INVESTIGATING THE MECHANISMS UNDERLYING CHOLINERGIC REGULATION OF DOPAMINE RELEASE



Stefania Vietti-Michelina

Department of Physiology, Anatomy and Genetics

Interdisciplinary Bioscience BBSRC DTP

Balliol College

University of Oxford

Thesis submitted for the degree of

Doctor of Philosophy

Hilary Term 2022

Table of Contents

STATEMENT OF AUTHORSHIP VII

CONFERENCE ABSTRACTS AND MANUSCRIPTS VIII

ACKNOWLEDGEMENTS IX

ABSTRACT X

ABBREVIATIONS XII

1. INTRODUCTION 1

1.1 THESIS OVERVIEW 2

1.2 ORGANISATION OF THE STRIATUM 3

1.2.1 Anatomy and function of the striatum 4

1.2.2 Neuronal composition of the striatum 7

1.3 STRIATAL CHOLINERGIC SYSTEM 10

1.3.1 Sources of striatal acetylcholine 10

1.3.2 Striatal cholinergic interneurons and their afferent connectivity 11

1.3.3 Striatal acetylcholine transmission 14

1.3.4 Muscarinic and nicotinic acetylcholine receptors 16

1.3.5 Behavioural implications of striatal cholinergic signalling 19

1.3.6 Acetylcholine detection 20

1.4 MESOSTRIATAL DOPAMINERGIC SYSTEM 24

1.4.1 Mesostriatal dopamine neurons and dopamine signalling 24

1.4.2 Local striatal modulation of dopamine release: role of acetylcholine 25

1.4.3 Dopamine receptors 28

1.4.4 Behavioural role of dopamine 30

1.5 PARKINSON'S DISEASE 32

1.5.1 Dopamine neuron degeneration in Parkinson's disease 33

1.5.2 Acetylcholine in Parkinson's disease 34

1.5.3 Alpha-synuclein in Parkinson's disease 36

1.5.4 Mouse models of Parkinson's disease 36

2. GENERAL METHODS 39

2.1 ANIMAL MODEL 40

2.1.1. Mice as a model organism to investigate striatal circuits 40

2.1.2 Transgenic mouse lines 41

2.1.3. Stereotaxic intracranial injections 43

2.2 FAST-SCAN CYCLIC VOLTAMMETRY FOR REAL-TIME DETECTION OF DA RELEASE 45

2.2.1. Slice preparation 48

2.2.2. Carbon fibre microelectrode fabrication 49

2.2.3. Electrical and light stimulation 50

2.2.4. FCV recording 52

2.3 IMAGING 55

2.3.1 GRAB sensor imaging 56

2.3.2. Calcium imaging 58

2.3.3. Slice preparation and recording 58

2.3.4. Image acquisition 60

2.3.5. Data processing 61

2.3.6. Viral serotype-driven differences in ACh signal measured with $GRAB_{ACh}$ 63

3. MODULATION OF STRIATAL ACETYLCHOLINE RELEASE 67

3.1 INTRODUCTION 68

3.2 METHODS 72

3.2.1 Animals and slice preparation 72

3.2.2 $GRAB_{ACh}$ and calcium imaging 72

3.2.3 Drugs 73

3.2.4 Immunohistochemistry and fluorescence microscopy 74

3.3 RESULTS 76

3.3.1 Properties of the ACh signal measured with $GRAB_{ACh}$ sensors in striatal slices 76

3.3.2 ACh release differs in dorsolateral and ventral striatum 81

3.3.3. ChI activation and ACh release follow stimulation frequency 82

3.3.4 Spatiotemporal dynamics of tonic and evoked ACh release are regulated by acetylcholinesterase 87

3.3.5. Antagonism of GABA receptors promotes ACh release signals 89

3.3.6. ACh release is under regulation by DA via D2Rs 92

3.4 DISCUSSION 103

3.4.1 $GRAB_{ACh}$ to measure real-time ACh release in striatal slices 103

3.4.2 Are dynamic changes in F_0 a measurement of tonic ACh levels? 105

3.4.3. Differences in evoked ACh release in dorsolateral and ventral striatum 106

3.4.4. Acetylcholinesterase as a regulator of ACh extracellular spatiotemporal dynamics 107

3.4.5. Potential tonic GABAergic inhibition of ACh release 109

3.4.6. DA regulation of ACh release via D2 receptors 111

4. EXPLORING THE MECHANISMS UNDERLYING ACETYLCHOLINE REGULATION OF DOPAMINE RELEASE VIA NICOTINIC ACETYLCHOLINE RECEPTORS 114

4.1 INTRODUCTION 115

4.2 METHODS 120

4.2.1 Animals and slice preparation 120

4.2.2 Fast-scan cyclic voltammetry 120

4.2.3 GRAB sensor and calcium imaging 122

4.2.4 Drugs 123

4.3 RESULTS 124

4.3.1 ACh-driven DA release is sensitive to changes in ACh release levels but insensitive to ChI stimulation frequency 124

4.3.2 Putative reduction in ACh levels driven by agonism of mAChRs partially promotes DA release sensitivity to stimulation of DA neurons but not ChIs 131

4.3.3. Putative increase in ACh levels driven by antagonism of mAChRs promotes DA release sensitivity to stimulation of DA neurons but not ChIs 136

4.3.4. nAChRs regulate short-term plasticity of DA release but not ACh release 142

4.3.5. Probing evidence for nAChR desensitisation by endogenous ACh 146

4.3.6. Calbindin D-28K does not interact with nAChRs in the ventral striatum 148

4.4 DISCUSSION 151

4.4.1 Changes in ACh release levels resulting from activity in ChIs are not translated into changes in ACh-driven DA release 151

4.4.2. nAChRs as regulators of DA but not ACh release plasticity 154

4.4.3. Probing potential nAChR desensitisation by endogenous ACh 156

4.4.4 Role of Calbindin-D28K in mediating nAChR function 157

4.4.5 Potential mechanisms operating downstream of nAChRs on DA axons 158

5. DYSFUNCTION IN STRIATAL ACETYLCHOLINE RELEASE IN A MOUSE MODEL OF EARLY PARKINSON'S DISEASE 161

5.1 INTRODUCTION 162

5.2 METHODS 166

5.2.1 Animals and slice preparation 166

5.2.2 $GRAB_{ACh}$ imaging 166

5.2.3 Drugs 167

5.3 RESULTS 169

5.3.1 Acetylcholinesterase regulates tonic levels of ACh more efficiently in SNCA-OVX mice 169

5.3.2 Evoked ACh release is lower in SNCA-OVX mice 172

5.3.3 SNCA-OVX mice show stronger D2R regulation of ACh release 173

5.3.4 Presumed tonic GABAergic inhibition of ACh release does not differ between SNCA-OVX and Snca -/- mice 176

5.4 DISCUSSION 179

5.4.1 Alterations in ACh tone regulation in the dorsolateral striatum of the early PD model SNCA-OVX 179

5.4.2 Alterations in evoked ACh release in the mouse model of early PD SNCA-OVX 180

5.4.3 Compensatory changes in D2R regulation of ACh release in SNCA-OVX mice 182

5.4.4 No changes in GABA receptor modulation of ACh release in SNCA-OVX versus Snca -/- 183

6. GENERAL DISCUSSION 185

6.1 MEASURING STRIATAL ACH RELEASE WITH $GRAB_{ACH}$ 187

6.2 ACH RELEASE IN THE STRIATUM 190

6.2.1 ChI activity and AChE in the regulation of ACh release dynamics 190

6.2.2 Potential tonic GABAergic inhibition of ACh release 192

6.2.3 Dopaminergic modulation of ACh release 193

6.3 CHOLINERGIC MODULATION OF DA RELEASE 196

6.3.1 Complexity of investigating cholinergic modulation of DA release short-term plasticity 196

6.3.2 Potential mechanisms operating downstream of nAChRs 198

6.4 STRIATAL ACH SIGNALLING IN A MODEL OF EARLY PD 200

6.5 CONCLUSION 204

REFERENCES 205

STATEMENT OF AUTHORSHIP

This thesis does not contain any material that has been accepted for the award of any other degree in any University or other institution. All data represented in this thesis are fully my own work, and where data has been contributed by others their contribution is stated below and in the main text.

The data included in **Chapter 5** are part of a wider study within the laboratory of Professor Stephanie Cragg and have been collected together with Dr Emanuel Lopes (Postdoctoral researcher). These data are provided with Dr Lopes' full permission and are identified in the corresponding figure legends.

CONFERENCE ABSTRACTS AND MANUSCRIPTS

CONFERENCE ABSTRACTS:

Vietti-Michelina S, Brimblecombe KR, Cragg SJ. Investigating the mechanisms underlying cholinergic regulation of dopamine release. DPhil poster day, Department of Physiology, Anatomy and Genetics (2019, Oxford, UK, poster).

Vietti-Michelina S, Brimblecombe KR, Cragg SJ. Presynaptic and postsynaptic components of dopamine release regulation by acetylcholine and nicotinic receptors. Virtual Dopamine Conference, ViDA (2020, online, poster).

Vietti-Michelina S, Lopes E, Brimblecombe KR, Cragg SJ. Dynamic regulation of striatal acetylcholine release by D2-dopamine receptors and adaptations in a mouse model of Parkinson's disease. Dopamine 2022 (Montréal, Canada, poster).

MANUSCRIPTS:

Condon MD, Platt NJ, Zhang Y, Roberts BM, Clements MA, **Vietti-Michelina S**, Tseu M, Brimblecombe KR, Threlfell S, Mann EO, Cragg SJ (2019) Plasticity in striatal dopamine release is governed by release-independent depression and the dopamine transporter. Nature communications 10: 4263.

Brimblecombe KR, **Vietti-Michelina S**, Platt NJ, Kastli R, Hnieno A, Gracie CJ, Cragg SJ (2019) Calbindin-D28K limits dopamine release in ventral but not dorsal striatum by regulating Ca^{2+} availability and dopamine transporter function. ACS Chemical Neuroscience 10: 3419-3426.

Pérez-Taboada I, Alberquilla S, Martìn ED, Anand R, **Vietti-Michelina S**, Tebeka NN, Cantley J, Cragg SJ, Moratalla R, Vallejo M (2020) Diabetes causes dysfunctional dopamine neurotransmission favoring nigrostriatal degeneration in mice. Movement Disorders 35: 1636-1648.

Jacob PF, Vargas-Gutierrez P, Okray Z, **Vietti-Michelina S**, Felsenberg J, Waddell S (2021) Prior experience conditionally inhibits the expression of new learning in Drosophila. Current Biology 31: 3490-3503.

ACKNOWLEDGEMENTS

There are several people I would like to thank, who made this experience unique and incredible. It was one of the most challenging but rewarding times of my life thus far and I'm grateful to the people that supported me through it.

First, I would like to sincerely thank my supervisor, Professor Stephanie Cragg for giving me the opportunity to work under her supervision. Her drive, passion, knowledge, and mentorship were truly inspiring and helped me grow both on a professional and personal level. I would also like to extend my gratitude to all the present and past members of the Cragg lab. You all made working in the lab a great experience, ensuring constant collaboration, open dialogue, and mutual support. In particular, I would like to thank Dr Sarah Threlfell for training me during my rotation, Dr Emanuel Lopes, Dr Bradley Roberts and Rishi Anand for being wonderful colleagues, always there to help when something doesn't work for mysterious reasons and to brainstorm ideas. I'm also deeply grateful to Dr Katherine Brimblecombe, whose guidance and expertise have helped me and taught me a lot.

I would like to thank the Doctoral Training Centre and the BBSRC for providing the fundings supporting this project. Thanks to all the DTPeeps, it was wonderful to meet so many talented scientists from different backgrounds, not to mention all the fun events we've organised! To my friends from Balliol college, in particular Laura and Dario, thank you for sharing this journey with me, this experience wouldn't have been the same without your friendship and support. To my best friends Lois, Chelsea and Chloe, you've truly been my rock in these past few years, I couldn't possibly imagine having done this without you. To my boyfriend Robert, thank you for your love and support and for being my voice of reason while writing this thesis.

A big thank you to all my friends from home in Turin, who have always been there for me despite the distance. Finally, I would like to deeply thank my parents, Maria Rita and Giovanni, for their unconditional support and all the sacrifices they made for me. Vi sono infinitamente grata e vi voglio bene.

ABSTRACT

Dopamine (DA) is a critical regulator of movement and motivation and disruptions to its signalling underlie various psychomotor disorders, including Parkinson's disease (PD) and addiction. DA neurons projecting from the midbrain to the striatum form extensive axonal arborisation which are subject to local neuromodulation, gating how action potential firing at the level of DA neuron soma is translated into axonal DA release. Unravelling these mechanisms is therefore fundamental to better understand DA regulation of striatal output in health and disease.

Acetylcholine (ACh) is one of the major local modulators of striatal DA release. ACh mainly originates from striatal cholinergic interneurons (ChIs) and dysregulation to striatal cholinergic signalling is also implicated in a range of neuropsychiatric and neurodegenerative disorders. ACh acts at nicotinic ACh receptors (nAChRs) localised on DA axons and modulates DA release in a multiplicity of ways, from directly driving DA release bypassing action potential firing by DA somata, to promoting short-term depression of DA released during burst stimulation. Despite this fundamental role, striatal ACh release dynamics are currently incompletely characterised, mainly due to a lack of tools for direct, real-time measurement of ACh release, only recently filled by the development of genetically encoded fluorescent sensors ($GRAB_{ACh}$). In this thesis, I used $GRAB_{ACh}$ in mouse striatal slices to characterise the major properties of striatal ACh release, a fundamental step to help unravel the mechanisms underlying cholinergic modulation of DA release. I found that ACh in dorsal and ventral striatum is dynamically released according to activity in ChIs and that acetylcholinesterase (AChE) modulates the spatiotemporal dynamics of evoked ACh release and tonic ambient levels of ACh. Furthermore, I show that ACh release is modulated by GABA acting at $GABA_A$ and $GABA_B$ receptors and inhibited by endogenous DA acting at D2-receptors (D2Rs). I then investigated the complex relationship between changes in ACh release and how these can dynamically gate DA release via nAChRs, combining $GRAB_{ACh}$ sensors and FCV to measure ACh and DA release in mouse striatal slices. I found that the magnitude of ACh-driven DA release is sensitive to changes in ACh

levels but insensitive to activity in ChIs. Furthermore, I found that nAChRs regulate short-term plasticity of DA but not ACh release and are not functionally associated with the calcium binding protein calbindin D-28K in DA axons. Finally, I've explored maladaptive alterations in striatal cholinergic signalling in a human α-synuclein overexpressing mouse model of early parkinsonism. In this model, we found lower ACh release and stronger regulation of tonic ACh by AChE. In the early parkinsonian model, we also reported stronger D2R-mediated regulation of ACh release and no changes in tonic GABAergic inhibition.

Overall, this thesis aimed at investigating the dynamic interplay between ACh and DA release in the striatum. The data here presented provide a novel characterisation of ACh release dynamics in health and early Parkinson's disease, together with previously unappreciated aspects of the dynamic gating of DA release by ACh.

ABBREVIATIONS

1p	Single pulse
5p	Train of 5 pulses
6-OHDA	6-hydroxydopamine
AAV	Adeno-associated virus
AC	Adenylyl cyclase
ACh	Acetylcholine
AChE	Acetylcholinesterase
aCSF	Artificial cerebrospinal fluid
AHP	Afterhyperpolarisation potential
AP	Action potential
AR	Asynchronous release
AUC	Area under curve
CaM	Calmodulin
cAMP	Cyclic adenosine monophosphate
CFM	Carbon fibre microelectrode
Ch	Choline
ChAT	Choline acetyltransferase
ChI	Cholinergic interneuron
ChOx	Choline oxidase
ChR2	Channelrhodopsin-2
CNS	Central nervous system
cpFP	Circularly permutated fluorescent protein
cpGFP	Circularly permutated green fluorescent protein
CPu	Caudate-putamen
D2R	Dopamine D2-receptor
DA	Dopamine
DAT	Dopamine transporter
DHβE	Dihydro-β-erythroidine

dMSN	Direct pathway medium spiny neuron
FCV	Fast-scan cyclic voltammetry
FRET	Fluorescence resonance energy transfer
FSI	Fast-spiking interneuron
GABA	γ-aminobutyric acid
GCaMP	Intracellular calcium sensor (calmodulin-M13-cpGFP)
GECI	Genetically encoded calcium indicator
GEVI	Genetically encoded voltage indicator
GPCR	G protein-coupled receptor
GPe	External segment of the globus pallidus
GPi	Internal segment of the globus pallidus
GRAB	GPCR-activation-based sensor
HPLC	High-performance liquid chromatography
hSyn	Human synapsin gene promoter
IHC	Immunohistochemistry
iMSN	Indirect pathway medium spiny neuron
IPSC	Inhibitory postsynaptic current
L-DOPA	Levodopa
LDT	Laterodorsal tegmental nucleus
LED	Light-emitting diode
LTSI	Low-threshold spiking interneuron
mAChR	Muscarinic acetylcholine receptor
MPTP	1-methyl-4-phenyl-1,2,3,6-tetrahydropyiridine
MSN	Medium spiny neuron
NAc	Nucleus accumbens
NAcC	Nucleus accumbens core
nAChR	Nicotinic acetylcholine receptor
NAcSh	Nucleus accumbens shell
PD	Parkinson’s disease
PKC	Protein kinase C

PLC	Phospholipase C
PPN	Pedunculopontine nucleus
PRiMA	Proline-rich membrane anchor
ROI	Region of interest
RPE	Reward prediction error
RPS6	Ribosomal protein S6
SNc	Substantia nigra pars compacta
SNCA	Human α-synuclein gene
Snca	Mouse α-synuclein gene
SNCA-OVX	Human α-synuclein overexpressing mouse model of PD
SNr	Substantia nigra pars reticulata
SNR	Signal-to noise-ratio
SPN	Spiny projection neuron
SST	Somatostatin
STD	Short-term depression
STN	Subthalamic nucleus
STP	Short-term plasticity
TAN	Tonically active neuron
TH	Tyrosine hydroxylase
THIN	TH-expressing interneuron
TTX	Tetrodotoxin
VAChT	Vesicular acetylcholine transporter
VGCC	Voltage-gated calcium channel
VTA	Ventral tegmental area
WT	Wild-type

1. Introduction

1.1 THESIS OVERVIEW

Dopamine (DA) plays a critical role in motor, motivational and reward-related functions and disruptions to its signalling underlie several psychomotor disorders, including Parkinson's disease (PD). DA release in the striatum is gated by a range of neuromodulators acting locally at the highly branched and widespread DA axons, so that activity in midbrain DA neurons does not necessarily correspond to DA release. Among the wide range of local axonal modulators of DA release, acetylcholine (ACh) is one of the most significant, with its effects dominating over concurrent modulators.

The striatum is one of the brain regions exhibiting the highest levels of ACh, enzymes for its synthesis and breakdown and ACh receptors (Mesulam et al., 1992; Zhou et al., 2002). ACh exerts a range of powerful effects on DA output, from directly driving striatal DA release bypassing action potential firing by midbrain DA soma, to promoting short-term depression of DA release during train stimulation, both via nicotinic ACh receptors (nAChRs) localised on DA axons (Rice and Cragg, 2004; Threlfell et al., 2012). To better understand the mechanisms underlying cholinergic modulation of DA release plasticity, unravelling the properties of striatal ACh release dynamics is fundamental. A lack of tools for direct real-time measurement of ACh release in intact brain tissue or *in vivo* has been an obstacle in the characterisation of ACh release dynamics. The recent development of genetically encoded fluorescent sensors for ACh release measurement (Jing et al., 2018, 2020) has filled this detection gap. In **Chapter 3**, I've used genetically encoded fluorescent sensors to measure ACh release in mouse striatal slices and examined the major properties of ACh release dynamics in dorsal and ventral striatum, including modulation by two key striatal neurotransmitters, γ-aminobutyric acid (GABA) and DA. In **Chapter 4**, I've explored the relationship between dynamic changes in ACh release and how these modulate the cholinergic and dopaminergic components of DA release via nAChRs. Finally, in **Chapter 5** I've explored maladaptive changes in striatal ACh transmission in a transgenic mouse model of early PD.

1.2 ORGANISATION OF THE STRIATUM

The basal ganglia are a group of subcortical nuclei comprising the striatum, the globus pallidus (GP), the substantia nigra (SN) and the subthalamic nucleus (STN) (**Figure 1.1**). The striatum is the major input structure of the basal ganglia, and it receives projections from the cortex, thalamus, and midbrain (Lanciego et al., 2012). The GP is divided into the external segment (GPe, often referred to simply as the globus pallidus in rodents) and the internal segment (GPi, known in rodents as the entopeduncular nucleus, EP). The SN includes two separate nuclei, the pars reticulata (SNr) and the pars compacta (SNc). The GPe, STN and SNc are intrinsic nuclei located between the input (striatum) and output nuclei in the transfer of information (Lanciego et al., 2012). The GPi and SNr constitute the principal output structure of the basal ganglia and send projections to the thalamus and brainstem (Crittenden and Graybiel, 2011; Lanciego et al., 2012). The basal ganglia cover a range of functions, from movement control to behaviour, cognition, and reward processing (Crittenden and Graybiel, 2011; Lanciego et al., 2012; Obeso et al., 2014). Accordingly, dysfunction in basal ganglia signalling underlies movement and psychiatric disorders, such as Parkinson's disease, Huntington's disease, addiction, and cognitive abnormalities (Crittenden and Graybiel, 2011; Obeso et al., 2014).

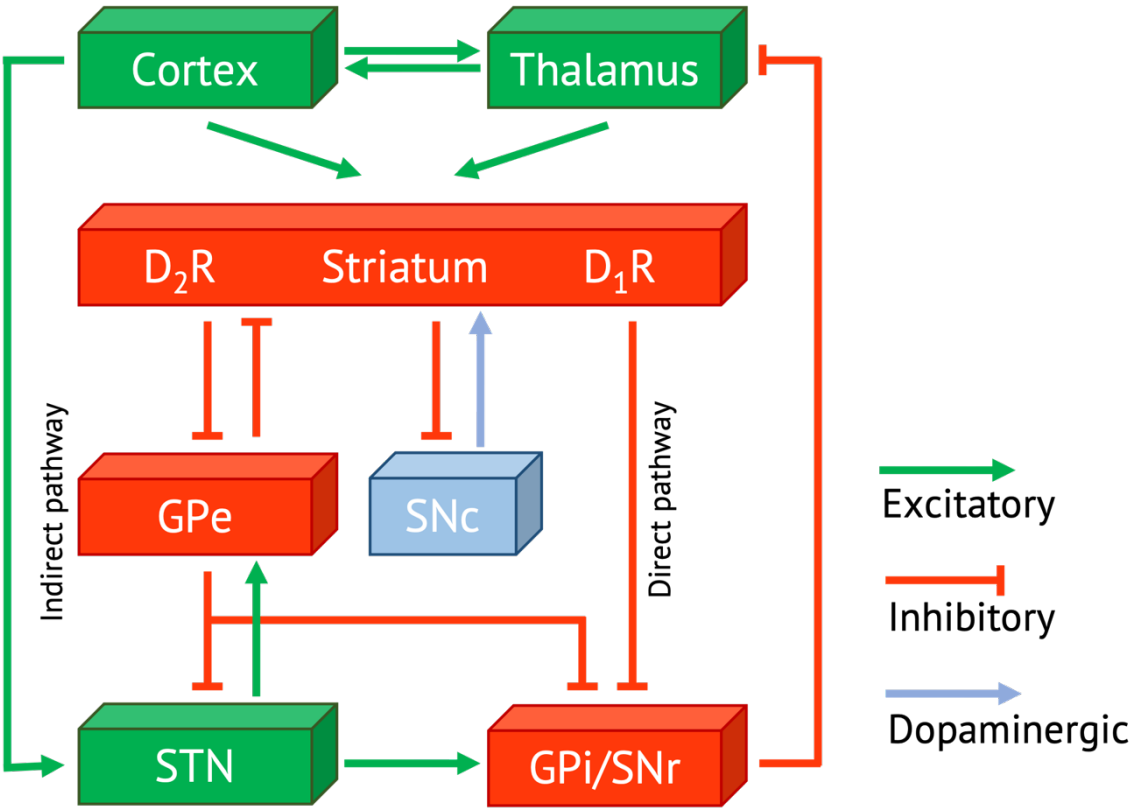


Figure 1.1. Classical model of basal ganglia connectivity.
A simplified representation showing the main connectivity between cortex, thalamus, and the basal ganglia nuclei. Notably, connectivity is more complex, with several transverse loops between nuclei. Inhibitory GABAergic pathways are indicated in red, glutamatergic excitatory projections in green and dopaminergic in light blue. GPe = external segment of the globus pallidus, GPi = internal segment of the globus pallidus, SNc = substantia nigra pars compacta, SNr = substantia nigra pars reticulata, STN = subthalamic nucleus, D1R = DA D1-receptor, D2R = DA D2-receptor. Indirect pathway represents D2R-positive medium spiny neuron projections to GPe, while direct pathway represents D1R-positive medium spiny neuron projections to the SNr/GPi.

1.2.1 Anatomy and function of the striatum

The striatum is the main input nucleus of the basal ganglia, and it receives projections from different brain areas, including the cortex, thalamus, midbrain, and brainstem (Gerfen, 1985; Doig et al., 2010; Lanciego et al., 2012; Dautan et al., 2014). The striatum integrates the different sensorimotor and limbic information conveyed by these inputs and projects to the output nuclei of the basal ganglia via direct and indirect pathway medium-sized spiny neurons (MSNs, **Figure 1.1**).

The striatum is functionally and topographically segregated along a dorsolateral to ventromedial axis (Voorn et al., 2004). For instance, cortical, thalamic and nigral input to the striatum distribute according to a dorsolateral-to-ventromedial gradient (Voorn et al., 2004). This topographical organisation is

consistent with a differential behavioural function across striatal regions. Indeed, the dorsal striatum, which includes the caudate nucleus and putamen, covers a role in sensorimotor related functions and habit formation (Knowlton et al., 1996; Packard, 1999; Yin et al., 2004; Quinn et al., 2013). On the other hand, the ventral striatum, which includes the nucleus accumbens (NAc), is thought to play a role in reward-based learning, reinforcement, motivated and appetitive behaviours (Carboni et al., 1989; McBride et al., 1999; Cardinal et al., 2002; Kalivas and McFarland, 2003; Kelley, 2004; Ikemoto, 2007). The cellular structure and function of the striatum is largely conserved between primates and rodents, however the relative positioning of striatal structures changes considerably. In primates, the caudate nucleus and putamen are structurally and functionally distinct, separated by white matter of the internal capsule. The NAc is adjacent to the two structures and delineated by the ventromedial end of the internal capsule. In rodents, the striatum is one structure and is positioned ventrally of the external capsule and lateral to the dorsal horns of the lateral ventricles. The caudate nucleus and putamen form one contiguous nucleus, referred to as the caudate-putamen (CPu), and the anatomical boundaries between CPu and NAc are less evident (**Figure 1.2**). The NAc is further organised in NAc core (NAcC) and NAc shell (NAcSh) (**Figure 1.2**), positioned more ventromedial and further subdivided into medial and lateral segments (Zahm, 1999; Ma et al., 2020). NAcSh subterritories are functionally heterogenous and differentially shape motivated and reward-related behaviours (Plasse et al., 2012; Yang et al., 2018; Smedley et al., 2019). Notably, most of the evidence reviewed in this chapter is based on studies conducted in rodents.

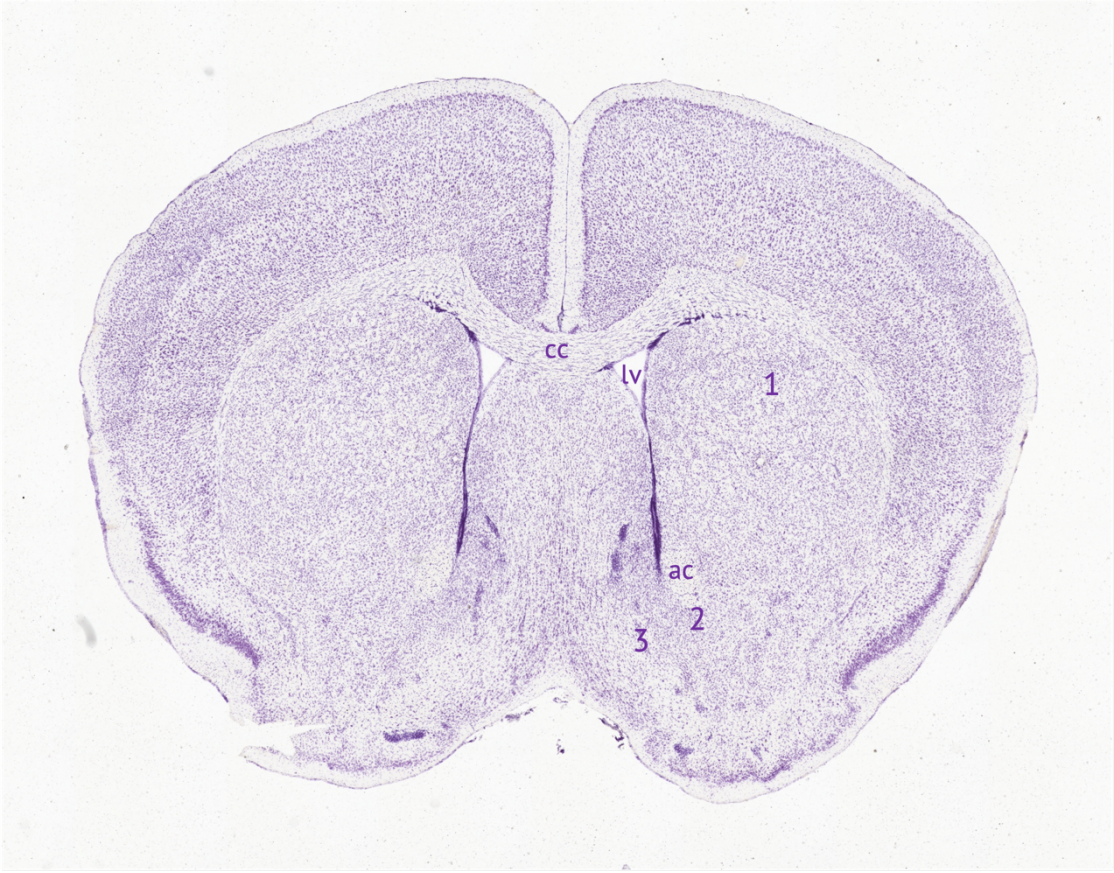


Figure 1.2. Coronal brain section of the mouse striatum with Nissl stain. Image adapted from the Allen Mouse Brain Atlas. *1: caudate-putamen (CPu), 2: nucleus accumbens core (NAcC), 3: nucleus accumbens shell (NAcSh), cc: corpus callosum, lv: lateral ventricle, ac: anterior commissure.*

The striatum is also organised in striosome (or patch) and matrix compartments, defined by the expression of different biochemical markers (Pert et al., 1976; Graybiel and Ragsdale, 1978; Gerfen et al., 1987). The striosomes occupy 10-15% of striatal volume and form a labyrinth-like structure embedded in the surrounding matrix (Crittenden and Graybiel, 2011; Brimblecombe and Cragg, 2017). They express high levels of μ-opioid receptor (MOR), D1-receptor (D1R), substance P (SP), met-enkephalin (met-ENK), calretinin, Nr4a1, pro-dynorphin, GAD-2, and EGR-1 (Pert et al., 1976; Besson et al., 1988; Sakamoto et al., 1992; Brimblecombe and Cragg, 2017). On the other hand, the matrix compartment is enriched with calbindin, somatostatin (SST), enkephalin (ENK), D2-receptor (D2R), and cholinergic markers such as acetylcholinesterase (AChE) and choline acetyltransferase (ChAT) (Graybiel and Ragsdale, 1978; Gerfen et al., 1987; Brimblecombe and Cragg, 2017). These compartments also have different anatomical connections, where the afferents

projecting to the matrix are principally related to associative and sensorimotor regions, while the striosome-projecting ones are limbic-related (Jimenez-Castellanos and Graybiel, 1987; Gerfen, 1989; Crittenden and Graybiel, 2011). Striosome and matrix compartmentalisation is also differentially involved in pathological processes underlying several psychomotor disorders, including PD, Huntington's disease, and addiction (Crittenden and Graybiel, 2011).

1.2.2 Neuronal composition of the striatum

Medium-sized spiny neurons (MSNs), also known as spiny projection neurons (SPNs), constitute the 90-95% of striatal neurons, while the remaining 3-5% are different populations of interneurons, classified according to their different morphology, protein content and electrophysiological properties (Kemp and Powell, 1971; Smith and Bolam, 1990; Kawaguchi, 1993; Kawaguchi et al., 1995; Bolam et al., 2000; Tepper and Bolam, 2004).

MSNs utilise GABA as their main neurotransmitter and constitute the primary input/output neurons of the striatum. Indeed, they integrate excitatory glutamatergic inputs from cortical and thalamic regions and dopaminergic inputs from the midbrain (**Section 1.4**) with local synaptic and neuromodulatory signalling, and project to the basal ganglia output nuclei (GPi, SNr) either directly or via the GPe (**Figure 1.1**) (Kawaguchi et al., 1990; Bolam et al., 2000; Lanciego et al., 2012). MSNs are also interconnected by local recurrent axon collateral, which mediate a network of inter-inhibition (Somogyi et al., 1981; Bolam et al., 2000; Tunstall et al., 2002; Taverna et al., 2008). MSNs can be divided into two populations based on their projections and protein expression (Smith and Bolam, 1990; Bolam et al., 2000). One subpopulation of MSNs expresses D1Rs, substance P and dynorphin and projects to the output nuclei of the basal ganglia, the GPi and SNr (Gerfen et al., 1990; Surmeier et al., 1996; Steiner and Gerfen, 1998; Bolam et al., 2000). These MSNs constitute the direct pathway (dMSNs) and their activation results in inhibition of neurons in the GPi/SNr and consequent disinhibition of their target regions (**Figure 1.1**). The other subpopulation expresses D2Rs and enkephalin and constitutes the indirect pathway (iMSNs),

projecting to the GPe (Gerfen et al., 1990; Steiner and Gerfen, 1998; Bolam et al., 2000). Activation of iMSNs inhibits neurons in the GPe, which will in turn disinhibit GPi neurons and therefore inhibit their target regions (**Figure 1.1**). Therefore, dMSNs and iMSNs exert opposing effects on basal ganglia-mediated behaviours. Indeed, activation of dMSNs promotes movement initiation and maintenance, reinforcement, and reward, while activation of the iMSNs suppresses these behaviours (Kravitz et al., 2010, 2012; Lobo et al., 2010; Freeze et al., 2013). However, this model oversimplifies basal ganglia connectivity and function and the role of these two subpopulations in shaping basal ganglia output is to date not fully characterised.

Other striatal neurons comprise different subtypes of interneurons. These interneurons are principally GABAergic, except for the cholinergic interneurons (ChIs) which signal through ACh (**Section 1.3.2**). There are several subtypes of striatal GABAergic interneurons, with new subtypes being discovered thanks to the availability of new transgenic mouse lines (Tepper et al., 2018). Here, I will briefly review three main classes of interneurons, the parvalbumin-expressing fast-spiking interneurons (FSIs), the neuropeptide Y/ somatostatin/ nitric oxide synthase low-threshold spiking interneurons (LTSIs), and the tyrosine hydroxylase (TH)-expressing interneurons (THINs).

FSIs express the calcium-binding protein parvalbumin (PV) and present fast firing frequencies (Gerfen et al., 1985; Kawaguchi, 1993; Tepper et al., 2010). FSIs receive cortical and, to a lesser extent, thalamic inputs (Kita et al., 1990; Kita, 1993; Ramanathan et al., 2002; Tepper et al., 2010), together with dopaminergic projections (Kubota et al., 1987) and GABAergic inputs originating from the GP (Bevan et al., 1998). There is electron microscopy evidence for cholinergic synapses onto FSIs (Chang and Kita, 1992) and these neurons express muscarinic and nicotinic acetylcholine receptors (Koós and Tepper, 2002; Luo et al., 2013a; Tepper et al., 2018). However, no apparent functional interaction between ChIs and FSIs has been described by local field stimulation or optogenetic studies (Koós and Tepper, 2002; English et al., 2012; Szydlowski et al., 2013). FSIs synapse onto direct and indirect pathways MSNs, providing strong feed-forward inhibition (Koós and Tepper, 1999;

Gittis et al., 2010; Planert et al., 2010). At a behavioural level, FSIs play a role in reward conditioning, associative learning, and habit formation (Lee et al., 2017; O'Hare et al., 2017; Owen et al., 2018; Tepper et al., 2018).

LTSIs are another class of striatal GABAergic interneurons. These interneurons are immunoreactive for SST, neuropeptide Y (NPY) and nitric oxide synthase (NOS) and present a low threshold calcium spike (LTS) and long-lasting plateau potentials following depolarisation (Kawaguchi, 1993; Tepper et al., 2010). LTSIs receive inputs from the cortex, dopamine axons and ChIs (Vuillet et al., 1989b, 1989a, 1992; Kawaguchi, 1993). The main efferent target of LTSIs are MSNs. Indeed, LTSIs synapse onto distal dendrites and spines of MSNs (DiFiglia and Aronin, 1982; Kubota et al., 1987; Vuillet et al., 1989b; Tepper et al., 2010). LTSIs also make synaptic contacts with ChIs (Vuillet et al., 1992). Behaviourally, LTSIs play an important role in goal-directed learning (Holly et al., 2019).

THINs are a subtype of GABAergic interneurons with heterogenous electrophysiological properties that have been grouped in four types (I-IV) (Ibanez-Sandoval et al., 2010). THINs receive inputs from cortex and thalamus (Ibanez-Sandoval et al., 2010; Assous et al., 2017; Tepper et al., 2018) and have been suggested to be potentially targeted by dopaminergic projections (Ibáñez-Sandoval et al., 2015; Xenias et al., 2015; Tepper et al., 2018). THINs target MSNs and LTSIs (Ibanez-Sandoval et al., 2010; Assous et al., 2017), express nicotinic ACh receptors (Luo et al., 2013a; Ibáñez-Sandoval et al., 2015) and mediate polysynaptic inhibition between striatal ChIs (Dorst et al., 2020).

1.3 STRIATAL CHOLINERGIC SYSTEM

1.3.1 Sources of striatal acetylcholine

The striatum is one of the brain regions exhibiting the highest levels of ACh, enzymes for its synthesis and breakdown and ACh receptors (Mesulam et al., 1992; Zhou et al., 2002). The major source of striatal ACh are intrinsic striatal ChIs (**Section 1.3.2**) (Contant et al., 1996; Calabresi et al., 2000). In rats, an additional source of ACh arising from cholinergic neurons projecting from the pedunculopontine (PPN) and laterodorsal tegmental nucleus (LDT) of the brainstem has been described (Woolf and Butcher, 1986; Dautan et al., 2014). PPN innervation of the striatum has also been reported in mice (Wall et al., 2013), although its cholinergic nature and functional role are yet to be defined. PPN/LDT cholinergic neurons directly innervate striatal MSNs and ChIs, with an inhibitory or excitatory effect, respectively (Dautan et al., 2020). These projections are also involved in the regulation of goal-directed behaviour and habit formation (Dautan et al., 2020). Despite the role of PPN/LDT cholinergic projections in modulating striatal function, ChIs alone have been found sufficient to provide a source of ACh that can modulate DA release (Brimblecombe et al., 2018). In rat striatal slices, targeted optogenetic activation of PPN/LDT cholinergic neurons did not result in a detectable modulation of striatal DA release measured with fast-scan cyclic voltammetry (FCV) (Brimblecombe et al., 2018). On the other hand, selective activation of ChIs directly drives and modulates DA release (Brimblecombe et al., 2018), reproducing previous findings in mouse (**Section 1.4.2**) (Cachope et al., 2012; Threlfell et al., 2012). These findings do not preclude PPN/LDT afferents from potentially modulating DA release *in vivo*, where they modulate activity in MSNs and ChIs (Dautan et al., 2020), which might in turn regulate DA release (Brimblecombe et al., 2018). Nonetheless, striatal ChIs are sufficient to account for local striatal cholinergic modulation of DA release.

1.3.2 Striatal cholinergic interneurons and their afferent connectivity

ChIs account for only 1-2% of striatal neurons, however their notable morphological features ensure widespread cholinergic innervation across the striatum (Phelps et al., 1985; Contant et al., 1996; Poppi et al., 2021). In rodents, ChIs present large cell bodies (20-40 μm) (Bolam et al., 1984; Phelps et al., 1985), long dendrites and extensive, highly branched axonal arbors (Bolam et al., 1984; Phelps et al., 1985; Wilson et al., 1990; Contant et al., 1996; Poppi et al., 2021). Quantitative electron microscopy studies in rat striatum estimated approximately 2 x 10^8 ACh varicosities/mm^3, inferring that each ChI possesses an average of around 500,000 axonal varicosities (Contant et al., 1996). ChIs generally occupy boundary regions between striosome and matrix compartments (Brimblecombe and Cragg, 2017) and are differentially distributed across the striatum. Quantitative imaging analysis of ChIs in the mouse striatum revealed that rostral portions of the striatum contain a higher number of ChIs than the caudal striatum and that NAcC presented lower ChI content than other striatal regions (Matamales et al., 2016). Furthermore, ChIs in the NAcC have shorter processes than those in the NAcSh or in the dorsal striatum (Matamales et al., 2016). However, ChI neuropil complexity, measured by the number of arbor bifurcations in a fixed distance, does not significantly differ between striatal regions (Matamales et al., 2016).

ChIs also present distinctive electrophysiological properties. ChIs have a depolarised resting membrane potential (around -60 mV) and are tonically active, firing action potentials at a rate of 2-10 Hz in absence of synaptic inputs (Wilson et al., 1990; Lee et al., 1998; Bennett and Wilson, 1999a). Furthermore, ChIs present prominent hyperpolarisation-activated cyclic nucleotide-gated (HCN) currents and large, slow afterhyperpolarisation potentials (AHPs) which contribute to their tonic activity (Kawaguchi, 1993; Bennett and Wilson, 1999b; Deng et al., 2007a; Poppi et al., 2021). These interneurons also show a dorsomedial-to-ventrolateral gradient of activity in the mouse striatum (Matamales et al., 2016). Indeed, studies using detection of phosphorylation of the ribosomal protein s6 (p-rpS6) as a measurement for baseline activity in ChIs (Bertran-Gonzalez et al., 2012; Matamales et al., 2016)

revealed that ChI cellular activity is higher in dorsomedial areas and gradually decreases towards ventrolateral areas (Matamales et al., 2016).

ChIs receive a vast range of excitatory, inhibitory and neuromodulatory inputs. ChIs receive excitatory glutamatergic inputs from cortex and thalamus and express a range of ionotropic and metabotropic glutamate receptors (**Figure 1.3**) (Bell et al., 2002; Deng et al., 2007b; Lim et al., 2014; Guo et al., 2015; Klug et al., 2018). ChIs also receive many inhibitory GABAergic projections and in the primate striatum it has been estimated that around 60% of synapses onto ChIs are GABAergic (Gonzales et al., 2013). ChIs express $GABA_A$ and $GABA_B$ receptors (Waldvogel et al., 1998; Yung et al., 1999; Rodríguez-Pallares et al., 2000) and GABA has been found to modulate ChI activity and ACh release acting at $GABA_A$ receptors on ChIs (DeBoer and Westerink, 1994; Rodríguez-Pallares et al., 2000; Lim et al., 2014; Sato et al., 2014). GABA has also been proposed to indirectly modulate ACh release by inhibiting glutamatergic corticostriatal inputs via $GABA_B$ receptors (DeBoer and Westerink, 1994; Poppi et al., 2021). Several GABAergic neurons synapse onto ChIs, including MSNs and striatal GABAergic interneurons (**Figure 1.3**) (Poppi et al., 2021). In the primate striatum, it has been estimated that around 24% of all synaptic contacts on ChIs originate from MSN axon collaterals (Gonzales et al., 2013). In mice, targeted optogenetic activation of MSNs evoked inhibitory postsynaptic currents (IPSCs) in the majority of ChIs, which were blocked by the $GABA_A$ receptor antagonist gabazine (Chuhma et al., 2011). Both LTSIs and THINs are functionally connected to ChIs and modulate their activity in the mouse striatum. Indeed, selective optogenetic activation of LTSIs triggered IPSCs in ChIs (Straub et al., 2016). THINs form recurrent inhibitory networks with ChIs which mediate polysynaptic GABAergic inhibition between neighbouring ChIs (Dorst et al., 2020). Finally, ChIs receive extrastriatal GABAergic inputs from the GPe and optogenetic activation of these projections elicited IPSCs in recorded ChIs (Klug et al., 2018).

ChI activity is also modulated by DA (**Figure 1.3**). There are reports of sparse synapses between DA axons and ChIs in the rat striatum (Hattori et al., 1976; Dimova et al., 1993), however DA is thought to act mainly as a volume transmitter (**Section**

1.4.1). In rodents and primates, ChIs express D2Rs and D5Rs and, to a lesser extent, D1Rs (Dawson et al., 1988; Bergson et al., 1995; Alcantara et al., 2003). DA has different outcomes on ChI excitability. For instance, in rodent striatal slices, bath application of DA excites ChIs via D1Rs and D5Rs (Aosaki et al., 1998; Centonze et al., 2003). On the other hand, in rodent striatal slices, DA acting at D2Rs can inhibit ChI firing and prolong slow afterhyperpolarisation duration (Maurice et al., 2004; Deng et al., 2007a). Co-release of glutamate from DA axons (Hnasko et al., 2010) can also modulate ChI activity (Chuhma et al., 2014, 2018; Cai and Ford, 2018).

ChIs also express muscarinic ACh receptors (mAChRs) and nAChRs. M_2 and M_4-mAChRs on ChIs act as autoreceptors and modulate ChI activation to prevent excessive ACh release (Bernard et al., 1992; Yan and Surmeier, 1996; Calabresi et al., 1998b; Lim et al., 2014). *In situ* hybridization in the rodent striatum showed that ChI express mRNA for α7 and β2 subunits of nAChRs (Azam et al., 2003; Abbondanza et al., 2022). In mice, ChIs appear to be the interneurons with highest expression of β2-subunit-containing nAChRs and deletion of these receptors in striatal interneurons leads to alterations in multiple behavioural domains (**Section 1.3.5**) (Abbondanza et al., 2022). Cholinergic neurons from the brainstem also project to and modulate ChI activity (**Section 1.3.1**).

As described above, ChIs project broadly throughout the striatum, which allows for widespread cholinergic modulation on a range of targets, such as MSNs, ChIs, GABAergic interneurons (**Section 1.2.2**), corticostriatal and dopaminergic terminals (**Section 1.4.2**) (Poppi et al., 2021). ChIs can directly modulate MSN activity via M_1- and M_4-mAChRs or inhibit their activity by recruiting GABAergic interneurons (Witten et al., 2010; Goldberg et al., 2011; English et al., 2012; Mamaligas and Ford, 2016; Cai and Ford, 2018). Furthermore, ChIs reduce glutamate release from corticothalamic terminals onto MSNs via activation of M_4- and M_2-mAChRs expressed by these projections (Pakhotin and Bracci, 2007; Goldberg et al., 2011; Pancani et al., 2014). Notably, ChI do not only release ACh but also co-release glutamate and GABA (Higley et al., 2011; Lozovaya et al., 2018a).

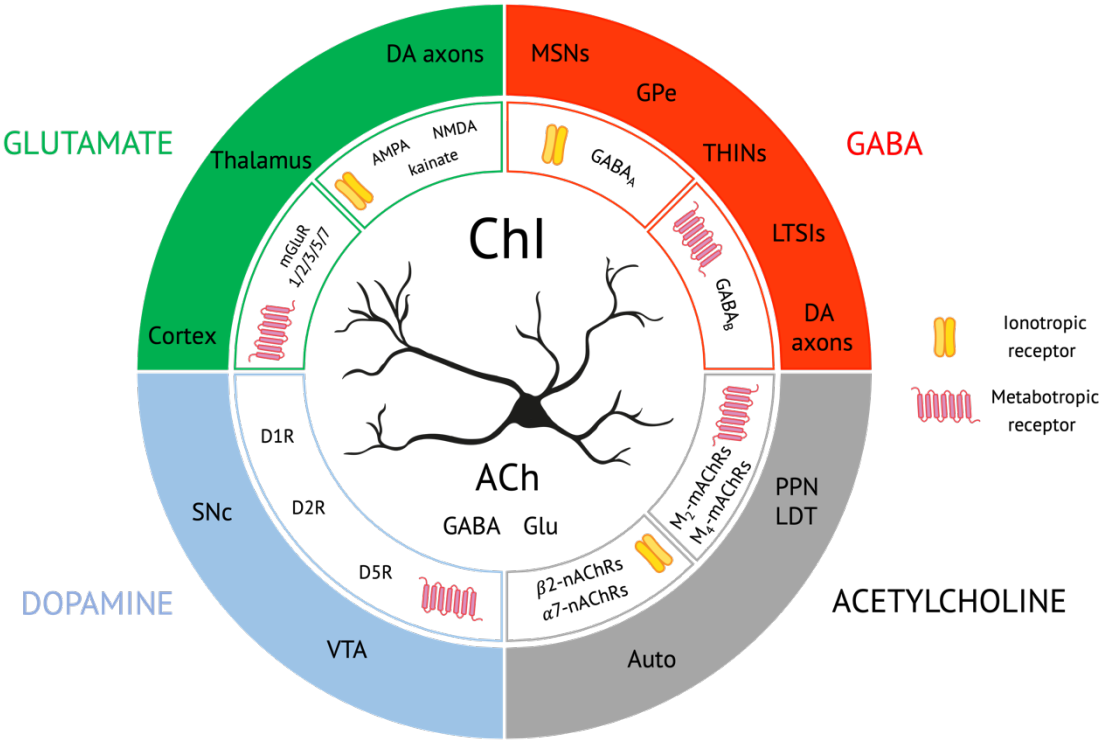


Figure 1.3. Schematic representation of the main inputs to ChIs and receptors expressed by ChIs.
ChIs receive excitatory glutamatergic projections (green) from cortex and thalamus and express a range of metabotropic and ionotropic glutamate (Glu) receptors. ChIs receive inhibitory GABAergic projections (red) from a range of sources and express $GABA_A$ and $GABA_B$ receptors. ChI activity is also modulated by dopaminergic projections from the midbrain (light blue) via DA receptors expressed on ChIs. Co-release of glutamate and GABA from DA neurons can also modulate ChI activity. ChIs receive projections from cholinergic neurons originating in the brainstem (PPN/LDT) and express nAChRs and mAChRs, which function as autoreceptors (grey). Ionotropic receptors are indicated in yellow, while metabotropic in pink. ChIs are the primary striatal source of ACh but they also co-release glutamate and GABA.

1.3.3 Striatal acetylcholine transmission

Historically, ACh is thought to signal as a volume transmitter and the dense innervation provided by ChI arbors, together with their tonic activity, is believed to result in continuous exposure of all tissue elements to ambient levels of ACh (Contant et al., 1996; Descarries et al., 1997). In this context, AChE has been proposed as a key player to maintain extracellular ACh levels within physiological limits (Contant et al., 1996; Descarries et al., 1997). Electron microscopy evidence from the rat striatum showed that ChIs give rise to a dense network of unmyelinated fibres studded with varicosities, i.e., axon dilations containing aggregated synaptic vesicles (Contant et al., 1996). Around less than 10% of these axonal varicosities displayed synaptic specialisation and more than 85% contained 10 or more synaptic vesicles (Contant et al., 1996; Nosaka and Wickens, 2022). These findings paved the way for the concept

of ACh volume transmission, where ACh is released from non-synaptic varicosities, diffuses in the extracellular space, and potentially exerts its effects on a range of targets spread in a large volume (Nosaka and Wickens, 2022).

To date, the exact modalities of ACh release from ChIs and the extent of its sphere of influence are still unresolved. The development of genetically encoded fluorescent sensors for real-time measurement of ACh release (Jing et al., 2018, 2020) might help to fill these knowledge gaps. For instance, work using G protein-coupled receptor (GPCR)-activation-based ACh sensor ($GRAB_{ACh}$) to measure evoked ACh release in mouse acute brain slices including either the medial entorhinal cortex (MEC) or hippocampus revealed that ACh signals through volume transmission with a spread-length constant of ~ 9-15 μm, depending on the brain region (Jing et al., 2018). On the other hand, work using a different type of fluorescent indicator (**Section 1.3.6**) suggested spatially restricted ACh signalling with spread length constant of ~ 1 μm (Zhu et al., 2020). Discrepancies between these reports might originate from the different tools used to measure ACh release and their relative spatial distribution and cellular localisation. Evidence from mathematical modelling of ChI activity and ACh release dynamics revealed a spatially segregated short-range signalling of ACh, where changes in ACh levels driven by changes in ChI firing result in differential regulation of the postsynaptic targets (Nosaka and Wickens, 2022). Together with these ACh transients adjacent to release sites, release from multiple sources originating from ChI tonic activity contributes to the overall ambient concentration of ACh, without interferences (Nosaka and Wickens, 2022). Consistently, AChE does not play a role in limiting the fast, point-to-point transmission but shapes the diffusion profile of ACh signals further away from release sites (> 5 μm) and over longer timescales (around 1 s) (Nosaka and Wickens, 2022).

Despite its role in shaping the extracellular dynamics of ACh release is currently incompletely characterised, AChE is a fundamental component in cholinergic systems. AChE catalyses the breakdown of ACh into choline and acetate and is among one of the fastest known enzymes (Descarries et al., 1997). *In situ* hybridization in the rat striatum showed that AChE is enriched in the striatum, and

it's expressed principally by ChIs, together with a small fraction of cholinoceptive neurons, such as SST-expressing interneurons and midbrain DA neurons (Bernard et al., 1995). AChE is found in different globular or asymmetric forms and the prevalent one in the mammalian brain is the globular form G_4 (Descarries et al., 1997; Dunant and Gisiger, 2017). In the rodent striatum, AChE is anchored on the plasma membrane of neuronal processes, as tetramers associated with a proline-rich membrane anchor (PRiMA) (Descarries et al., 1997; Perrier et al., 2002; Dobbertin et al., 2009). In the rat striatum, AChE secretion has also been reported (Sarno et al., 1987; Descarries et al., 1997). Microdialysis studies of the rat striatum have shown a steady-state basal level of ACh in the extracellular space, which is increased by anti-AChE treatment (Xu et al., 1991; Messamore et al., 1993; Descarries et al., 1997), highlighting the importance of AChE in shaping ACh release dynamics.

1.3.4 Muscarinic and nicotinic acetylcholine receptors

ACh exerts its effect via nAChRs and mAChRs, which are expressed by most striatal afferents and neurons (Poppi et al., 2021). Generally, activation of ionotropic nAChRs has a rapid, excitatory effect, while activation of metabotropic mAChRs has a long-term modulatory role. Muscarinic receptors are GPCRs and are grouped into two classes according to their intracellular signalling cascades (Lim et al., 2014). M_1-like receptors (comprising M_1, M_3, M_5-mAChRs) are generally regarded as excitatory and are coupled to $G_{q/11}$ and induce activation of the phospholipase C (PLC) pathway, which leads to production of inositol triphosphate (IP_3) and diacylglycerol (DAG), resulting in activation of protein kinase C (PKC) and release of Ca^{2+} from intracellular stores (Lin et al., 2004; Lim et al., 2014; Abudukeyoumu et al., 2019). The M_2-like receptors (including M_2 and M_4-mAChRs) have an inhibitory role and are coupled to $G_{i/o}$, decrease the activity of adenylyl cyclase and lead to G protein-mediated inhibition of voltage-gated Ca^{2+} channels (VGCCs) (Wess, 1996; Lim et al., 2014; Abudukeyoumu et al., 2019). Activation of mAChRs can control gene expression, including that of AChE (Nitsch et al., 1998; Kammer et al., 2001). All mAChRs subtypes are expressed at various levels in the rodent striatum and these receptors operate a

long-term modulatory role which results in increase or decrease of cellular excitability (Lim et al., 2014). M_2 and M_4-mAChRs are expressed on the terminals of striatal glutamatergic afferents and their activation reduces glutamate release and the excitatory drive on MSNs (Levey et al., 1991; Hersch et al., 1994a; Calabresi et al., 1998a; Pakhotin and Bracci, 2007; Pancani et al., 2014; Assous, 2021). MSNs express M_1 and M_4-mAChRs which have opposing effects on their activity. Activation of M_1-mAChRs results in an increase of MSN excitability, while activation of M_4-mAChRs leads to a decrease in excitability (Galarraga et al., 1999; Lin et al., 2004; Perez-Rosello et al., 2005; Yamamoto et al., 2013; Mamaligas and Ford, 2016; Mamaligas et al., 2019; Assous, 2021). MAChRs are also expressed by GABAergic interneurons, such as FSIs and LTSIs (Bernard et al., 1992; Koós and Tepper, 2002). Furthermore, M_5-mAChRs mRNA is expressed by DA neurons (Vilaró et al., 1990; Weiner et al., 1990). Finally, M_2 and M_4-mAChRs act as autoreceptors on ChIs (Bernard et al., 1992; Yan and Surmeier, 1996).

Nicotinic receptors belong to a ligand-gated ion channel superfamily with cation selective permeability and are formed by homomeric or heteromeric combinations of five different $\alpha\beta$ subunits (Dani and Bertrand, 2007). The different possible subunit combinations confer specific structural and functional properties to the receptor, influencing agonist binding affinity, channel permeability and desensitisation kinetics (Dani and Bertrand, 2007; Exley and Cragg, 2008). In general, activation of presynaptic nAChRs in the central nervous system (CNS) has a rapid excitatory effect, promoting neurotransmitter release through downstream Ca^{2+}-dependent mechanisms which include increase in intracellular Ca^{2+} by direct permeation of the receptor channel, activation of VGCCs, Na^+-dependent membrane depolarization and indirect stimulation of Ca^{2+} release from intracellular stores (Dani and Bertrand, 2007; McKay et al., 2007). In the mouse striatum, the most abundant nAChR subtypes are either homomeric α7-nAChRs or heteromeric receptors containing the β2 subunit together with a combination of α4, α6, and β3 subunits. (Champtiaux et al., 2003; Quik et al., 2007). The homomeric and highly Ca^{2+} permeable α7-nAChRs (Dajas-Bailador and Wonnacott, 2004) are primarily associated

with Ca^{2+}-dependent facilitation of neurotransmitter release and alterations in intracellular Ca^{2+} signalling due to release from intracellular stores (Gray et al., 1996; Dajas-Bailador et al., 2002; Dickinson et al., 2007). β2-nAChRs present lower Ca^{2+} permeability than the homomeric receptors and have been described to regulate neurotransmitter release via membrane depolarization and recruitment of voltage-gated Ca^{2+} channels (VGCCs) (Dajas-Bailador and Wonnacott, 2004; Dani and Bertrand, 2007; Dickinson et al., 2007; McKay et al., 2007). In striatum, different subtypes of nAChRs are expressed on a range of striatal neurons, where they modulate neurotransmitter release and cellular excitability via mechanisms which have only been party elucidated. Glutamatergic terminals express α7-nAChRs and their activation enhances glutamate release (Kaiser and Wonnacott, 2000; Campos et al., 2010; Howe et al., 2016). Direct cholinergic modulation of MSNs is mediated by mAChRs, and MSNs are generally thought not to express nAChRs (Luo et al., 2013a; Assous, 2021). THINs and LTSIs express a combination of αβ-nAChRs. Indeed, application of nAChR agonists induces depolarisation in THINs, putatively via α3β4-nAChRs (Luo et al., 2013a; Ibáñez-Sandoval et al., 2015; Assous, 2021). Application of nAChR agonists has a dual effect on LTSIs, either excitatory via β2-nAChRs, or inhibitory potentially through the recruitment of THINs (Luo et al., 2013b; Elghaba et al., 2016; Assous and Tepper, 2019; Assous, 2021). Moreover, DA axons express β2-nAChRs which have a fundamental role in shaping DA release plasticity (**Section 1.4.2**). Finally, ChIs express α7 and β2 subunit-containing nAChRs, whose function is only recently being elucidated (**Section 1.3.5**) (Azam et al., 2003; Abbondanza et al., 2022).

Neuronal nAChRs can undergo desensitisation upon sustained application of agonists and their subunit composition influences desensitisation susceptibility and kinetics (Giniatullin et al., 2005; Dani and Bertrand, 2007). NAChRs can undergo agonist-mediated desensitisation either via a canonical mechanism (starting from an open receptor state) in milliseconds to seconds, or via high affinity desensitisation (HAD), mediated by low agonist concentrations and proceeding from the closed receptor state, in the order of seconds to minutes (Giniatullin et al., 2005). β2-subunit

containing nAChRs have high agonist binding affinity and are prone to desensitisation, while α7-nAChRs show less desensitisation (Quick and Lester, 2002; Giniatullin et al., 2005). For instance, in the striatum, nicotine induces rapid desensitisation of β2-nAChRs, promoting DA release sensitivity to stimulation (**Section 1.4.2**) (Rice and Cragg, 2004; Zhang and Sulzer, 2004). Moreover, in the VTA concentrations of nicotine seen in smokers appear to preferentially desensitise β2-nAChRs on dopaminergic and GABAergic neurons, while promoting α7-nAChR-mediated glutamatergic excitation of DA neurons (Mansvelder and McGehee, 2000, 2002; Wooltorton et al., 2003). While nicotine-mediated desensitisation of nAChRs is well documented, desensitisation of striatal nAChRs by endogenous ACh is incompletely defined. β2-nAChRs can be desensitised by prolonged exposure to ACh (Quick and Lester, 2002; Paradiso and Steinbach, 2003), but it is thought that its fast clearance under physiological conditions might preclude significant nAChR desensitisation (Cragg, 2006).

1.3.5 Behavioural implications of striatal cholinergic signalling

ChIs cover a fundamental role in regulating a range of behaviours, as shown by the variety of movement and psychiatric disorders associated with ChI signalling. In the primate striatum, tonically active neurons (TANs, putatively ChIs) fire action potentials at a frequency of 2-5 Hz and respond to reward-related stimuli with a pause in their tonic firing (Kimura et al., 1984; Aosaki et al., 1994b; Apicella et al., 1997; Morris et al., 2004). This response is a multiphasic event which can be preceded by a burst of action potentials and/or followed by a rebound increase in firing (Apicella, 2002, 2017). Furthermore, TANs change their responses in a way that reflects discrepancies between actual and predicted rewards (Joshua et al., 2008; Apicella et al., 2009, 2011). The ability to encode reward prediction errors (RPEs) and the fact that TAN responses are time-locked with changes in DA neuron firing suggest that these two systems work closely to integrate information about stimuli and outcomes, to guide motivated actions (Morris et al., 2004; Apicella, 2017). TANs are generally involved in detecting the motivational significance of environmental

stimuli, however their pause responses present a degree of heterogeneity due to behavioural task, degree of conditioning and the nature of the stimulus and reward (Apicella, 2017; Poppi et al., 2021). The mechanisms mediating and modulating this pause response are still unresolved, and a potential role for DA and D2Rs, or excitatory corticothalamic projections have been reported (Chuhma et al., 2014; Straub et al., 2014; Zhang et al., 2018; Gallo et al., 2021; Martyniuk et al., 2021).

In rodents, TANs present less homogeneous responses to reward-related cues, with either increase or decrease in firing at different stages of the behavioural task and depending on striatal regions (Atallah et al., 2014; Benhamou et al., 2014; Thorn and Graybiel, 2014). Striatal ChIs in rodents are also involved in flexible shifting of learning upon changes in contingencies, encode changes in the state of the environment and signal changes in movement states (Ragozzino, 2003; Ragozzino et al., 2009; Bradfield et al., 2013; Apicella, 2017; Howe et al., 2019). Striatal ACh release measured with $GRAB_{ACh}$ in freely moving mice also correlates with movement direction (Liu et al., 2022). ACh signalling is also involved in stereotyped behaviours, as shown by an exacerbation of drug-induced stereotypic behaviours in transgenic mice with increased ACh release due to overexpression of the vesicular ACh transporter (VAChT) (Crittenden et al., 2014). Moreover, eliminating ACh synthesis via deletion of ChAT in the mouse forebrain leads to hyperactive behaviour in a novel environment (Patel et al., 2012). Striatal cholinergic signalling via β2-nAChRs is also central to the regulation of a range of striatal-dependent behaviours. Indeed, the selective deletion of β2-nAChRs in mouse striatal interneurons led to an increase in anxiety-like behaviour, alterations in social preference task, and impairments in initial discrimination learning (Abbondanza et al., 2022).

1.3.6 Acetylcholine detection

Several different approaches have been developed to measure ACh release, each with its own advantages and disadvantages. Recently, genetically encoded fluorescent sensors for real-time detection of ACh release ($GRAB_{ACh}$) have been developed (Jing et al., 2018, 2020), allowing an unprecedented resolution to

investigate ACh release dynamics in intact tissue. $GRAB_{ACh}$ sensors were developed by inserting a conformationally sensitive circularly permutated green fluorescent protein (cpGFP) into the third intracellular loop of M_3-mAChRs, which undergoes a conformational change upon ACh binding (Baird et al., 1999; Jing et al., 2018, 2020). It has been shown that in cell culture these sensors present negligible internalisation and coupling with G protein-mediated downstream signalling pathways (Jing et al., 2018, 2020). Furthermore, these sensors have fast on-off kinetics and report rapid conformational changes upon ligand binding, making them well-suited to detect ACh release in real-time. Nonetheless, these sensors are sensitive to agonists and antagonists of the GCPRs they're modelled on, limiting potential pharmacological manipulations, and do not provide information on neurotransmitter concentration. These tools have been adopted throughout this thesis and a more detailed description of their use can be found in **Chapter 2** (**Section 2.2**), for general implications, and **Section 2.3** for $GRAB_{ACh}$ in particular. Further discussion about the implications of using $GRAB_{ACh}$ sensors for measuring ACh release is found in **Chapter 3** (**Section 3.4**) and in **Chapter 6** (**Section 6.1**)**.**

Microdialysis is another method used to monitor ACh release. Microdialysis provides a direct measurement of ACh content in tissue and allows to measure absolute baseline concentration of neurotransmitter, however it has poor spatiotemporal resolution (order of minutes), unsuitable to investigate real-time release dynamics. Attempts to improve microdialysis temporal resolution were made by combining it with a segmented flow microfluidic device, which increased temporal resolution up to around 15 s (Wang et al., 2008). Nonetheless, to better appreciate ACh release dynamics in real-time subsecond resolution is needed.

Electrophysiological recordings of ChIs or postsynaptic neurons expressing ACh receptors are also an alternative approach used to study cholinergic transmission. For instance, patch-clamp provides a good measurement of ACh receptor-mediated effects on postsynaptic cell excitability. However, this technique is limited by the number of cells that can be recorded and the desensitisation of

cholinergic currents (Dani and Bertrand, 2007; Jing et al., 2018). Moreover, when using these methods, extracellular ACh release dynamics are not measured directly.

Electrochemical approaches to measure ACh or its precursor choline (Ch) have also been developed. Generally, an electrode is coated with enzymes that break down the non-electroactive ACh (or Ch) to H_2O_2 which is then oxidised, and the resulting current measured with constant potential amperometry or FCV. One approach combined a carbon fibre microelectrode (CFM) coated with AChE and choline oxidase (ChOx) and FCV to measure evoked ACh in mouse striatal slices (Asri et al., 2016). Alternatively, ChOx-coated biosensors to use in combination with amperometry were also developed (Schuvailo et al., 2005; Baker et al., 2014, 2017). One prominent advantage of the use of these tools is the ability to calibrate the electrodes and hence directly measure ACh concentration. Disadvantages include relatively slow temporal resolution and potential non-specific detection of other electroactive species, such as DA. Furthermore, ChOx-based biosensor responses can be affected by physiological variations in O_2, a co-substrate of ChOx (Santos and Sirota, 2021). A version of these Pt-based polymer enzyme composite biosensor (Baker et al., 2014, 2017) was previously tested in the lab. Prominent responses to DA and inability to insert the probe sufficiently into tissue due to its size made these tools unsuitable for further use in investigating ACh release dynamics.

A further approach is based on fluorescence resonance energy transfer (FRET) to measure GPCR activation. M_1, M_2, M_3, M_5-mAChRs have been linked to a donor/acceptor pair so that ligand-induced conformational changes are reported by changes in FRET (Maier-Peuschel et al., 2010; Ziegler et al., 2011; Markovic et al., 2012). Advantages of these tools include rapid responses to receptor agonists (order of ms) and high binding affinity (Wang et al., 2018). However, these tool present generally low sensitivity and have only been validated in cell culture.

Cell-based neurotransmitter fluorescent engineered reporters (CNiFERs) have also been used to measure ACh release via mAChR activation. CNiFERs are cultured cells engineered to express a GPCR of choice (e.g., M_1-mAChR) and signal an increase in cytosolic calcium following G protein-coupled receptor cascade with a genetically

encoded calcium sensor (Nguyen et al., 2010). These tools have high sensitivity and were validated for use *in vivo*, however disadvantages include the requirement for invasive cell transplantation.

Finally, using a similar strategy as the one adopted in the development of GRAB sensors, intensity-based ACh sensing fluorescent reporters (iAChSnFR) were developed (Borden et al., 2020). These sensors are based on a microbial periplasmic binding protein (PBP) that binds to ACh linked to a cpFP and allow real-time measurement of ACh signals *in vivo* (Borden et al., 2020).

1.4 MESOSTRIATAL DOPAMINERGIC SYSTEM

1.4.1 Mesostriatal dopamine neurons and dopamine signalling

DA neurons originate in the midbrain and send projections to a range of brain areas, including different cortical regions, the lateral septum, the amygdala, the lateral habenula, the entorhinal cortex and hippocampus, the STN, and the striatum (Yetnikoff et al., 2014). In particular, DA neurons of the SNc (A9 group) preferentially innervate the CPu, constituting the nigrostriatal projection system (Yetnikoff et al., 2014). DA neurons in the ventral tegmental area (VTA, A10 group) project primarily to the NAc, forming the mesolimbic DA system (Yetnikoff et al., 2014). Despite this subdivision, overlap between the terminal fields of SNc and VTA neurons has been reported (Björklund and Dunnett, 2007; Yetnikoff et al., 2014).

DA neurons present distinctive morphological characteristics. In the rat brain, each SNc DA neuron project a single unmyelinated axon to the CPu, where it forms a widespread, complex, and highly dense axonal arbor (Matsuda et al., 2009). Each reconstructed DA axon was estimated to have a total length of up to 780,000 µm (467,000 µm on average) and to occupy up to 5.7% of striatal volume (Matsuda et al., 2009). Computational modelling of the axon of individual DA neurons showed high energetic demand required for efficient action potential propagation associated with these highly branched large axonal arborisations (Pissadaki and Bolam, 2013). These morphological features, together with the presence of several neuromodulatory receptors on DA axons suggest that the correspondence between action potential firing by midbrain DA neurons and striatal DA release is a complex event influenced by mechanisms occurring locally at axonal level (Rice et al., 2011).

In vivo, DA neurons in the rat exhibit autonomous tonic firing at frequencies ranging from 1 to 10 Hz, together with burst firing of 2-5 spikes at 20-40 Hz, with bursts up to 100 Hz occasionally reported (Grace and Bunney, 1984a, 1984b; Hyland et al., 2002). Switching in firing mode from low to high firing frequencies is thought to encode information about reward prediction and delivery as well as salient stimuli (**Section 1.4.4**).

Striatal DA is thought to signal through diffusion-based volume transmission (Rice and Cragg, 2008). Indeed, DA neurons form a small number of symmetrical synapses, with 60-70% of axonal varicosities being asynaptic (Descarries et al., 1996). Furthermore, striatal DA receptors are metabotropic receptors (**Section 1.4.3**), with slower response times than ionotropic receptors, and are mainly localised extrasynaptically (Yung et al., 1995; Caillé et al., 1996; Missale et al., 1998; Rice et al., 2011). Further evidence is provided by the fact that the DA transporter (DAT) is characterised by low transport rate, exclusive expression by DA neurons and extrasynaptic localisation in striatum (Hersch et al., 1997; Povlock and Schenk, 1997; Rice and Cragg, 2008; Rice et al., 2011). Hence, DATs do not regulate DA spillover or clearance from a release site which depends on diffusion, but they regulate the sphere of influence of DA (Rice and Cragg, 2008; Rice et al., 2011). DATs are also major regulators of short-term plasticity of DA release, together with mechanisms governing axonal excitability (Condon et al., 2019).

1.4.2 Local striatal modulation of dopamine release: role of acetylcholine

The correspondence between action potential firing by midbrain DA neurons and striatal DA release is a complex event, influenced by mechanisms occurring locally at axonal level. Indeed, the widespread and complex axonal arbors characteristic of DA neurons (**Section 1.4.1**) together with the presence of several neuromodulatory receptors on DA axons suggest that striatal DA release is gated by axonal mechanisms and striatal neuromodulators and neurotransmitters (Rice et al., 2011). For example, DA release in the mouse striatum is under regulation by GABA, adenosine, nitric oxide, hydrogen peroxide, and substance P (Avshalumov et al., 2003; Hartung et al., 2011; Brimblecombe and Cragg, 2015; Lopes et al., 2019; Roberts et al., 2020, 2022).

Nonetheless, one of the main local modulators of striatal DA release is ACh, which regulates striatal DA release plasticity via nAChRs and mAChRs. In rats, DA neurons in the midbrain express mRNA for the nAChR subunits α3-7 and β2-4 (Azam et al., 2002; Sulzer et al., 2016). In the rodent striatum, DA axons express the β2

subunit, forming heteropentameric receptors with different combinations of the α4-6 and β3 subunits (**Figure 1.4**) (Jones et al., 2001; Grady et al., 2007; Sulzer et al., 2016). FCV studies using subunit-specific antagonists and mice with knockout of specific subunits revealed that DA release plasticity is regulated by different nAChRs across striatal territories, namely α4α5β2 and α6β2β3 in dorsal striatum and α4α6β2β3 in ventral striatum (**Figure 1.4**) (Exley and Cragg, 2008; Exley et al., 2008, 2011, 2012, 2013). In rodents, activation of β2-nAChRs enhances DA release evoked by single pulses or low frequency pulse trains and consequently promotes short-term depression (STD) of DA release evoked by trains of pulses at higher frequencies (Rice and Cragg, 2004). Hence, nAChRs can limit how well striatal DA release correlates with activity in midbrain DA neurons (Threlfell and Cragg, 2011). Lack of activation, antagonism, desensitisation by an agonist (e.g., nicotine), or deletion of β2-nAChRs suppresses DA release by single pulse or low frequency pulse trains, relieving STD and facilitating release by high frequency trains (Rice and Cragg, 2004; Zhang and Sulzer, 2004; Patel et al., 2012). Therefore, when nAChRs are turned off, DA release better reflects frequency of activity in DA neurons (Threlfell and Cragg, 2011). The mechanisms via which nAChRs on DA axons modulate short-term plasticity of DA release are currently incompletely characterised.

In rodents, ACh released following synchronous activation of a population of ChIs can directly evoke DA release via β2-nAChRs, bypassing action potential firing in DA neuron cell bodies (Cachope et al., 2012; Threlfell et al., 2012; Brimblecombe et al., 2018). Moreover, striatal DA release measured with continuous amperometry shows a biphasic profile, characterised by an initial dopaminergic component and a subsequent cholinergic component with a total latency of 17.8 ms (Wang et al., 2014a, 2014b). Therefore, electrical stimulation evokes an initial DA release event via direct depolarisation of DA axons, which summates with a second DA release event driven by ACh released from ChIs (Sulzer et al., 2016). Notably, this cholinergic component of DA release does not convey information on activity in ChIs (Threlfell et al., 2012; Shin et al., 2017). Recent evidence in mouse striatal slices has shown that ACh can induce action potential firing in distal DA axons as a mechanism to

regulate striatal DA signalling (Liu et al., 2022). Indeed, selective optogenetic activation of ChIs evoked action potentials in DA axons which were abolished by the β2-nAChR antagonist DHβE (Liu et al., 2022). Evidence collected expressing $GRAB_{ACh}$ and $GRAB_{DA}$ sensors selectively on DA axons also showed that spontaneous activity in ChIs resulted in DA release that was extended beyond the ACh-signalling domains (Liu et al., 2022). Further evidence also showed that, in mouse and primate dorsal striatal slices, ACh-mediated activation of α6β2-nAChRs resulted in excitatory postsynaptic potential-like depolarisations in DA axons (axEPSPs) (Kramer et al., 2022). Summation of these nicotinic axEPSPs can trigger action potentials locally in DA axons (Kramer et al., 2022). Despite these recent advances, the mechanisms underlying ACh-driven DA insensitivity to differential activation of ChIs are still incompletely characterised.

ACh can also modulate DA release plasticity via mAChRs. In this context, the main role of mAChRs is to regulate ACh release levels which subsequently act at nAChRs on DA axons to modulate DA release (Sulzer et al., 2016). Agonism of mAChRs on ChIs inhibits their firing, which will in turn reduce ACh release and nAChR activation on DA axons, relieving the nAChR-mediated STD of DA release (Threlfell et al., 2010). Work in mice with selective knockout of M_2, M_4, or M_5-mAChRs revealed the predominant role of M_4-mAChRs in the NAc and M_2 and M_4-mAChRs in the CPu, which are localised on ChIs and act as autoreceptors (**Section 1.3.4**), and no role for M_5-mAChRs (Threlfell et al., 2010). Midbrain DA neurons in rats express the mRNA for M_5-mAChRs (Vilaró et al., 1990; Weiner et al., 1990), but direct anatomical evidence for localisation of these receptors on DA axons is lacking. Nonetheless, M_5-mAChRs have been reported to have a direct facilitatory role on DA axons, promoting DA release (Zhang et al., 2002; Shin et al., 2015).

Finally, ChIs can also mediate the effects of other neurotransmitters on DA release, such as glutamate, nitric oxide, opioids, and insulin (Britt and McGehee, 2008; Hartung et al., 2011; Stouffer et al., 2015; Kosillo et al., 2016).

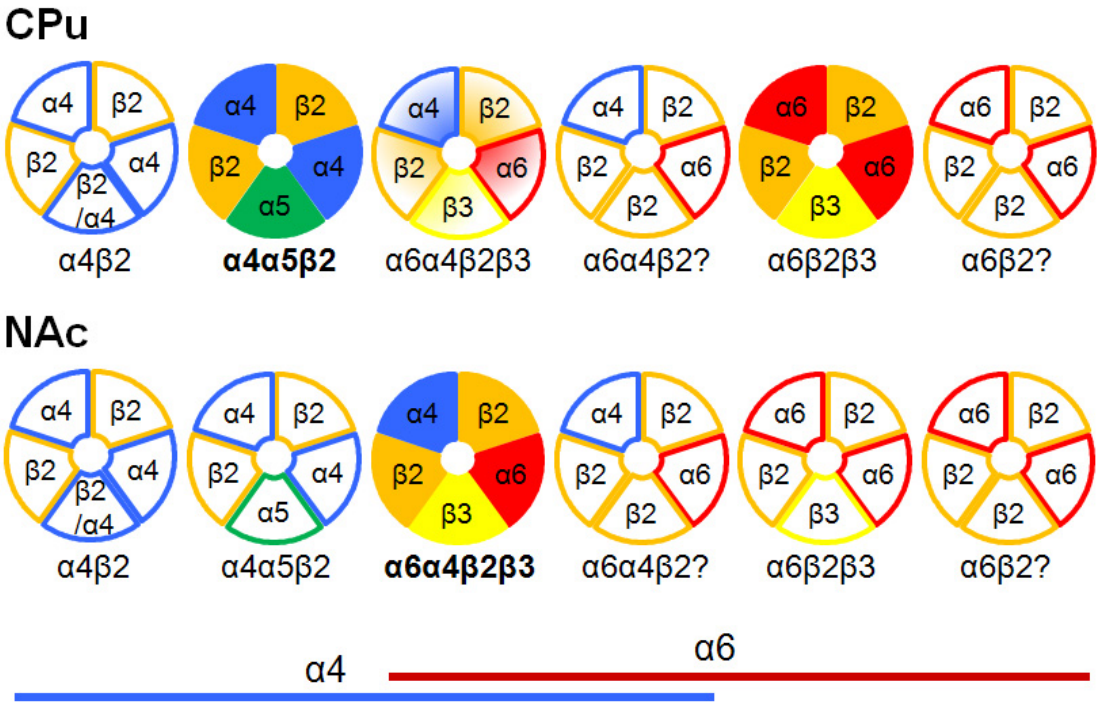


Figure 1.4. Subunit composition of nAChRs expressed on DA axons in the mouse striatum (schematic by Dr R. Exley). *Striatal nAChRs localised on DA axons are composed by combinations of different $\alpha\beta$ subunits. The different subunit composition gives the receptors specific structural and functional properties, influencing binding affinity, channel permeability and desensitisation kinetics. Receptors formed by different subunit combinations preferentially regulate DA release in dorsal (CPu) and ventral striatum (NAc). In particular, $\alpha4\alpha5\beta2$ and $\alpha6\beta2\beta3$ nAChRs in dorsal striatum and $\alpha4\alpha6\beta2\beta3$ in ventral striatum.*

1.4.3 Dopamine receptors

DA mediates its effects via five types of GPCRs (D1-D5), divided into two groups: the D1-class and the D2-class (Beaulieu and Gainetdinov, 2011). The D1-class receptors, which comprises D1R and D5R, activate the $G\alpha_{s/olf}$ postsynaptic protein complex to promote cyclic adenosine monophosphate (cAMP) production by adenylyl cyclase (AC) (Beaulieu and Gainetdinov, 2011). The D2-class receptors, including D2R, D3R, and D4R, couple to the $G\alpha_{i/o}$ family of G protein and inhibit AC and decrease cAMP production (Beaulieu and Gainetdinov, 2011). In rodents, there are two major splice variants of D2Rs, namely D2S (D2-short) and D2L (D2-long), which differ for the presence of an additional 29 amino acids in the third intracellular loop of D2L (Giros et al., 1989; Monsma et al., 1989; Beaulieu and Gainetdinov, 2011). D2S isoforms are mainly presynaptic and function as autoreceptors, while D2L isoforms are predominantly postsynaptic (Usiello et al., 2000; Beaulieu and Gainetdinov, 2011).

In the striatum, D1 and D2 are the most abundantly expressed DA receptor types (Levey et al., 1993). These receptors are differentially expressed on MSNs, with D1Rs expressed by dMSNs and D2Rs expressed by iMSNs (**Section 1.2.2**). In rodents, DA increases excitability of dMSNs via D1Rs and decreases excitability of iMSNs via D2Rs, thus modulating excitability of the two output pathways of the striatum in opposite directions (Planert et al., 2013). DA regulates excitability of GABAergic interneurons via D1 and D5 receptors, expressed by FSIs and LTSIs (Moine et al., 1991; Rivera et al., 2002). In particular, activation of D1-like receptors induces depolarisation in rodent striatal FSIs and LTSIs (Bracci et al., 2002; Centonze et al., 2002, 2003). ChIs also express D1 (low expression), D5 and D2 receptors (**Section 1.3.2**). In particular, in rodent striatal slices, activation of D2Rs on ChIs inhibits ChI autonomous firing and Ca^{2+} entry in ChIs (Yan et al., 1997; Maurice et al., 2004; Deng et al., 2007a), decreasing ACh release more strongly in the dorsal striatum (Henselmans and Stoof, 1991).

DA neurons express D2Rs, which function as autoreceptors regulating axonal and somatodendritic DA release. In mouse midbrain slices, somatodendritic DA release acts D2Rs on DA neurons and modulates their activity (Beckstead et al., 2004). In particular, somatodendritic DA released by SNc DA neurons primarily autoinhibits the releasing neuron via D2Rs (Hikima et al., 2021). In rodent striatal slices, agonism of D2Rs suppresses single pulse evoked DA release in a concentration dependent manner (Palij et al., 1990; Bull and Sheehan, 1991; Kennedy et al., 1992; Rice et al., 2011). On the other hand, antagonism of D2Rs has no effect on single pulse-evoked DA release, suggesting no basal DA tone, but amplifies subsequent DA release evoked by train stimulation (Limberger et al., 1991; Patel et al., 1992; Cragg and Greenfield, 1997; Rice et al., 2011). In rodent striatal slices, the onset of D2R-mediated inhibition of DA release is by 100 ms, with a maximal effect around 500 ms and a duration up to 5 s (Lee et al., 2002; Phillips et al., 2002; Rice et al., 2011; Sulzer et al., 2016). *In vivo*, basal extracellular DA is sufficient for tonic stimulation of D2 autoreceptors (May and Wightman, 1989; Sulzer et al., 2016). Furthermore, autoreceptor activation presents faster kinetics *in vivo*, with a maximal effect around 150-300 ms and

termination around 600-800 ms, possibly reflecting higher basal DA tone (Benoit-Marand et al., 2001; Rice et al., 2011).

1.4.4 Behavioural role of dopamine

DA plays a fundamental role in regulating movement, as degeneration of nigrostriatal DA neurons in PD results in loss of motor control and movement deficits (**Section 1.5**). Studies in non-human primates report increased DA neuron firing upon action initiation (Schultz et al., 1983; Romo and Schultz, 1990). A similar role was also showed in rodents, where phasic increase in DA neuron signalling is associated to and triggers locomotion (Howe and Dombeck, 2016). Furthermore, in freely moving mice DA levels correlate with movement initiation and direction, concomitantly with ACh (Liu et al., 2022).

DA also plays a key role in processing reward-related information. Studies in non-human primates show strong phasic activation of DA neurons in response to unpredicted appetitive stimuli (unconditioned stimuli, US), such as liquid and food rewards, as well as to reward-predicting cues (conditioned stimuli, CS) (Mirenowicz and Schultz, 1996). The observed responses to appetitive events do not encode reward per se, but rather an error in the prediction of reward, encoding the discrepancy between the reward received and the predicted one (Schultz et al., 1997). Indeed, DA neurons are activated when an unpredicted reward occurs (positive prediction error, the event is better than predicted), inhibited when a predicted reward is omitted (negative prediction error, the event is worse than predicted) and are uninfluenced when a reward occurs as expected (Schultz, 1998). Predictions are fundamental to acquire advanced information on future events and conform behavioural responses accordingly, increasing approach or avoidance behaviour (Schultz, 1998). These prediction error responses scale according to reward probability and value (Fiorillo et al., 2003; Morris et al., 2004; Tobler et al., 2005) and correspond to an increase in striatal DA levels (Phillips et al., 2003; Roitman, 2004; Day et al., 2007). Furthermore, DA neuron responses to reward prediction have also been reported in rodents and humans (Pan, 2005; Roesch et al., 2007; D'Ardenne et

al., 2008; Rutledge et al., 2010; Cohen et al., 2012). DA signals encoding RPE are also shaped by subjective value and motivational state (Bassareo and Chiara, 1999; Lak et al., 2014; Papageorgiou et al., 2016). In rodents, DA release in the NAcC in response to reward-predicting cues is also modulated by correct movement initiation (Syed et al., 2016).

In non-human primates, phasic responses in DA neurons are time-locked with pauses in TANs (**Section 1.3.5**) (Morris et al., 2004), further suggesting a functional interaction between these two systems *in vivo*. In rodents, the cholinergic and dopaminergic systems also closely regulate one another. For instance, DA at D2Rs on ChIs modulates ACh release response to a reward-predicting cue (Gallo et al., 2021; Martyniuk et al., 2021), while ACh at nAChRs and mAChRs modulates DA release in response to reward-predicting cues (Collins et al., 2016).

1.5 PARKINSON'S DISEASE

PD is a neurodegenerative disease affecting millions of patients worldwide. PD was identified between the neurological disorders examined in the Global Burden of Disease, Injuries and Risk Factors Study (2015) as the fastest growing disease in prevalence and mortality (Group et al., 2017; Dorsey et al., 2018). The number of PD patients between 1990 and 2016 has more than doubled, from 2.5 million patients to 6.1 million, and projections of increasing incidence of the disease suggest a doubling of PD patients by 2050 (Bach et al., 2011; Dorsey et al., 2018; Rocca, 2018). Therefore, PD represents a significant health and economic burden and understanding the underlying causes of PD progression is fundamental to develop more effective treatments.

PD is most frequently an idiopathic disorder, however rare genetically inherited forms of the disease do exist (Singleton et al., 2003; Chartier-Harlin et al., 2004). Overall, PD is characterised by neurodegeneration of nigrostriatal neurons (Kish et al., 1988), which results in reduced DA signalling in the striatum and disrupted basal ganglia function (**Section 1.5.1**). This leads to a range of motor symptoms, including bradykinesia, muscle tone rigidity, resting tremor, and non-motor symptoms, such as sleep disturbances, depression, and dementia (Poewe et al., 2017).

An increase in the risk of developing PD could be potentially driven by pre-existing chronic diseases, such as diabetes. Indeed, epidemiology studies have reported an increased risk of developing PD in patients with diabetes (Xu et al., 2011; Sun et al., 2012; Yang et al., 2017; Pablo-Fernandez et al., 2018; Pagano et al., 2018). The reported link between higher incidence of PD and diabetes might be due to potential shared genetic factors or pathogenic mechanisms (Pablo-Fernandez et al., 2018). Network-based analysis reported evidence for genes associated with PD and diabetes, suggesting a link at a molecular level between the two diseases (Santiago and Potashkin, 2013, 2014). Furthermore, patients with diabetes have dysfunctions in DA signalling, such as lower striatal DAT binding, and have higher α-synuclein levels (Pagano et al., 2018). To further investigate the link between diabetes and PD, I collaborated in a study aimed at assessing diabetes-induced molecular markers of

DA neuron damage and the impact of diabetes on the vulnerability of nigrostriatal DA neurons to neurodegeneration (Pérez-Taboada et al., 2020). We found that mouse models of type 1 and type 2 diabetes presented increased oxidative stress, decreased levels of proteins regulating DA transmission and altered DA release and reuptake measured with FCV (Pérez-Taboada et al., 2020). Diabetic mice also presented higher susceptibility to nigrostriatal degeneration leading to motor impairments than their healthy control counterpart (Pérez-Taboada et al., 2020). Overall, these findings support the hypothesis that diabetes increases vulnerability to neurodegenerative damage in striatal DA signalling leading to motor impairments. In particular, my contribution to this study involved the characterisation of DA release alterations measured with FCV in mouse striatal slices from both diabetes models. These data are not included in this thesis and are published in Pérez-Taboada et al. (2020) (see Conference Abstracts and Manuscripts Section).

1.5.1 Dopamine neuron degeneration in Parkinson's disease

The pathological hallmarks of PD are degeneration of DA neurons in the SNc and accumulation of intracellular inclusions containing aggregates of α-synuclein (**Section 1.5.3**). Degeneration of neuromelanin-positive and calbindin-negative ventral tier SNc DA neurons results in dopaminergic denervation of the dorsolateral striatum (Kish et al., 1988; Iacopino et al., 1992; Surmeier and Sulzer, 2013). Consequently, decrease in striatal DA leads to aberrant downstream synaptic weighting of basal ganglia activity and the manifestation of motor symptoms (Albin et al., 1989; DeLong, 1990). Potential mechanisms underlying DA neuron death include α-synuclein proteostasis, oxidative stress, mitochondrial dysfunction, neuroinflammation and aging (Poewe et al., 2017). Furthermore, the unique morphology of nigrostriatal DA neurons has been proposed as an additional factor that underlies their selective vulnerability (Bolam and Pissadaki, 2012; Pissadaki and Bolam, 2013). Nigrostriatal DA neurons form extensive unmyelinated axonal arbors in the dorsal striatum (**Section 1.4.1**) and the higher energy demand required for maintenance of normal function (resting membrane potential maintenance, action

potential propagation) in these arbors makes them particularly susceptible to metabolic and oxidative stress (Bolam and Pissadaki, 2012; Pissadaki and Bolam, 2013). The striatum is therefore a critical site for studying the disease. Consistently, human imaging studies have reported early alterations in the striatum of PD patients, even preceding diagnosis, and post-mortem studies suggest that DA neuron terminals in striatum degenerate before their cell bodies in the SNc (Sossi et al., 2004; Kordower et al., 2013; Poewe et al., 2017).

The gold standard treatment for PD patients consists in substituting striatal DA loss with administration of the DA precursor levodopa (L-DOPA) (Poewe et al., 2017; Tubert and Murer, 2021). However, after prolonged use, L-DOPA induces unwanted motor-related side effects, such as dyskinesia (Poewe et al., 2017). Alternative therapies can include other dopaminergic medications, such as monoamine oxidase type B inhibitors (MAOB), and DA receptor agonists (Schaeffer et al., 2014; Poewe et al., 2017). Before L-DOPA, anticholinergic drugs were used to treat motor symptoms in PD patients. These treatments are generally less effective than L-DOPA and can lead to cognitive and autonomic side effects with continuous use (Lim et al., 2014; Tubert and Murer, 2021). Nonetheless, cholinesterase inhibitors are highly effective in improving symptoms in PD patients with dementia (Rolinski et al., 2012; Wang et al., 2015; Poewe et al., 2017).

1.5.2 Acetylcholine in Parkinson's disease

Historically, PD has been considered as an hypercholinergic and hypodopaminergic disease and, before L-DOPA, anticholinergic drugs were the preferred treatment for PD patients (Barbeau, 1962). Following the discovery that DA transmission is reduced in PD, it has been proposed that DA and ACh in the striatum are in equilibrium to guarantee normal movement control and that this equilibrium is altered in PD, where a loss of DA results in an hypercholinergic state (Barbeau, 1962). Hence, DA depletion is accompanied by an increase in ChI signalling which exacerbates the aberrant rearrangement of striatal circuitry and leads to the appearance of motor symptoms (Pisani et al., 2007). α-synuclein inclusions, a

pathological hallmark of PD, have also been reported in ChIs of PD patients at the latest stages of disease progression (Mori et al., 2008).

In PD animal models, alterations in striatal ChI signalling have also been reported. In parkinsonian non-human primates, TANs lose their pause response, and their density is increased in the caudate nucleus (Aosaki et al., 1994a; Petryszyn et al., 2016; Villalba et al., 2019). In PD rodent models, microdialysis and high-performance liquid chromatography (HPLC) studies reported higher extracellular levels of ACh, increasing gradually with damage in SNc DA neurons (DeBoer et al., 1993; Ikarashi et al., 1997; Cao et al., 2012). Findings from different rodent models of PD provided contrasting results on how loss of nigrostriatal DA neurons impacted on ChI excitability, overall pointing towards aberrant ChI transmission. In 6-hydroxydopamine (6-OHDA) rat models (**Section 1.5.4**), loss of DA neurons drove a reduction of the slow afterhyperpolarisation current in ChIs which resulted in increased ChI excitability (Sanchez et al., 2011). DA depletion in 6-OHDA mice also led to an attenuation of M_4-mAChR coupling with Ca^{2+} channels regulating ChI firing due to an upregulation of expression of the regulator of G protein signalling (RGS) 4, resulting in an overall loss of autoreceptors control of ChI firing (Ding et al., 2006). Optogenetic inhibition of ChIs improved motor deficits in the 6-OHDA PD mouse model (Maurice et al., 2015; Ztaou et al., 2016). On the other hand, in mice lesioned with 6-OHDA, DA loss was found to decrease ChI spontaneous firing (Choi et al., 2020). In a mouse model of progressive DA loss (*Slc6a3*$^{DTR+/-}$ diphtheria-toxin-sensitive), ChI tonic activity was decreased via a reduction in ACh availability and transcription of HCN channels (McKinley et al., 2019). Moreover, 6-OHDA partial lesions in mice led to downregulation of metabotropic glutamate receptors (mGluR1) on ChIs and loss of glutamate co-release-mediated excitation of ChIs in the dorsolateral striatum, which underlies parkinsonian motor impairments (Cai et al., 2021).

1.5.3 Alpha-synuclein in Parkinson's disease

The other feature of PD besides DA neuron degeneration is the accumulation of filamentous cytoplasmic protein aggregates (Lewy bodies), which are principally comprised of α-synuclein (Baba et al., 1998; Spillantini et al., 1998). Genome-wide association studies (GWAS) have revealed that point mutations, together with locus multiplication of the gene encoding for α-synuclein (*SNCA*) are associated with sporadic and familial forms of PD (Singleton et al., 2003; Bekris et al., 2010; Venda et al., 2010).

The normal function of the protein α-synuclein is not fully understood, but it appears to cover an important role in the maintenance of synaptic function and integrity (Burré, 2015). Indeed, α-synuclein interacts with synaptic vesicles regulating mobilisation, reclustering and neurotransmitter release (Cabin et al., 2002; Nemani et al., 2010; Burré, 2015; Lautenschläger et al., 2018). Furthermore, α-synuclein has a role in regulating DA synthesis, storage, release, and reuptake (Senior et al., 2008; Anwar et al., 2011; Janezic et al., 2013; Burré, 2015; Threlfell et al., 2021).

In PD, α-synuclein undergoes a pathogenic process in which α-synuclein monomers progressively aggregate to form large α-synuclein fibrils, which are the aggregates that make up the Lewy bodies (Poewe et al., 2017). For instance, aggregation of α-synuclein promotes progressive nigrostriatal neuron degeneration in rats (Taschenberger et al., 2012; Paumier et al., 2015). The underlying mechanisms for α-synuclein accumulation and aggregation can include protein overproduction, and mutations which increase the likelihood of misfolding and oligomerisation, but they are still incompletely characterised (Poewe et al., 2017).

1.5.4 Mouse models of Parkinson's disease

A variety of animal models have been generated to study the pathogenesis and therapeutic development of PD. Rodent models of PD can be grouped in neurotoxin and genetic models (Chia et al., 2020). Neurotoxin models can be generated with the administration of neurotoxins such as 6-OHDA or 1-methyl-4-

phenyl-1,2,3,6-tetrahydropyiridine (MPTP), which leads to oxidative stress and induce rapid degeneration of nigrostriatal DA neurons (Perese et al., 1989; Sauer and Oertel, 1994; Chia et al., 2020). Despite producing a consistent behavioural phenotype and predictable degeneration of DA neurons, toxin models lack the formation of Lewy bodies and are unsuitable to study early stages of disease progression (Chia et al., 2020).

Genetic models can be generated by overexpressing or knocking out genes associated with PD and allow to investigate disease progression at different stages. Genetic models include overexpression of α-synuclein and leucine-rich repeat kinase 2 (LRKK2) or knockout/knockdown of Parkin, protein deglycase (*DJ-1*) and Pten-induced kinase 1 (*PINK1*) (Chia et al., 2020). Given the importance of α-synuclein in the pathogenesis of PD, several transgenic rodent models with manipulations in the expression of this protein have been developed. α-synuclein can be overexpressed with a vector-based approach which leads to cytosolic protein aggregation, deficits in striatal DA signalling and loss of nigral DA neurons (Bianco et al., 2002; Kirik et al., 2002; Lundblad et al., 2012). A progressive and highly physiological transgenic mouse model of PD that overexpresses human α-synuclein at disease relevant levels was developed at the Oxford Parkinson's Disease Centre and used for experiments in this thesis. This model (*SNCA*-OVX) was generated using a BAC construct carrying the complete wild-type human *SNCA* locus on a mouse *Snca* knockout background, allowing to explore the pathological mechanisms triggered by progressive human α-synuclein accumulation (Janezic et al., 2013). *SNCA*-OVX mice show early deficits in DA release (3-4 months old) in the dorsal striatum that precede DA neuron loss, together with alterations in the GABAergic regulation of DA release (Janezic et al., 2013; Roberts et al., 2020). Furthermore, *SNCA*-OVX mice present an age-dependent loss of nigrostriatal DA neurons, a reduction in midbrain DA neuron firing rates and a motor phenotype (Janezic et al., 2013; Dodson et al., 2016).

Overall, the main aim of this thesis was to investigate the dynamic interplay between ACh and DA release in the striatum, using FCV and GRAB sensors to measure neurotransmitter release dynamics in real-time in mouse striatal slices. In **Chapter 3**, I probed ACh release dynamics across striatal regions, testing the frequency dependency of ACh release and its regulation by AChE, GABA and DA. Subsequently, in **Chapter 4**, I've expanded upon these findings to investigate how dynamic changes in ACh release modulate DA release plasticity via nAChRs. Here, I assessed the contributions of ACh release levels, activity in ChIs and mechanisms operating downstream of nAChRs. Finally, in **Chapter 5**, we investigated alterations in striatal ACh signalling in a human α-synuclein overexpressing mouse model of early PD, focussing on the role of AChE, GABA and DA.

2. General Methods

2.1 ANIMAL MODEL

2.1.1. Mice as a model organism to investigate striatal circuits

Striatal mouse brain slices were used in this body of work to study cholinergic modulation of DA release. Mice were chosen as a model organism for a variety of reasons. Firstly, they present conserved neuronal structures that have close similarity to humans, which allows to perform more invasive experiments to record neurotransmitter dynamics. Secondly, mice can be genetically manipulated, and several transgenic strains are already available. Finally, mice are widely used in neuroscience research and in most studies investigating striatal DA transmission, and therefore, by adopting this model, we can directly compare the results in this work with previous studies.

Acute *ex vivo* coronal mouse brain slices containing ventral and dorsal striatum were used in all experiments monitoring real-time neurotransmitter release. Slices were preferred to an *in vitro* approach because they preserve typical striatal connectivity and maintain striatal neuron spatial organisation, including the complex arborisation of DA axons (Matsuda et al., 2009). Slices were also preferred to an *in vivo* approach because they allow to carry out a more straightforward manipulation and measurement of striatal neurotransmitters, such as DA and ACh. Indeed, drugs at defined concentrations can be consistently bath administered and the extracellular environment can be easily manipulated, for example with changes in ionic concentration. Furthermore, it is easier to maintain environmental conditions, like pH and temperature, constant across different sets of experiments. Finally, from one experimental animal, several striatal slices can be collected and used for different experiments, in line with the idea of reduction of the number of experimental animals in use.

Nonetheless, there are some disadvantages to slice use. While preparing coronal striatal slices, DA neuron projections from the midbrain are severed, so that there is no tonic DA neuron activity and striatal DA axons need to be stimulated to

evoke DA release. However, this allows to selectively investigate axonal modulation of striatal DA release, in absence of presynaptic activity. Notably, in the slice preparation used throughout this thesis, the cholinergic system responsible for local modulation of DA release is intact. Indeed, ChIs are tonically active and able to modulate axonal DA release (Threlfell et al., 2012). Brainstem cholinergic projections to the striatum are also severed, however it was previously shown that these are not responsible for the modulation of striatal DA release (Brimblecombe et al., 2018).

Even though striatal mouse slices are a suitable model to examine the local interplay between DA and ACh, *in vivo* experiments are necessary to understand the implications of these *ex vivo* observations for the whole CNS and for behaviour.

2.1.2 Transgenic mouse lines

Animals were group-housed and maintained on a 12-hour light/dark cycle (lights on 7 a.m. to 7 p.m.) at 22°C and 60-70% humidity. *Ad libitum* access to food and water was provided. All procedures were carried out in accordance with the Animals in Scientific Procedures Act 1986 (Amended 2012) with ethical approval from the University of Oxford and under the authority of a UK Home Office Project Licence (P9371BF54).

For all experiments adult male and female mice were used. Historically, there has been an underrepresentation of female subjects in animal research (Beery, 2018), and there is a strong sex bias towards only including male subjects in neuroscience research using rodents (Will et al., 2017). The reason behind such bias is based on the assumption that females are more variable than males and that they have to be tested across the phases of the oestrus cycle (Prendergast et al., 2014; Beery, 2018). However, a thorough analysis of behavioural, morphological, physiological, and molecular traits revealed that there is no significantly greater variability in female than male mice (Prendergast et al., 2014). Furthermore, oestrus cycle variability is no greater than intrinsic variability in males (Prendergast et al., 2014; Beery, 2018). It is therefore fundamental to include both sexes in preclinical research, to help building

a knowledge base that better reflects the human population and better contributes to the design of clinical research (Clayton, 2016). As a research group, we've introduced the use of mixed sex cohorts in our experiments. In this work, data originating from cohorts of similar numbers of male and female subjects were plotted together unless sex-specific effects were identified.

Wild-type C57BL/6J mice (Charles River) were used for GRAB sensor imaging and FCV experiments (**Chapter 3-4**). This strain is preferred in the study of DA neurotransmission because it carries a wild-type gene for α-synuclein, a protein fundamental for regulation of DA release (Abeliovich et al., 2000), distinct to some other C57BL/6 strains in which spontaneous deletion of this gene has been observed (Specht and Schoepfer, 2001).

For experiments involving selective optogenetic activation of ChIs (**Chapter 4**), ChAT-Cre;Ai32 mice (aged 9-15 weeks) were used. These mice were generated by crossing homozygous ChAT-Cre mice (B6;129S6-*Chat*$^{tm2(cre)Lowl}$/J, Jax ID 006410) with homozygous Ai32 mice (B6;129S-*Gt(ROSA)26Sor*$^{tm32(CAG-COP4*H134R/EYFP)Hze}$/J, Jax ID 012569) and express channelrhodopsin-2 (ChR2) globally in cholinergic neurons.

For calcium imaging experiments, ChAT-Cre;Ai95D mice (aged 9-12 weeks) were used. ChAT-Cre;Ai95D mice (**Chapter 3-4**) express GCaMP6f selectively in cholinergic neurons and were generated by crossing homozygous ChAT-Cre mice (B6;129S6-*Chat*$^{tm2(cre)Lowl}$/J, Jax ID 006410) with homozygous Ai95D mice (B6;129S-*Gt(ROSA)26Sor*$^{tm95.1(CAG-GCaMP6f)Hze}$/J, Jax ID 024105).

For experiments investigating the role of calbindin-D28K (calb1) in DA axons, mice with knockdown of calb1 selectively in DA neurons were used (aged 7-9 months, **Chapter 4**). Double heterozygous mice with decreased calb1 expression in DA neurons (calbKD) were generated crossing homozygous Calb$_{TM2}$ (B6N.129-*Calb*$^{tm2.1Mpin}$/MmyrJ, Jax ID 031936) with homozygous DAT^{IREScre} mice (B6.SJL-*Slc6a3*$^{tm1.1(cre)Bkmn}$/J, Jax ID 006660). Heterozygous knockdown was chosen instead of homozygous deletion to minimise potential confounding adaptations that might accompany deletion of Ca^{2+} buffer (Brimblecombe et al., 2019). Control animals with

wild-type levels of calb1 (calbWT) were DAT^{IREScre} mice, matching for age and sex the calbKD mice.

For experiments probing striatal ACh transmission in a model of early Parkinson's disease (**Chapter 5**), mice overexpressing human α-synuclein (*SNCA*-OVX, aged 3-4 months) at disease-relevant levels were used (Janezic et al., 2013). These mice (B6.Cg-Tg(SNCA)OVX37Rwm *Snca^{tm1Rosl}*/J, Jax ID 023837) were generated by injection of BAC DNA containing the human α-synuclein locus into C56BL6 mouse pronuclei and back-crossed onto an α-synuclein-null (*Snca* -/-) pure C57BL6 background (Janezic et al., 2013). *SNCA*-OVX mice show early deficits in DA release at 3-4 months old, age-dependent reduction in SNc DA neuron firing, loss of nigrostriatal DA neurons and PD-related motor phenotypes (Janezic et al., 2013). *Snca* -/- mice were chosen as a control because they don't express endogenous synuclein, avoiding confounding interactions, and they allow littermate pairing with overexpressors. Furthermore, *Snca* -/- present no differences in storage and release of DA compared to mice expressing moderate levels of human α-synuclein, suggesting that the reported deficits in DA neurotransmission are due to overexpression of α-synuclein rather than expression per se (Janezic et al., 2013).

2.1.3. Stereotaxic intracranial injections

Stereotaxic intracranial injections in the striatum were performed on either wild-type (C57BL/6J) or transgenic (*SNCA*-OVX, *Snca* -/-) mice to deliver adeno-associated virus (AAV)-packaged GRAB sensors for expression in striatal neurons. Surgical procedures were carried out aseptically and according to the Project Licence.

First, isoflurane (IsoFlo) was used to induce general anaesthesia (4%). Once the mouse was anaesthetised, the fur was thoroughly clipped to ensure a good surface for incision. The mouse was then transferred to the stereotaxic frame (Kopf Instruments) and isoflurane levels were lowered for maintenance of anaesthesia (1-2%). The pedal withdrawal reflex was monitored throughout the procedure to ensure adequate anaesthetic depth. A rectal thermometer was used to check internal

temperature and an eye ointment was applied to protect the eyes. Then, the incision site was cleaned with chlorexidine gluconate (Chloraprep) and bupivacaine hydrochloride (Marcaine polyamp) was locally injected (2 mg/kg). Sub cut fluids (sterile saline, Vetivex) and analgesic meloxicam (Metacam, 5mg/kg) were also administered.

The skull was exposed, and craniotomies performed with a small drill. AAV-packaged sensors were injected bilaterally (1 µL/site) in either CPu (ML ± 2.2, AP + 0.65, DV -2.7/-2.5) or NAcC (ML ± 0.9, AP + 1.4, DV -3.8/-3.5) at a rate of 200 nL/min with a 32-gauge Hamilton syringe (Hamilton Company), withdrawn 5 minutes after injection. The constructs injected at a titre of 10^{13} genome copies/mL were AAV5.hSyn.ACh3.0 (Jing et al., 2020), AAV9.hSyn.ACh3.0 (Jing et al., 2020) and AAV5.hSyn.DA2m (Sun et al., 2020) and were all purchased from WZ Bioscience.

The wound was then closed using sterile monofilament suture (Monocryl). Mice were monitored and weighted daily for post-operative days 0-7, then once a week until used for experiments. Medicated jelly to alleviate postoperative pain was provided for days 0-2. Mice were maintained at least 2-3 weeks after injection, to allow construct expression.

2.2 FAST-SCAN CYCLIC VOLTAMMETRY FOR REAL-TIME DETECTION OF DA RELEASE

Fast-scan cyclic voltammetry (FCV) at carbon fibre microelectrodes (CFMs) was the preferred method used throughout this thesis to measure DA release in real-time. FCV is an electrochemical technique that uses the faradaic current resulting from a change in the oxidation state of an electroactive substance to quantify its concentration. DA is an electroactive molecule with two hydroxyl groups that can be readily oxidised and reduced, making it suitable for detection with FCV (**Figure 2.1**). A potential is applied at the recording electrode in the form of a triangular scan wave and across a range predicted to oxidise and reduce the molecule to measure. On the forward sweep (negative to positive potential), the substrate is oxidised, while on the reverse sweep it is subsequently reduced, yielding measurable faradaic currents at both oxidation and reduction potentials. DA is oxidised to DA-o-quinone on the forward sweep at approximately +600 mV, while it is reduced on the reverse sweep back to dopamine at around -200 mV (**Figure 2.1**). The sweep frequency is 8Hz, corresponding to one current measurement every 125 ms. In order to obtain the faradaic current attributable to DA there's need to subtract a large background current due to charging of the electrode, which is done digitally with the Millar voltammeter (Hermans et al., 2008).

FCV is one of the best techniques for real-time detection of DA release dynamics in a DA-rich area like the striatum for several reasons. Firstly, it has good sensitivity (nM range) and temporal resolution (ms range). Secondly, the CFM used to detect DA currents is small enough to ensure minimal tissue damage and big enough to measure extrasynaptic DA, fundamental given that DA signals as a volume transmitter (Rice et al., 2011). Finally, FCV allows to calibrate DA signals, given that the measured faradaic current is proportional to DA concentration. Indeed, by calibrating the CFM with known concentrations of DA, it is possible to convert current values into concentration.

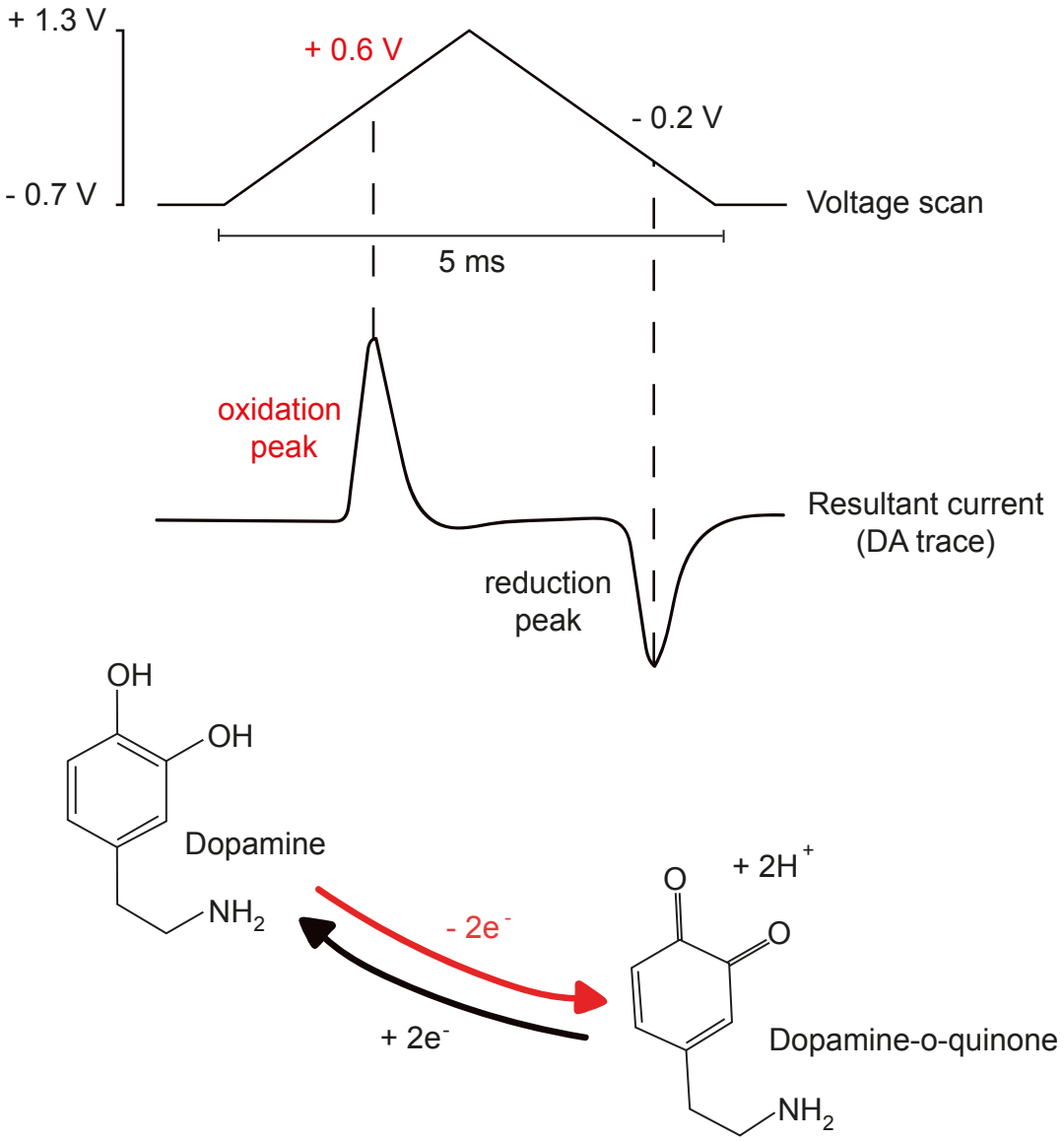


FIGURE 2.1. Fast-scan cyclic voltammetry to measure DA release.
A triangular voltage waveform is scanned across the recording electrode. During the positive phase of the scan (from -0.7 V to +1.3 V) DA is oxidised to DA-o-quinone (red), while during the negative phase (from +1.3 V to -0.7 V) DA-o-quinone is reduced back to DA (black). The current resulting from these redox reactions is recorded and produces a voltammogram showing typical oxidation peak at +0.6 V and reduction peak at -0.2 V. The scan duration is 5 ms and the scan rate is 800 V/s.

Despite these advantages, FCV has low molecular selectivity (for instance, it cannot distinguish between DA and norepinephrine) and low spatial resolution, given that it cannot sample DA levels in proximity of specific cell types.

There are several alternative methods that can be used to detect DA release in real-time in *ex vivo* slices. I will focus on microdialysis and genetically encoded fluorescent sensors, given that these tools provide either higher molecular or temporal and spatial selectivity than FCV.

Microdialysis with high-performance liquid chromatography (HPLC) coupled to electrochemical detection has higher chemical selectivity than FCV, allowing to distinguish between electroactive species with similar chemical structure, such as DA and norepinephrine (NE). Microdialysis can also measure absolute baseline concentration of neurotransmitter, which is not possible with FCV. However, this technique has poor temporal resolution, with samples that can be collected at a maximum rate of 1 sample per minute, inadequate to measure DA release dynamics in real-time. Microdialysis temporal resolution was improved by combination with a segmented flow system up to 15 s (Wang et al., 2008). Despite this improvement, subsecond temporal resolution is needed to better appreciate real-time dynamic changes in extracellular DA.

During the course of this thesis work, new tools for imaging neurotransmitter release based on GPCRs have been developed. The two different genetically encoded fluorescent sensors to measure DA release are dLight (Patriarchi et al., 2018, 2020) and $GRAB_{DA}$ (Sun et al., 2018, 2020). These tools are either D1 or D2 DA receptors bound to a circularly permutated fluorescent protein (cpFP) so that, upon binding of the endogenous ligand (in this case DA), the receptor undergoes a conformational change which results in an increase in fluorescence. These DA indicators yield large fluorescent responses upon ligand binding, making them particularly well suited for *in vivo* use (Labouesse et al., 2020). These tools also have higher molecular selectivity and spatial resolution than FCV, given that they present high specificity for their endogenous ligands and can be selectively expressed in specific cell types using a Cre recombinase-dependent approach (Labouesse et al., 2020). Furthermore, DA sensors undergo rapid conformational changes following ligand binding and have fast on/off rates, making them well-suited to detect DA release in real-time. Despite the multiple advantages and the growing body of work using these tools for DA monitoring, there are several considerations to be aware of. For instance, these GPCR-based sensors can buffer endogenous ligand and hence reduce DA availability at wild-type DA receptors (Labouesse et al., 2020). Fluorescent sensors might also be expressed ubiquitously throughout the membrane and so they might not reflect

the location of endogenous DA receptors and report levels of DA to which endogenous receptors might not be exposed to (Labouesse et al., 2020). Furthermore, given that these sensors are modelled on endogenous GPCRs, they are sensitive to agonists and antagonists of said receptors. It has been reported that these indicators present no downstream signalling and no internalisation in cell culture (Patriarchi et al., 2018; Sun et al., 2018), however additional work is needed to determine whether the tools are stably expressed and inert in intact brain tissue and upon dynamic changes in the volume of ligand. Finally, fluorescent sensors report neurotransmitter release as a change in fluorescence from baseline and do not provide information about the concentration of the ligand, which is instead possible to measure when using FCV.

In **Chapter 4**, I've used one of the two DA indicators ($GRAB_{DA}$) to replicate the effects of nAChR antagonism on DA release, well established with FCV (Rice and Cragg, 2004). I showed that $GRAB_{DA}$ sensors can measure dynamic changes in DA release plasticity, consistent with FCV findings. However, it is not possible to calibrate DA signals measured with $GRAB_{DA,}$ and the fluorescent signal is stable only for a limited time (**Figure 2.4B**). Overall, FCV remains the preferred technique to measure DA release in DA-rich regions like the striatum and in *ex vivo* slices for a number of reasons, including ability to calibrate DA signals and recording stability over time. The development of genetically encoded GPCR-based fluorescent sensors is nonetheless a revolutionary step for neurotransmitter release monitoring, bridging the gap in detection for a range of neurotransmitters, such as ACh.

2.2.1. Slice preparation

Mice were sacrificed by cervical dislocation and subsequently decapitated for collection of the brain. Acute 300 μm thick striatal coronal slices were prepared using a vibratome (VT1200S, Leica) in ice-cold HEPES-based buffer saturated with 95% O_2/ 5% CO_2, containing (in mM): NaCl (120), $NaHCO_3$ (20), HEPES acid (6.7), KCl (5), HEPES salt (3.3), $CaCl_2$ (2), $MgSO_4$ (2), KH_2PO_4 (1.2), glucose (10). Slices were

maintained in a holding chamber for at least one hour at room temperature (20-22° C) in HEPES-based buffer before transferral to the recording chamber.

2.2.2. Carbon fibre microelectrode fabrication

CFMs are ideal to measure DA release with FCV. These electrodes have an optimal diameter (around 7 µm) to measure DA spillover and therefore volume transmission, thought to be the main signalling modality of striatal DA. CFMs were produced in-house and one electrode was used for a single experiment, given that repeated exposure to DA and tissue fouling can alter electrode sensitivity and kinetics. Borosilicate capillary tubes (2.0 mm outside diameter, 1.16 mm inside diameter, Harvard Apparatus) were threaded with a single epoxy-free carbon fibre (7 µm diameter, Goodfellow Cambridge Ltd.). To facilitate insertion and clean the carbon fibre, each capillary tube was filled with acetone, which was subsequently removed by drying the tube on filter paper. The capillary tube was then sealed around the carbon fibre using a PE-2 vertical microelectrode puller (Narishige, Japan). The microelectrode puller was set at a high heat setting to ensure the formation of a tight seal between the glass tube and the carbon fibre, which resulted in high electrode signal-to-noise ratio (SNR). The seal was then visually inspected for damage under 100x magnification, and the carbon fibre was cut to a length of 50-100 µm from seal to tip. This carbon fibre length typically produced a sensitivity to DA within the desired range. Shorter CFMs have reduced sensitivity to DA, while longer electrodes have higher noise levels. Insulated copper wire (0.1 mm in diameter) was coated with silver conductance paint and inserted in the open end of the capillary tube, in electrical contact with the carbon fibre close to the tip and secured with cyanoacrylate glue.

2.2.3. Electrical and light stimulation

Throughout this work, I used striatal coronal slices which only contained DA axons, so that DA release cannot occur from midbrain DA neuron firing. Therefore, local stimulation was needed to evoke DA release.

One stimulation approach adopted was electrical stimulation delivered using a surface bipolar concentric Pt/Ir electrode (25 μm tip diameter, FHC Inc.). The stimulating electrode was positioned on the surface of striatal tissue at circa 100 μm from the recording electrode. Stimulation pulses lasted for 200 μs, were generated out-of-phase with FCV scans and were applied at 0.6 mA, to ensure minimal site variability in evoked $[DA]_o$ and synchronous release from multiple synapses near the stimulating electrode (Cragg, 2003; Threlfell et al., 2010). Indeed, DA release evoked with this stimulation (inter-stimulus interval 2.5 minutes) was stable over time (**Figure 2.2C**. Two-tailed paired Student's t-test, p = 0.11, n = 17 slices in N = 11 mice). In drug-free conditions, this stimulation evoked near maximal (perimaximal) DA release as previously described (Cragg, 2003). This stimulation was also used to measure neuronal activation with calcium imaging and DA or ACh release with $GRAB_{DA/ACh}$ (**Section 2.3.3**). Despite being a reliable method, electrical stimulation activates all circuit elements in the stimulation range besides DA axons, which can alter DA release. To achieve a more selective approach, I turned to optogenetics.

To evaluate the effects of ACh and nAChRs on DA release in isolation, I used an optogenetic approach to selectively light-activate ChIs and FCV to measure subsequent DA release. ChR2-expressing cholinergic fibres from ChATCre;Ai32 slices (**Section 2.1.2**) were activated using a 470 nm LED (OptoLED, Cairn Research). Blue light pulses were delivered at a duration of 2 ms and an intensity of ~ 11 mW, as previously described to successfully trigger ACh-evoked DA release (Threlfell et al., 2012). Slices were visualised on an upright microscope (Olympus BX50WI) under a 10x immersion objective with fluorescence optics for visualising eYFP (ChR2 expression). Light-evoked DA under these conditions was stable over time (**Figure 2.2F**. Two-tailed paired Student's t-test, p = 0.80, n = 8 slices in N = 4 mice) and similar to that obtained with electrical stimulation (Threlfell et al., 2012).

DA release evoked by light and electrical stimulation was Ca^{2+} dependent and action potential dependent (TTX sensitive) (Threlfell et al., 2010, 2012). Light and electrical pulses were delivered every 2.5 minutes, to ensure full recovery of DA terminals between pulses.

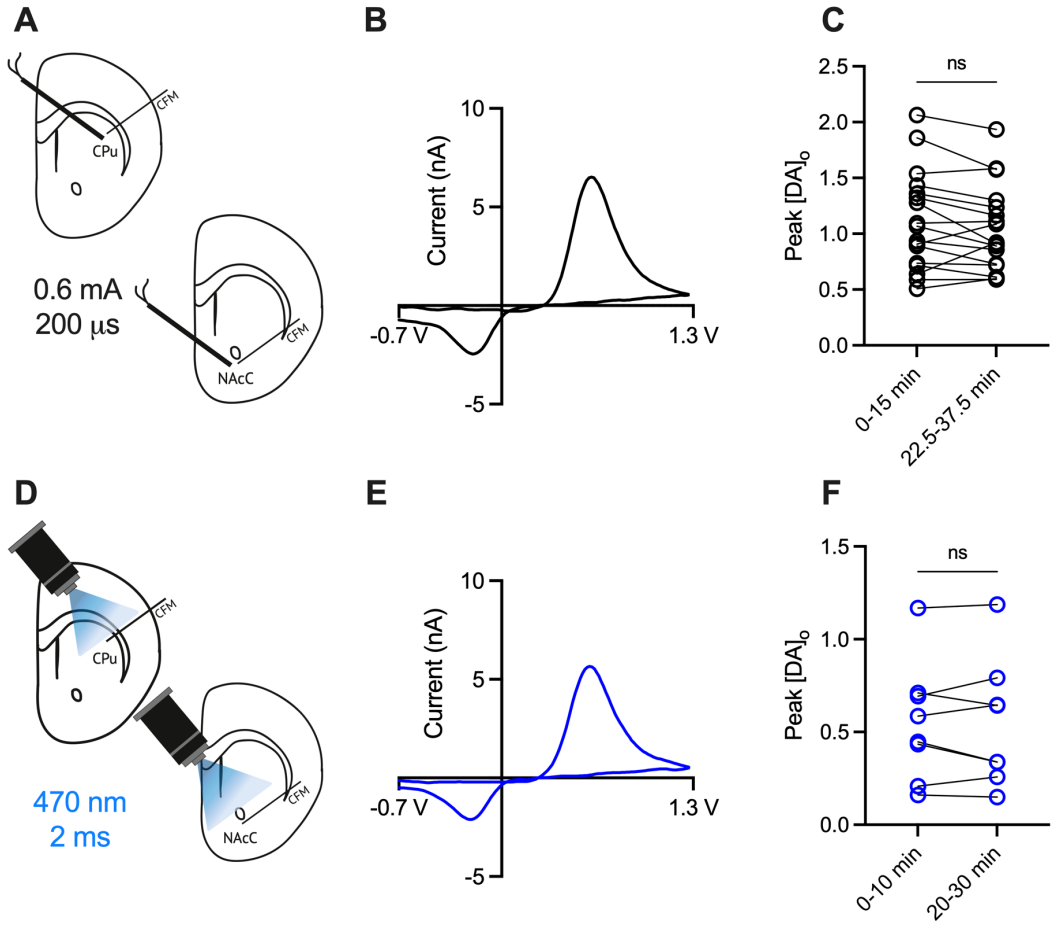


FIGURE 2.2. Electrically and light-evoked $[DA]_o$ is stable over time.
(A) *Schematic representation of the recording configuration in dorsolateral striatum (CPu) and ventral striatum (NAcC). Recording sites were chosen in dorsolateral regions of the CPu and in proximity of the anterior commissure in the NAcC. DA release was evoked with electrical pulses at 0.6 mA and lasting 200 µs and recorded with a CFM.*
(B) *Representative cyclic voltammogram of electrically evoked $[DA]_o$. DA oxidation and reduction potentials are +0.6 V and -0.2 V, respectively.*
(C) *Mean peak $[DA]_o$ (± SEM) evoked by single electrical pulses in the first 15 minutes of an experiment and in the last 15 minutes, in one recording site. Recordings were performed in wild-type mice and in drug-free conditions. Two-tailed paired Student's t-test: p = 0.11, n = 17 slices in N = 11 mice.*
(D) *Schematic representation of the recording configuration in dorsolateral sites of the CPu and in the NAcC. ChR2-expressing ChIs were stimulated with blue light pulses (470 nm) lasting 2 ms to evoke ACh-driven DA release measured with a CFM.*
(E) *Representative cyclic voltammogram of light evoked $[DA]_o$ release.*
(F) *Mean peak $[DA]_o$ (± SEM) evoked by single light pulses in the first 10 minutes of an experiment and after 20 minutes, in the same recording site. Recordings were performed in ChAT-Cre;Ai32 mice and in drug-free conditions. Two-tailed paired Student's t-test: p = 0.80, n = 8 slices in N = 4 mice.*

2.2.4. FCV recording

Slices were bisected and transferred to the recording chamber where they were superfused at ~ 1.8 ml/min in bicarbonate-buffer based artificial cerebrospinal fluid (aCSF) containing (in mM): NaCl (125), $NaHCO_3$ (26), KCl (3.8), $CaCl_2$ (2.4), $MgSO_4$ (1.3), KH_2PO_4 (1.2), glucose (10), saturated with 95% O_2/5% CO_2, at 31-33° C. Slices were left to equilibrate in the bath for 30 minutes prior recording and the recording electrode was charged in tissue during this time, to equilibrate the recording conditions and to minimise baseline drift during the experiment.

After slice equilibration, the CFM was lowered 100 μm into tissue in the chosen recording site. CFMs with a full signal gain in the range of 3-9 mV/nA were used for recording and the full signal gain was monitored and adjusted throughout the experiment. Recordings were performed in the dorsolateral CPu and in the NAcC. Stably releasing recording sites in each region were chosen for all experiments. Single pulses were delivered until a stable release baseline was reached, allowing a maximum release variability of 10% in successive stimulations. For experiments combining light and electrical stimulation, site release stability was assessed for both stimulations.

Evoked extracellular DA concentration ($[DA]_o$) was measured using FCV with the custom-made CFMs (**Section 2.2.2**) and a Millar voltammeter (Julian Millar, Barts and the London School of Medicine and Dentistry). A triangular voltage waveform (-700 to +1300 mV range vs Ag/AgCl reference) was scanned across the CFM at a scan rate of 800 V/s and sampling frequency of 8 Hz. Evoked currents were attributed to DA by comparison of the potentials for peak oxidation and reduction with those of DA in aCSF (oxidation peak +500-600 mV, reduction peak -200 mV). Currents sampled at the DA oxidation peak potential were measured in each voltammogram from baseline and plotted against time, to provide profiles of $[DA]_o$ versus time. Recording electrodes were calibrated in 2 μM DA in each experimental media at the end of each experiment. Calibration solutions were prepared before use from 2.5/5 mM DA in 0.1 M $HClO_4$ stock solution stored at 4°C.

For experiments requiring changes in extracellular calcium ($[Ca^{2+}]_o$), [$CaCl_2$] was changed accordingly. For experiments using different compounds, drugs were diluted from frozen stock aliquots in aCSF and washed on while stimulating with single pulses for a minimum time of 10-15 minutes.

Data were acquired and analysed using Axoscope 10.5 (Molecular Devices) and locally-written Microsoft Excel macros (Visual Basic). DA oxidation currents values were measured from background-subtracted voltammograms, converted to concentration using the electrode calibration factor and plotted against time to obtain $[DA]_o$ transients.

Statistical analysis was carried out using GraphPad Prism. Parametric statistical tests, namely Student's t-test and Analysis of Variance (ANOVA) test, were used to compare data groups, assuming normal distribution, similar variance, and independence of data in each group. Post hoc multiple comparison tests were performed to assess specific differences between pairs of data groups when the interaction between factors in the analysis of variance was significant. Sample size (n) for each experiment refers to the number of slices used. Slices were considered as an independent statical unit since they meet the requirements for genuine replication, namely independent allocation to an experimental condition, independent treatment application and lack of influence between each other (Lazic et al., 2018). Indeed, slices along the rostrocaudal axis were randomly and independently chosen for a particular experiment, drugs were applied independently to each slice and only local microcircuits within a given slice were considered. Higher degree of variability within samples was observed in each recoding site, and recordings were performed in one site per slice. Sample size was informed by estimation of variance in the data, considering expected variability between slices known from previous work conducted in similar experimental conditions (e.g., recording solutions). The number of experimental animals for each dataset was also reported and was $N \geqslant 3$. Pilot data for which $N \geqslant 2$ have also been included and are labelled as such in their respective chapters. The threshold for statistical significance

was $p < 0.05$. Statistical significance was reported as: * $p < 0.05$; ** $p < 0.01$; *** $p < 0.001$; **** $p < 0.0001$.

2.3 IMAGING

Recently, the field has seen the development of genetically encoded fluorescent sensors which allow to image neurotransmitter release *ex vivo* and *in vivo*. These sensors are based on a GPCR linked to a circularly permutated fluorescent protein (cpFP) and measure neurotransmitter release via an increase in fluorescence which occurs following a conformational change upon ligand binding. This approach allows an unprecedented level of spatial and temporal resolution, and, given that GPCRs are a large family of receptors, can be developed to probe several endogenous neurochemicals (Ravotto et al., 2020). In particular, the development of these tools has been advantageous for measuring neurotransmitters for which there was an historical lack of reliable methods, like ACh (Jing et al., 2018). An overview of the methods previously developed to measure ACh release and their advantages and disadvantages is provided in **Chapter 1** (**Section 1.3.6**). In this thesis, I've used GRAB (GPCR-activation based) sensors to measure ACh and DA release in striatal slices from healthy (**Chapter 3-4**) and parkinsonian mouse models (**Chapter 5**).

To be probe neuronal activation, I've used GCaMP6f (Chen et al., 2013) to measure intracellular calcium level in selective neuronal types (**Chapter 3-4**).

Notably, control preparations such as calcium or neurotransmitter insensitive reporters were not used in this body of work in the interest of reduction of the number of experimental animals in use, in line with the 3R guidelines. Furthermore, the use of brain slices allows to perform within-slice pharmacological control experiments. For instance, in **Figure 3.1D**, I showed that fluorescent responses measured with $GRAB_{ACh}$ are sensor specific given that they are abolished by a mAChR antagonist. Ligand-insensitive $GRAB_{ACh}$ sensors were also previously validated in cell culture (Jing et al., 2020).

2.3.1 GRAB sensor imaging

To measure striatal ACh release, I used next-generation $GRAB_{ACh}$ sensors (Jing et al., 2020). $GRAB_{ACh}$ sensors were packaged in AAV5 or AAV9 vectors (AAV5.hSyn.ACh3.0, AAV9.hSyn.ACh3.0, WZ Bioscience) and injected in dorsal and ventral striatum of adult mice (**Figure 2.3**). After a 3-week waiting period to ensure optimal sensor expression (Jing et al., 2018, 2020), mice were sacrificed, and acute striatal slices were prepared for recording. $GRAB_{ACh}$ sensors were developed combining a human M_3-mAChR with a cpGFP (Baird et al., 1999; Jing et al., 2018, 2020). When ACh is released, it binds to the sensor provoking a conformational change which is translated into an increase in fluorescence. In cell culture, $GRAB_{ACh}$ sensors have negligible coupling with major GPCR-mediated downstream pathways and no internalisation upon sustained exposure to ACh (Jing et al., 2018, 2020). Moreover, the human synapsin promoter (hSyn) ensures stable and long-term expression of the sensor globally in striatal neurons (Kügler et al., 2003). The considerations on the use of fluorescent sensors to monitor DA release outlined in **Section 2.2** are also valid for the use of $GRAB_{ACh}$ to measure ACh release.

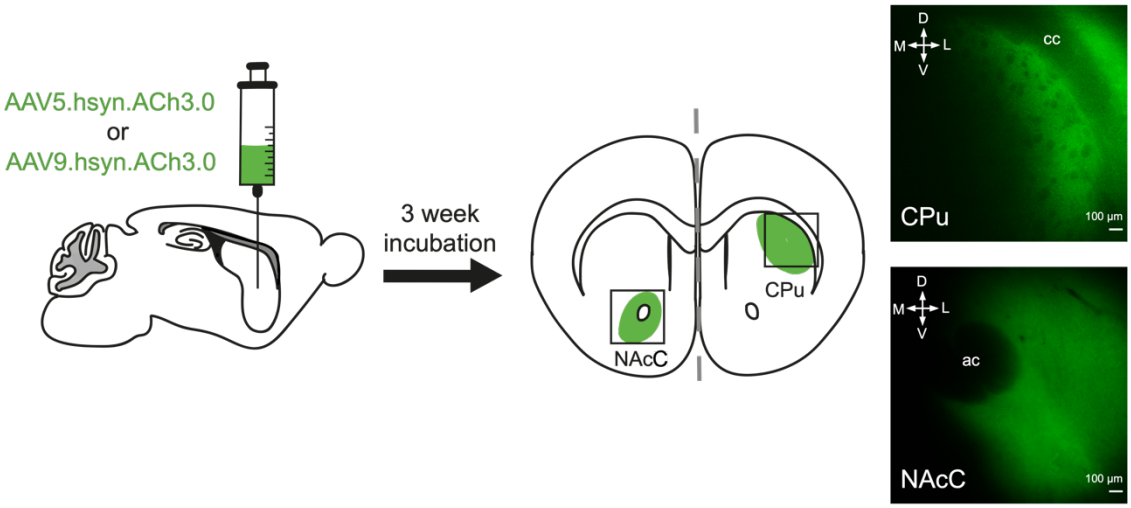


FIGURE 2.3. Schematic representation of the experimental procedure for GRAB$_{ACh}$ expression in mouse striatum. *AAV-packaged GRAB$_{ACh}$ sensors (ACh3.0) were injected in each hemisphere of wild-type mice in either dorsal (targeting dorsolateral CPu) or ventral striatum (targeting the NAcC). After at least 3 weeks of incubation, mice were sacrificed, and slices prepared for recording. Example images from dorsal and ventral slices show bright and uniform sensor expression. A similar experimental procedure was adopted to deliver GRAB$_{DA}$ sensors in the CPu of wild-type mice and GRAB$_{ACh}$ sensors in the CPu of parkinsonian mice and their littermate controls.*

GRAB$_{DA}$ sensors were used to measure DA release and gain insights into how this receptor-based approach can report extracellular dynamics of neurotransmitters. GRAB$_{DA}$ are human D2Rs linked to a cpGFP (Sun et al., 2018). Similarly to ACh sensors, DA released extracellularly binds to the receptor provoking a conformational change which leads to an increase in fluorescence. First and second generation GRAB$_{DA}$ sensors show negligible coupling to downstream GPCR signalling, stable membrane expression upon prolonged exposure to DA, and high specificity and sensitivity for DA (Sun et al., 2018, 2020). I've been using next-generation GRAB$_{DA}$ (AAV5.hSyn.DA2m, WZ Bioscience) with optimised coupling between the cpGFP and the GPCR to obtain higher fluorescent responses (Sun et al., 2020). GRAB$_{DA}$ sensors packaged in AAV5 were injected in the dorsal striatum of adult wild-type mice and acute striatal slices were prepared after a two-week incubation period, to ensure appropriate sensor expression (Sun et al., 2018). The hSyn promoter ensures stable and long-term expression of the sensor globally in striatal neurons (Kügler et al., 2003), which allows to measure bulk extracellular DA signal comparable to that measured with FCV.

2.3.2. Calcium imaging

Genetically encoded calcium indicators (GECIs) measure changes in intracellular calcium levels ($[Ca^{2+}]_i$). This is a reliable proxy for neuronal activity given that large changes in $[Ca^{2+}]_i$ result from action potential firing and synaptic transmission (Luo et al., 2018). GCaMP (Nakai et al., 2001) is a GECI that is composed by a cpGFP (Baird et al., 1999), the calcium-binding protein calmodulin (CaM) and the CaM-interacting M13 peptide (Crivici and Ikura, 1995). Calcium ions bind to CaM and drive a conformational change in the CaM-M13 complex which results in an increase in fluorescence. There is a large family of different GCaMPs (Luo et al., 2018) and GCaMP6 sensors were developed by optimising the interface between cpGFP-CaM and M13-CaM, to obtain indicators with higher sensitivity, faster kinetics, and stronger fluorescence responses (Chen et al., 2013). In this thesis, I've been using a transgenic line expressing GCaMP6f (**Section 2.1.2**), the fastest genetically encoded indicator for sensing $[Ca^{2+}]_i$ (Chen et al., 2013). Advantages of the use of GCaMP6f include expression in selective neuronal subtypes, ability to image large groups of neurons or small synaptic compartments (Chen et al., 2013) and good temporal resolution which allows detection of individual spike events (Chen et al., 2013).

Despite these advantages, calcium indicators measure changes in the cytosolic free calcium ions and thereby act as exogenous calcium buffers (Grienberger and Konnerth, 2012). GECIs can therefore contribute to the total amount of cellular calcium buffer molecules and change the intracellular calcium dynamics (Grienberger and Konnerth, 2012).

2.3.3. Slice preparation and recording

For all imaging experiments performed in this thesis, slices were prepared as described in **Section 2.2.1**. Following one hour incubation in HEPES-based buffer, slices were bisected and transferred to the recording chamber. Here, they were superfused at ~ 2-2.5 ml/min in aCSF (**Section 2.2.4**) and left to equilibrate in the bath for at least 30 minutes prior recording.

Expression levels were checked under a 10x objective using a sCMOS camera (IRIS9, Teledyne Photometrics) and the stimulating electrode was positioned in dorsolateral or ventral striatal (NAcC) sites with the brightest expression. Slices were electrically stimulated as described in **Section 2.2.3**, with electrical pulses delivered every 2.5 minutes. In drug-free conditions, the size of fluorescent responses measured with $GRAB_{ACh}$ sensors evoked by single electrical stimuli (filled circles) is stable over time in CPu and NAcC (**Figure 2.4A**. Two-way ANOVA, time x region interaction: F (18, 379) = 0.27, p = 0.99; time effect: F (18,379) = 1.5, p = 0.086; region effect: F (1,379) = 0.02, p = 0.88, n = 11 slices in CPu: N = 8 mice, NAcC: N = 10 mice). Peak fluorescence is also stable for $GRAB_{DA}$ and Ca^{2+} imaging when recordings lasted under 30 minutes (**Figure 2.4B**. Simple linear regression and slope significantly non-zero, R^2 = 0.02, p = 0.16, n = 6 slices in N = 6 mice. **2.4C**. Simple linear regression and slope significantly non-zero, R^2 = 0.002, p = 0.70, n = 5 slices in N = 5 mice). Furthermore, the chosen stimulation parameters known to evoke perimaximal DA release also evoke perimaximal ACh release (**Chapter 3**, **Figure 3.1E-F**).

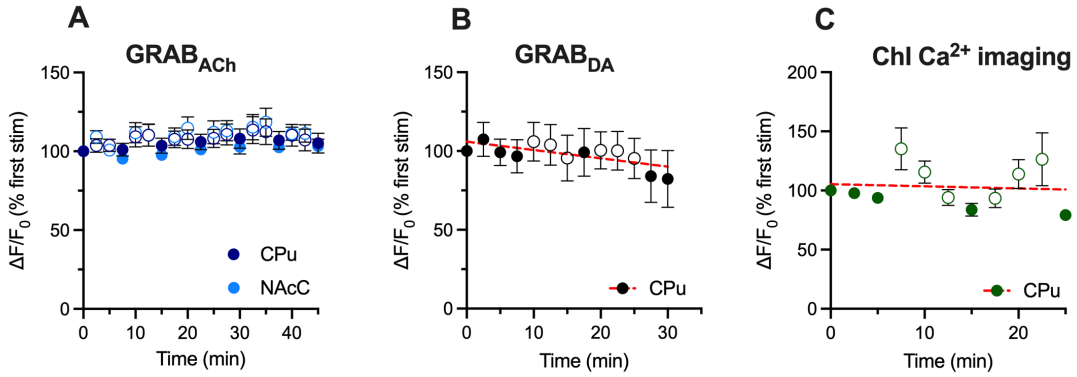


FIGURE 2.4. Fluorescent responses measured with GRAB sensors and Ca^{2+} imaging are stable over time.
(A) *Mean peak $\Delta F/F_0$ (± SEM) for ACh release measured with $GRAB_{ACh}$ in dorsolateral (CPu) and ventral (NAcC) striatum in drug-free conditions. Filled circles represent single electrical pulses, while empty circles represent trains of pulses at different frequencies. Data are normalised to the first single stimulus applied. Two-way ANOVA: time x region interaction: F (18, 379) = 0.27, p = 0.99; time effect: F (18,379) = 1.5, p = 0.086; region effect: F (1,379) = 0.02, p = 0.88, n = 11 slices in CPu: N = 8 mice NAcC: N = 10 mice.*
(B) *Mean peak $\Delta F/F_0$ (± SEM) for DA release measured with $GRAB_{DA}$ sensors in drug-free conditions in dorsolateral striatum (CPu). Filled circles represent single electrical pulses, while empty circles represent trains of pulses at different frequencies. Data are normalised to the first single stimulus applied. Simple linear regression and slope significantly different from zero: R^2 = 0.02, p = 0.16, n = 6 slices in N = 6 mice.*
(C) *Mean peak $\Delta F/F_0$ (± SEM) for calcium imaging responses in drug-free conditions in dorsolateral striatum (CPu). Filled circles represent single electrical pulses, while empty circles represent trains of pulses at different frequencies. Data are normalised to the first stimulus given. Simple linear regression and slope significantly different from zero: R^2 = 0.002, p = 0.7, n = 5 slices in N = 5 mice.*

2.3.4. Image acquisition

Images were acquired under a 10x immersion objective using a sCMOS camera (IRIS9, Teledyne Photometrics) and an ImageJ plugin (MicroManager). The camera default acquisition speed was 30 frames per second (fps, 30 Hz) and pixel size of 4.25 µm x 4.25 µm. An advantage of using imaging over FCV is that it is possible to manipulate the acquisition parameters to achieve higher sampling frequencies and potentially resolve individual events in train stimulations. Hence, in experiments assessing evoked neurotransmitter release or neuronal activation, I've binned the camera pixels (2x2) and defined a rectangular recording window of active pixels (**Figure 2.6A**) to achieve sampling frequencies as high as 100 Hz (100 fps). These manipulations impact on the camera resolution but increase its sensitivity so that it is possible to resolve individual events upon train stimulation. However, it is important to note that resolution of discrete events in a train also depends on the kinetics of the fluorescent sensor used. In experiments investigating tonic changes in neurotransmitter release, the camera default acquisition rate and recording window were maintained, to ensure sampling of a surface wide enough to detect potential spontaneous release events. The detailed acquisition parameters used for each set of experiments are described in each chapter as appropriate.

All genetically encoded fluorescent sensors used in this thesis have a fluorophore (cpGFP) as an output, therefore the signal relies on excitation by a light source. A blue light LED (470 nm) at a range of intensities (2-11 mW) was used to excite the cpGFP. Changes in excitation light intensity can impact on SNR and sensor photostability so they were optimised considering experiment duration and recording time. Notably, the acquisition parameters chosen ensured stable recordings with minimal photobleaching and baseline fluorescence shift (F_0) over time (**Figure 2.5**). Indeed, F_0 monitored from electrically evoked ACh signals measured with $GRAB_{ACh}$ is stable over time in both CPu and NAcC (**Figure 2.5A**. Two-way ANOVA, time x region interaction: $F(18, 360) = 0.37$, $p = 0.99$; time effect: $F(18,360) = 1.14$, $p = 0.30$; region effect: $F(1,20) = 0.60$, $p = 0.45$, n = 11 slices in CPu: N = 8 mice, NAcC: N = 10 mice). Dynamic changes in F_0 might therefore suggest

changes in ACh ambient levels as discussed in **Chapter 3** (**Section 3.4.2**). F_0 is also stable for calcium imaging recordings (**Figure 2.5B**. Simple linear regression and slope significantly non-zero, R^2 = 0.05, p = 0.095, n = 5 slices in N = 5 mice).

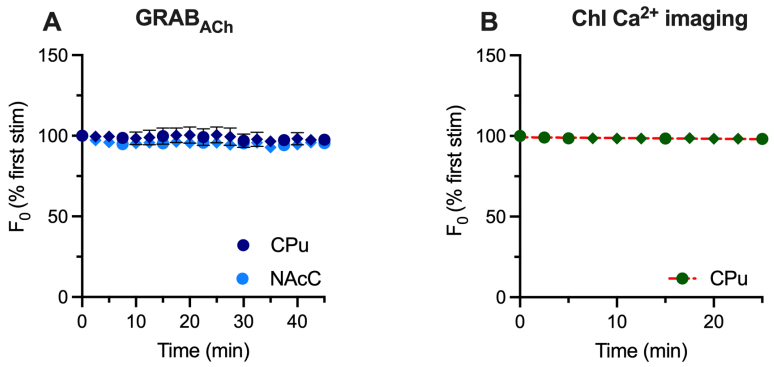


Figure 2.5. Baseline fluorescence F_0 is stable over time for GRAB$_{ACh}$ and Ca^{2+} imaging.
(A) *Mean F_0 (± SEM) measured with GRAB$_{ACh}$ in drug-free conditions in CPu and NAcC. Data are normalised to the first stimulus applied. Circles represent single electrical pulses, while diamonds represent trains of pulses at different frequencies Stimuli were delivered every 2.5 minutes. Two-way ANOVA, time x region interaction: F (18, 360) = 0.37, p = 0.99; time effect: F (18,360) = 1.14, p = 0.30; region effect: F (1,20) = 0.60, p = 0.45, n = 11 slices in CPu: N = 8 mice, NAcC: N = 10 mice.*
(B) *Mean Ca^{2+} imaging F_0 (± SEM) normalised to the first stimulus applied in drug-free conditions in CPu. Circles represent single electrical pulses, while diamonds represent trains of pulses at different frequencies Stimuli were delivered every 2.5 minutes. Simple linear regression and slope significantly non-zero: R^2 = 0.05, p = 0.095, n = 5 slices in N = 5 mice.*

2.3.5. Data processing

For calcium imaging and GRAB experiments looking at evoked transients, the size of each acquired image was calculated in ImageJ using information about pixel size and objective magnification. The stimulating electrode angle was calculated to ensure that the sampling region of interest (ROI) was positioned with the same orientation (**Figure 2.6A**). A square ROI (100 µm x 100 µm) was positioned so that its centre was at 100 µm from the stimulating electrode, consistently with FCV experiments (**Section 2.2.3**). Frame number and fluorescence values were then extracted for the recording ROI and the background ROI with a custom written ImageJ macro. These parameters were then analysed with a custom written MATLAB code (MATLAB R2020_a, MathWorks). First, frames were converted into time (s) and then background was subtracted as previously described (Condon et al., 2019). In brief, the chosen background was a static value obtained from a ROI positioned on the

stimulating electrode, matching the size and orientation of the sampling ROI. The sensors used in this body of work are globally expressed in the tissue included in the recording window so that choosing a background ROI on tissue could lead to subtracting a signal resulting from neurotransmitter release. Choosing a background ROI on the stimulating electrode ensured that variations in environmental light conditions were accounted for without subtracting a biologically meaningful signal.

Then, the change in fluorescence from baseline was calculated (**Figure 2.6B**). A two-term exponential decay function,

$$f(x) = a^{bx} + c^{dx}$$

('exp2' MATLAB function) was fit to the pre and post-peak raw fluorescence values (F) to obtain baseline fluorescence values (F_0). Fluorescent responses were then calculated as

$$\frac{\Delta F}{F_0} = \frac{F - F_0}{F_0}$$

(**Figure 2.6B**). The baseline fluorescence value corresponding to the peak $\Delta F/F_0$ value (F_0 peak) was also extracted to monitor basal fluorescence changes over time and in different drug conditions.

For experiments looking at tonic levels of neurotransmitter, frame and fluorescence values were extracted using ImageJ from square ROIs (100 µm x 100 µm) positioned at locations of high sensor expression. Change in fluorescent responses from baseline driven by compound application were calculated as $\Delta F/F_0$, where F_0 corresponds to pre-drug basal fluorescence.

The number of animals for each dataset is $N \geqslant 4$. Preliminary data for which $N \geqslant 2$ have also been included and are labelled as such in their respective chapters. Statistical analysis was carried out using GraphPad Prism and the threshold for statistical significance was $p < 0.05$. The statistical tests, assumptions and statistical units used are specified in **Section 2.2.4**.

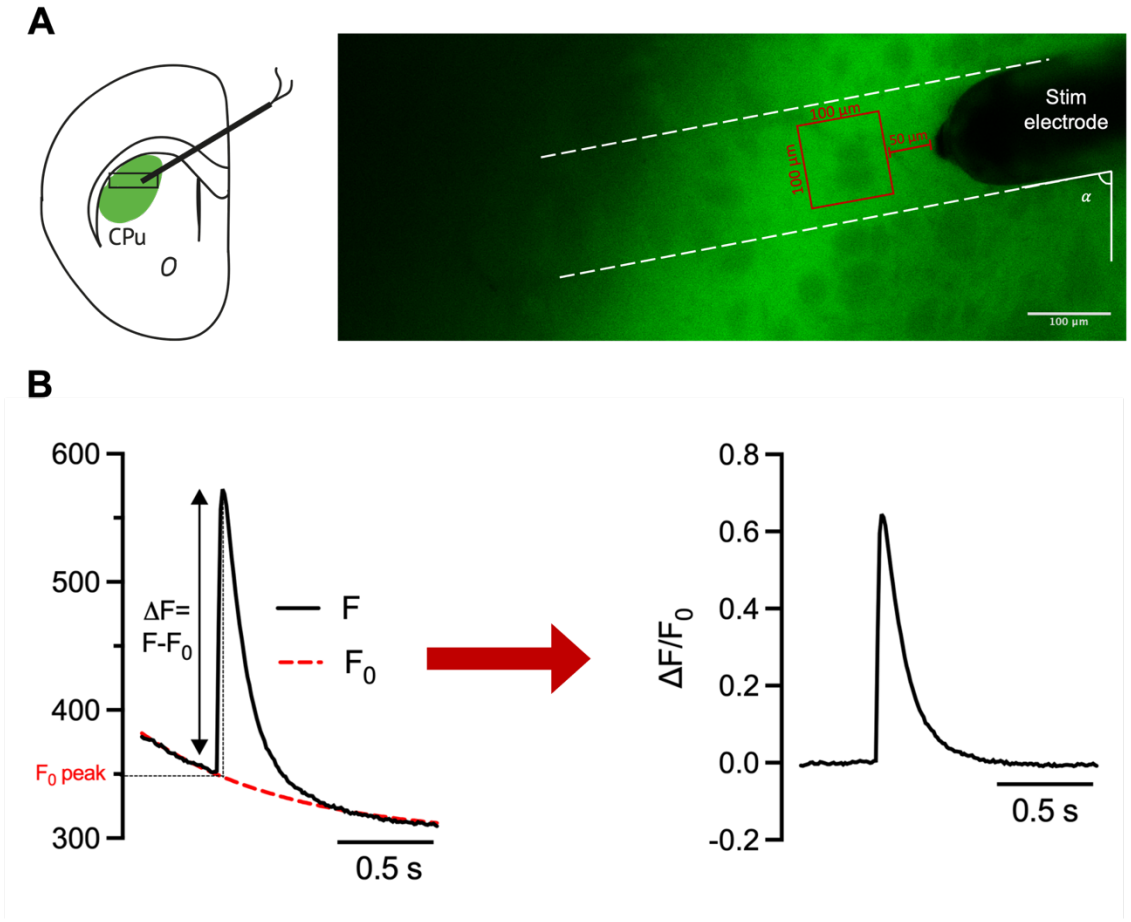


FIGURE 2.6. Data extraction and processing for imaging experiments involving electrical stimulation.
(A) *Right, schematic representation of the recording configuration in CPu. To achieve the highest sampling frequency (100 Hz), a rectangular recording window containing the stimulating electrode was selected. Left, example recording window ($GRAB_{ACh}$). The angle of the stimulating electrode was calculated and a square region of interest (ROI) of 100 µm x 100 µm was positioned accordingly. The ROI was positioned so that its centre would be at 100 µm from the stimulating electrode, similarly to FCV (where the stimulating and recording electrodes are placed at ~ 100 µm).*
(B) *Example trace to calculate $\Delta F/F_0$. An exponential decay function was fit in MATLAB to raw fluorescence values (F) to obtain baseline fluorescence F_0. The change in fluorescence from baseline ($\Delta F=F-F_0$) was then calculated and divided by baseline fluorescence to obtain $\Delta F/F_0$ values. The baseline fluorescence value corresponding to the peak $\Delta F/F_0$ value (F_0 peak) was also extracted to monitor basal fluorescence changes over time and in different drug conditions.*

2.3.6. Viral serotype-driven differences in ACh signal measured with $GRAB_{ACh}$

To monitor real-time ACh release, I used $GRAB_{ACh}$ sensors packaged in two different adeno-associated viral vectors, AAV5 and AAV9 (**Section 2.3.1**). These differences in viral serotype were responsible for alterations in the temporal dynamics of the measured ACh signals.

To ensure the maintenance of standard experimental conditions across different experimental groups, I injected the same viral titre and amount, in mice

with the same genotype and in the same age group (**Section 2.1.3**). Furthermore, the constructs were packaged under the same promoter (hSyn), which should ensure global neuronal expression in striatal neurons (Kügler et al., 2003), and with the same version of the sensor (ACh3.0) (Jing et al., 2020). Hence, the differences appeared to be driven by the viral serotype.

The expression of the construct in dorsolateral striatum was similar for both AAV5 and AAV9-driven GRABs (**Figure 2.7A**), characterised by global localisation in neuronal processes as further described in **Chapter 3** (**Section 3.3.1**). However, the temporal profiles of single pulse-evoked ACh signal in drug-free were different (**Figure 2.7B**). AAV5-driven GRABs showed fast ACh signals (**Figure 2.7B**, *top*), while the ones measured with AAV9-driven sensors showed slower decay kinetics (**Figure 2.7B**, *bottom*). Consistently, the half-lives of ACh transients measured with AAV9-$GRAB_{ACh}$ were higher than those measured with AAV5-$GRAB_{ACh}$ (**Figure 2.7C**. Two-tailed unpaired Student's t-test, $p < 0.0001$. AAV5: n = 77 transients in N = 8 mice, AAV9: n = 55 transients in N = 6 mice).

Several reasons could explain the described differences in the signal. First, different viral serotypes might be responsible for driving sensor expression in different cell types, changing the sites from which ACh release is sampled. However, AAV5 and AAV9 have been shown to transfect with similar efficiency striatal neurons, interneurons, oligodendrocytes, and microglia (Aschauer et al., 2013). Furthermore, the two serotypes show similar spread from injection site and anterograde and retrograde transport (Haery et al., 2019).

The kinetics of the fluorescent responses measured with genetically encoded sensors are generally a function of on/off rates of ligand binding to the sensor and ligand concentration (Sabatini, 2019). Given that the sensor encoded by the two viral vectors is the same (ACh3.0), I can exclude an effect of sensor affinity and on/off binding kinetics. However, different viral serotypes might drive expression of the sensor in different neuronal compartments, so that the GRABs can be exposed to different concentration of the ligand, resulting in altered readout kinetics. For instance, AAV9-GRAB might be expressed closer to ACh release sites and yield a

longer lasting signal, while AAV5-GRABs might localise further away from the release sites measuring a faster signal which has already been partially degraded. To test whether changes in the temporal dynamics of ACh signals are driven by sampling distance from release sites, AAV9 or AAV5-DIO-$GRAB_{ACh}$ (Cre-dependent) could be expressed selectively in ChIs (by injecting in ChAT-Cre mice) to measure the most local ACh signal and assess if the differences persist.

Finally, differences in the signal measured in the two serotypes could be driven by differences in the transfection efficacy. For instance, higher GRAB expression could result in increased capacity to measure the ligand, higher receptor occupancy and longer lasting signals. I showed that the signal appeared to be overall equally distributed in neuronal projections in the two serotypes (**Figure 2.7A**), however a more thorough quantitative analysis is needed to determine percentage expression of $GRAB_{ACh}$ molecules driven by each vector.

Overall, to interpret the results in the experimental chapters of this thesis, it is important to note that the timescales of fluorescent responses measured with GPCR-based sensors are a function of ligand binding/unbinding, fluorophore conformational change induction/reversal, sensor localisation and expression levels. Therefore, the signal measured with these tools might not accurately reflect endogenous timescales of neurotransmitter release. Nonetheless, these tools can still measure dynamic changes in neurotransmitter release and how pharmacological manipulations might alter release properties.

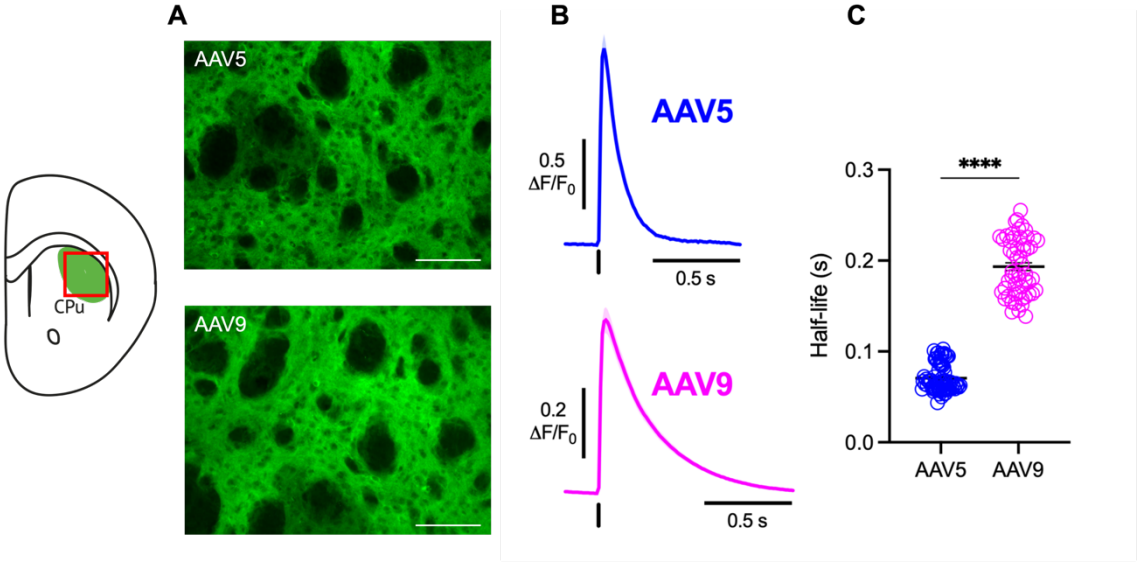


FIGURE 2.7. Differences in GRAB$_{ACh}$ signal expressed by different viral serotypes.
(A) *Fluorescent images showing GFP (GRAB$_{ACh}$) expression driven by AAV5 or AAV9-packaged constructs in dorsolateral striatum (CPu). Scale bar indicates 100 µm. GRAB$_{ACh}$ is densely expressed in striatal neuropil by both serotypes.*
(B) *Mean (± SEM) ACh transients evoked by single electrical pulses measured with AAV5 or AAV9-driven GRAB$_{ACh}$ sensors in drug-free conditions. When GRAB$_{ACh}$ are expressed via AAV9, the decay kinetics of ACh signal are slower.*
(C) *Half-lives of ACh transients evoked by single electrical stimuli measured with GRAB$_{ACh}$ driven by either AAV5 or AAV9. Half-lives were calculated from falling phases of ACh transients and are significantly higher for AAV9-packeged GRABs. Two-tailed unpaired Student's t test: $p < 0.0001$, AAV5: $n = 77$ transients in $N = 8$ mice, AAV9: $n = 55$ transients in $N = 6$ mice.*

3. Modulation of striatal acetylcholine release

3.1 INTRODUCTION

The striatum is one of the brain regions exhibiting the highest levels of ACh, enzymes for its synthesis and breakdown and ACh receptors (Mesulam et al., 1992; Contant et al., 1996; Zhou et al., 2002). The primary source of ACh are striatal cholinergic interneurons (ChIs) (Contant et al., 1996; Calabresi et al., 2000), together with an external source originating from the pedunculopontine and laterodorsal tegmental nuclei (Dautan et al., 2014). ACh covers a fundamental role in modulating striatal circuits and output and ChIs can be described as gatekeepers of striatal circuitry, with implications in a range of neuropsychiatric and neurodegenerative disorders (Pisani et al., 2007; Poppi et al., 2021).

Despite this essential role, striatal ACh release properties are incompletely characterised, mainly due to a lack of tools for direct real-time measurement of extracellular ACh. An overview of the various tools available to measure ACh release and their limitations is provided in **Chapter 1** (**Section 1.3.6**). This gap in ACh detection has only recently been filled with the development of GPCR-activation-based ACh sensors ($GRAB_{ACh}$) (Jing et al., 2018, 2020), however a characterisation of ACh release dynamics across striatal regions is still lacking. In this chapter, I set out to investigate the major properties of ACh release in dorsolateral and ventral striatum, including modulation by two key striatal neurotransmitters, GABA and DA.

As described in **Chapter 1** (**Section 1.3**), ChIs constitute only 1-2% of striatal neurons, however they have large cell bodies, long dendrites, and extensive, highly branched axonal arborisations, sending projections widely across the striatum (Bolam et al., 1984; Lim et al., 2014). Quantitative electron microscopy studies in rat striatum estimated approximately $2x10^8$ ACh varicosities/mm^3, inferring that each ChI possesses an average of around 500,000 axonal varicosities, allowing widespread release of ACh (Contant et al., 1996; Abudukeyoumu et al., 2019). The neuropil complexity of ChIs appears to be constant along the dorsoventral striatal axis (Matamales et al., 2016), however regional differences in ChI anatomy have been reported. Indeed, ChIs in the NAc core (NAcC) are less dense (Matamales et al., 2016),

have smaller cell bodies (Gonzales and Smith, 2015) and shorter processes (Matamales et al., 2016) compared to those in the NAc shell (NAcSh) and dorsal striatum (CPu). ChIs also form a small number of conventional synaptic connections and ACh main signalling modality is thought to be volume transmission (Descarries et al., 1997; Threlfell and Cragg, 2011; Dunant and Gisiger, 2017; Poppi et al., 2021).

ChIs are tonically active neurons and can fire action potentials at 2-10 Hz in absence of synaptic inputs (Wilson et al., 1990; Bennett and Wilson, 1999a). ChIs also encode reward-related and salient events by pausing their firing activity (Morris et al., 2004; Joshua et al., 2008). This pause response can be preceded by bursts of action potentials and followed by rebound excitation (Apicella, 2002; Morris et al., 2004). Overall, dynamic changes in ChI firing are a fundamental aspect of striatal cholinergic signalling and are thought to contribute to associative learning in a reward-related context (Lim et al., 2014). Nonetheless, how changes in ChI activity impact on ACh release levels have not been completely characterised. To investigate this, in **Section 3.3.3** I stimulated with a range of tonic-like and burst-like frequencies mimicking ChI firing and measured ChI activation and ACh release across striatal regions.

The dense innervation and tonic activity of ChIs ensure continuous exposure to tonic ambient levels of ACh (Descarries et al., 1997; Abudukeyoumu et al., 2019) and acetylcholinesterase (AChE) is a potential candidate proposed to regulate the spatiotemporal dynamics of ACh release (Descarries et al., 1997; Zhou et al., 2002; Pisani et al., 2007; Dunant and Gisiger, 2017). AChE, which catalyses ACh breakdown, is among the fastest known enzymes (Descarries et al., 1997) and is highly expressed in the striatum mainly by ChIs, together with other interneurons and midbrain DA neurons (Bernard et al., 1995). AChE is mostly found anchored on the plasma membrane of neurons and their processes (Descarries et al., 1997; Dobbertin et al., 2009), but can also be secreted (Descarries et al., 1997). Therefore, AChE is ideally positioned to regulate several aspects of ACh release dynamics including tonic levels, frequency dependency and time course of extracellular signal, but this role has not been fully characterised in real-time. In **Section 3.3.4**, I explored the role of AChE in

modulating tonic and evoked levels of ACh release and shaping its spatiotemporal dynamics.

ChI excitability and ACh release can be modulated by a range of striatal neuromodulators. ChIs receive a high number of inhibitory projections from MSNs (Chuhma et al., 2011; Gonzales et al., 2013) and GABAergic interneurons (Sullivan et al., 2008; Elghaba et al., 2016). GABA inhibits ChI activity either via $GABA_A$ receptors on ChIs (DeBoer and Westerink, 1994; Lim et al., 2014; Sato et al., 2014) or by inhibiting glutamatergic corticostriatal inputs via $GABA_B$ receptors (DeBoer and Westerink, 1994; Poppi et al., 2021). Moreover, there is ambient GABA tone in the striatum (Ade et al., 2008; Kirmse et al., 2008, 2009), which tonically inhibits DA release (Lopes et al., 2019; Roberts et al., 2020). The effect of GABA tone and GABAergic receptors on ACh release dynamics in real-time have not been previously characterised. Hence, in **Section 3.3.5**, I tested whether ACh release was under tonic GABAergic inhibition mediated via $GABA_A$ and $GABA_B$ receptors.

DA is another major regulator of ACh release. DA axons surround ChIs in a fashion suitable for volume transmission, as well as forming sparse synaptic connections (Dimova et al., 1993; Li et al., 2002; Goldberg and Reynolds, 2011). DA can act at D2 receptors (D2Rs) on ChIs to inhibit their firing (Alcantara et al., 2003; Maurice et al., 2004; Deng et al., 2007a). Recent *in vivo* studies suggest that DA acting at D2Rs on ChIs regulates the size and length of the dip in ACh release which follows ChI pause (Gallo et al., 2021; Martyniuk et al., 2021). Despite these advances, how DA levels modulate ACh release dynamics via D2Rs across striatal regions is still incompletely defined. In **Section 3.3.6**, I investigated the role of D2Rs in modulating ACh release in real-time and the effects of a pathological increase in DA levels driven by cocaine on ACh release in dorsolateral and ventral striatum.

Overall, the work included in this chapter aimed at providing a characterisation of the major properties of ACh release across striatal regions. First, I defined the properties of the ACh signal measured with $GRAB_{ACh}$ sensors, by testing whether fluorescence responses were sensor, stimulation current, action potential and Ca^{2+} dependent (**Section 3.3.1**). I then tested if ACh release differed between

dorsolateral and ventral striatum (**Section 3.3.2**). Moreover, I tested if ACh was released according to stimulation frequency (**Section 3.3.3**) and if AChE regulated evoked and ambient levels of ACh (**Section 3.3.4**). Finally, I investigated whether ACh release was under tonic GABAergic inhibition (**Section 3.3.5**) and endogenous regulation by DA via D2Rs (**Section 3.3.6**).

3.2 METHODS

3.2.1 Animals and slice preparation

Wild-type C57BL6/J mice (6-7 weeks old, mixed sex) were injected with either AAV5.hSyn.ACh3.0 or AAV9.hSyn.ACh3.0 with a titre of ~ 0.8 x 10^{13} gc/ml as described in **Chapter 2** (**Section 2.1.3**). Mice were sacrificed from 3 weeks after injection and acute *ex vivo* coronal slices containing dorsal and ventral striatum were prepared as previously described in **Section 2.2.1** and **2.3.3**.

For calcium imaging experiments, male and female ChAT-Cre;Ai95D mice were used. These mice were aged 9-12 weeks to match with the $GRAB_{ACh}$ injected ones and expressed GCaMP6f selectively in cholinergic neurons. Acute *ex vivo* striatal slices were prepared as described in **Chapter 2** (**Section 2.2.1** and **2.3.3**).

Recordings were carried out in the dorsolateral striatum (labelled as CPu in the figures) and in the nucleus accumbens core (labelled as NAcC in the figures).

3.2.2 $GRAB_{ACh}$ and calcium imaging

For $GRAB_{ACh}$ imaging experiments involving electrical stimulation, recordings were carried out as described in **Chapter 2** (**Section 2.3.3** and **2.3.4**). To achieve a sampling frequency of 100 Hz, a recording window of active pixels was defined, the camera exposure rate set to 10 ms and the pixels binned 2x2. These acquisition parameters allowed to resolve individual release events in train stimulations, depending on the sensor off kinetics (e.g., **Figure 3.5**). Excitation light consisted of a blue LED (470 nm) and was turned on continuously to record each ACh release event (1p/trains at 5-100 Hz: 2 s; 2 Hz trains: 3.5 s) with an intensity of ~ 10-11 mW. Data were extracted and processed as described in **Section 2.3.5**. For experiments on evoked ACh involving AChE inhibition (**Section 3.3.4**), the duration of the acquisition was increased to 4.5 s given the highly different decay dynamics of the signal. Acquisition time was kept constant in both control and AChE inhibition conditions. To avoid bleaching given the increased exposure time to excitation light, light power

was reduced to ~2mW. Evoked ACh signals in the presence of an AChE inhibitor did not reach baseline (**Figure 3.6A**) and therefore fluorescence responses could not be processed in MATLAB as described in **Section 2.3.5**, for which pre and post-stimulation baseline values are needed to obtain F_0. Hence, $\Delta F/F_0$ was calculated using the average pre-stimulation fluorescence values as F_0.

For $GRAB_{ACh}$ experiments investigating tonic ACh levels or calibration of ACh signal, fluorescence sampling was performed for 1 s intermittently every 30 s. The whole recording window was maintained, and the camera exposure rate was increased to 100 ms, while the excitation light was lowered to ~2 mW, to ensure minimal bleaching. Data were extracted as described in **Chapter 2** (**Section 2.3.5**).

For calcium imaging experiments, recordings were carried out as described in **Chapter 2** (**Section 2.3.3** and **2.3.4**). Given the different nature of the fluorescent indicator, some acquisition parameters were optimised from $GRAB_{ACh}$ imaging. Camera exposure time was increased to 100 ms, which resulted in lower sampling frequency but higher signal-to-noise. Exposure light power was also optimised for GCaMP and set at ~5 mW. Notably, all acquisition parameters were optimised for each fluorescent indicator to ensure low noise levels and minimise baseline fluorescence shift over time (**Chapter 2**, **Figure 2.5**).

For all experiments involving electrical stimulation, stimulation protocols were repeated in duplicates and the order of stimuli was randomised.

For each set of experiments the number of experimental animals was $N \geq 4$. Experiments included in **Figure 3.2E-F** and **Figure3.4C-D** are preliminary observations, with N = 2 and N = 3 respectively. Comparisons for statistical significance were assessed by two-way ANOVA, Student's t-test and regression analysis using GraphPad Prism 9.

3.2.3 Drugs

Drugs were diluted in either dH_2O or DMSO (dymethil sulfoxide) to 1,000x stock aliquots and stored at -20°C. Final drug concentrations (**Table 3.1**) were prepared in aCSF saturated with 95% O_2/ 5% CO_2 right before use.

DRUG	SUPPLIER	ACTION	CONCENTRATION	REFERENCES
Acetylcholine	Bio-Techne	Endogenous ACh	10-50-100 µM	(Jing et al., 2018)
Ambenonium	Bio-Techne	AChE inhibitor	5 µM	(Exley et al., 2008)
Atropine	Tocris Bioscience	mAChR antagonist	2 µM	(Threlfell et al., 2010)
Bicuculline	Abcam	$GABA_A$ receptor antagonist	10 µM	(Lopes et al., 2019)
CGP 55845	Abcam	$GABA_B$ receptor antagonist	4 µM	(Roberts et al., 2020)
Cocaine	Sigma-Aldrich	DAT inhibitor	5 µM	(Condon et al., 2019)
DHβE	Tocris Bioscience	β2-nAChR antagonist	1 µM	(Threlfell et al., 2012)
L-741,626	Abcam	D2R antagonist	1 µM	(Condon et al., 2019)
Quinpirole	Cambridge Bioscience	D2R agonist	5 µM	(Brimblecombe et al., 2019)
Tetrodotoxin	Bio-Techne	Na^+ channel blocker	1 µM	(Threlfell et al., 2012)

Table 3.1. List of drugs used in Chapter 3 with mode of action and references clarifying concentration choice.

3.2.4 Immunohistochemistry and fluorescence microscopy

Immunohistochemistry (IHC) was used to confirm the localisation of $GRAB_{ACh}$ sensors. These sensors are packaged in a viral construct under the human synapsin (hSyn) promoter, which promotes global expression in striatal neurons (Kügler et al., 2003). To better define $GRAB_{ACh}$ localisation in different neuronal subtypes, I looked at co-localisation with markers for MSNs (Ctip2), ChIs (choline acetyltransferase, ChAT), DA neurons (tyrosine hydroxylase, TH) and GFP ($GRAB_{ACh}$). Slices for IHC were either obtained from perfused brains or re-sectioned slices used for recording. Mice for perfusion were injected with $GRAB_{ACh}$ as described in **Chapter 2** (**Section 2.1.3**).

After 3 weeks, mice were anaesthetised with an overdose of pentobarbital and then transcardially perfused with 5 mL of phosphate saline buffer (PBS 1x) and then 5 mL of 4% paraformaldehyde (PFA). Brains were removed and fixed in 4% PFA for 24 hours. Brains were then sectioned with a vibrating microtone (VT1000S, Leica biosystems) into 40-50 µm thick coronal slices containing striatum and midbrain. Sections were stored in PBS 0.05% sodium azide. Alternatively, at the end of each recording, 300 µm thick striatal slices were fixed for 24-48 hours in 4% PFA and then stored in PBS 0.05% sodium azide until re-sectioning. Striatal slices were then re-sectioned using a vibrating microtome (VT1000S, Leica biosystems) to 40-50 µm thickness and stored in PBS 0.05% sodium azide.

For IHC, slices were washed in PBS and then blocked for 90 minutes in a solution of PBS-T (0.5% Trixon X-100) and 10% normal donkey or goat serum. Sections were then incubated in primary antibodies overnight in PBS-T with 2% serum at 4°C. The primary antibodies used were rat anti-Cip2 (1:500, ab18465), goat anti-ChAT (1:200, ab144p), rabbit anti-TH (1:750, ab112). The next day, sections were washed in PBS and incubated in species-appropriate secondary antibodies for 2 hours at room temperature (RT). The secondary antibodies used were, respectively, Alexa 594 goat anti-rat, Alexa 594 donkey anti-goat and Alexa 594 goat anti-rabbit, all used at 1:1000 dilution. All secondaries were on the red shifted spectrum to avoid cross talk with GFP from $GRAB_{ACh}$. Slices were then washed in PBS and mounted on glass slides and cover-slipped using Vectashield (Vector Labs). Coverslips were sealed using nail varnish and stored at 4°C. Images were acquired with an Olympus BX41 microscope with Q-Click cooled monochrome CCD camera (Olympus Medical) and a 10x or 20x objective. Monochrome images were converted to pseudocolored in ImageJ.

3.3 RESULTS

3.3.1 Properties of the ACh signal measured with $GRAB_{ACh}$ sensors in striatal slices

Next generation $GRAB_{ACh}$ sensor, ACh3.0 (Jing et al., 2020), was used in the experiments described in this chapter to measure striatal ACh release. This sensor is based on a M_3-muscarinic ACh receptor (mAChR) linked to a circularly permutated GFP (cpGFP), which converts the ACh-induced change in the receptor conformation into a change in fluorescence (Jing et al., 2020). This optimised $GRAB_{ACh}$ sensor shows high sensitivity, specificity, photostability, temporal and spatial resolution (Jing et al., 2020), making it suitable to measure striatal ACh release dynamics in real-time.

First, I looked at $GRAB_{ACh}$ sensor expression. As discussed in **Chapter 2** (**Section 2.3.1** and **2.3.6**), $GRAB_{ACh}$ sensors are under the hSyn promoter, which targets construct expression exclusively to striatal neurons (Kügler et al., 2003; Haery et al., 2019). Furthermore, in cultured neurons, $GRAB_{ACh}$ sensors localised to the plasma membrane of the soma and were trafficked to dendrites and axons (Jing et al., 2020). In striatal slices, $GRAB_{ACh}$ sensors (labelled by GFP) showed dense neuropil expression (**Figure 3.1A**). No co-labelling with ChAT (marker of ChIs) was seen in the cell body but only in the processes (**Figure 3.1A**). In the midbrain, $GRAB_{ACh}$ sensors were expressed in the SNr but not in the SNc (labelled by TH), consistent with the sensor being expressed by striatal MSNs and carried forward to the midbrain (**Figure 3.1A**). Overall, these data suggest that $GRAB_{ACh}$ sensors are expressed in the predominant striatal neuronal population (MSNs) and globally in neuronal projections, making them suitable to measure bulk extracellular ACh signal. A more thorough anatomical characterisation is needed to determine the exact location in different neuronal compartments and neuronal subtypes.

I then defined the properties of the signal measured with $GRAB_{ACh}$ by examining signal calibration, specificity and working range. As discussed in **Chapter 2** (**Section 2.2**), fluorescent sensors do not provide information about neurotransmitter concentration but only measurement of a change in fluorescence from baseline. To calibrate the fluorescent responses measured with $GRAB_{ACh}$, I briefly

bath-applied known concentration of ACh ($[ACh]_o$, 10-100 µM range) in presence of the AChE inhibitor ambenonium (5 µM). Fluorescence was sampled intermittently every 30 s and in absence of stimulation, while ACh was washed on and off twice (**Figure 3.1B**). Fluorescence changed linearly with $[ACh]_o$ in dorsal striatum (**Figure 3.1C**. Simple linear regression, $R^2 = 0.85$, n ⩾ 16 wash ons/concentration in N ⩾ 5 mice/concentration), suggesting that the size of fluorescent responses is proportional to $[ACh]_o$.

Next, I tested whether the electrically evoked signals measured with $GRAB_{ACh}$ were sensor specific. Given that $GRAB_{ACh}$ are M_3-mAChRs, I used a broad spectrum mAChR antagonist (atropine) to test if the evoked ACh signal would be abolished. Indeed, atropine (2 µM) abolished fluorescent responses in both dorsolateral and ventral striatum (**Figure 3.1D**. Two-tailed paired Student's t-test, control: $p < 0.0001$, atropine: $p = 0.48$, n = 13 slices in N = 6 mice), suggesting sensor specificity.

Finally, to define the sensor working range and the relationship between ACh release and stimulation, I used a range of stimulation currents (0.05-0.9 mA) and durations (20-1000 µs) to electrically evoke ACh release. ACh was released according to stimulation current intensity similarly in both dorsolateral and ventral striatum (**Figure 3.1E**. Two-way ANOVA, current x region interaction: $F(4,50) = 0.68$, $p = 0.60$; current effect: $F(4,50) = 91.39$, $p < 0.0001$; region effect: $F(1,50) = 0.23$, $p = 0.63$, n = 6 slices/region, CPu: N = 5 mice, NAcC: N = 6 mice). ACh release also varied according to stimulation duration, equally in dorsolateral and ventral striatum (**Figure 3.1F**. Two-way ANOVA, pulse width x region interaction: $F(5,60) = 0.25$, $p = 0.93$; pulse width effect: $F(5,60) = 33.40$, $p < 0.0001$; region effect: $F(1,60) = 0.66$, $p = 0.41$, n = 6 slices/region in N = 6 mice/region). Notably, electrical pulses applied at 0.6 mA and lasting 200 µs, known to evoke perimaximal DA release in drug-free conditions (**Chapter 2**, **Section 2.2.3**), also evoked perimaximal ACh release. These parameters were then chosen as standard for experiments where ACh was electrically evoked.

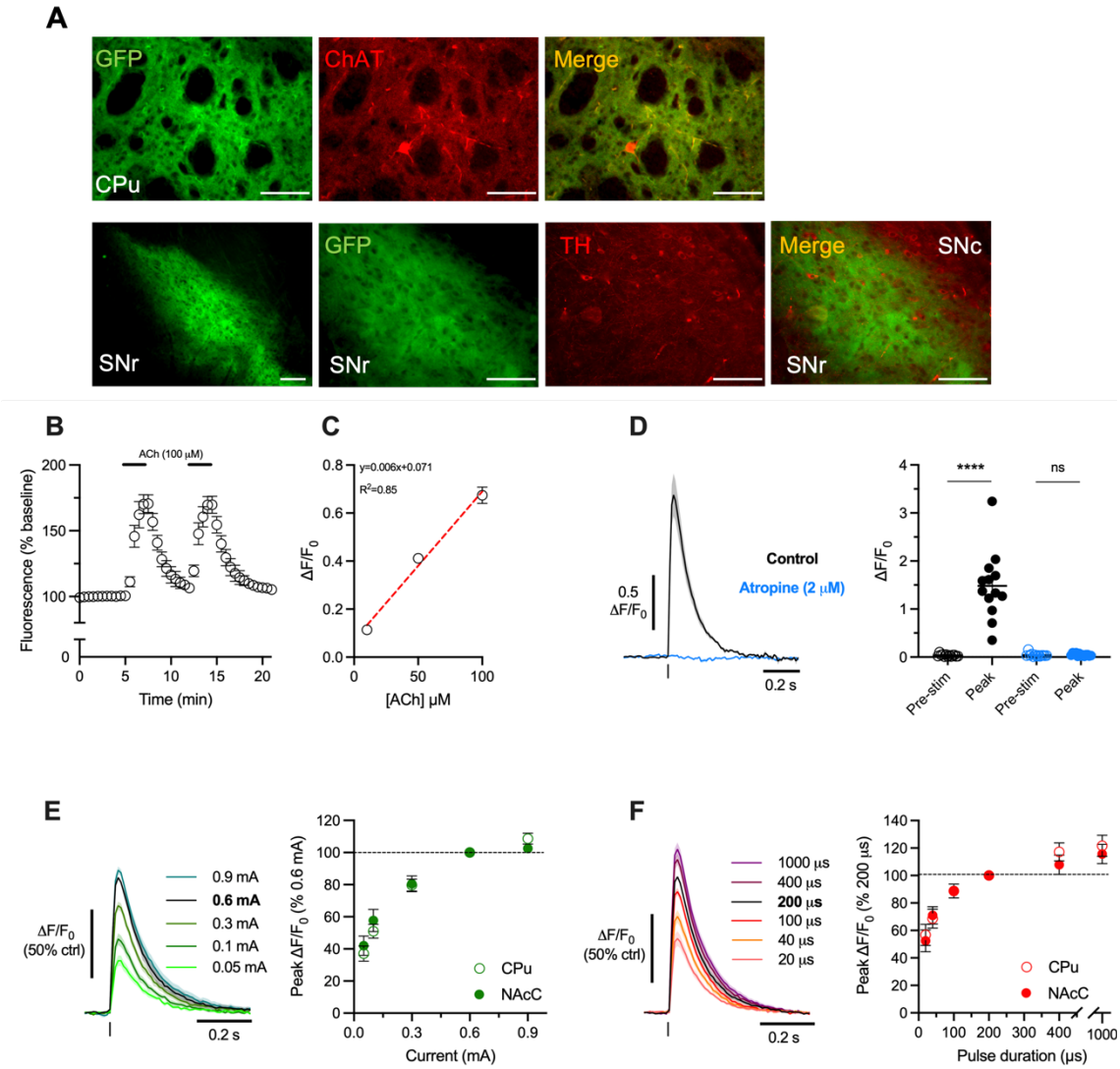


FIGURE 3.1. ACh signal measured with GRAB$_{ACh}$ is sensor specific and stimulation dependent.
(A) *Fluorescence images showing GRAB$_{ACh}$ expression (GFP, green) co-labelled with ChAT (ChIs, red) in striatum and TH (DA neurons, red) in the midbrain. Scale bar indicates 100 µm. GRAB$_{ACh}$ are densely expressed in striatal neuropil and by MSNs.* ***(B)*** *Example of the experimental design used to calibrate ACh signals measured with GRAB$_{ACh}$. ACh (10-100 µM) was washed on for 2 min and washed off for 5 min, while sampling fluorescence every 30 s. Calibrations were performed in presence of ambenonium (5 µM, AChE inhibition) and randomising the order of [ACh]$_o$ washed on, n = 16 wash-ons for 10/100 µM and n = 18 wash-ons for 50 µM in N ⩾ 5 mice/concentration.* ***(C)*** *Mean peak ΔF/F$_0$ (± SEM) plotted against [ACh]$_o$. Fluorescence changes linearly with [ACh]$_o$. Simple linear regression fit in dorsal striatum: R^2 = 0.85.* ***(D)*** *Left, mean (± SEM) ACh transients evoked by single electrical pulses before (control, black) and after washing on atropine (blue). Right, peak ΔF/F$_0$ in the 100 ms prior electrical stimulation (pre-stim) and in the 100 ms post (peak) in control conditions and atropine. There is a significant effect of stimulation in drug-free conditions but not in presence of atropine. Two-tailed paired Student's t-test: control: p < 0.0001; atropine: p = 0.48, n = 13 slices in N = 6 mice. Data are plotted together for dorsolateral and ventral striatum.* ***(E)*** *Left, mean (± SEM) ACh transients evoked by single electrical pulses applied at different intensities. Right, mean peak ΔF/F$_0$ (± SEM) plotted against current intensity in CPu and NAcC. Values are normalised to control current 0.6 mA, routinely used in the lab to elicit perimaximal DA release. ACh release scales according to current intensity, similarly in both regions. Two-way ANOVA: current x region interaction: F (4,50) = 0.68, p = 0.60; current effect: F (4,50) = 91.39, p < 0.0001; region effect: F (1,50) = 0.23, p = 0.63, n = 6 slices/region, CPu: N = 5 mice, NAcC: N = 6 mice.* ***(F)*** *Left, mean (± SEM) ACh transients evoked by single electrical pulses applied with different durations. Right, mean peak ΔF/F$_0$ (± SEM) plotted against pulse duration in CPu and NAcC. Values are normalised to control current 200 µs, routinely used in the lab to elicit perimaximal DA release. ACh release varies according to pulse duration, similarly in dorsal and ventral striatum. Two-way ANOVA: pulse width x region interaction: F (5,60) = 0.25, p = 0.93; pulse width effect: F (5,60) = 33.40, p < 0.0001; region effect: F (1,60) = 0.66, p = 0.41, n = 6 slices/region in N = 6 mice/region.*

Tetrodotoxin (TTX) is a neurotoxin that blocks Na^+ channels, which are involved in driving the ascending phase of action potentials (APs) (Debanne et al., 2011). Therefore, I used TTX to test if evoked ACh measured with $GRAB_{ACh}$ sensors was AP-dependent. Electrically-evoked ACh release was abolished by TTX (1 μM) in dorsolateral and ventral striatum (**Figure 3.2A-B**. Two-tailed paired Student's t-test, control: p = 0.0025, TTX: p = 0.20, n = 9 slices in N = 6 mice). Baseline fluorescence F_0 was unaltered by application of TTX (**Figure 3.2C**. Two-tailed paired Student's t-test, p = 0.79, n = 9 slices in N = 6 mice).

Another property of neurotransmitter release is its calcium dependency. Hence, I examined whether ACh release measured with $GRAB_{ACh}$ was Ca^{2+}-dependent and the relationship between ACh release and extracellular Ca^{2+} concentration ($[Ca^{2+}]_o$). ACh released by single electrical pulses scaled according to $[Ca^{2+}]_o$ (**Figure 3.2D**). Changing $[Ca^{2+}]_o$ alters ACh release probability and so I expect in low $[Ca^{2+}]_o$ ACh release to be lower, while in high $[Ca^{2+}]_o$ I expect it to be higher. Indeed, ACh signals increased according to $[Ca^{2+}]_o$ (**Figure 3.2E-F**). However, the relationship between $[Ca^{2+}]_o$ and ACh release differed depending on the parameter considered to quantify ACh release. The relationship between $[Ca^{2+}]_o$ and area under the curve (AUC) of ACh responses was linear and similar in both ventral and dorsolateral striatum (**Figure 3.2E**. Simple linear regression and slope comparison, CPu: R^2 = 0.91, NAcC: R^2 = 0.96, p = 0.17. CPu 0 mM: n = 7 slices in N = 4 mice, 1.2 mM: n = 6 slices in N = 4 mice; 3.6 mM: n = 4 slices in N = 4 mice. NAcC 0 mM: n = 5 slices in N = 4 mice, 1.2 mM: n = 4 slices in N = 3 mice; 3.6 mM: n = 3 slices in N = 2 mice). On the other hand, measuring peak $\Delta F/F_0$ indicated that ACh release approached a plateau at 3.6 mM $[Ca^{2+}]_o$ in the dorsolateral but not ventral striatum (**Figure 3.2F**. One-phase association and test if one curve fits both datasets, CPu: R^2 = 0.98, NAcC: R^2 = 0.97, p < 0.0001). Altering $[Ca^{2+}]_o$ can also impact on ChI tonic firing (Poppi et al., 2021), which might alter tonic ACh levels in the slice. To test potential changes in baseline ACh tone, I looked at whether changing $[Ca^{2+}]_o$ altered baseline fluorescence F_0. There is no significant change in F_0 driven by lowering or increasing $[Ca^{2+}]_o$ (**Figure 3.2G**.

Two-tailed paired Student's t-test for 2.4-1.2 mM: p = 0.84, n = 9 slices in N = 7 mice, 2.4-3.6 mM: p = 0.067, n = 7 slices in N = 6 mice).

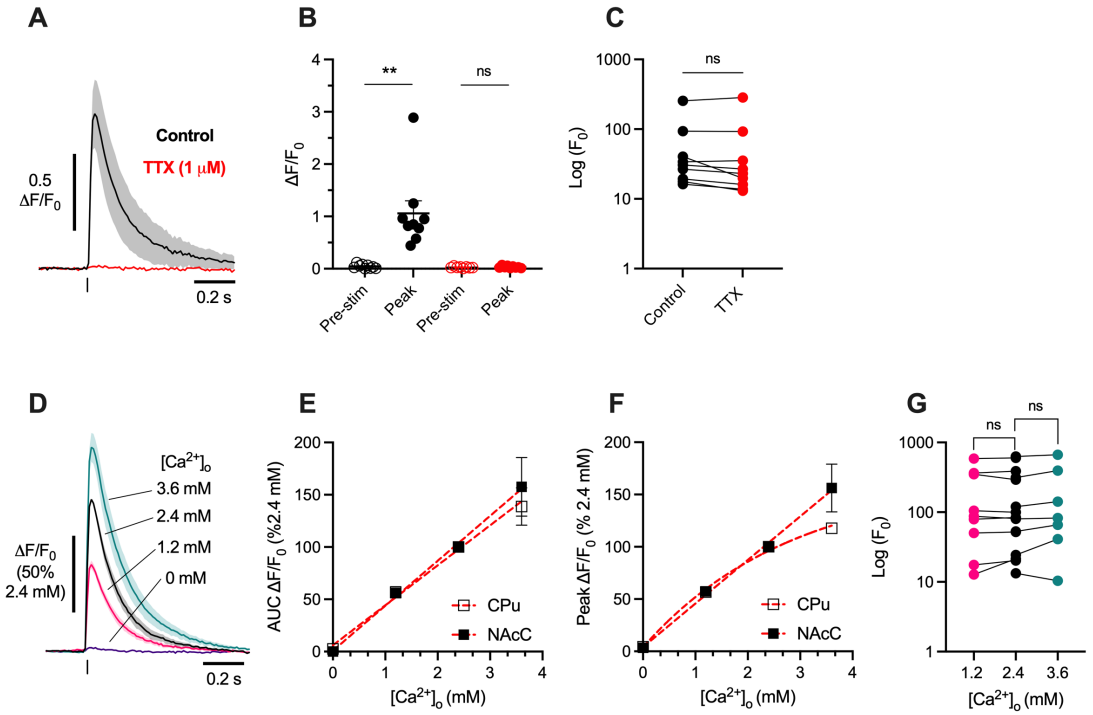


Figure 3.2. ACh release measured with GRAB$_{ACh}$ is action potential and Ca^{2+}-dependent.
(A) *Mean (± SEM) ACh transients evoked by single electrical pulses before (control, black) and after washing on TTX (red), n = 9 slices in N = 6 mice. Data are plotted together for CPu and NAcC.*
(B) *Peak $\Delta F/F_0$ in the 100 ms prior electrical stimulation (pre-stim) and in the 100 ms post stimulation (peak) in control drug-free conditions (black) and TTX (red). There is a significant effect of stimulation in drug-free conditions but not in presence of TTX, suggesting that the signal is AP-dependent. Two-tailed paired Student's t-test: control: p = 0.0025, TTX: p = 0.20, n = 9 slices in N = 6 mice. Data are plotted together for CPu and NAcC.*
(C) *Baseline fluorescence F_0 in control (black) and TTX (red). F_0 was not altered by TTX wash on. Two-tailed paired Student's t-test: p = 0.79; n = 9 slices in N = 6 mice. Data are plotted together for CPu and NAcC.*
(D) *Mean (± SEM) ACh transients evoked by single electrical pulses in different $[Ca^{2+}]_o$ in CPu and NAcC. Experiments were carried out starting in control Ca^{2+} levels (2.4 mM) and then washing on aCSF with one altered $[Ca^{2+}]_o$, so that only two $[Ca^{2+}]_o$ conditions were tested in one site. Each condition is normalised to its true control (2.4 mM Ca^{2+}).*
(E) *Mean (± SEM) AUC $\Delta F/F_0$ plotted against $[Ca^{2+}]_o$. There is a linear relationship between Ca^{2+} and AUC of ACh release, which describes both CPu and NAcC. Simple linear regression and slope comparison: CPu: R^2 = 0.91, NAcC: R^2 = 0.96, p = 0.17; CPu 0mM: n = 7 slices in N = 4 mice, 1.2 mM: n = 6 slices in N = 4 mice, 3.6 mM: n = 4 slices in N = 4 mice. NAcC 0mM: n = 5 slices in N = 4 mice, 1.2 mM: n = 4 slices in N = 3 mice, 3.6 mM: n = 3 slices in N = 2 mice.*
(F) *Mean (± SEM) peak $\Delta F/F_0$ plotted against $[Ca^{2+}]_o$. Peak fluorescence change tends to plateau at high Ca^{2+} (3.6 mM) in CPu but not NAcC. One-phase association and test if one curve fits both datasets: CPu: R^2 = 0.98, NAcC: R^2 = 0.97, p < 0.0001. Number of slices and mice for each condition is the same as above.*
(G) *Baseline fluorescence F_0 in all $[Ca^{2+}]_o$ conditions. F_0 is unaltered by $\Delta[Ca^{2+}]_o$. Two-tailed paired Student's t-test for paired experiments: 2.4 mM to 1.2 mM: p = 0.84, 2.4 mM to 3.6 mM: p = 0.067; for 2.4 mM to 1.2 mM n = 9 slices in N = 7 mice, for 2.4 mM to 3.6 mM n = 7 slices in N = 6 mice. Data are plotted together for CPu and NAcC.*
The data here represented were collected using AAV5.hSyn.ACh3.0.

3.3.2 ACh release differs in dorsolateral and ventral striatum

Dorsal and ventral striatum are functionally heterogeneous regions, with differences in the activity levels, density, and spatial organisation of ChIs (Matamales et al., 2016). Therefore, I investigated potential regional differences in evoked ACh release by measuring ACh release from dorsolateral (CPu) and ventral (NAcC) striatum of the same injected mouse. I examined the size of ACh transients, the half-life of the signals and basal fluorescence F_0.

Single pulse-evoked ACh release was higher in peak size in dorsolateral compared to ventral striatum (**Figure 3.3B**. Two-tailed unpaired Student's t-test, p = 0.0042. CPu: n = 58 stimuli, NAcC: n = 81 stimuli in N = 13 mice). AUC of ACh signals was also bigger in dorsolateral (CPu) compared to ventral striatum (NAcC) (**Figure 3.3C**. Two-tailed unpaired Student's t-test, p=0.011). To test potential differences in ACh clearance between regions, I looked at the half-lives of the ACh transients. Half-lives did not significantly differ in dorsolateral and ventral striatum (**Figure 3.3D**. Two-tailed unpaired Student's t test, p=0.095). Dorsolateral striatum also presented higher baseline fluorescence F_0 (**Figure 3.3E.** Two-tailed unpaired Student's t test, p=0.0006). In this case, differences in baseline fluorescence could be a function of regional differences in ACh tone or indicate different levels of expression of the sensor (**Section 3.4.2**).

I then looked at differences in the recovery profile of ACh release in both regions by stimulating with pairs of single electrical pulses at increasing intervals (0.5 s to 20 s, **Figure 3.3F-G**). Overall, the dorsolateral striatum (CPu) had faster recovery than NAcC (**Figure 3.3H**. One-phase association and test if one curve fits both datasets, CPu: $R^2 = 0.94$, NAcC: $R^2 = 0.94$, $p < 0.0001$. CPu: n = 6 slices in N = 4 mice, NAcC: n = 5 slices in N = 5 mice).

Overall, these findings suggest that ACh release is higher and recovers faster in the dorsolateral compared to ventral striatum.

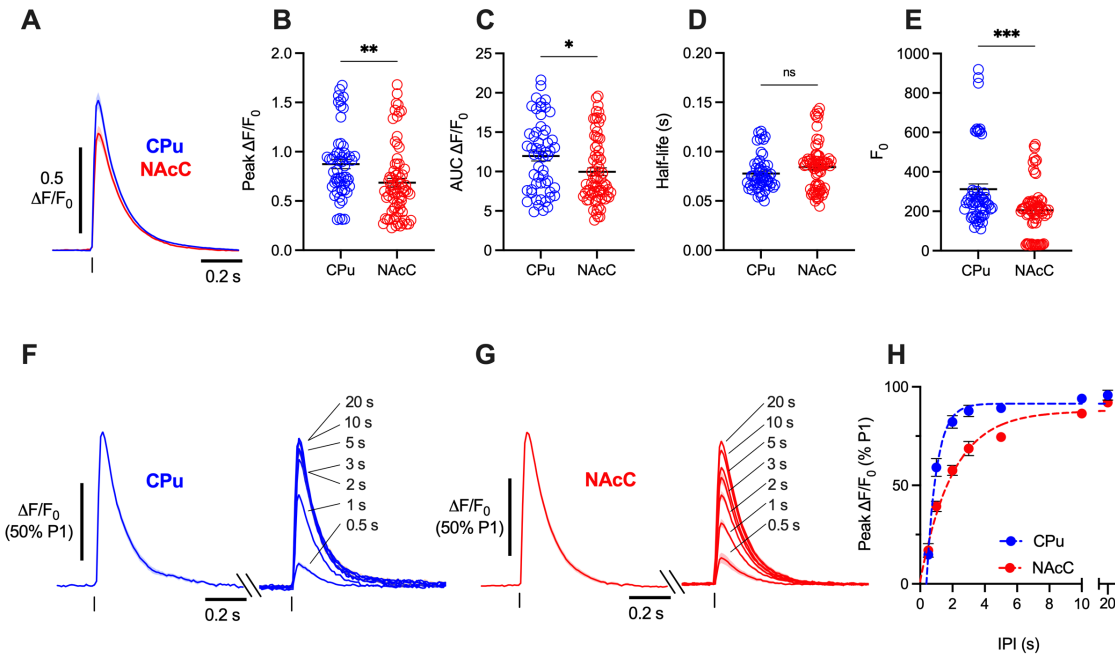


Figure 3.3. ACh release is higher and recovers faster in dorsolateral compared to ventral striatum.
(A) *Mean (± SEM) ACh transients evoked by single electrical pulses in dorsolateral (CPu) and ventral (NAcC) striatum. Dorsolateral or ventral striatal recordings were performed in slices from the same animal, which was bilaterally injected. Each individual single stimulation is considered, CPu: n = 58 stimuli, NAcC: n = 81 stimuli in N = 13 mice.*
(B) *Peak ΔF/F₀ in dorsolateral (CPu) and ventral (NAcC) striatum. ACh release measured by peak size is higher in dorsolateral striatum (CPu). Two-tailed unpaired Student's t-test: p = 0.0042. CPu: n = 58 stimuli, NAcC: n = 81 stimuli in N = 13 mice.*
(C) *AUC ΔF/F₀ in dorsolateral (CPu) and ventral (NAcC) striatum. ACh release measured with AUC is higher in dorsolateral striatum (CPu). Two-tailed unpaired Student's t-test: p = 0.011. CPu: n = 58 stimuli, NAcC: n = 81 stimuli in N = 13 mice.*
(D) *Half-lives of ACh transients in dorsolateral (CPu) and ventral (NAcC) striatum. Half-lives were calculated from the falling phases of ACh transients and do not significantly differ between regions. Two-tailed unpaired Student's t-test: p = 0.095. CPu: n = 58 stimuli, NAcC: n = 81 stimuli in N = 13 mice.*
(E) *Baseline fluorescence F₀ in dorsolateral (CPu) and ventral (NAcC) striatum. Dorsolateral striatum presents higher F₀. Two-tailed unpaired Student's t-test: p = 0.0006. CPu: n = 58 stimuli, NAcC: n = 81 stimuli in N = 13 mice.*
(F) *Mean (± SEM) ACh transients evoked by pairs of electrical pulses at increasing intervals (0.5-20 s) in dorsolateral striatum (CPu). Data are normalised to the first stimulus given (P1), n = 6 slices in N = 4 mice.*
(G) *Mean (± SEM) ACh transients evoked by pairs of electrical pulses at increasing intervals (0.5-20 s) in NAcC. Data are normalised to the first pulse, n = 5 slices in N = 5 mice.*
(H) *Mean peak ΔF/F₀ (± SEM) plotted against inter pulse interval (IPI) in dorsolateral (CPu) and ventral (NAcC) striatum. Data are normalised to the first pulse given. ACh release recovery differs between dorsolateral (CPu) and ventral (NAcC) striatum. One-phase association and test if one curve fits both datasets: CPu: $R^2 = 0.94$, NAcC: $R^2 = 0.94$, $p < 0.0001$. CPu: n = 6 slices in N = 4 mice, NAcC: n = 5 slices in N = 5 mice.*
The data here represented were collected using AAV5.hSyn.ACh3.0.

3.3.3. ChI activation and ACh release follow stimulation frequency

ChIs display multiple firing patterns *in vivo*. They are tonically active neurons firing APs at frequencies of 2-10 Hz (Bolam et al., 1984; Wilson et al., 1990; Bennett and Wilson, 1999b; Goldberg and Reynolds, 2011). ChIs also presents irregular and/or bursting firing patterns, consisting of 3-5 spikes with highly variable interspike

intervals (range of ~ 10-25 Hz) (Bennett and Wilson, 1999a; Sharott et al., 2012). Furthermore, ChIs encode reward-related and salient event by pausing their firing activity (Morris et al., 2004; Joshua et al., 2008; Goldberg and Reynolds, 2011). Such pause response can be flanked by high frequency bursts of APs (Morris et al., 2004; Joshua et al., 2008). Given that changing in ChI firing is a fundamental aspect of ACh signalling in striatum, I set out to investigate if ACh is released following differential activation of ChIs.

To test whether activity in ChIs follows stimulation frequency, I turned to calcium imaging of ChIs using slices from ChATCre;Ai95D mice (which express GCaMP6f selectively in ChIs). ChI activation followed stimulation frequency in dorsolateral (**Figure 3.4A-B**. Simple linear regression and slope significantly non-zero, $R^2 = 0.68$, $p < 0.0001$, n = 5 slices in N = 5 mice) and ventral striatum (**Figure 3.4C-D**. Simple linear regression and slope significantly non-zero, $R^2 = 0.68$, $p = 0.0008$, n = 3 slices in N = 3 mice).

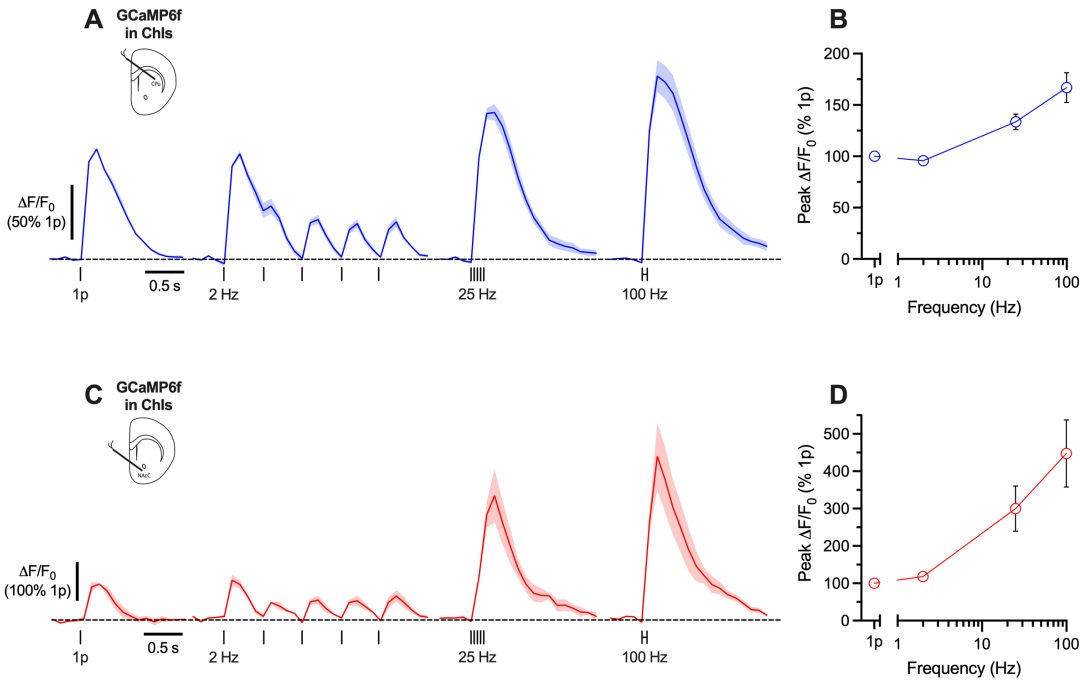


FIGURE 3.4. ChI activation measured with calcium imaging follows stimulation frequency.
(A) *Mean (± SEM) Ca^{2+} transients evoked by single electrical pulses (1p) or trains of 5 pulses at 2-25-100 Hz in dorsolateral striatum (CPu). Data are normalised to single pulse, n = 5 slices in N = 5 mice.*
(B) *Mean peak $\Delta F/F_0$ (± SEM) plotted against stimulation frequency in dorsolateral striatum (CPu). Data are normalised to single pulse. ChI activation varies according to stimulation frequency. Simple linear regression (curve not shown) and slope significantly non-zero: $R^2 = 0.68$, $p < 0.0001$, n = 5 slices in N = 5 mice.*
(C) *Mean (± SEM) Ca^{2+} transients evoked by single electrical pulses or trains of 5 pulses at 2-25-100 Hz in NAcC. Data are normalised to single pulse, n = 3 slices in N = 3 mice.*
(D) *Mean peak $\Delta F/F_0$ (± SEM) plotted against stimulation frequency in NAcC. Data are normalised to single pulse. ChI activation varies according to stimulation frequency. Simple linear regression (curve not shown) and slope significantly non-zero: $R^2 = 0.68$, $p = 0.0008$, n = 3 slices in N = 3 mice.*

To test whether ACh is released according to stimulation frequency, I used $GRAB_{ACh}$ to measure ACh release and stimulated with trains of 5 pulses (5p) at low "tonic-like" frequencies (2-10 Hz), or high "burst-like" frequencies (25-100 Hz). For low frequency stimulation, it was possible to resolve individual release events in the train (**Figure 3.5A**), suggesting that ACh was released according to stimulation. There were no regional differences in ACh released by 2 Hz trains (**Figure 3.5B**. Two-way ANOVA, stim number x region interaction: F (3,36) = 0.34, p = 0.79; stim number effect: F (3,36) = 7.28 p = 0.0006; region effect: F (1,36) = 1.47, p = 0.23. CPu: n = 6 slices in N = 4 mice, NAcC: n = 5 slices in N = 5 mice). There was higher ACh re-release in the NAcC following stimulation with 5 and 10 Hz trains (**Figure 3.5C**. Two-way ANOVA, stim number x region interaction: F (3,36) = 0.49, p = 0.68; stim number effect: F (3,36) = 1.113, p = 0.35, region effect: F (1,36) = 6.25, p = 0.017. CPu: n = 6 slices in N = 4

mice, NAcC: n = 5 slices in N = 5 mice). It was not possible to quantify ACh released by individual pulses in 10 Hz trains because there was still significant summation even after subtraction of the first pulse, due to $GRAB_{ACh}$ sensor off kinetics (Jing et al., 2020).

When I stimulated with high frequency trains, I observed regional differences in how the signal summates extracellularly (**Figure 3.5D**). Hence, information on whether ACh is released according to stimulation frequency were dependent on the metric of release used. In the ventral striatum (NAcC), the peak size of fluorescence responses increased according to stimulation frequency (**Figure 3.5E**. Two-way ANOVA, frequency x region interaction: $F(3,36) = 7.14$, $p = 0.0007$; frequency effect: $F(3,36) = 33.43$, $p < 0.0001$; region effect: $F(1,36) = 21.21$, $p < 0.0001$. Bonferroni multiple comparisons, 1p: $p > 0.99$; 25 Hz: $p > 0.99$; 40 Hz: $p = 0.14$; 100 Hz: $p < 0.0001$. CPu: n = 5 slices in N = 4 mice, NAcC: n = 6 slices in N = 5 mice). On the other hand, in the dorsolateral striatum (CPu), the AUC increased according to stimulation frequency (**Figure 3.5F**. Two-way ANOVA, frequency x region interaction: $F(3,47) = 4.40$, $p = 0.0082$; frequency effect: $F(3,47) = 97.05$, $p < 0.0001$; region effect: $F(1,47) = 16.95$, $p = 0.0002$. Bonferroni multiple comparisons, 1p: $p > 0.99$; 25 Hz: $p > 0.99$; 40 Hz: $p = 0.045$; 100 Hz: $p = 0.0006$. CPu: n = 5 slices in N = 4 mice, NAcC: n = 6 slices in N = 5 mice). These differences could reflect differential expression of the sensor, different ACh clearance or synchronous and asynchronous release contributions.

Overall, these data indicate that ACh is released according to stimulation frequency, fundamental to interpret the regulation of ACh-driven DA (**Chapter 4**).

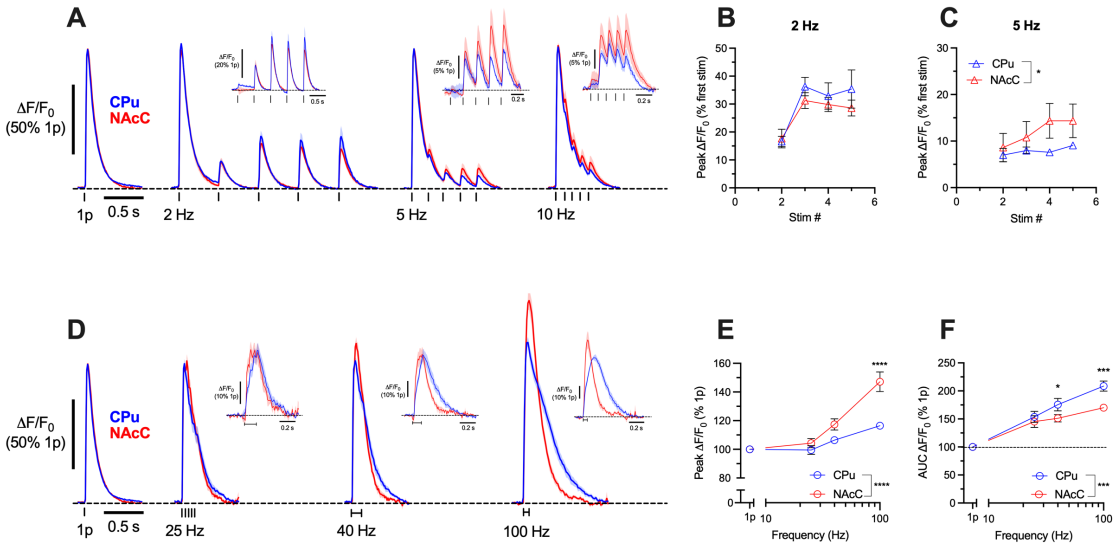


FIGURE 3.5. ACh is released according to stimulation frequency in dorsolateral and ventral striatum.

(A) *Mean (± SEM) ACh transients evoked by single electrical pulses (1p) or trains of 5p at 2-5-10 Hz in dorsolateral (CPu, blue) and ventral (NAcC, red) striatum. Data are normalised to single pulse for each region. ACh is released according to stimulation frequency and it is possible to resolve individual release events in the train. First pulse subtracted transients are shown in the inset. CPu: n = 6 slices in N = 4 mice, NAcC: n = 5 slices in N = 5 mice.*

(B) *Mean peak ΔF/F₀ (± SEM) plotted against stimulus number (stim #) for 2 Hz trains in dorsolateral (CPu, blue) and ventral (NAcC, red) striatum. Each peak was calculated from first pulse subtracted transients and normalised to the first pulse in the train. There are no regional differences in ACh release profiles upon 2 Hz stimulation. Two-way ANOVA: stim number x region interaction: F (3,36) = 0.34, p = 0.79; stim number effect: F (3,36) = 7.28, p = 0.0006; region effect: F (1,36) = 1.47, p = 0.23. CPu: n = 6 slices in N = 4 mice, NAcC: n = 5 slices in N = 5 mice.*

(C) *Mean peak ΔF/F₀ (± SEM) plotted against stimulus number (stim #) for 5 Hz trains in dorsolateral (CPu, blue) and ventral (NAcC, red) striatum. Each peak was calculated from first pulse subtracted transients and normalised to the first pulse in the train. There are regional differences in ACh release profiles at 5 Hz stimulation. Two-way ANOVA: stim number x region interaction: F (3,36) = 0.49, p = 0.68; stim number effect: F (3,36) = 1.113, p = 0.35, region effect: F (1,36) = 6.25, p = 0.017. CPu: n = 6 slices in N = 4 mice, NAcC: n = 5 slices in N = 5 mice.*

(D) *Mean (± SEM) ACh transients evoked by single electrical pulses or trains of 5p at 25-40-100 Hz in dorsolateral (CPu, blue) and ventral (NAcC, red) striatum. Data are normalised to single pulse. ACh is released according to stimulation frequency, but different release metrics report this effect in the two regions. First pulse subtracted transients are shown in the inlet. CPu: n = 5 slices in N = 4 mice, NAcC: n = 6 slices in N = 5 mice.*

(E) *Mean peak ΔF/F₀ (± SEM) plotted against stimulation frequency in dorsolateral (CPu, blue) and ventral (NAcC, red) striatum. Data are normalised to single pulses. In the NAcC, peak size increased according to stimulation frequency more than in the CPu. Two-way ANOVA: frequency x region interaction: F (3,36) = 7.14, p = 0.0007; frequency effect: F (3,36) = 33.43, p < 0.0001; region effect: F (1,36) = 21.21, p < 0.0001. Bonferroni multiple comparisons: 1p: p > 0.99; 25 Hz: p > 0.99; 40 Hz: p = 0.14; 100 Hz: p < 0.0001. CPu: n = 5 slices in N = 4 mice, NAcC: n = 6 slices in N = 5 mice.*

(F) *Mean AUC ΔF/F₀ (± SEM) plotted against stimulation frequency in dorsolateral (CPu, blue) and ventral (NAcC, red) striatum. Data are normalised to single pulses. In the CPu, AUC size increased according to stimulation frequency more than in the NAcC. Two-way ANOVA: frequency x region interaction: F (3,47) = 4.40, p = 0.0082; frequency effect: F (3,47) = 97.05, p < 0.0001; region effect: F (1,47) = 16.95, p = 0.0002. Bonferroni multiple comparisons: 1p: p > 0.99; 25 Hz: p > 0.99; 40 Hz: p = 0.045; 100 Hz: p = 0.0006. CPu: n = 5 slices in N = 4 mice, NAcC: n = 6 slices in N = 5 mice. The data here represented were collected using AAV5.hSyn.ACh3.0.*

3.3.4 Spatiotemporal dynamics of tonic and evoked ACh release are regulated by acetylcholinesterase

AChE is a highly efficient enzyme, is particularly enriched in striatum and is in a key position to regulate the extracellular dynamics of ACh (Descarries et al., 1997). To test the role of AChE in regulating evoked ACh release, I used an AChE inhibitor (ambenonium) and stimulated with single electrical stimuli or trains of 5p at "tonic/phasic" frequencies (2/25 Hz). AChE inhibition greatly altered ACh release profiles in dorsolateral striatum (**Figure 3.6A**). The peak size of ACh release evoked by single pulses was decreased in ambenonium (**Figure 3.6B**. Two-tailed paired Student's t-test, $p = 0.0027$, $n = 5$ slices in $N = 4$ mice). The duration ACh transients evoked by single pulses was increased as showed by an increase in the half-lives (**Figure 3.6C**. Two-tailed paired Student's t-test, $p = 0.0005$, $n = 5$ slices in $N = 4$ mice). The 5p:1p ratio was increased upon high frequency stimulation in presence of the AChE inhibitor ambenonium (**Figure 3.6D**. Two-way ANOVA, frequency x drug interaction: $F(1,8) = 138.6$, $p < 0.0001$; drug effect: $F(1,8) = 123.3$, $p < 0.0001$; frequency effect: $F(1,8) = 204.1$, $p < 0.0001$. Bonferroni multiple comparisons, 2 Hz: $p > 0.99$; 25 Hz: $p < 0.0001$, $n = 5$ slices in $N = 4$ mice), suggesting that AChE limits ACh frequency sensitivity in the dorsolateral striatum. Blocking AChE also promoted an increase in F_0 (**Figure 3.6E**. Two-tailed unpaired Student's t-test, $p = 0.0008$, $n = 5$ slices in $N = 4$ mice), which could indicate an increase in ACh tonic levels. To further assess how changes in F_0 might impact on fluorescent responses, I plotted ΔF against F_0 in drug-free (control) and in ambenonium. In control conditions, there is a linear relationship between ΔF and F_0 and this relationship changes and becomes less steep upon ambenonium wash on (**Figure 3.6F**. Simple linear regression and slope comparison, control: $R^2 = 0.67$, ambenonium: $R^2 = 0.45$, $p < 0.0001$, $n = 35$ stimulations/condition), suggesting that the changes in F_0 after ambenonium wash on are not sufficient to explain the concomitant changes in fluorescent responses.

I then tested whether AChE regulated ambient levels of ACh. Without stimulating, I intermittently sampled fluorescence change upon wash on of the AChE inhibitor ambenonium (5 μM) in presence/absence of TTX (1 μM), to determine AP

dependency. AChE inhibition significantly increased fluorescent responses in a TTX-sensitive way, suggesting that AChE limits tonic ambient ACh levels (**Figure 3.6G**. Two-way ANOVA, time x drug interaction: $F(39, 440) = 3.13$, $p < 0.0001$; drug effect: $F(1, 440) = 220.2$, $p < 0.0001$; time effect: $F(39, 440) = 9.65$, $p < 0.0001$. Control: n = 7 slices in N = 6 mice, TTX: n = 6 slices in N = 5 mice).

Overall, these data indicate that AChE limits the duration and frequency sensitivity of evoked ACh signals, together with regulating striatal ACh tone.

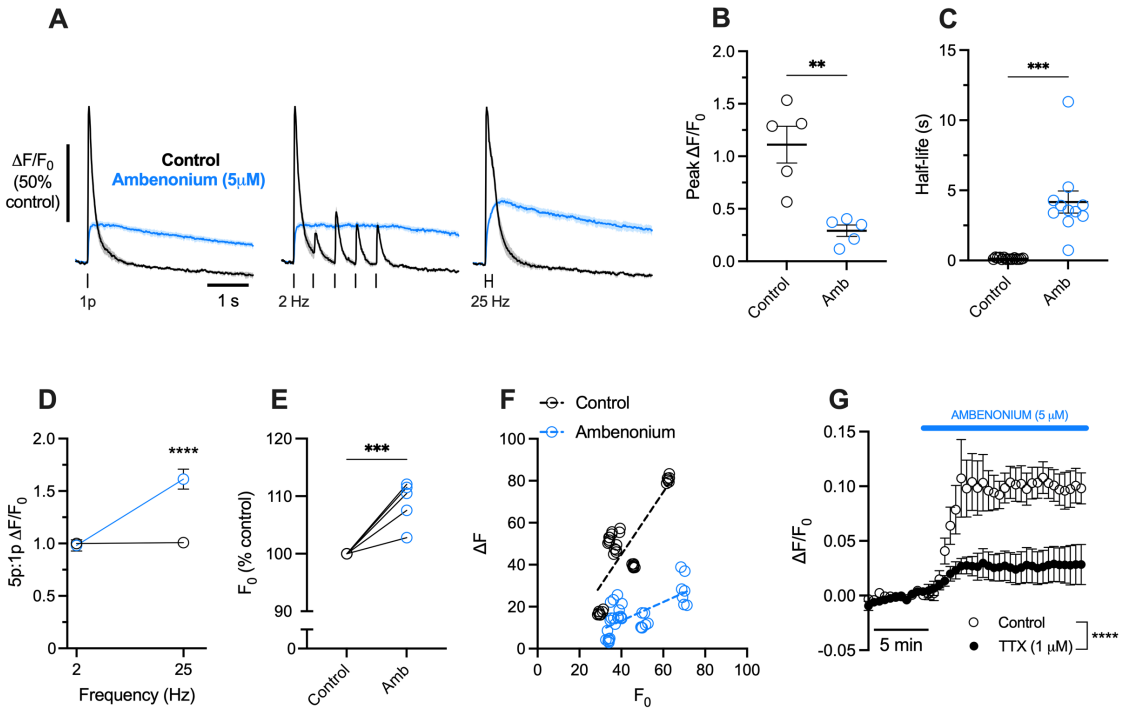


FIGURE 3.6. AChE regulates evoked and tonic ACh release in dorsolateral striatum.
(A) *Mean (± SEM) ACh transients evoked by single electrical pulses (1p) or trains of 5p at 2-25 Hz in control (drug-free, black) and ambenonium (5 μM, blue), an AChE inhibitor. Data are normalised to single pulse in control conditions. AChE inhibition causes a drop in the peak of the transient and an increase in the duration of the ACh signal, n = 5 slices in N = 4 mice.*
(B) *Mean peak ΔF/F₀ (± SEM) of single pulse-evoked transients. Ambenonium causes a drop in peak size. Two-tailed paired Student's t test: p = 0.0027, n = 5 slices in N = 4 mice.*
(C) *Half-lives of 1p-evoked transients calculated from their falling phases. Ambenonium enhanced the half-lives of ACh signal. Two-tailed paired Student's t-test: p = 0.0005, n = 5 slices in N = 4 mice.*
(D) *Mean ΔF/F₀ 5p:1p ratios (± SEM) in control conditions and AChE inhibition. Ratios at high stimulation frequency (25 Hz) are increased in ambenonium, suggesting that AChE inhibition promotes frequency sensitivity of ACh release. Two-way ANOVA: frequency x drug interaction: F (1,8) = 138.6, p < 0.0001; drug effect: F (1,8) = 123.3, p < 0.0001; frequency effect: F (1,8) = 204.1, p < 0.0001. Bonferroni multiple comparisons: 2 Hz: p > 0.99; 25 Hz: p < 0.0001, n = 5 slices in N = 4 mice.*
(E) *Baseline fluorescence F₀ normalised to control conditions (drug-free). Ambenonium significantly increases F₀. Two-tailed unpaired Student's t-test: p = 0.0008, n = 5 slices in N = 4 mice.*
(F) *ΔF plotted against F₀ for each stimulation in/out of ambenonium. The relationship between ΔF and F₀ in the two conditions segregates in two different populations. Simple linear regression and slope comparison: control: R^2 = 0.67; ambenonium: R^2 = 0.45, p < 0.0001, n = 35 stimulations per condition.*
(G) *Mean (± SEM) ΔF/F₀ sampled every 30 s in presence/absence of TTX. Change in fluorescence responses from baseline driven by AChE application were calculated as ΔF/F₀, where F₀ corresponds to pre-drug basal fluorescence. Inhibition of AChE with ambenonium (5 μM) increases ACh levels in a TTX-dependent way, suggesting that AChE limits ambient ACh levels arising from APs. Two-way ANOVA: time x drug interaction: F (39, 440) = 3.13, p < 0.0001; drug effect: F (1, 440) = 220.2, p < 0.0001; time effect: F (39, 440) = 9.65, p < 0.0001. Control: n = 7 slices in N = 6 mice, TTX: n = 6 slices in N = 5 mice.*
The data here represented were collected using AAV5.hSyn.ACh3.0 for panel (A-F) and AAV5.hSyn.ACh3.0 or AAV9.hSyn.ACh3.0 for panel (G).

3.3.5. Antagonism of GABA receptors promotes ACh release signals

The striatum is highly GABAergic and in both dorsal and ventral regions there is ambient GABA tone (Ade et al., 2008; Kirmse et al., 2008, 2009), which inhibits DA

release (Lopes et al., 2019; Roberts et al., 2020). Here, I tested whether striatal ACh release was under tonic GABAergic inhibition by looking at the effect of $GABA_A$ and $GABA_B$ receptor antagonists on single pulse-evoked ACh release. Wash on of GABA receptor antagonists (bicuculline: 10 μM, CGP 55845: 4 μM) increased the size (measured by AUC) of 1p-evoked ACh release in dorsolateral striatum (**Figure 3.7A**. Two-way ANOVA, time x drug interaction: $F(110,444) = 6.90$, $p < 0.0001$; time effect: $F(110,444) = 210.7$, $p < 0.0001$; drug effect: $F(1,444) = 479.4$, $p < 0.0001$, n = 5 slices in N = 5 mice). Striatal DA is under tonic GABAergic inhibition and so wash on of GABA receptor antagonists will increase single pulse DA release, which could potentially act at D2Rs on ChIs to inhibit ACh release, limiting the effects of GABA receptor antagonists on ACh release. To test whether the effect of GABA receptors antagonism on ACh release was limited by the increase in DA levels, I blocked D2Rs with the antagonist L-741,626 (1 μM). In D2R block, single pulse-evoked ACh release is increased upon antagonism of GABA receptors (**Figure 3.7B**. Two-way ANOVA, time x drug interaction: $F(109,440) = 11.77$, $p < 0.0001$; time effect: $F(109,440) = 158.2$, $p < 0.0001$; drug effect: $F(1,440) = 984.5$, $p < 0.0001$, n = 5 slices in N = 4 mice). D2R antagonism slightly promotes the effect of GABA receptor antagonists on ACh release, suggesting that the increase of DA levels upon relief of tonic GABAergic inhibition might feebly limit the effect of GABA receptor antagonism on ACh release (**Figure 3.7C**. Two-way ANOVA, time x drug interaction: $F(11,96) = 0.74$, $p = 0.69$; time effect: $F(11,96) = 15.84$, $p < 0.0001$; drug effect: $F(1,96) = 6.47$, $p = 0.012$. Control: n = 5 slices in N = 5 mice, L-741,626: n = 5 slices in N = 4 mice).

In the NAcC, AUC of 1p-evoked ACh transients was also enhanced by GABA receptor antagonism (**Figure 3.7D**. Two-way ANOVA, time x drug interaction: $F(110,444) = 3.62$, $p < 0.0001$; time effect: $F(110,444) = 92.11$, $p < 0.0001$; drug effect: $F(1,444) = 336.6$, $p < 0.0001$, n = 5 slices in N = 5 mice). The effect of washing on GABA receptor antagonists on ACh release was analogous in ventral and dorsolateral striatum (**Figure 3.7E**. Two-way ANOVA, time x region interaction: $F(11,96) = 0.088$, $p > 0.99$; time effect: $F(11,96) = 9.43$, $p < 0.0001$; region effect: $F(1,96) = 0.058$, $p = 0.81$, n = 5 slices in N = 5 mice). Overall, these findings suggest that the size of ACh

release transients (measured by AUC) is limited by GABA acting at $GABA_A$ and $GABA_B$ receptors, in dorsolateral and ventral striatum.

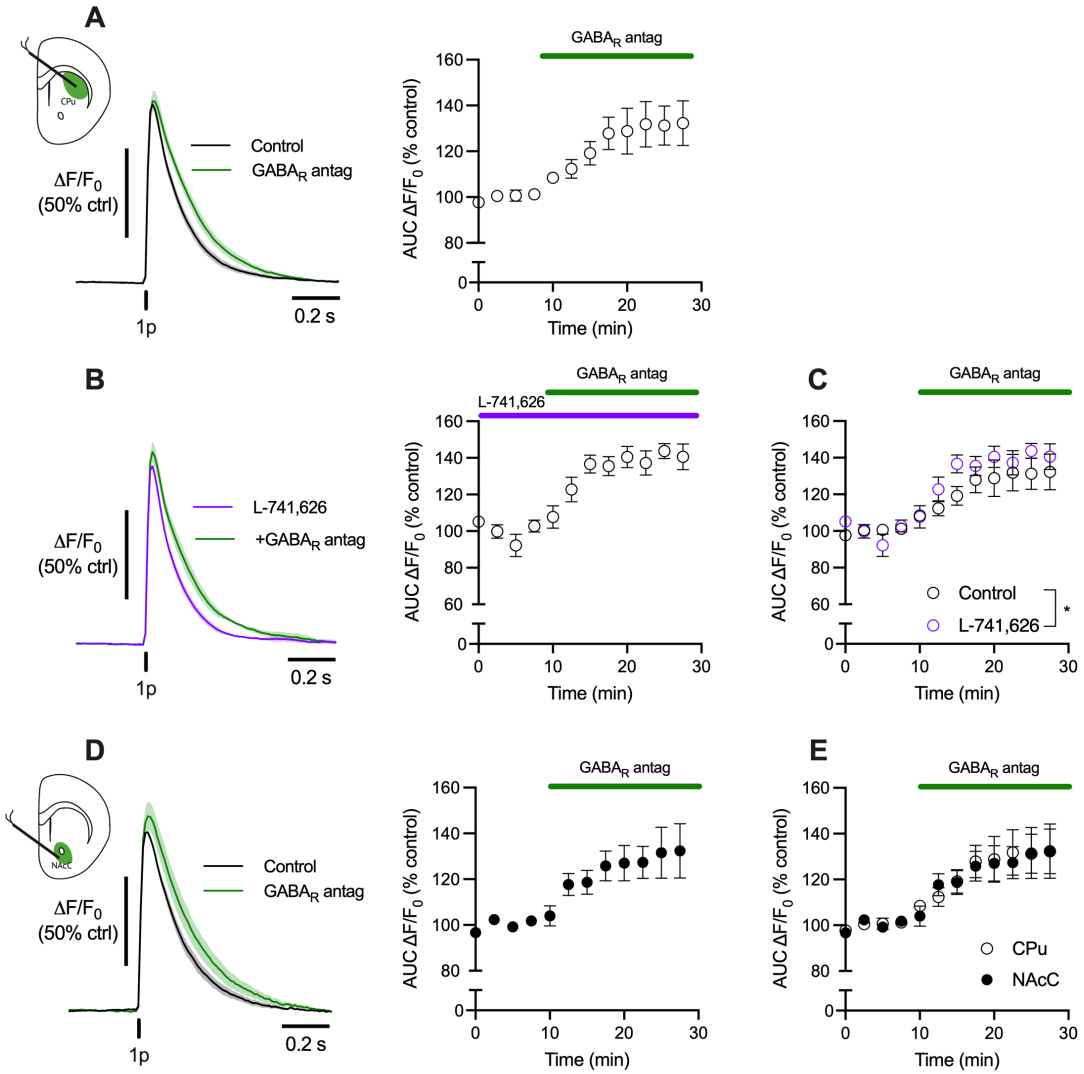


FIGURE 3.7. AUC of ACh transients is increased upon antagonism of $GABA_A$ and $GABA_B$ receptors in ventral and dorsolateral striatum.

(A) *Left, mean (± SEM) ACh transients in dorsolateral striatum (CPu) evoked by single electrical pulses (1p) in control (drug-free, black) and in presence of $GABA_A$ and $GABA_B$ receptor antagonists ($GABA_R$ antag) , respectively bicuculline (10 μM) and CGP 55845 (4 μM). Transients are normalised to 1p control. Right, mean AUC $\Delta F/F_0$ (± SEM) plotted against time. Data are normalised to pre-wash on baseline (indicated as control). AUC is increased by GABA receptor block. Two-way ANOVA: time x drug interaction: $F(110,444) = 6.90$, $p < 0.0001$; time effect: $F(110,444) = 210.7$, $p < 0.0001$; drug effect: $F(1,444) = 479.4$, $p < 0.0001$, n = 5 slices in N = 5 mice.* ***(B)*** *Left, mean (± SEM) ACh transients in dorsolateral striatum (CPu) evoked by 1p in D2R antagonism (L-741-626 1 μM, purple) and in presence of GABA receptor antagonists. Transients are normalised to 1p control (L-741,626). Right, mean AUC $\Delta F/F_0$ (± SEM) plotted against time. Data were normalised to pre-wash on baseline (L-741,626). ACh release is increased by GABA receptor antagonists in presence of the D2R antagonist L-741,626. Two-way ANOVA: time x drug interaction: $F(109,440) = 11.77$, $p < 0.0001$; time effect: $F(109,440) = 158.2$, $p < 0.0001$; drug effect: $F(1,440) = 984.5$, $p < 0.0001$, n = 5 slices in N = 4 mice.* ***(C)*** *Mean AUC $\Delta F/F_0$ (± SEM) plotted against time in control (drug-free, black) or L-741-626 (purple). There is a small but significant effect of D2R antagonism. Two-way ANOVA: time x drug interaction: $F(11,96) = 0.74$, $p = 0.69$; time effect $F(11,96) = 15.84$, $p < 0.0001$; drug effect $F(1,96) = 6.47$, $p = 0.012$. Control: n = 5 slices in N = 4 mice, L-741-626: n = 5 slices in N = 4 mice.* ***(D)*** *Left, mean (± SEM) ACh transients in NAcC evoked by 1p in control (drug-free, black) and in presence of $GABA_R$ antagonists. Transients are normalised to 1p control (drug-free). Right, mean AUC $\Delta F/F_0$ (± SEM) plotted against time. Data are normalised to pre-wash on baseline. ACh release is increased*

(cont.) by GABA receptor antagonism. Two-way ANOVA: time x drug interaction: F (110,444) = 3.62, p < 0.0001; time effect: F (110,444) = 92.11, p < 0.0001; drug effect: F (1,444) = 336.6, p < 0.0001, n = 5 slices in N = 5 mice. ***(E)*** *Mean AUC $\Delta F/F_0$ (± SEM) plotted against time in CPu and NAcC. There are no regional differences in the size of the effect of GABA receptor-mediated inhibition of ACh transient AUC. Two-way ANOVA: time x region interaction: F (11,96) = 0.088, p > 0.99; time effect: F (11,96) = 9.43, p < 0.0001; region effect: F (1,96) = 0.058, p = 0.81, n = 5 slices in N = 5 mice. The data here represented were collected using AAV5.hSyn.ACh3.0.*

3.3.6. ACh release is under regulation by DA via D2Rs

The dopaminergic and cholinergic systems in the striatum are strongly interconnected and DA can modulate ChI firing activity via D2Rs localised on ChIs (Alcantara et al., 2003; Maurice et al., 2004; Lim et al., 2014). Therefore, I investigated the role of D2Rs in regulating ACh release and the effect of pathological levels of DA (obtained with cocaine) on ACh release.

To test if D2Rs regulate ACh release, I examined the effect of the D2R agonist quinpirole (5 µM) on 1p and 5p (2 Hz) evoked ACh release. This 2 Hz stimulation paradigm is in the range of ChI tonic firing frequencies (Wilson et al., 1990; Bennett and Wilson, 1999b) and allows to resolve release events at 500 ms, when D2R activation is reported to be maximal (Sulzer et al., 2016). In dorsolateral striatum (CPu), quinpirole inhibited ACh released by single pulses (**Figure 3.8A-B**. Two-tailed paired Student's t-test, p = 0.0005, n = 5 slices in N = 4 mice). Quinpirole also inhibited ACh released by 2Hz trains (**Figure 3.8A-C**. Two-way ANOVA, drug x stim number interaction: F (4,20) = 15.82, p < 0.0001; stim number effect: F (4,20) = 14.07, p < 0.0001; drug effect: F (1,20) = 173.1, p < 0.0001. Bonferroni multiple comparisons, stim 1: p < 0.0001; stim 2: p = 0.043; stim 3: p = 0.0003; stim 4: p = 0.0014; stim 5: p = 0.0020, n = 5 slices in N = 4 mice). In the NAcC, quinpirole reduced ACh released by single pulses (**Figure 3.8D-E**. Two-tailed paired Student's t-test, p = 0.044, n = 5 slices in N = 4 mice). D2R activation with quinpirole also overall decreased ACh released by 2 Hz trains, particularly at the first pulse (**Figure 3.8F**. Two-way ANOVA, drug x stim number interaction: F (4,20) = 6.55, p = 0.0015; stim number effect: F (4,20) = 18.38, p < 0.0001; drug effect: F (1,40) = 16.98, p = 0.0005. Bonferroni multiple comparisons, stim 1: p < 0.0001; stim 2: p > 0.99; stim 3: p > 0.99; stim 4: p > 0.99; stim 5: p > 0.99, n = 5 slices in N = 4 mice). Overall, these results show that activation of D2Rs inhibits

ACh released by single and tonic-like trains of pulses in dorsolateral and ventral striatum.

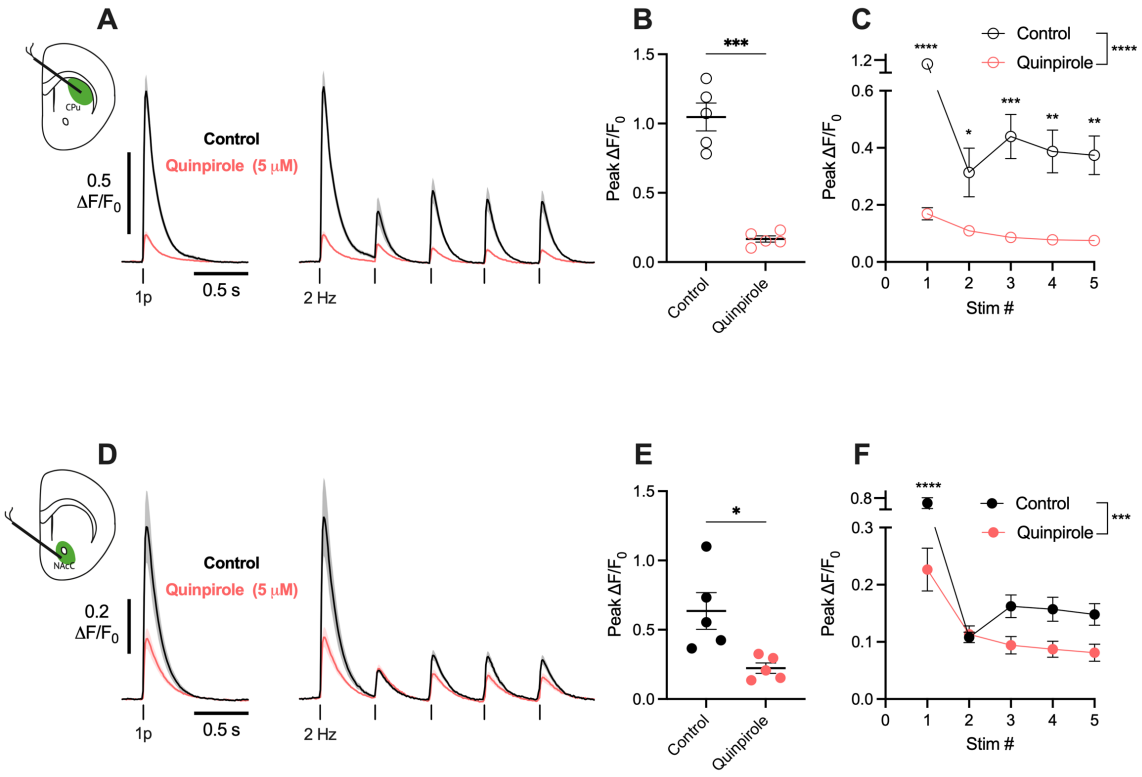


Figure 3.8. Agonism of D2Rs inhibits ACh release.
(A) *Mean (± SEM) ACh transients in dorsolateral striatum (CPu) evoked by single electrical pulses (1p) or trains of 5 pulses at 2 Hz in control (drug-free, black) and in presence of the D2R agonist quinpirole (5 μM), n = 5 slices in N = 4 mice.*
(B) *Peak ΔF/F₀ in control and quinpirole. Agonism of D2Rs reduces 1p-evoked ACh release in dorsolateral striatum. Two-tailed paired Student's t-test: p = 0.0005, n = 5 slices in N = 4 mice.*
(C) *Mean peak ΔF/F₀ (± SEM) plotted against stimulus number (stim #) in 2 Hz trains for control and quinpirole. Agonism of D2Rs inhibits ACh released by each stimulus in the train. Two-way ANOVA: drug x stim number interaction: F (4,20) = 15.82, p < 0.0001; stim number effect: F (4,20) = 14.07, p < 0.0001; drug effect: F (1,20) = 173.1, p < 0.0001. Bonferroni multiple comparisons: stim 1: p < 0.0001; stim 2: p = 0.043; stim 3: p = 0.0003; stim 4: p = 0.0014; stim 5: p = 0.0020, n = 5 slices in N = 4 mice.*
(D) *Mean (± SEM) ACh transients in NAcC evoked by single electrical pulses or trains of 5 pulses at 2Hz in control (drug-free, black) and in presence of D2R agonist quinpirole (5 μM), n = 5 slices in N = 4 mice.*
(E) *Peak ΔF/F₀ in control or quinpirole. Agonism of D2Rs reduces 1p-evoked ACh release in ventral striatum. Two-tailed paired Student's t-test: p = 0.044, n = 5 slices in N = 4 mice.*
(F) *Mean peak ΔF/F₀ (± SEM) plotted against stimulus number (stim #) in 2 Hz trains for control and quinpirole. Agonism of D2Rs overall inhibits ACh release, particularly at the first stimulation pulse. Two-way ANOVA: drug x stim number interaction: F (4,20) = 6.55, p = 0.0015; stim number effect: F (4,20) = 18.38, p < 0.0001; drug effect: F (1,20) = 16.98, p = 0.0005. Bonferroni multiple comparisons: stim 1: p < 0.0001; stim 2: p > 0.99; stim 3: p > 0.99; stim 4: p > 0.99; stim 5: p > 0.99, n = 5 slices in N = 4 mice.*
The data here represented were collected using AAV5.hSyn.ACh3.0.

To look at regional differences in the effect of D2R agonism, I directly compared ACh released by trains of pulses in drug-free (control) or in presence of

quinpirole in dorsolateral and ventral striatum, by means of a three-way ANOVA (**Figure 3.9A**). An overall effect of stimulus number in the train was reported, similar in both regions and differing for each treatment condition (**Figure 3.9A**. Stimulus number effect: $F(4,40) = 30.91$, $p < 0.0001$; Stimulus number x region (CPu vs NacC) interaction: $F(4,40) = 0.26$, $p = 0.90$; Stimulus number x treatment (control vs quinpirole) interaction: $F(4,40) = 21.39$, $p < 0.0001$), consistent with observations reported in **Figure 3.5**. An effect of quinpirole wash on was reported, with differences in dorsolateral compared to ventral striatum (**Figure 3.9A**. Treatment (control vs quinpirole) effect: $F(1,40) = 150.1$, $p < 0.0001$; treatment (control vs quinpirole) x regions (CPu vs NAcC) interaction: $F(1,40) = 41.63$, $p < 0.0001$). Finally, an effect of regions (dorsolateral, CPu, vs ventral, NAcC) was observed (**Figure 3.9A**. Regions (CPu vs NAcC) effect: $F(1,40) = 23.62$, $p < 0.0001$). Given these significant interactions, I directly compared the effect of region in control conditions and in presence of quinpirole. In control conditions, ACh release was overall smaller in NAcC (**Figure 3.9B**. Two-way ANOVA, region x stim number interaction: $F(4,40) = 0.59$, $p = 0.66$; stim number effect: $F(4,40) = 27.61$, $p < 0.0001$; region effect: $F(1,40) = 32.98$, $p < 0.0001$, $n = 5$ slices/region in $N = 4$ mice/region), consistent with previous findings (**Figure 3.3**). When D2Rs were activated, ACh release in the two regions was levelled, suggesting a stronger inhibition mediated by D2Rs in dorsolateral striatum (**Figure 3.9C**. Two-way ANOVA, region x stim number interaction: $F(4,40) = 0.79$, $p = 0.53$; stim number effect: $F(4,40) = 14.88$, $p < 0.0001$; region effect: $F(1,40) = 2.20$, $p = 0.14$, $n = 5$ slices/region in $N = 4$ mice/region). Overall, I found a stronger D2R-mediated inhibition of ACh release in dorsolateral striatum.

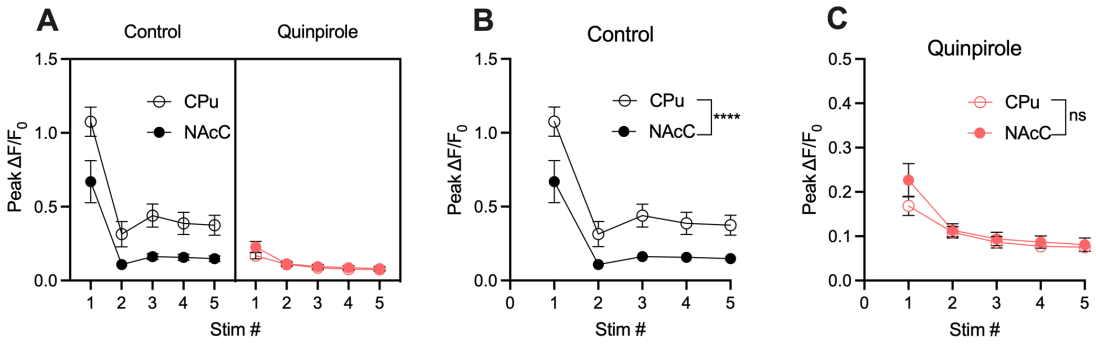


FIGURE 3.9. The effect of D2R agonism on ACh release is stronger in dorsolateral than ventral striatum.
(A) *Mean peak ΔF/F₀ (± SEM) plotted against stimulus number (stim #) in 2 Hz trains in a three-way graph. A three-way ANOVA was performed to determine the effect of stimulation pulse, region and D2R agonism (quinpirole). Three-way ANOVA: stim number effect: F(4,40) = 30.91, p < 0.0001; treatment (control vs quinpirole) effect: F(1,40) = 150.1, p < 0.0001; region effect (CPu vs NAcC): F(1,40) = 23.62, p < 0.0001; stim number x treatment (control vs quinpirole) interaction: F(1,40) = 23.62, p < 0.0001; stim number x region (CPu vs NAcC) interaction: F(4,40) = 0.26, p = 0.90; treatment (control vs quinpirole) x region (CPu vs NAcC) interaction: F(1,40) = 41.63, p < 0.0001; stim number x treatment x region interaction: F(4,40) = 1.08, p = 0.37, n = 5 slices/region in N = 4 mice/region.*
(B) *Mean peak ΔF/F₀ (± SEM) plotted against stimulus number (stim #) in 2 Hz trains in control conditions (drug-free) in dorsolateral (CPu) and ventral (NAcC) striatum. ACh release is overall lower in NAcC than CPu. Two-way ANOVA: region x stim number interaction: F (4,40) = 0.59, p = 0.66; stim number effect: F (4,40) = 27.61, p < 0.0001; region effect: F (1,40) = 32.98, p < 0.0001, n = 5 slices/region in N = 4 mice/region.*
(C) *Mean peak ΔF/F₀ (± SEM) plotted against stimulus number (stim #) in 2 Hz trains in presence of D2R agonist quinpirole in dorsolateral (CPu) and ventral (NAcC) striatum. ACh release is equalised by D2R agonism in CPu and NAcC, suggesting stronger effect in dorsal striatum. Two-way ANOVA: region x stim number interaction: F (4,40) = 0.79, p = 0.53; stim number effect: F (4,40) = 14.88, p < 0.0001; region effect: F (1,40) = 2.20, p = 0.14, n = 5 slices/region in N = 4 mice/region.*

To test whether ACh release is under regulation by endogenous DA acting at D2Rs, I examined the effect of a selective D2R antagonist (L-741,626) on 1p and 5p (2Hz) evoked ACh release. In dorsolateral striatum, antagonism of D2Rs with L-741,626 (1 µM) did not alter 1p-evoked ACh release (**Figure 3.10A-B**. Two-tailed paired Student's t-test, p = 0.84, n = 5 slices in N = 5 mice). D2Rs antagonism enhanced ACh released by 2Hz trains (**Figure 3.10C**. Two-way ANOVA, drug x stim number interaction: F (4,20) = 9.18, p = 0.0002; stim number effect: F (4,20) = 22.58, p < 0.0001; drug effect: F (1,20) = 81.00, p < 0.0001. Bonferroni multiple comparisons, stim 1: p > 0.99; stim 2: p < 0.0001; stim 3: p = 0.056; stim 4: p = 0.0009; stim 5: p = 0.0012, n = 5 slices in N = 5 mice). The absence of effect of D2R antagonism on ACh release evoked by single pulses or the first stimulus in a train is consistent with absence of striatal DA tone and D2Rs being GPCRs. In rodent striatal slices, D2R activation is maximal at ~500 ms (Sulzer et al., 2016). In all previous observations, when I stimulated with trains of pulses at 2 Hz, ACh released by the second pulse in

the train (500 ms) was lower than ACh released by successive pulses (**Figure 3.5A-B**). To determine whether this effect was due to endogenous activation of D2Rs, I looked at the effect of D2R block on ACh released by the second stimulus in the train, when D2R activation should be maximal. In dorsolateral striatum, ACh released by the second stimulus in 2 Hz trains is significantly enhanced when D2Rs are antagonised (**Figure 3.10D-E**. Two tailed paired Student's t-test, $p = 0.0035$, $n = 5$ slices in $N = 5$ mice).

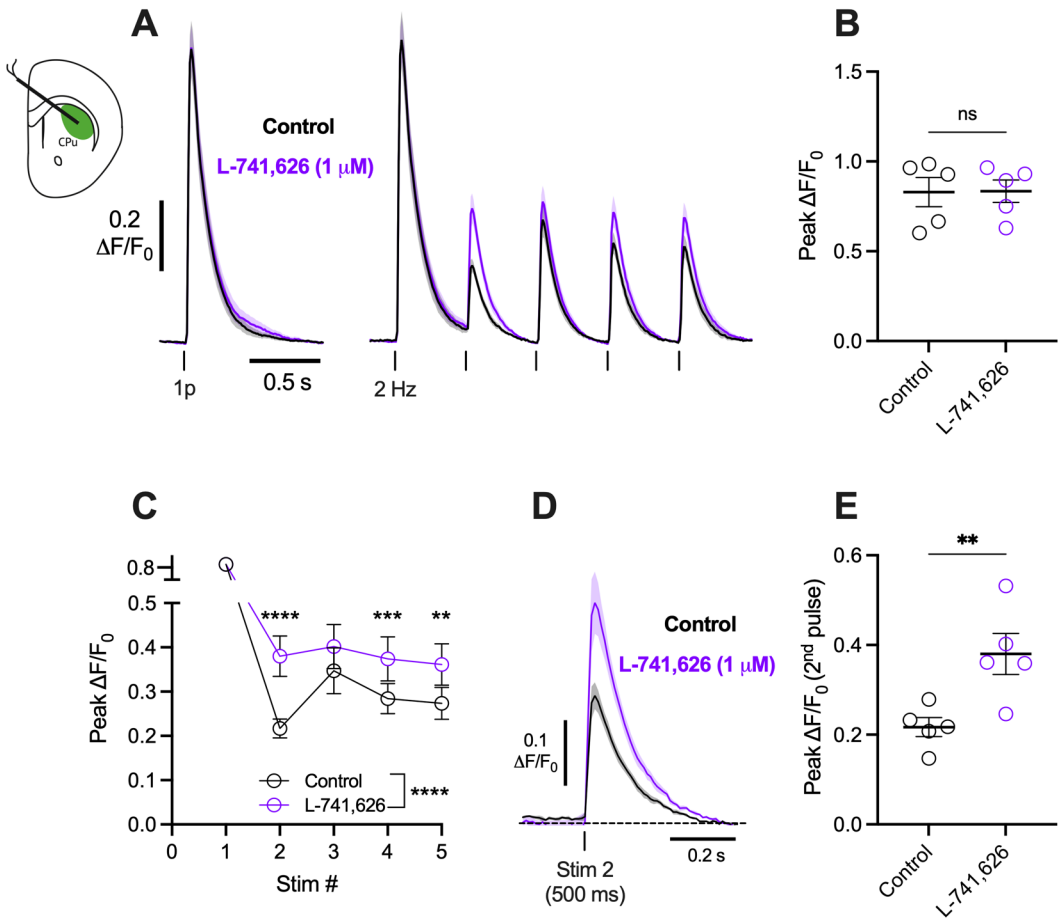


Figure 3.10. DA inhibits ACh release via D2Rs in the dorsolateral striatum.
(A) *Mean (± SEM) ACh transients in dorsolateral striatum (CPu) evoked by single electrical pulses or trains of 5 pulses at 2Hz in control (drug-free, black) and in presence of the D2R antagonist L-741,626 (1 μM), n = 5 slices in N = 5 mice.*
(B) *Peak $\Delta F/F_0$ in control or L-741,626. Antagonism of D2Rs does not alter 1p-evoked ACh release in dorsolateral striatum. Two-tailed paired Student's t-test: p = 0.84, n = 5 slices in N = 5 mice.*
(C) *Mean peak $\Delta F/F_0$ (± SEM) plotted against stimulus number (stim #) in 2 Hz trains for control and L-741,626. Antagonism of D2Rs promotes ACh re-release for successive pulses in the train. Two-way ANOVA: drug x stim number interaction: F (4,20) = 9.18, p = 0.0002; stim number effect: F (4,20) = 22.58, p < 0.0001; drug effect: F (1,20) = 81.00 p < 0.0001. Bonferroni multiple comparisons: stim 1: p > 0.99; stim 2: p < 0.0001; stim 3: p = 0.056; stim 4: p = 0.0009; stim 5: p = 0.0012, n = 5 slices in N = 5 mice.*
(D) *Mean (± SEM) ACh transients for the second stimulus (stim 2) in 2 Hz 5p trains in dorsolateral striatum (CPu). Transients were calculated from 1p-subtracted traces.*
(E) *Peak $\Delta F/F_0$ in control and L-741,626 for ACh released by stimuli delivered at 500 ms (2^{nd} pulse in 2 Hz 5p trains). Two-tailed paired Student's t-test: p = 0.0035, n = 5 slices in N = 5 mice. The data here represented were collected using AAV5.hSyn.ACh3.0.*

In the NAcC, D2Rs antagonism did not alter 1p-evoked ACh release (**Figure 3.11A-B**. Two-tailed paired Student's t-test, p = 0.45, n = 5 slices in N = 5 mice). ACh released by 2Hz trains was also enhanced (**Figure 3.11C**. Two-way ANOVA, drug x stim number interaction: F (4,20) = 0.87, p = 0.49; stim number effect: F (4,20) = 23.79, p < 0.0001; drug effect: F (1,20) = 15.29, p = 0.0009, n = 5 slices in N = 5 mice).

Moreover, ACh released by stimuli delivered at 500 ms was enhanced in presence of the D2R antagonist L-741,626 (**Figure 3.11D-E**. Two tailed unpaired Student's t-test, p = 0.047, n = 5 slices in N = 5 mice).

Overall, these data suggest that ACh release is under regulation by endogenous striatal DA acting at D2Rs.

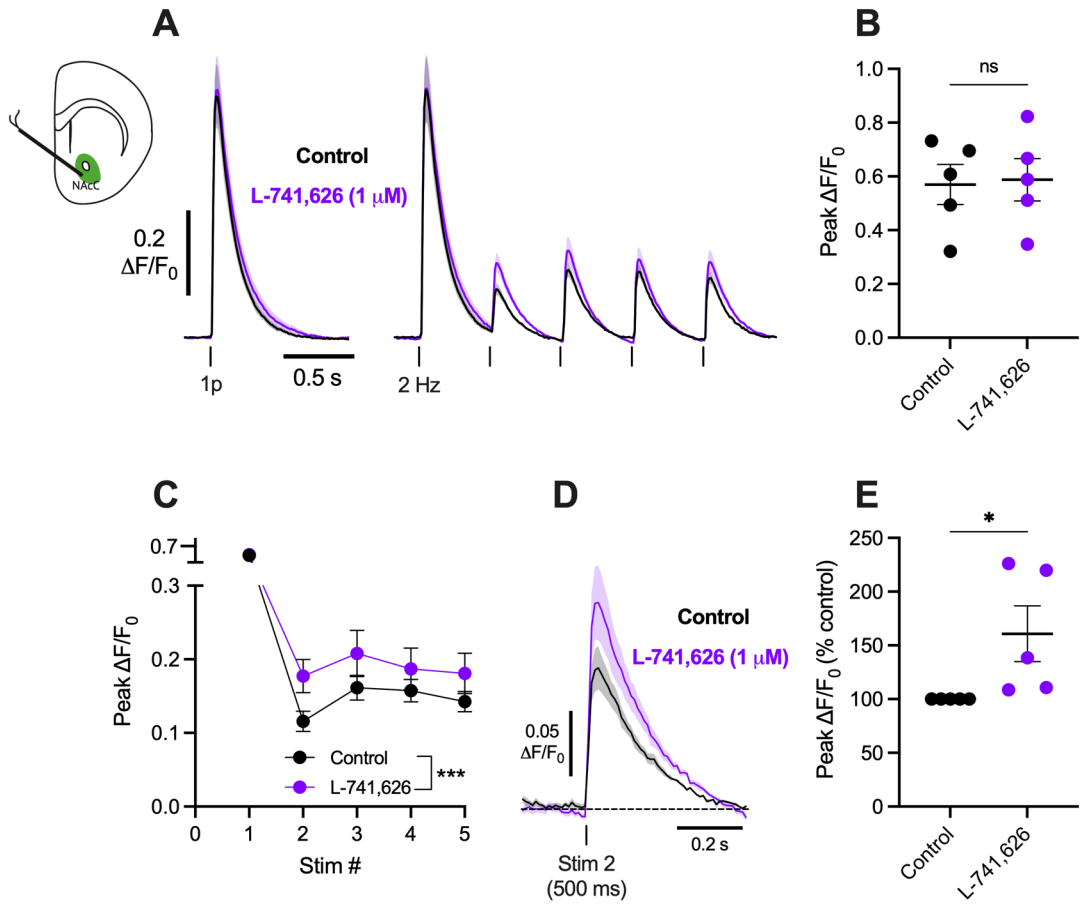


Figure 3.11. DA inhibits ACh release via D2Rs in the ventral striatum.
(A) *Mean (± SEM) ACh transients in NAcC evoked by single electrical pulses or trains of 5 pulses at 2Hz in control (drug-free, black) and in presence of D2R antagonist L-741,626 (1 μM), n = 5 slices in N = 5 mice.*
(B) *Peak ΔF/F₀ in control or L-741,626. Antagonism of D2Rs does not alter 1p-evoked ACh release in ventral striatum. Two-tailed paired Student's t-test: p = 0.45, n = 5 slices in N = 5 mice.*
(C) *Mean peak ΔF/F₀ (± SEM) plotted against stimulus number (stim #) in 2 Hz trains for control and L-741,626. Antagonism of D2Rs promotes ACh re-release for successive pulses in the train. Two-way ANOVA: drug x stim number interaction: F (4,20) = 0.87, p = 0.49; stim number effect: F (4,20) = 23.79, p < 0.0001; drug effect: F (1,20) = 15.29, p = 0.0009, n = 5 slices in N = 5 mice.*
(D) *Mean ACh transients for the second stimulus in 2 Hz 5p trains in NAcC. Transients were calculated from 1p-subtracted traces.*
(E) *Peak ΔF/F₀ in control and L-741,626 (D2R block) for ACh released by stimuli at 500 ms (2nd pulse in 2 Hz 5p trains). Data are normalised to control (drug-free) conditions. Two-tailed unpaired Student's t-test: p = 0.047, n = 5 slices in N = 5 mice. The data here represented were collected using AAV5.hSyn.ACh3.0.*

After characterising endogenous dopaminergic regulation of ACh release, I investigated how this circuit is altered when dysregulation occurs, like in the instance of the drug of abuse cocaine. Cocaine blocks the DA transporter (DAT), resulting in an increase in extracellular levels of DA ($[DA]_o$). I hypothesise that this increase in $[DA]_o$ will act at D2Rs on ChIs to inhibit ACh release. To test this, I first measured ACh release driven by single pulses or trains of pulses at tonic/phasic frequencies in presence/absence of cocaine (5 μM). In dorsolateral striatum, ACh released by single electrical pulses was slightly decreased by cocaine (**Figure 3.12A-B.** Two-tailed paired Student's t-test, p = 0.036, n = 8 slices in N = 5 mice). ACh driven by trains of 5p at 25 Hz was also slightly decreased, although not significantly (**Figure 3.12A-C**. Two-tailed paired Student's t-test, p = 0.06, n = 8 slices in N = 5 mice). Cocaine also decreased ACh released by 2 Hz trains (**Figure 3.12A-D**. Two-way ANOVA, drug x stim number interaction: F (4,35) = 1.69, p = 0.17; stim number effect: F (4,35) = 29.39, p < 0.0001; drug effect: F (1,35) = 86.40, p < 0.0001, n = 8 slices in N = 5 mice). To test whether the cocaine-mediated inhibition of ACh release was due to increased activation of D2Rs on ChIs, I blocked D2Rs with a selective antagonist (L-741,626, 1 μM) and measured ACh release in presence/absence of cocaine. When D2Rs were blocked, cocaine failed to significantly inhibit ACh release driven by single pulse (**Figure 3.12F**. Two-tailed paired Student's t-test, p = 0.061, n = 5 slices in N = 5 mice), trains of pulses at 25 Hz (**Figure 3.12G**. Two-tailed paired Student's t-test, p = 0.067, n = 5 slices in N = 5 mice) and 2 Hz (**Figure 3.12H**. Two-way ANOVA, drug x stim number interaction: F (4,40) = 0.09, p = 0.98; stim number effect: F (4,40) = 11.19, p < 0.0001; drug effect: F (1,40) = 3.05, p = 0.088, n = 5 slices in N = 5 mice). Overall, these data show that the enhanced levels of $[DA]_o$ in presence of cocaine act at D2Rs on ChIs to inhibit ACh release in dorsolateral striatum.

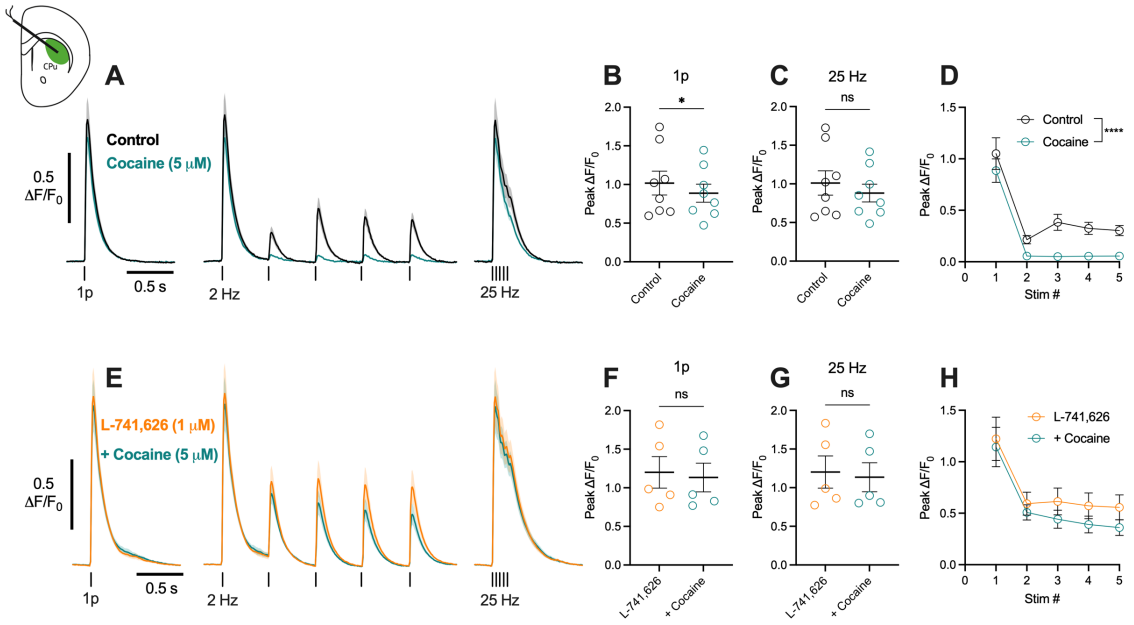


FIGURE 3.12. Enhanced [DA]₀ levels given by cocaine act at D2Rs to inhibit ACh release in dorsolateral striatum.
(A) *Mean (± SEM) ACh transients in dorsolateral striatum (CPu) evoked by single electrical pulses or trains of 5 pulses at 2-25 Hz in control (drug-free, black) and in presence of cocaine (5 μM, green), n = 8 slices in N = 5 mice.*
(B) *Peak ΔF/F₀ in control or cocaine. Cocaine slightly decreases ACh released by 1p. Two-tailed paired Student's t-test: p = 0.036, n = 8 slices in N = 5 mice.*
(C) *Peak ΔF/F₀ in control or cocaine. Cocaine does not alter ACh released by trains of 5p at 25 Hz. Two-tailed paired Student's t-test: p = 0.06, n = 8 slices in N = 5 mice.*
(D) *Mean peak ΔF/F₀ (± SEM) plotted against stimulus number (stim #) in 2 Hz trains for control and cocaine. Cocaine decreases ACh released by 2 Hz train stimulation. Two-way ANOVA: drug x stim number interaction: F (4,35) = 1.69, p = 0.17; stim number effect: F (4,35) = 29.39, p < 0.0001; drug effect: F (1,35) = 86.40, p < 0.0001, n = 8 slices in N = 5 mice.*
(E) *Mean (± SEM) ACh transients in dorsolateral striatum (CPu) evoked by 1p or trains of 5p at 2-25 Hz in presence of the D2R antagonist L-741,626 (1 μM, orange) and after wash-on of cocaine (5 μM, green), n = 5 slices in N = 5 mice.*
(F) *Peak ΔF/F₀ in L-741,626 and after wash-on of cocaine. When D2Rs are blocked, cocaine does not alter 1p-evoked ACh release. Two-tailed paired Student's t-test: p = 0.061, n = 5 slices in N = 5 mice.*
(G) *Peak ΔF/F₀ in L-741,626 and after wash-on of cocaine. When D2Rs are blocked, cocaine does not alter 5p (25 Hz)-evoked ACh release. Two-tailed paired Student's t-test: p = 0.067, n = 5 slices in N = 5 mice.*
(H) *Mean peak ΔF/F₀ (± SEM) plotted against stimulus number (stim #) in 2 Hz trains for L-741,626 and L-741,626 + cocaine. When D2Rs are blocked, the cocaine-induced decrease in ACh release is rescued. Two-way ANOVA: drug x stim number interaction: F (4,40) = 0.09, p = 0.98; stim number effect: F (4,40) = 11.19, p < 0.0001; drug effect: F (1,40) = 3.05, p = 0.088, n = 5 slices in N = 5 mice. The data here represented were collected using AAV5.hSyn.ACh3.0.*

In the ventral striatum, cocaine did not significantly decrease ACh release evoked by single pulses (**Figure 3.13B**. Two-tailed paired Student's t-test, p = 0.14, n = 5 slices in N = 4 mice). Cocaine modestly decreased ACh released by 2Hz trains (**Figure 3.13C**. Two-way ANOVA, drug x stim number interaction F (4,20) = 1.98, p = 0.13; stim number effect: F (4,20) = 76.80, p < 0.0001; drug effect: F (1,20) = 90.84, p < 0.0001, n = 5 slices in N = 4 mice). Cocaine also slightly decreased ACh release driven by 5p at 25 Hz, but not significantly (**Figure 3.13.D**. Two-tailed paired Student's t-test, p = 0.051, n = 5 slices in N = 4 mice). Overall, these data indicate that in the

ventral striatum increasing DA levels with cocaine only modestly inhibits ACh released by train stimulations. To test whether this effect was mediated by D2Rs, I used the D2R antagonist L-741,626 (1 μM) and measured ACh release upon cocaine (5 μM) wash-on. The effect of cocaine was rescued by D2R block (**Figure 3.13F**. Two-tailed paired Student's t-test, $p = 0.71$. **Figure 3.13G**. Two-way ANOVA, drug x stim number interaction: $F(4,20) = 0.11$, $p = 0.97$; stim number effect: $F(4,20) = 6.77$, $p = 0.0013$; drug effect: $F(1,20) = 1.82$, $p = 0.19$. **Figure 3.13H**. Two-tailed paired Student's t-test, $p = 0.81$, $n = 5$ slices in $N = 5$ mice), which suggests that the small effect of cocaine is mediated by DA via D2Rs.

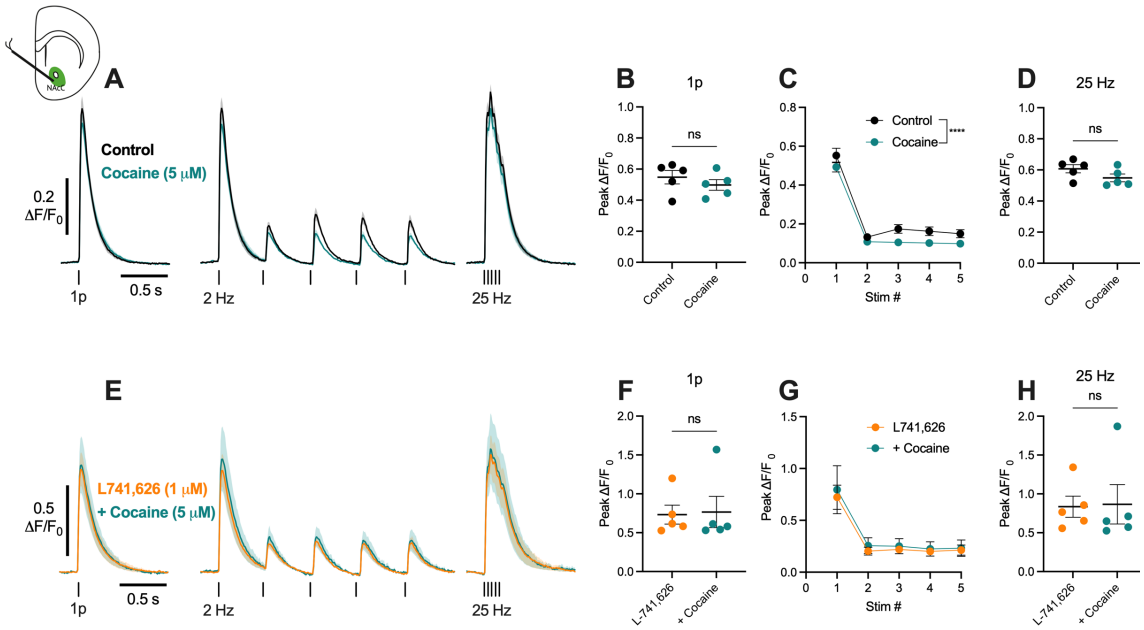


FIGURE 3.13. High [DA]$_o$ levels given by cocaine only modestly inhibit ACh release via D2Rs in ventral striatum.
(A) *Mean (± SEM) ACh transients in NAcC evoked by single electrical pulses or trains of 5 pulses at 2-25 Hz in control (drug-free, black) and in presence of cocaine (5 μM, green), n = 5 slices in N = 4 mice.*
(B) *Peak ΔF/F$_0$ in control or cocaine. Cocaine did not significantly decrease ACh released by 1p. Two-tailed paired Student's t test: p = 0.14, n = 5 slices in N = 4 mice.*
(C) *Mean peak ΔF/F$_0$ (± SEM) plotted against stimulus number (stim #) in 2 Hz trains for control and cocaine. Cocaine slightly decreases ACh released by 2 Hz train stimulation. Two-way ANOVA: drug x stim number interaction F (4,20) = 1.98, p = 0.13; stim number effect: F (4,20) = 76.80, p < 0.0001; drug effect: F (1,20) = 90.84, p < 0.0001, n = 5 slices in N = 4 mice.*
(D) *Peak ΔF/F$_0$ in control or cocaine. Cocaine slightly decreased ACh released by trains of 5 pulses at 25 Hz, but the effect did not reach significance. Two-tailed paired Student's t-test: p = 0.051, n = 5 slices in N = 4 mice.*
(E) *Mean (± SEM) ACh transients in NAcC evoked by single electrical pulses or trains of 5 pulses at 2-25 Hz in presence of the D2R antagonist L-741,626 (1 μM, orange) and after wash-on of cocaine (5 μM, green), n = 5 slices in N = 5 mice.*
(F) *Peak ΔF/F$_0$ in L-741,626 and L-741,626 + cocaine wash-on. When D2Rs are blocked, cocaine does not alter 1p-evoked ACh release. Two-tailed paired Student's t-test: p = 0.71, n = 5 slices in N = 5 mice.*
(G) *Mean peak ΔF/F$_0$ (± SEM) plotted against stimulus number (stim #) in 2 Hz trains for L-741,626 and L-741,626 + cocaine. When D2Rs are blocked, the small cocaine-induced decrease in ACh release is rescued. Two-way ANOVA: drug x stim number interaction: F (4,20) = 0.11, p = 0.97; stim number effect: F (4,20) = 6.77, p = 0.0013; drug effect: F (1,20) = 1.82, p = 0.19, n = 5 slices in N = 5 mice.*
(H) *Peak ΔF/F$_0$ in L-741,626 and L-741,626 + cocaine. When D2Rs are blocked, cocaine does not alter 5p (25 Hz)-evoked ACh release. Two-tailed paired Student's t-test, p= 0.81, n = 5 slices in N = 5 mice. The data here represented were collected using AAV5.hSyn.ACh3.0.*

3.4 DISCUSSION

In this chapter, I've investigated the major properties of striatal ACh release across striatal regions with a new generation genetically encoded fluorescent sensor ($GRAB_{ACh}$). Overall, I showed that ACh release measured with $GRAB_{ACh}$ was proportional to ACh concentration, sensor-specific, positively correlated to stimulation intensity (**Figure 3.1**), and AP and Ca^{2+}-dependent (**Figure 3.2**). The findings included in this chapter also showed regional differences in evoked ACh release and its recovery profile, with overall higher ACh release in dorsolateral striatum (**Figure 3.3**). Furthermore, I reported that ChI are activated and ACh is released according to stimulation frequency, with regional differences in extracellular summation of the signal (**Figure 3.4** and **3.5**). I also showed that AChE spatiotemporally regulates evoked ACh release and its frequency response, together with limiting tonic ambient ACh levels (**Figure 3.6**). Finally, I found that ACh release was under GABAergic modulation (**Figure 3.7**) and was inhibited by DA acting at D2Rs, more strongly in dorsolateral than ventral striatum (**Figure 3.8** to **3.13**).

3.4.1 $GRAB_{ACh}$ to measure real-time ACh release in striatal slices

In cultured cells, $GRAB_{ACh}$ sensors show affinity for ACh comparable to wild-type M_3-mAChRs (Jakubík et al., 1997), negligible internalisation and coupling with G protein-mediated downstream signalling pathways (Jing et al., 2018, 2020). Furthermore, in cultured hippocampal brain slices, these sensors show minimal perturbation of cellular physiology and membrane properties (Jing et al., 2018). Given all these characteristics, these tools are ideal for real-time measurement of ACh release with minimal disruption to the native properties of the systems in which they are expressed.

One important aspect that can impact upon the ACh signal measured with these sensors is their localisation. In **Figure 3.1A**, I characterised $GRAB_{ACh}$ expression profiles in striatal and midbrain slices. I showed dense and even distribution in neuronal processes in the striatum, which made exact co-localisation with specific

neuronal subtypes difficult. I also found that $GRAB_{ACh}$ sensors were trafficked to the midbrain in the SNr, consistent with expression by striatal MSNs, and were not expressed by SNc DA neurons. Previous studies showed that in cultured hippocampal neurons, $GRAB_{ACh}$ sensors localised on the plasma membrane of somata, dendrites, and axons (Jing et al., 2018, 2020). However, these experiments were performed using a different transfection method from AAVs and not in intact brain tissue. Therefore, a detailed description of $GRAB_{ACh}$ expression patterns in brain slices is still lacking. Inferring GRAB localisation in neuronal subtypes by looking at wild-type M_3-mAChRs expression is also difficult, because these receptors are expressed in striatum at low levels (Brann et al., 1988; Hersch et al., 1994b). Indeed, endogenous M_3-mAchRs appeared to be exclusively expressed in axon terminals of cortical and thalamic glutamatergic afferent to the striatum (Weiner et al., 1990; Hersch et al., 1994b). Overall, $GRAB_{ACh}$ appeared to be densely expressed on the membrane of axons and dendrites in the most prevalent neuronal population of the striatum (MSNs), making them a suitable tool to detect bulk extracellular ACh signal. To confirm the exact expression of the GRABs in different striatal neuronal subtypes and their localisation in different neuronal compartments, future experiments could provide a more thorough anatomical characterisation. Further spatial resolution can also be achieved by targeting the expression of $GRAB_{ACh}$ sensors to specific neuronal subtypes via Cre recombinase-dependent approach. Nonetheless, defining where these sensors localise in the neuron is still relevant to better interpret the extracellular dynamics of the signal (e.g., spread constant of release, distance from release sites).

As previously discussed in **Chapter 2** (**Section 2.2**), fluorescent sensors do not provide information about neurotransmitter concentration. In **Figure 3.1B-C**, I calibrated the fluorescent signal measured with $GRAB_{ACh}$ by rapidly washing on/off known concentrations of the substrate ACh and found a linear relationship between the size of fluorescent responses and ACh concentration. The fluorescence measured in this way cannot be used as a calibration factor to normalise ACh signals for a number of reasons. For instance, the ACh concentration that will penetrate the tissue and reach $GRAB_{ACh}$ indicators is going to be lower than the one bath applied, despite

blocking ACh breakdown with an inhibitor of AChE. Moreover, measured responses are a function of sensor expression, binding kinetics, and acquisition parameters. Nevertheless, I showed that these indicators report fluorescence in a way that is proportional to concentration of neurotransmitter release. *In vivo* microdialysis studies in the striatum of freely moving or anaesthetised rats reported basal levels of ACh in the nanomolar range, markedly increased upon administration of AChE inhibitors (Xu et al., 1991; Messamore et al., 1993; Descarries et al., 1997; Farar et al., 2012; Nosaka and Wickens, 2022). All $[ACh]_o$ here used to calibrate the $GRAB_{ACh}$ sensors (**Table 3.1**) were higher than those measured *in vivo* and were chosen in accordance with $GRAB_{ACh}$ dose-response curve in HEK293T cells (Jing et al., 2018, 2020). In particular, a saturating (100 μM), intermediate (50 μM) and lower concentration yielding detectable fluorescent responses (10 μM) were washed on briefly to test whether fluorescent signal measured with $GRAB_{ACh}$ was proportional to $[ACh]_o$.

3.4.2 Are dynamic changes in F_0 a measurement of tonic ACh levels?

Upon wash on of the AChE inhibitor ambenonium, I reported an increase in baseline fluorescence F_0 (**Figure 3.6E**). Generally, imaging signals are measured as $\Delta F/F_0$ to correct for the effects of different levels of indicator expression, excitation intensity and chosen sampling region. F_0 is a measure of baseline fluorescence and it's fundamental to estimate this parameter correctly, to limit the error in calculating $\Delta F/F_0$ (Chen et al., 2006; Balkenius et al., 2015). Here, I calculated F_0 as described in **Chapter 2** (**Section 2.3.5**), obtaining a baseline fluorescence level inferred from a non-linear fit for each stimulation, instead of choosing a constant value averaged across the whole experiment, to minimise estimation errors (Chen et al., 2006; Balkenius et al., 2015). Hence, F_0 thus calculated is a good estimation of baseline fluorescence in each condition and for each stimulation paradigm. Generally, absolute F_0 values depend upon sensor expression and acquisition parameters, but dynamic changes in F_0 might serve as a measurement of ambient ACh tone for a number of reasons. Firstly, changes in F_0 were only seen upon wash on of a compound known to increase

extracellular ACh levels (ambenonium). Indeed, in drug-free conditions, F_0 is stable over time in both ventral and dorsolateral striatum (**Chapter 2**, **Figure 2.5A**). Secondly, shifts in F_0 were not associated to changes in ambient illumination conditions given that an image-specific background was subtracted to account for changes in environmental conditions (as described in **Chapter 2**, **Section 2.3.5**). Shifts in baseline fluorescence driven by potential changes in pH can also be excluded, given that fluorescence measured with $GRAB_{ACh}$ is only weakly pH-dependent (Jing et al., 2018). Finally, if a temperature shift was responsible for alteration to basal fluorescence, this would also impact receptor kinetics and enzymatic activity in the slice, changing the overall dynamics of the signal, which was not seen.

In **Figure 3.3E**, I reported significantly higher F_0 in dorsolateral than ventral striatum. Higher F_0 in dorsolateral striatum could represent overall higher tonic levels of ACh, consistent with higher ChI basal activity in dorsal regions (Matamales et al., 2016). However, an indirect measurement of ACh tone at nAChRs achieved by assessing DA release probability revealed no underlying differences in ACh tone in the two regions (Exley et al., 2008). Therefore, F_0 could simply reflect differences in the levels of sensor expression. The development of ratiometric sensors would be fundamental to better understand whether parameters like F_0 can cover a biologically meaningful role in estimating basal neurotransmitter levels.

3.4.3. Differences in evoked ACh release in dorsolateral and ventral striatum

In **Section 3.3.2**, I've found that single pulse-evoked ACh release measured in dorsolateral and ventral striatum of the same animal is higher in CPu (**Figure 3.3B-C**). This is consistent with previous reports of differences in ChI anatomy, density, and activity across striatal regions (Gonzales and Smith, 2015; Matamales et al., 2016). Indeed, in the NAcC, there are less ChIs than in other striatal regions and their baseline intrinsic activity is lower than in dorsal regions (Matamales et al., 2016). However, it is important to note that the measured ACh signal is a function of $GRAB_{ACh}$ sensor expression. For instance, lower transfection efficiency in the ventral striatum will result in lower sensor expression and wrongly undersampled ACh release levels.

Indeed, F_0 was overall lower in NAcC, which suggests lower sensor expression (as discussed above in **Section 3.4.2**). Future work providing a quantification of $GRAB_{ACh}$ expression levels across striatal regions could be important to allow an accurate estimation of the regional differences in ACh release levels.

In **Figure 3.5**, I showed that ACh is released according to stimulation frequency and pulse number with regional differences in the extracellular summation of the signal, particularly upon high frequency stimulation. In the CPu, AUC increased upon higher stimulation frequency, while in the NAcC, peak size reported frequency information (**Figure 3.5D-F**). These differences could reflect differential expression of the sensor, different ACh diffusion and clearance from the extracellular space or the differential contributions of synchronous and asynchronous release (AR). Indeed, high frequency stimulation, which initially evokes synchronous release, can additionally evoke AR, which lasts for tens or hundreds of ms after the end of the AP burst (Kaeser and Regehr, 2014; Rozov et al., 2019). The molecular mechanisms and physiological relevance of AR are currently incompletely characterised. It has been proposed that AR might play a role in the generation of long-lasting forms of synaptic plasticity mediated by extrasynaptic metabotropic receptors (Rozov et al., 2019). The increase in AUC upon higher frequency stimulation in CPu could therefore indicate the contribution of AR to extracellular ACh levels. The slow Ca^{2+} chelator EGTA has been found to abolish AR, while substitution of extracellular Ca^{2+} with Sr^{2+} increases the amplitude and duration of AR (Kaeser and Regehr, 2014; Rozov et al., 2019). These approaches could therefore be used in future work to determine AR contribution in shaping ACh signal dynamics across striatal regions.

3.4.4. Acetylcholinesterase as a regulator of ACh extracellular spatiotemporal dynamics

In **Section 3.3.4** I found that blocking AChE dramatically altered the temporal profiles of evoked ACh release and increased ambient ACh levels. AChE, which catalyses ACh breakdown into choline and acetate, is one of the fastest known enzymes (Descarries et al., 1997) and is enriched in striatum (Bernard et al., 1995). It

has been proposed that AChE could be a key regulator of extracellular ACh signal dynamics. Consistently with this idea, I provided evidence that AChE limits the duration of evoked ACh transients and their frequency dependency (**Figure 3.6A-D**).

Somewhat surprisingly, I showed that upon AChE inhibition the size of the peak of evoked fluorescent responses is prominently decreased (**Figure 3.6B**). This drop in peak $\Delta F/F_0$ could be due to a mathematical artefact driven by an increase in the denominator F_0 (**Figure 3.6E**). However, I showed that the increase in baseline fluorescence was not sufficient to explain the peak drop (**Figure 3.6F**) and might instead indicate an increase in ambient ACh levels. Another candidate mechanism could be autoreceptor activation. Indeed, ChI regulate their own ACh release via M_2 and M_4-mAChRs (Yan and Surmeier, 1996; Calabresi et al., 1998b; Poppi et al., 2021), but investigating the contribution of autoreceptor activation is difficult. All mAChR subtypes have a high degree of similarity in the ligand-binding site, limiting the availability of subtype-selective ligands (Eglen, 2006; Abudukeyoumu et al., 2019). Hence, M_2 and M_4-mAChR antagonists can also bind to and block the $GRAB_{ACh}$ sensors (M_3-mAChRs), making it difficult to interpret the measured signals. Indeed, I piloted the use of two M_2 and M_4-mAChR selective antagonists (AF-DX116 and PD102807, respectively) and observed a concentration dependent decrease in ACh signal measured with $GRAB_{ACh}$ sensors. Given that autoreceptors antagonism should promote ACh release, these findings suggested a non-specific effect of the antagonists on the $GRAB_{ACh}$ itself. Potential experiments to investigate the role of autoreceptors could be carried out in transgenic mice with selective knock-out of different mAChR subtypes. The drop in peak size could also be due to substrate-mediated internalisation of the sensor. In cell culture, it was shown that $GRAB_{ACh}$ sensors are stably expressed in membrane upon prolonged exposure to high concentration of ligand (Jing et al., 2018). However, additional work is needed to determine whether the tools are stably expressed and inert in intact brain tissue. One final candidate mechanism could be ACh depletion, which could be tested in future experiments by supplementing with choline (which does not bind to the $GRAB_{ACh}$

sensor, (Jing et al., 2018)), or by testing whether the effect of AChE inhibition is replicated with an inhibitor of the choline transporter.

It has been proposed that the dense striatal ChI innervation and their tonic activity results in continuous exposure of all tissue elements to tonic ambient levels of ACh (Contant et al., 1996; Descarries et al., 1997). Recent evidence in mouse striatal slices expressing $GRAB_{ACh}$ to measure ACh release has also reported frequently occurring spontaneous ACh release events in dorsal and ventral striatum (Liu et al., 2022). In this context, AChE appears to be a good candidate for the regulation of ambient ACh levels (Descarries et al., 1997; Pisani et al., 2007; Dunant and Gisiger, 2017). Here, I found that AChE inhibition increased fluorescence levels in absence of stimulation in a TTX-dependent manner (**Figure 3.6G**), suggesting that the signal measured is ambient striatal ACh tone resulting from tonic ChI activity. This is consistent with microdialysis studies which showed a steady-state basal level of ACh in the extracellular space which is increased by anti-AChE treatment (Xu et al., 1991; Messamore et al., 1993; Descarries et al., 1997). Recent evidence from mouse striatal slices measuring spontaneous nAChR-mediated excitatory postsynaptic potentials in DA axons (axEPSPs) reported that inhibition of AChE transiently increased the frequency of spontaneous axEPSPs and slowed their decay kinetics, suggesting that AChE regulates the spatiotemporal dynamics of ACh release onto DA axons (Kramer et al., 2022). Notably, AChE inhibition did not impact on axEPSPs peak amplitude, suggesting that a fraction of ChI terminals exist in proximity to nAChRs on DA axons and that ACh might also operate via fast, synaptic-like neurotransmission (Kramer et al., 2022).

3.4.5. Potential tonic GABAergic inhibition of ACh release

In **Section 3.3.5**, I found that the AUC of ACh release transients was increased upon antagonism of GABA receptors in both dorsolateral and ventral striatum. These findings point towards the idea of a potential tonic GABAergic inhibition of striatal ACh release. This is not surprising given that the striatum is predominantly GABAergic

and there is ambient GABA tone which modulates DA release (Lopes et al., 2019; Roberts et al., 2020, 2021). These findings are also consistent with microdialysis studies which showed that GABA receptors can tonically inhibit the output of striatal ACh (DeBoer and Westerink, 1994). DA is under tonic GABAergic inhibition in the striatum and the increase in DA levels resulting from relief of tonic inhibition via antagonism of GABA receptors was found to act at D2Rs to feebly limit the relief of tonic ACh inhibition (**Figure 3.7C**). To better understand whether DA feedforwards to modulate ACh release via D2Rs upon antagonism of GABA receptors, future effort should consider a different stimulation paradigm through which the time course of D2R activation can be appreciated (e.g., trains of pulses at low frequencies). Such experiments could be particularly relevant in a disease model of Parkinson's disease, where tonic GABAergic inhibition of DA release is disrupted.

The GABA responsible for mediating this inhibition can originate from several sources. Indeed, ChIs receive many intrastriatal and extrastriatal GABAergic projections, and around 60% of synapses onto ChIs are estimated to be GABAergic (Gonzales et al., 2013; Poppi et al., 2021). GABA exerts its effects directly inhibiting ChI firing via $GABA_A$ receptors (Lim et al., 2014; Sato et al., 2014) and indirectly through presynaptic inhibition of corticostriatal terminals via $GABA_B$ receptors (DeBoer and Westerink, 1994; Poppi et al., 2021). MSNs form synaptic connections with ChIs and their optogenetic activation leads to postsynaptic IPSCs in ChIs (Chuhma et al., 2011), suggesting that GABA released from MSNs onto ChIs is a major determinant of ChI excitability (Lim et al., 2014). ChIs also receive inhibitory inputs from GABAergic interneurons (INs). For instance, THINs form recurrent inhibitory networks with ChIs (Sullivan et al., 2008; Dorst et al., 2020). LTSIs synapse onto ChIs and trigger IPSCs when optogenetically stimulated (Vuillet et al., 1992; Straub et al., 2016). GABA can also be co-released by ChIs and DA neurons (Tritsch et al., 2012; Lozovaya et al., 2018b). It seems unlikely that GABA co-released from ChIs could regulate ACh released at the same time. Instead, GABA co-released from DA axons might impact on ChI activity. However, it has been shown that dopaminergic afferents

seem to regulate ChI inhibitory networks principally via DA at D2Rs (Dorst et al., 2020).

3.4.6. DA regulation of ACh release via D2 receptors

In **Section 3.3.6**, I investigated DA regulation of ACh release, focussing on the role of inhibitory D2Rs. I found that there is endogenous inhibition of ACh release by DA acting at D2Rs on ChIs in dorsolateral and ventral striatum (**Figure 3.10-3.11**). This is consistent with electrophysiology studies that show that DA acts at D2Rs to inhibit ChI firing (Maurice et al., 2004; Deng et al., 2007a; Chuhma et al., 2014). These findings are also consistent with recent *in vivo* studies which show that DA acting at D2Rs can modulate the size and length of the ACh release dip that follows pauses in ChIs (Gallo et al., 2021; Martyniuk et al., 2021).

When activating D2Rs with the agonist quinpirole, I found that the D2R activation effect on ACh release was stronger in dorsolateral striatum (**Figure 3.8-3.9**). This is consistent with studies in rat striatal slices monitoring radiolabelled ACh release which reported stronger effect of quinpirole in the dorsal striatum (Henselmans and Stoof, 1991). Notably, quinpirole will also activate D2 autoreceptors on DA axons and consequently decrease DA release. If the effect of quinpirole in inhibiting DA release is different in the two regions, then D2Rs on ChIs will be differentially activated by their endogenous ligand DA. However, unpublished observations from the lab showed that agonism of D2Rs (in presence of the nAChR antagonist DHβE) dose-dependently inhibited electrically evoked DA release with similar efficacy in CPu and NAcC. Differences in D2R regulation of ACh release across striatal regions could arise from differences in the expression of D2Rs by ChIs and their affinity for DA. There have been reports of heterogeneity in the timing and sensitivity of D2R signalling and D2R expression across striatal subregions. For instance, D2Rs on MSNs in the NAcSh are more sensitive to DA and have slower activation kinetics (Marcott et al., 2018). Furthermore, there is lower expression of ChI markers in striatal neurons expressing D2Rs along the dorsoventral axis,

suggesting molecular heterogeneities among ChIs across striatal regions (Puighermanal et al., 2020).

In **Figure 3.10** and **3.11**, I reported that selective antagonism of D2Rs with L-741,626 resulted in enhanced ACh release by successive pulses in low frequency train stimulation (2 Hz). In particular, endogenous DA at D2Rs mediated maximal inhibition of ACh release at 500 ms, consistently with the time course of D2R activation in rodent striatal slices (Lee et al., 2002; Phillips et al., 2002; Rice et al., 2011; Sulzer et al., 2016). Recent evidence using $GRAB_{ACh}$ sensors selectively expressed on DA axons in mouse striatal slices also showed that D2R blockade enhanced ACh released by pairs of electrical pulses and induced an additional ACh release that peaked around 600 ms after the first stimulation (Liu et al., 2022). The delay seen in these responses could be due to the segregated expression of $GRAB_{ACh}$ on DA axons.

In **Figure 3.12**, I found that cocaine decreased ACh release in CPu, in a D2R-dependent manner. This is consistent with a DA-mediated increase in D2R activation which resulted in ACh inhibition. This DA-mediated decrease in ACh levels might then lead to reduced ACh tone at nAChRs on DA axons, lower activation of nAChRs and relief of the nAChR-mediated STD of DA release. In support of this hypothesis, unpublished observations from the lab measuring DA release with FCV at a second epoch reported a relief of the nAChR-mediated STD of DA release in the presence of cocaine.

In **Figure 3.13**, I found that the effects of cocaine on ACh release were less pronounced in the NAcC, consistent with a stronger effect of D2R agonism in the dorsolateral striatum (**Figure 3.9**). These findings are also consistent with previous studies reporting regional differences in cocaine effects on striatal microcircuits. For instance, repeated exposure to cocaine produced a decrease in the sensitivity of postsynaptic D2R-mediated signalling only in the NAc (Marcott et al., 2018). Other studies reported an increase in ACh levels upon exposure to cocaine by activation of excitatory D1Rs on ChIs exclusively in the NAcSh (Imperato et al., 1992; Consolo et al., 1999; Mark et al., 1999). A balancing effect on ACh release via activation of excitatory D1-like receptors (D5Rs and D1Rs) could be at play, however more recent

evidence showed that the D2R-dependent inhibition of ACh signalling is fundamental to mediate cocaine-related behavioural responses (Lewis et al., 2020). Indeed, selective ablation of D2Rs from ChIs in mice reduced motor responses to cocaine and its reinforcing properties (Lewis et al., 2020). Furthermore, blockade of D1-like receptors did not alter ACh release evoked by paired pulse stimulation measured by $GRAB_{ACh}$ at DA axons (Liu et al., 2022). A different mechanism regulating the DA-ACh axis in presence of cocaine might therefore be at play in the ventral striatum. Unpublished observations from the lab seems to support this hypothesis and point toward a potential role of D2Rs on DA axons in the NAcC in modulating short-term plasticity of DA release in presence of cocaine.

Overall, in this chapter I've outlined a range of properties of ACh striatal signalling. This is a fundamental step to better understand how ACh dynamically modulates DA release plasticity, which will be investigated in the next chapter.

4. Exploring the mechanisms underlying acetylcholine regulation of dopamine release via nicotinic acetylcholine receptors

4.1 INTRODUCTION

In **Chapter 3**, I defined a range of properties of striatal ACh release, a fundamental step to better understand how ACh can modulate striatal DA release and its plasticity. In this chapter, I'm going to explore how dynamic changes in ACh release can modulate DA release plasticity.

Midbrain DA neurons project to the striatum where they form complex and dense axonal arborisations (Matsuda et al., 2009). These morphological features, together with the presence of several neuromodulatory receptors on DA axons suggest that the correspondence between action potential firing by midbrain DA neurons and striatal DA release might be influenced by mechanisms occurring locally at axonal level (Rice et al., 2011). ACh is one of the major local modulators of striatal DA transmission and acts via nicotinic ACh receptors (nAChRs) and muscarinic ACh receptors (mAChRs) to regulate DA release plasticity in multiple ways.

In rodents, ACh released following synchronous activation of a population of cholinergic interneurons (ChIs) can directly evoke DA release, bypassing action potential firing in DA somata (Cachope et al., 2012; Threlfell et al., 2012; Brimblecombe et al., 2018). Cholinergic driven DA release requires activation of nAChRs on DA axons (Cachope et al., 2012; Threlfell et al., 2012). Furthermore, studies measuring DA release with continuous amperometry showed that electrically-evoked DA release currents present a biphasic profile, characterised by an initial dopaminergic component and a subsequent cholinergic component (Wang et al., 2014a, 2014b). In rats, an additional source of ACh arising from cholinergic neurons originating in the pedunculopontine nucleus (PPN) and laterodorsal tegmentum (LDT) in the brainstem has been described (Dautan et al., 2014). Nonetheless, ChIs alone have been found sufficient to provide a source of ACh that can modulate DA release (Brimblecombe et al., 2018), and no detectable modulation of striatal DA release was reported by targeted optogenetic activation of PPN/LDT projections (Brimblecombe et al., 2018). A major property of ACh-driven DA release is that it does not convey information about activity in ChIs. Indeed, selective light-activation of ChIs with trains at increasing frequencies failed to evoke more DA release than a

single stimulus in dorsal and ventral striatum (NAc core) (Threlfell et al., 2012; Shin et al., 2017). This depression of ACh-driven DA re-release is not due to spike attenuation in ChIs (Threlfell et al., 2012). Conversely, selective optogenetic activation of DA axons results in DA released proportionally to stimulation frequency and pulse number (Threlfell et al., 2012). Local activation of both ChIs and DA axons with electrical stimulation shows that the overall DA release is insensitive to stimulation frequency, consistent with previous studies (Rice and Cragg, 2004; Zhang and Sulzer, 2004). Hence, the cholinergic component of DA release dominates over concurrent activity in DA neurons and shunts the efficacy of activity in DA neurons in evoking DA release (Threlfell et al., 2012). The mechanisms limiting the sensitivity of ACh-driven DA release to stimulation frequency are currently incompletely characterised. In particular, the role of ChI firing modalities in modulating the dynamic range of ACh release and the consequent effect on the dynamic gating of DA release is undefined. To address these unknowns, in **Section 4.3.1** I explored whether dynamic changes in ACh release levels can modulate short-term plasticity of ACh-driven DA release using a combination of optogenetics to activate ChIs, $GRAB_{ACh}$ imaging to measure ACh release and FCV to measure ACh-driven DA release.

Together with driving DA release, ACh can act at β2-nAChRs localised on DA axons (Jones et al., 2001; Champtiaux et al., 2003) to modulate short-term plasticity of DA release. Work in rodent striatal slices measuring DA release with FCV showed that activation of β2-nAChRs drives DA release evoked by single pulse and promotes short-term depression (STD) of DA release in train stimulation (Rice and Cragg, 2004). Therefore, nAChRs prevent DA re-release driven by multiple pulses at any frequency and limit how action potential firing in DA neurons is translated into DA release (Threlfell and Cragg, 2011). Lack of activation, antagonism, deletion, or desensitisation of β2-nAChRs reduces single pulse-driven DA release and relieves STD, enhancing burst-driven release in a way proportional to frequency and pulse number (Rice and Cragg, 2004; Zhang and Sulzer, 2004; Patel et al., 2012). Given the growing body of work using fluorescent indicators to measure DA release, in **Section 4.3.4** I used new generation $GRAB_{DA}$ sensors to monitor DA release plasticity in

response to antagonism of nAChRs, replicating FCV findings. β2-nAChRs are also found on ChIs (Azam et al., 2003; Abbondanza et al., 2022) and deletion of these receptor in striatal interneurons leads to profound behavioural changes, including anxiety, social and explorative behaviours (Abbondanza et al., 2022). Nonetheless, the role of β2-nAChRs in gating striatal ACh release dynamics has not been fully characterised. In **Section 4.3.4**, I investigated the role of nAChRs in modulating ACh release in dorsolateral and ventral striatum. Furthermore, in **Section 4.3.5**, I explored evidence for desensitisation of β2-nAChRs by endogenous ACh looking at nAChR-mediated regulation of burst versus single pulse-evoked DA release measured with FCV.

Despite the strong modulation of striatal DA short-term plasticity mediated by nAChRs on DA axons, the mechanisms operating downstream of these receptors are incompletely characterised. In general, activation of presynaptic nAChRs in the CNS promotes neurotransmitter release through a downstream Ca^{2+}-dependent mechanism which includes increase in intracellular Ca^{2+} by direct permeation of the receptor channel, activation of voltage-gated Ca^{2+} channels (VGCCs), Na^{+}-dependent membrane depolarization and indirect stimulation of Ca^{2+} release from intracellular stores (Dani and Bertrand, 2007; McKay et al., 2007). In particular, β2-nAChRs have also been found to operate through Ca^{2+}-related mechanisms involving membrane depolarization and recruitment of voltage-gated Ca^{2+} channels (VGCCs) (Dani and Bertrand, 2007; Dickinson et al., 2007; McKay et al., 2007). In the midbrain, β2-nAChRs on DA neurons operate in Ca^{2+} mobilization mechanisms that are followed by Na^{+} and T-type Ca^{2+} channels activation (Tsuneki et al., 2000), whereas at striatal synaptosomes β2-nAChRs on DA axons appears to be functionally associated to different types of VGCCs, recruited through local membrane depolarization (Soliakov and Wonnacott, 1996; Kulak et al., 2001). In the mouse striatum, β2-nAChR activation induces action potential firing in distal DA axons followed by opening of P/Q-type and N-type Ca^{2+} channels (Liu et al., 2022). Furthermore, quantitative proteomics analysis revealed that several proteins are associated with mouse neuronal β2-nAChRs, including proteins involved in Ca^{2+} signalling (McClure-Begley et al., 2013).

Hence, it is plausible that striatal nAChRs on DA axons might exert their effects on DA release plasticity through Ca^{2+}-related mechanisms, potentially limiting intracellular Ca^{2+} summation and VGCCs opening through interactions with intracellular Ca^{2+} buffer proteins. An unexplored and potentially relevant candidate to operate downstream of nAChR activity is the Ca^{2+} chelator calbindin D-28k (calb1), which is preferentially expressed in VTA DA neurons (Greene et al., 2005). Calb1 is a fast, high affinity Ca^{2+} buffer, which also operates as a Ca^{2+} sensor and transporter (Schmidt, 2012) and is involved in forms of hippocampal short-term plasticity (Blatow et al., 2003). In the ventral striatum, calb1 limits DA release by reducing intracellular Ca^{2+} availability and interacting with the DA transporter (DAT) (Brimblecombe et al., 2019). In **Section 4.3.6**, I tested whether calb1 mediates nAChR regulation of DA release in the NAcC in striatal slices of mice with selective knock-down of calb1 in DA neurons.

ACh can also modulate DA release via mAChRs. ACh acts at M_2 and M_4-mAChRs localised on ChIs (Yan and Surmeier, 1996; Alcantara et al., 2001) and at M_5-mAChRs, whose mRNA is expressed by DA neurons but have not been directly localised on DA axons (Vilaró et al., 1990; Weiner et al., 1990). Agonism of M_2/M_4-mAChRs on ChIs inhibits their firing (Yan and Surmeier, 1996; Calabresi et al., 1998b; Ding et al., 2006), which will in turn reduce ACh release and nAChR activation on DA axons, relieving the nAChR-mediated depression of DA re-release (Threlfell et al., 2010). FCV experiments on slices from mice with deletion of specific mAChRs subtypes revealed the prevalent role of M_4-mAChRs in the NAc and M_2 and M_4-mAChRs in the CPu, but no prominent role for M_5-mAChRs (Threlfell et al., 2010). Instead, M_5-mAChRs directly act on DA axons to potentiate DA release in the ventral striatum (Shin et al., 2015). The contribution of the mAChR regulation of DA release on the cholinergic and dopaminergic component of DA release remains to be defined. In **Section 4.3.2** and **4.3.3**, I tested if putative changes in ACh levels driven by agonism and antagonism of mAChRs regulate ACh-driven and DA-driven DA release dynamics measured with FCV.

Overall, the work included in this chapter aimed at investigating cholinergic regulation of DA release by defining the contribution of ACh release levels, activity in ChIs and mechanisms operating downstream of nAChRs on DA axons. First, I tested whether ACh-driven DA release was sensitive to dynamic changes in ACh release plasticity driven by activity in ChIs and changes in ACh release probability (**Section 4.3.1**, **4.3.2**, **4.3.3**). I then tested if FCV findings assessing nAChR-mediated regulation of DA release short-term plasticity were replicated when DA release was measured by new generation fluorescent sensors ($GRAB_{DA}$) (**Section 4.3.4**). Furthermore, I tested if ACh release was regulated by nAChRs either directly or via DA (**Section 4.3.4**). Finally, I investigated a potential role for calb1 in mediating nAChR STD of DA release (**Section 4.3.6**).

4.2 METHODS

4.2.1 Animals and slice preparation

Different mouse lines were used for the experiments in this chapter and details are found in **Chapter 2** (**Section 2.1.2**). For experiments investigating ACh-driven DA release, slices from ChAT-Cre;Ai32 mice were used (9-15 weeks, mixed sex cohorts). These mice express channelrhodopsin2 (ChR2) selectively in cholinergic interneurons which allow to achieve targeted light activation of ChIs. Light activation of ChIs can drive DA release (Threlfell et al., 2012) and this approach was used to investigate properties of the ChI-driven component of DA release in isolation.

For experiment monitoring DA or ACh release with $GRAB_{DA/ACh}$, wild-type C57BL6/J mice (6-7 weeks old, mixed sex) were injected with either AAV5/9.hSyn.ACh3.0 (Jing et al., 2020) or AAV5.hSyn.DA2m (Sun et al., 2020) with a titre of ~ 0.8 x 10^{13} gc/ml (**Section 2.1.3**).

For experiments investigating the role of calb1 in DA axons, I used slices from mice with knockdown of calb1 selectively in DA neurons (calbKD) and slices from control mice with wild-type levels of calb1 (calbWT, DAT-Cre background), (see **Section 2.1.2**). Knockdown and control mice were matched for age (7-9 months) and sex (males and females).

Acute *ex vivo* coronal slices containing dorsal and ventral striatum were prepared for recordings as previously described in **Section 2.2.1** and **2.3.3**. Recordings were carried out in the dorsolateral striatum (labelled as CPu in the figures) and in the nucleus accumbens core (labelled as NAcC in the figures).

4.2.2 Fast-scan cyclic voltammetry

FCV at CFMs was used to monitor DA release in the majority of the experiments described in this chapter. Recordings were performed as described in **Chapter 2** (**Section 2.2.4**). Stably releasing recording sites in each region were chosen for all experiments described. Single pulses were delivered until a stable release

baseline was reached, allowing a maximum release variability of 10% in successive stimulations. For experiments combining light and electrical stimulation, site release stability was assessed with both stimulations. In these experiments, light stimulation (Lstim) selectively activated ChIs (expressing ChR2) and allows to monitor ACh-driven DA release in isolation. Electrical stimulation (Estim) provided a generalised local depolarisation which activated both ChIs and DA axons, allowing to assess the dual cholinergic and dopaminergic components of release (**Figure 4.1**). Both stimulation parameters were delivered as previously described in **Chapter 2** (**Section 2.2.3**).

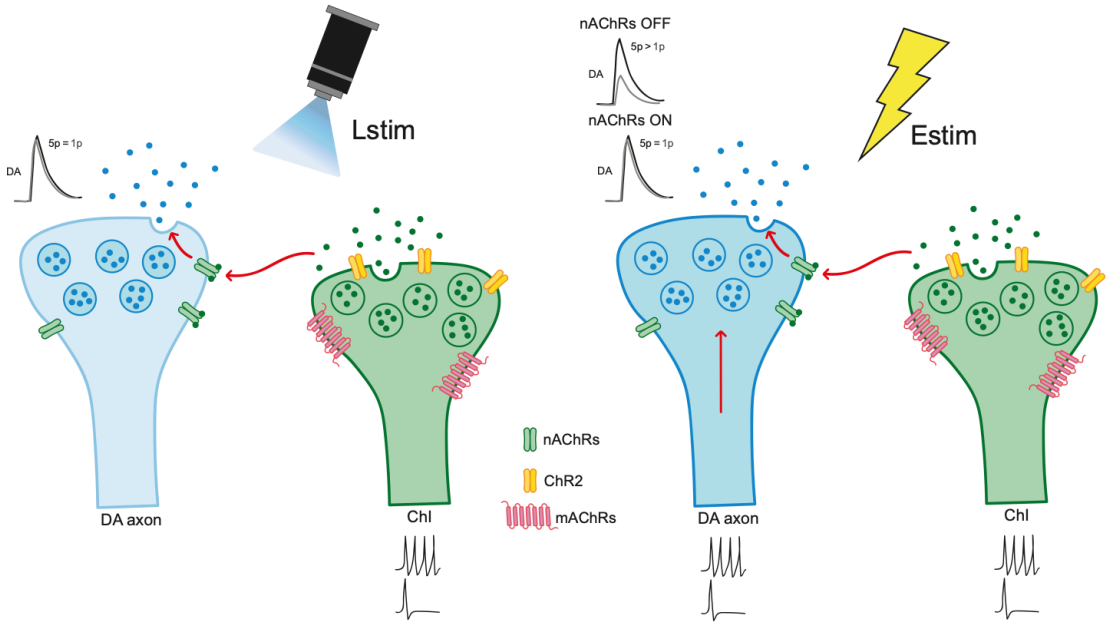


Figure 4.1. Schematic representation of the pathways recruited with the different stimulations used.
(A) *Light stimulation (Lstim) selectively activates ChIs (expressing channelrhodopsin2, ChR2), which release ACh that binds to nAChRs on DA axons and drives DA release. Single pulse (1p) or burst of pulses (5p) at any frequency do not alter the magnitude of ACh-driven DA release.*
(B) *Electrical stimulation (Estim) provides a generalised depolarisation which activates DA neurons and ChIs. Stimulating with 5p at any frequency does not drive more DA release than a single pulse when nAChRs are on. When nAChRs are off, DA released by burst stimulation at high frequency is higher than DA released by a single pulse. The abbreviation nAChRs indicates β2-subunit-containing nicotinic ACh receptors, while mAChRs indicate M_2 and M_4-muscarinic autoreceptors on ChIs.*

Different stimulation protocols were designed comprising single pulses or train of pulses at different frequencies delivered in a pseudorandom order. Chosen frequencies span the range of DA neurons firing frequencies *in vivo*. Simplified protocols delivering single pulses or 5 pulses at 40 Hz in a pseudorandom order were used for experiments combining light and electrical stimulation. Frequency of 40 Hz

was chosen as a tool to explore cholinergic function since it is the highest frequency for reliable ChR2-driven ChI firing (Threlfell et al., 2012). Stimulation protocols were repeated in triplicates in each recording site. Drug or modified aCSF wash-ons were performed in the same recording sites and single light/electrical pulses were given prior protocol start to reach stable effect on DA release. For experiments requiring changes in $[Ca^{2+}]_o$, $[CaCl_2]$ was changed accordingly and CFMs were calibrated in each $[Ca^{2+}]_o$. Mg^{2+}-substitution was not used when lowering $[Ca^{2+}]_o$ to avoid confounding effects of Mg^{2+}-mediated NMDA receptor block (Nowak et al., 1984).

For experiments comparing the effect of genotype (calbKD vs calbWT), slices from both genotypes were prepared in one experimental day and recordings were carried out with slices from both genotypes in the bath at the same time, to allow direct comparisons.

Data were acquired and analysed using Axoscope 10.5 (Molecular Devices) and locally-written Microsoft Excel macros. DA oxidation currents values were measured from background-subtracted voltammograms, converted to concentration using the electrode calibration factor and plotted against time to obtain $[DA]_o$ transients. Electrode calibration was carried out in each recording solution. The number of animals for each dataset is $N \geqslant 3$. Pilot observations with a $N = 2$ were reported in **Figure 4.16B**.

Statistical analysis was carried out using GraphPad Prism. To assess statistical significance, two-way ANOVA and Student's t-test were performed, together with linear regression analysis.

4.2.3 GRAB sensor and calcium imaging

For $GRAB_{ACh}$ and $GRAB_{DA}$ imaging experiments recordings were carried out as described in **Chapter 2** (**Section 2.3.3** and **2.3.4**). To achieve a sampling frequency of 100 Hz, a recording window of active pixels was defined, the camera exposure rate set to 10 ms and the pixels binned 2x2. Excitation light consisted of a blue LED (470 nm) and was turned on continuously to record each neurotransmitter release event

($GRAB_{ACh}$: 2s; $GRAB_{DA}$: 2.5s) with an intensity of ~10-11 mW. Data were extracted and processed as described in **Section 2.3.5**.

For calcium imaging experiments, recordings were carried out as described in **Chapter 2** (**Section 2.3.3** and **2.3.4**). Exposure time was increased to 100 ms and excitation light intensity was lowered to ~5 mW to minimise bleaching.

For all experiments, stimulation protocols were carried out in duplicates and the order of stimuli was randomised. For $GRAB_{ACh}$ experiments probing ACh release in response to changes in extracellular calcium concentration ($[Ca^{2+}]_o$), recordings started in control $[Ca^{2+}]_o$ (2.4 mM) and either high $[Ca^{2+}]_o$ (3.6 mM) or low $[Ca^{2+}]_o$ (1.2 mM) aCSF were subsequently washed on. Data are expressed as normalised to their true control $[Ca^{2+}]_o$ levels.

For each set of experiments the number of experimental animals was $N \geqslant 3$. Pilot observations with a N = 2 were reported in **Figure4.4A-B** and **Figure4.15**. Comparisons for statistical significance were assessed by two-way ANOVA, Student's t-test or linear regression using GraphPad Prism 9.

4.2.4 Drugs

Drugs were diluted in either dH_2O or DMSO (dymethil sulfoxide) to 1,000x stock aliquots and stored at -20°C. Final drug concentrations (**Table 4.1**) were prepared in aCSF saturated with 95% O_2/ 5% CO_2 right before use.

DRUG	SUPPLIER	ACTION	CONCENTRATION	REFERENCES
Atropine	Tocris Bioscience	mAChR antagonist	2-50 µM	(Threlfell et al., 2010)
DHβE	Tocris Bioscience	β2-nAChR antagonist	1 µM	(Threlfell et al., 2012)
Oxotremorine-M	Tocris Bioscience	mAChR agonist	180 nM-10 µM	(Threlfell et al., 2010)

Table 4.1. List of drugs used in Chapter 4 with mode of action and references clarifying concentration choice.

4.3 RESULTS

4.3.1 ACh-driven DA release is sensitive to changes in ACh release levels but insensitive to ChI stimulation frequency

ACh released following synchronous activation of ChIs can directly evoke DA release, bypassing action potential firing in DA somata (Threlfell et al., 2012). Furthermore, DA release presents a biphasic profile characterised by an initial dopaminergic component and a subsequent cholinergic-driven component (Wang et al., 2014a, 2014b). Given this strong cholinergic-driven component of DA release, I investigated the relationship between dynamic changes in ACh release driven by activity in ChIs and subsequent gating of DA release.

To directly test the effects of ChI activation on DA release, I used mouse striatal slices expressing the light-activated ion channel ChR2 selectively in ChIs (ChAT-Cre;Ai32) and FCV to measure light-evoked DA release. To measure dynamic changes in ACh release, I used the globally expressed $GRAB_{ACh}$ sensor (Jing et al., 2020).

First, I tested whether ACh-driven DA was released according to stimulation intensity. I hypothesise that changes in the light intensity used to activate ChIs should result in higher or lower ACh release, which will in turn drive more or less DA release. Indeed, I previously showed that ACh is released according to stimulation current intensity (**Chapter 3**, **Figure 3.1E**), similarly in both dorsolateral and ventral striatum. Consistently, DA release evoked by single light pulses delivered at different intensities scaled according to light power, with regional differences (**Figure 4.2A-B**. Two-way ANOVA, current x region interaction: $F(5,48) = 5.81$, $p = 0.0003$; current effect: $F(5,48) = 100.4$, $p < 0.0001$; region effect: $F(1,48) = 22.93$, $p < 0.0001$. Bonferroni multiple comparisons, 1 mW: $p > 0.99$; 2 mW: $p = 0.0002$; 5 mW: $p < 0.0001$; 8 mW: $p = 0.15$; 11 mW: $p > 0.99$; 15 mW: $p > 0.99$. CPu: n = 6 slices in N = 4 mice, NAcC: n = 4 slices in N = 4 mice).

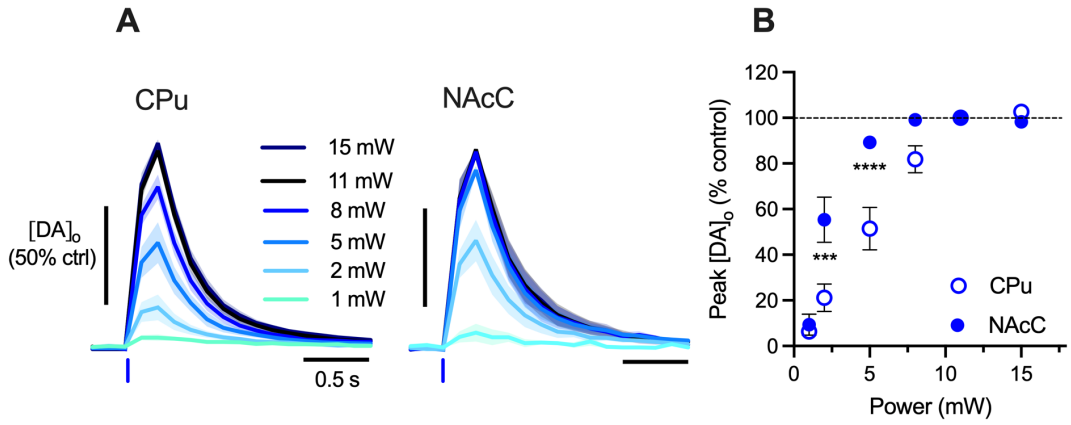


Figure 4.2. ACh-driven DA release evoked by single light pulses scales according to stimulation light intensity.
(A) *Mean $[DA]_o$ transients (± SEM) over time evoked by different light intensities in dorsolateral (CPu) and ventral (NAcC) striatum. Data are normalised to control light power 11 mW and evoked by single light stimuli. CPu: n = 6 slices in N = 4 mice, NAcC: n = 4 slices in N = 4 mice.*
(B) *Mean peak $[DA]_o$ (± SEM) plotted against light power intensity in dorsolateral (CPu) and ventral (NAcC) striatum.. Data are normalised to control power 11 mW. Light-driven DA release is released according to stimulation light intensity, with differences in dorsal compared to ventral striatum. Two-way ANOVA: current x region interaction: $F(5,48) = 5.81$, $p = 0.0003$; current effect: $F(5,48) = 100.4$, $p < 0.0001$; region effect: $F(1,48) = 22.93$, $p < 0.0001$. Bonferroni multiple comparisons: 1 mW: $p > 0.99$; 2 mW: $p = 0.0002$; 5 mW: $p < 0.0001$; 8 mW: $p = 0.15$; 11 mW: $p > 0.99$; 15 mW: $p > 0.99$. CPu: n = 6 slices in N = 4 mice, NAcC: n = 4 slices in N = 4 mice.*

Overall, these findings suggest that ACh-driven DA release is positively correlated to ACh release levels. However, targeted optogenetic activation of ChIs with multiple stimuli delivered at different frequencies did not result in alterations in DA release levels, suggesting that the cholinergic component of DA release is not a straightforward readout of activity in ChIs (Threlfell et al., 2012). In **Chapter 3** (**Section 3.3.3**), I showed that ACh is released according to stimulation frequency in dorsolateral and ventral striatum. These results further support the notion that changes in ACh levels resulting from activity in ChIs do not impact on the levels of ACh-driven DA release. To better understand the underlying mechanisms, I set out to investigate how dynamic changes in ACh release levels can modulate short-term plasticity (STP) of ChI-driven and DA-driven DA.

The first strategy used to dynamically vary ACh release levels was changing extracellular calcium concentration ($\Delta[Ca^{2+}]_o$), which altered ACh release probability as previously described (**Chapter 3**, **Figure 3.2D-G**). To test whether ACh was released according to stimulation frequency and $\Delta[Ca^{2+}]_o$, I varied $[Ca^{2+}]_o$ and measured ACh released by either single electrical pulses or trains of 5 pulses at different frequencies

(5-40 Hz). In dorsolateral striatum, ACh release scaled according to $[Ca^{2+}]_o$ for all stimulation conditions (**Figure 4.3A**. Two-way ANOVA, $[Ca^{2+}]_o$ effect for 1p: $F(2,1300) = 486.8$, $p < 0.0001$; 5p at 5 Hz: $F(2,2890) = 528.8$, $p < 0.0001$; 5p at 25 Hz: $F(2,3399) = 542.1$, $p < 0.0001$; 5p at 40 Hz: $F(2,3400) = 561.8$, $p < 0.0001$. 2.4-3.6 mM: n = 4 slices in N = 4 mice, 2.4-1.2 mM: n = 6 slices in N = 4 mice). To evaluate the effect of $\Delta[Ca^{2+}]_o$ and stimulation frequency on ACh release STP, I looked at 5p:1p ratios in each $[Ca^{2+}]_o$ condition. Ratios were increased according to stimulation frequency (**Figure 4.3B**. Simple linear regression and slope significantly non-zero for paired experiments, 2.4-3.6 mM: $R^2 = 0.88$, $p < 0.0001$; $R^2 = 0.85$, $p < 0.0001$, n = 4 slices in N = 4 mice. 2.4-1.2 mM: $R^2 = 0.68$, $p < 0.0001$, $R^2 = 0.23$, $p = 0.043$, n = 6 slices in N = 4 mice). Ratios were also overall higher in high $[Ca^{2+}]_o$ (3.6 mM), but the same relationship between $[Ca^{2+}]_o$ and frequency was maintained in all $[Ca^{2+}]_o$ conditions (**Figure 4.3B**. Simple linear regression with slope and elevation comparison for paired experiments, 2.4-3.6 mM: slopes do not significantly differ, $p = 0.65$, elevations significantly differ, $P = 0.035$, n = 4 slices in N = 4 mice. 2.4-1.2 mM: slopes and elevations do not significantly differ, $p = 0.97$ and $p = 0.71$ respectively, N = 6 slices in N = 4 mice). Overall, these findings suggest that ACh is released dynamically according to $[Ca^{2+}]_o$ and stimulation frequency in dorsolateral striatum.

I then tested if these dynamic changes in ACh release would differentially drive DA release. I selectively light activated ChIs with single pulses or trains of 5p at different frequencies (5-40 Hz) and changed $[Ca^{2+}]_o$, while monitoring DA release with FCV. These stimulation parameters were chosen to mimic the range of tonic and phasic firing in ChIs and DA neurons. Furthermore, ChIs activated with ChR2 can reliably fire action potentials at all chosen stimulation frequencies (Threlfell et al., 2012). In dorsolateral striatum (CPu), light-driven DA release was reduced in low $[Ca^{2+}]_o$ and enhanced in high $[Ca^{2+}]_o$ (**Figure 4.3C**. Two-way ANOVA, $[Ca^{2+}]_o$ effect for 1p: $F(1.018,58.00) = 41.82$, $p < 0.0001$; 5p at 5 Hz: $F(1.020,58.14) = 42.95$, $p < 0.0001$; 5p at 25 Hz: $F(1.022,58.27) = 42.32$, $p < 0.0001$; 5p at 40 Hz: $F(1.019,58.06) = 49.00$, $p < 0.0001$, n = 4 slices in N = 4 mice), consistently with the $[Ca^{2+}]_o$-driven changes in ACh release. However, trains of 5p at increasing frequencies failed to promote

additional DA release, in contrast with promoting dynamic changes in ACh release. Indeed, 5p:1p ratios were unaffected by changes in $[Ca^{2+}]_o$ and frequency (**Figure 4.3D**. Two-way ANOVA, $[Ca^{2+}]_o$ x frequency interaction: $F(4,18) = 0.124$, $p = 0.97$; frequency effect: $F(2,9) = 0.19$, $p = 0.82$; $[Ca^{2+}]_o$ effect: $F(1.205, 10.85) = 0.091$, $p = 0.81$, $n = 4$ slices in $N = 4$ mice). Overall, these results suggest that ACh-driven DA release depends upon ACh levels but is insensitive to ChI stimulation frequency in the dorsolateral striatum.

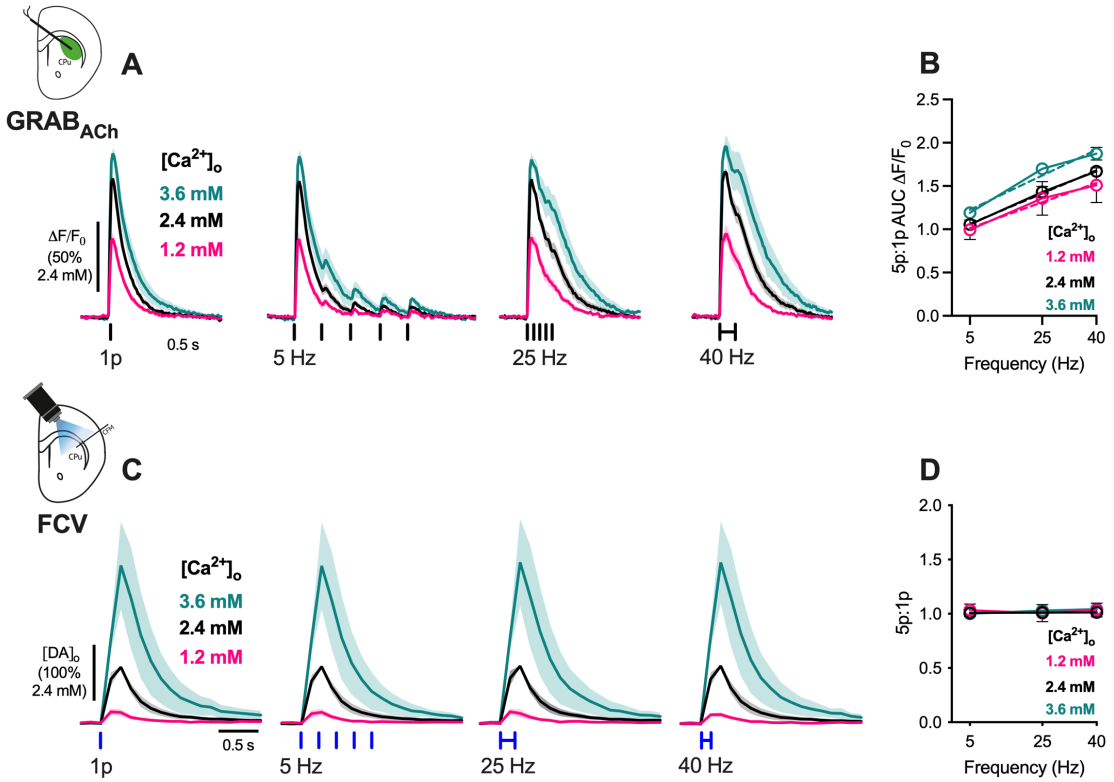


Figure 4.3. In dorsolateral striatum, changes in [Ca^{2+}]$_o$ and stimulation frequency change ACh release accordingly, but corresponding ACh-driven DA release does not reflect the changes in ACh release.

(A) *Mean (± SEM) ACh transients evoked by single electrical pulses (1p) or trains of 5 pulses (5p) at 5-40 Hz in dorsolateral striatum (CPu) in different [Ca^{2+}]$_o$ conditions. Experiments were carried out starting in control Ca^{2+} levels (2.4 mM) and then washing on aCSF with altered [Ca^{2+}]$_o$, so that only two [Ca^{2+}]$_o$ conditions were tested in one site. Each condition is normalised to its true control (2.4 mM [Ca^{2+}]$_o$). 2.4 mM to 3.6 mM: n = 4 slices in N = 4 mice. 2.4 mM to 1.2 mM: n = 6 slices in N = 4 mice. ACh is released according to [Ca^{2+}]$_o$ levels. Two-way ANOVA: [Ca^{2+}]$_o$ effect for 1p: F (2,1300) = 486.8, p < 0.0001; 5p at 5 Hz: F (2,2890) = 528.8, p < 0.0001; 5p at 25 Hz: F (2,3399) = 542.1, p < 0.0001; 5p at 40 Hz: F (2,3400) = 561.8, p < 0.0001. 2.4-3.6 mM: n = 4 slices in N = 4 mice, 2.4-1.2 mM: n = 6 slices in N = 4 mice.*

(B) *Mean (± SEM) 5p:1p ΔF/F$_0$ (calculated from AUC) plotted against stimulation frequency in different [Ca^{2+}]$_o$ conditions. Ratios are increased according to stimulation frequency in all [Ca^{2+}]$_o$ conditions. Simple linear regression and slope significantly non-zero for paired experiments: 2.4 mM to 3.6 mM: R^2 = 0.88, p < 0.0001; R^2 = 0.85, p < 0.0001, n = 4 slices in N = 4 mice. 2.4 mM to 1.2 mM: R^2 = 0.68, p < 0.0001, R^2 = 0.23, p = 0.043, n = 6 slices in N = 4 mice. Ratios were also overall higher in high [Ca^{2+}]$_o$ (3.6 mM), but the same relationship between [Ca^{2+}]$_o$ and frequency was maintained in all [Ca^{2+}]$_o$ conditions. Simple linear regression with slope and elevation comparison for paired experiments: 2.4 mM to 3.6 mM: slopes do not significantly differ, p = 0.65, elevations significantly differ, p = 0.035, n = 4 slices in N = 4 mice. 2.4 mM to 1.2 mM: slopes and elevations do not significantly differ, p = 0.97 and p = 0.71, respectively, n = 6 slices in N = 4 mice. The data here represented were collected using AAV5.hSyn.ACh3.0.*

(C) *Mean [DA]$_o$ transients (± SEM) over time in different [Ca^{2+}]$_o$ evoked by 1p or trains of 5p at different frequencies in the dorsolateral striatum (CPu). Transients are normalised to 1p 2.4 mM [Ca^{2+}]$_o$. Changes in [Ca^{2+}]$_o$ alter 1p and 5p light-driven DA release in a similar way. Two-way ANOVA: [Ca^{2+}]$_o$ effect for 1p: F (1.018,58.00) = 41.82, p < 0.0001; 5p at 5 Hz: F (1.020,58.14) = 42.95, p < 0.0001; 5p at 25 Hz: F (1.022,58.27) = 42.32, p < 0.0001; 5p at 40 Hz: F (1.019,58.06) = 49.00, p < 0.0001, n = 4 slices in N = 4 mice.*

(D) *Mean (± SEM) 5p:1p peak [DA]$_o$ plotted against stimulation frequency. Ratios were unaffected by changes in [Ca^{2+}]$_o$ and frequency. Two-way ANOVA: [Ca^{2+}]$_o$ x frequency interaction: F (4,18) = 0.124, p = 0.97; frequency effect: F (2,9) = 0.19, p = 0.82; [Ca^{2+}]$_o$ effect: F (1.205, 10.85) = 0.091, p = 0.81, n = 4 slices in N = 4 mice.*

In the NAcC, ACh release also varied according to [Ca^{2+}]$_o$ (**Figure 4.4A**. Two-way ANOVA, [Ca^{2+}]$_o$ effect for 1p: F (2,808) = 983.5, p < 0.0001; 5p at 5 Hz: F (2,1650)

= 1130, $p < 0.0001$; 5p at 25 Hz: F (2,1111) = 396.4, $p < 0.0001$; 5p at 40 Hz: F (2,1111) = 327.2, $p < 0.0001$. 2.4-3.6 mM: n = 3 slices in N = 2 mice, 2.4-1.2 mM: n = 4 slices in N = 3 mice). To test the effect of stimulation frequency on ACh release in different $[Ca^{2+}]_o$ conditions, I calculated 5p:1p ratios. Ratios are proportional to stimulation frequency in all $[Ca^{2+}]_o$ (**Figure 4.4B**. Simple linear regression and slope significantly non-zero for paired experiments, 2.4-3.6 mM: $R^2 = 0.87$, $p = 0.0002$; $R^2 = 0.83$, $p = 0.0006$, n = 3 slices in N = 2 mice. 2.4-1.2 mM: $R^2 = 0.70$, $p = 0.0006$, $R^2 = 0.60$, $p = 0.0029$, n = 4 slices in N = 3 mice), suggesting that ACh is released according to stimulation.

DA release evoked by light stimuli to activate ChIs was also positively correlated with $[Ca^{2+}]_o$ (**Figure 4.4C.** Two-way ANOVA, $[Ca^{2+}]_o$ effect for 1p: F (1.028,78.15) = 89.19, $p < 0.0001$; 5p at 5 Hz: F (1.029,78.19) = 85.58, $p < 0.0001$; 5p at 25 Hz: F (1.032,78.42) = 85.77, $p < 0.0001$; 5p at 40 Hz: F (1.022,77.66) = 97.26, $p < 0.0001$, n = 5 slices in N = 5 mice), consistently with changes in ACh release. However, 5p:1p ratios were unaltered by changes in $[Ca^{2+}]_o$ and stimulation frequency (**Figure 4.4D**. Two-way ANOVA frequency x $[Ca^{2+}]_o$ interaction: F (4,24) = 2.193, $p = 0.1$; frequency effect: F (2,12) = 3.144, $p = 0.08$; $[Ca^{2+}]_o$ effect: F (1.198,14.38) = 0.86, $p = 0.38$, n = 5 slices in N = 5 mice). Taken together, these data suggest that dynamic changes in ACh release levels impact on ACh-driven DA in a way independent from ChI stimulation frequency in the ventral striatum.

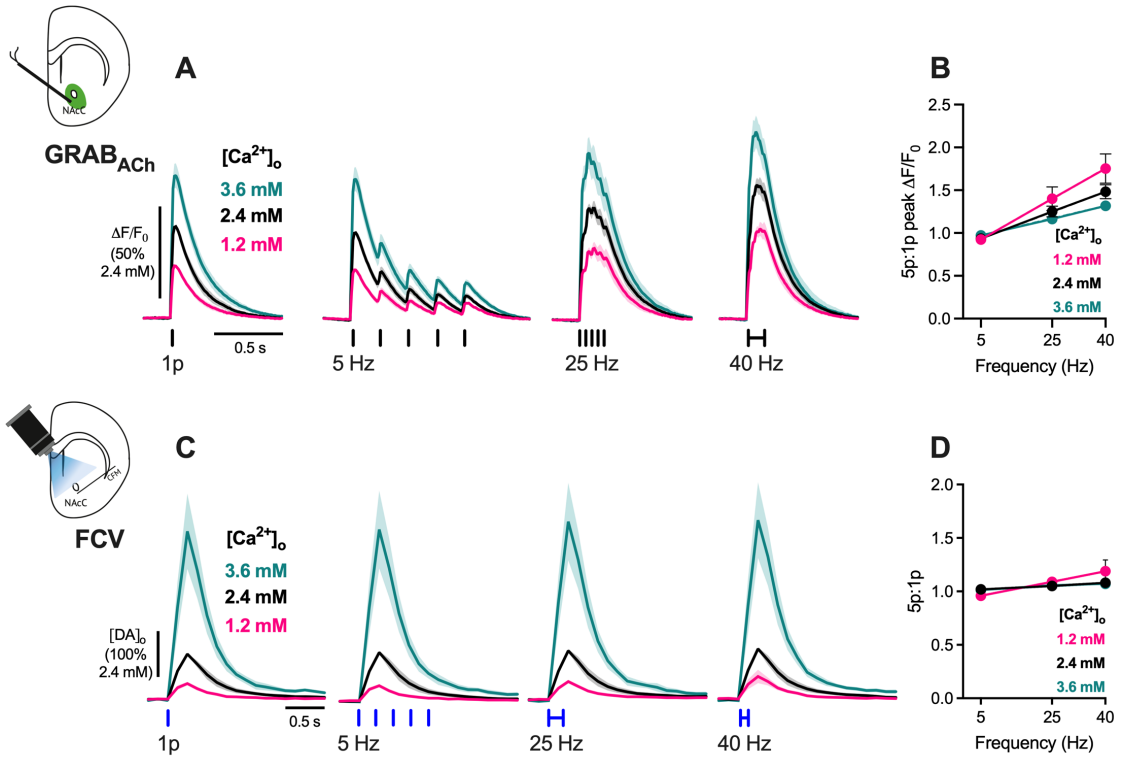


Figure 4.4. ACh is released according to stimulation frequency and [Ca^{2+}]$_o$, but these changes are not reflected in ACh-driven DA release in the ventral striatum.

(A) *Mean (± SEM) ACh transients evoked by single electrical pulses or trains of 5 pulses at 5-40 Hz in NAcC in different [Ca^{2+}]$_o$ conditions. Experiments were carried out starting in control Ca^{2+} levels (2.4 mM) and then washing on aCSF with altered [Ca^{2+}]$_o$, so that only two [Ca^{2+}]$_o$ conditions were tested in one site. Each condition is normalised to its true control (2.4 mM [Ca^{2+}]$_o$). ACh is released according to [Ca^{2+}]$_o$ levels. Two-way ANOVA: [Ca^{2+}]$_o$ effect for 1p: F (2,808) = 983.5, p < 0.0001; 5p at 5 Hz: F (2,1650) = 1130, p < 0.0001; 5p at 25 Hz: F (2,1111) = 396.4, p < 0.0001; 5p at 40 Hz: F (2,1111) = 327.2, p < 0.0001. 2.4-3.6 mM: n = 3 slices in N = 2 mice, 2.4-1.2 mM: n = 4 slices in N = 3 mice.*

(B) *Mean (± SEM) 5p:1p ΔF/F$_0$ (calculated from peak values) plotted against stimulation frequency in different [Ca^{2+}]$_o$ conditions. Ratios are increased according to stimulation frequency in all [Ca^{2+}]$_o$ conditions. Simple linear regression and slope significantly non-zero for paired experiments: 2.4-3.6 mM: R^2 = 0.87, p = 0.0002; R^2 = 0.83, p = 0.0006, n = 3 slices in N = 2 mice. 2.4-1.2 mM: R^2 = 0.70, p = 0.0006, R^2 = 0.60, p = 0.0029, n = 4 slices in N = 3 mice. The data here represented were collected using AAV5.hSyn.ACh3.0.*

(C) *Mean [DA]$_o$ transients (± SEM) over time in different [Ca^{2+}]$_o$ evoked by 1p or trains of 5p at different frequencies in the NAcC. Changes in [Ca^{2+}]$_o$ altered 1p and 5p light-driven DA release in a similar way. Transients are normalised to 1p 2.4 mM [Ca^{2+}]$_o$. Two-way ANOVA: [Ca^{2+}]$_o$ effect for 1p: F (1.028,78.15) = 89.19, p < 0.0001; 5p at 5 Hz: F (1.029,78.19) = 85.58, p < 0.0001; 5p at 25 Hz: F (1.032,78.42) = 85.77, p < 0.0001; 5p at 40 Hz: F (1.022,77.66) = 97.26, p < 0.0001, n = 5 slices in N = 5 mice.*

(D) *Mean (± SEM) 5p:1p peak [DA]$_o$ plotted against stimulation frequency. Ratios were unaffected by changes in [Ca^{2+}]$_o$ and frequency. Two-way ANOVA: frequency x [Ca^{2+}]$_o$ interaction: F (4,24) = 2.193, p = 0.1; frequency effect: F (2,12) = 3.144, p = 0.08; [Ca^{2+}]$_o$ effect: F (1.198,14.38) = 0.86, p = 0.38, n = 5 slices in N = 5 mice.*

Overall, I've showed that ACh-driven DA release depends upon levels of ACh release. However, dynamic changes in ACh release resulting from ChI activity do not result in a dynamic response of ChI-driven DA release.

4.3.2 Putative reduction in ACh levels driven by agonism of mAChRs partially promotes DA release sensitivity to stimulation of DA neurons but not ChIs

Levels of ACh and ChI excitability can also be affected by mAChR agonism and antagonism (Yan and Surmeier, 1996; Ding et al., 2006; Bonsi et al., 2008). The broad spectrum mAChR agonist oxotremorine decreased 1p electrically evoked DA release and enhanced burst-driven release measured with FCV in mouse striatal slices (Threlfell et al., 2010). This suggests that activation of mAChRs on ChIs, which inhibits their firing, decreased ACh release and deactivated nAChRs, allowing an increase in DA release sensitivity to presynaptic depolarisation frequency (Threlfell et al., 2010). That study used electrical stimulation, which recruits simultaneously DA axons and ChIs (**Figure 4.1**). Thus, the individual contribution of the cholinergic and dopaminergic components of DA release remains to be defined.

I tested whether a reduction in ACh levels mediated by mAChR agonism could promote DA release sensitivity to changes in stimulation of ChIs or DA axons and whether there were differences between the two components. To separate the cholinergic component from the dopaminergic component, I used striatal slices from ChAT-Cre;Ai32 mice (selective light activation of ChIs) and combined light stimulation (ChIs only) with electrical stimulation (ChIs + DA axons) (**Figure 4.1**). To test if agonism of mAChRs promoted DA release responsiveness to stimulation, I used FCV to detect DA release, the broad-spectrum mAChRs agonist oxotremorine-M and a stimulation protocol alternating between either electrical or light single pulses (1p) or trains of 5 pulses (5p) at 40 Hz. This paradigm was chosen because frequencies of 40 Hz are in the range of DA neuron burst firing and can reliably evoke action potentials in ChIs expressing ChR2 (Threlfell et al., 2012).

In the dorsolateral striatum, wash on of increasing concentrations of oxotremorine (500 nM-10 μM) progressively decreased electrically-evoked DA release (**Figure 4.5A-B**. Two-way ANOVA, concentration x frequency interaction: $F(3,24) = 0.13$, $p = 0.93$; frequency effect: $F(1,8) = 13.84$, $p = 0.0059$; concentration effect: $F(3,24) = 40.15$, $p < 0.0001$, n = 5 slices in N = 4 mice). Light-evoked DA release was also decreased progressively by increasing concentrations of oxotremorine

(**Figure 4.5C-D**. Two-way ANOVA, concentration x frequency interaction: F (3,24) = 0.049, p = 0.98; frequency effect: F(1,8) = 0.0052, p = 0.94; concentration effect: F (3,24) = 107.8, p < 0.0001, n = 5 slices in N = 4 mice). These findings suggest that agonism of mAChRs reduced ACh release and activation of nAChRs by released ACh, decreasing ACh-evoked DA release.

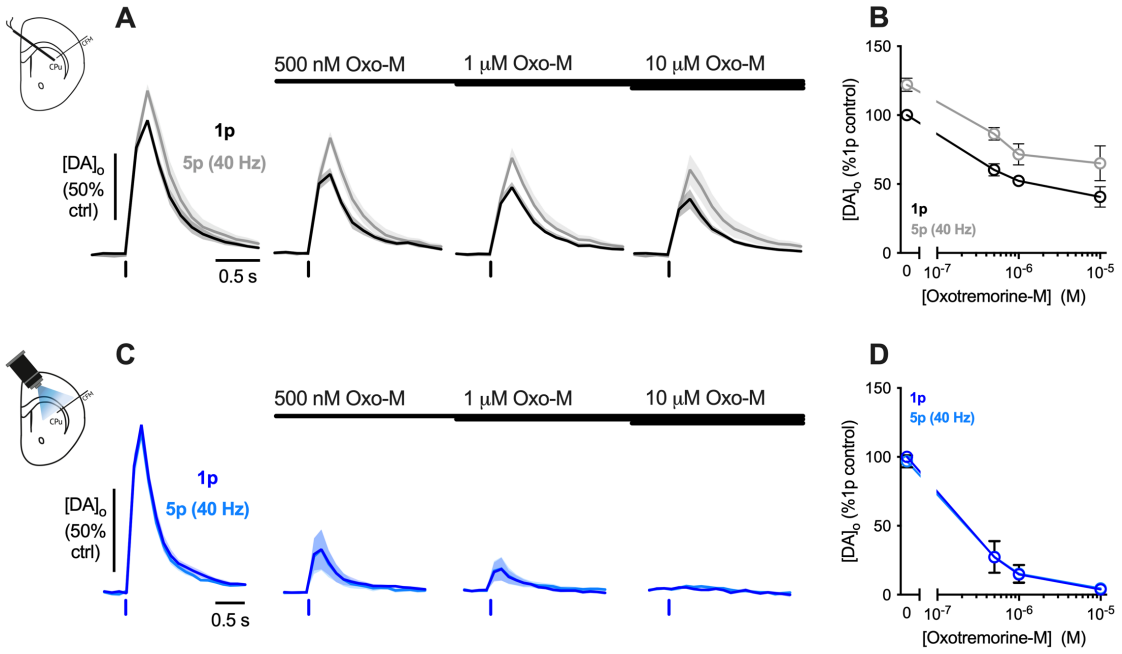


Figure 4.5. Agonism of mAChRs reduced electrically and light-evoked DA release in the dorsolateral striatum.
(A) *Mean [DA]o transients (± SEM) against time in different oxotremorine-M concentrations evoked by single electrical pulses (1p) trains of 5 pulses (5p) at 40 Hz in dorsolateral striatum (CPu). Transients are normalised to 1p in control conditions (drug-free). Overall, oxotremorine decreased electrically-evoked DA release (quantified in B), n = 5 slices in N = 4 mice.*
(B) *Mean peak [DA]o electrically evoked by 1p or 5p (40 Hz) plotted against oxotremorine-M concentration. Agonism of mAChR reduced electrically-evoked DA release. Two-way ANOVA: concentration x frequency interaction: F (3,24) = 0.13, p = 0.93; frequency effect: F (1,8) = 13.84, p = 0.0059; concentration effect: F (3,24) = 40.15, p < 0.0001, n = 5 slices in N = 4 mice.*
(C) *Mean [DA]o transients (± SEM) against time in different oxotremorine-M concentrations evoked by single light pulses (1p) trains of 5p at 40 Hz in dorsolateral striatum. Transients are normalised to 1p in control conditions (drug-free). Oxotremorine decreased light-evoked DA release (quantified in D), n = 5 slices in N = 4 mice.*
(D) *Mean peak [DA]o light-evoked by 1p or 5p plotted against oxotremorine-M concentration. Agonism of mAChR reduced light-evoked DA release. Two-way ANOVA: concentration x frequency interaction: F (3,24) = 0.049, p = 0.98; frequency effect: F (1,8) = 0.0052, p = 0.94; concentration effect: F(3,24) = 107.8, p < 0.0001, n = 5 slices in N = 4 mice.*

To test the effect of mAChR agonism (oxotremorine) on the frequency response of electrically and light-evoked DA release, I examined whether there were differences in DA release driven by 1p or 5p. With electrical stimulation, 5p (40 Hz) evoked more DA release than 1p in all conditions (**Figure 4.6A**. Linear regression and

slope comparison with x = y line, aCSF: R^2 = 0.98; 500 nM: R^2 = 0.99; 1 µM: R^2 = 0.98; 10 µM: R^2 = 0.92, p < 0.0001, n = 5 slices in N = 4 mice). 5p:1p ratios were not significantly altered by oxotremorine (**Figure 4.6B**. Linear regression and slope significantly non-zero, R^2 = 0.64, p = 0.19, n = 5 slices in N = 4 mice). Taken together, these results suggest that a reduction in ACh levels driven by agonism of mAChRs overall decreased DA release but failed to promote DA release sensitivity to stimulation. These findings are apparently in contrast with previous observations, which reported a strong effect of oxotremorine in facilitating burst-driven DA release (Threlfell et al., 2010). However, in the study conducted by Threlfell et al. (2010), a higher stimulation frequency was used (100 Hz). The small effect here described is due to the use of a lower stimulation frequency (40 Hz). This frequency was chosen to better mimic physiological burst firing in DA neurons and to reliably activate ChR2-expressing ChIs with light stimuli (Threlfell et al., 2012).

To test whether reduction in ACh levels driven by agonising of mAChRs unveiled any frequency sensitivity in light-evoked release, I looked at the differences between DA evoked by single light stimuli or a burst of pulses. In all oxotremorine concentrations, ACh-evoked DA release elicited by 1p or 5p was the same (**Figure 4.6C**. Linear regression and slope comparison with x = y line, aCSF: R^2 = 0.90; 500 nM: R^2 = 0.95; 1 µM: R^2 = 0.83; 10 µM: R^2 = 0.46, p = 0.56, n = 5 slices in N = 4 mice), suggesting that reduction in ACh levels driven by mAChR agonism did not unveil stimulation dependence of ACh-driven DA release. In 10 µM oxotremorine there was no more detectable DA release, and peak DA evoked by 5p and 1p were both close to zero (**Figure 4.6C**. Linear regression, R^2 = 0.46, X-intercept = -0.062, Y-intercept = 0.021).

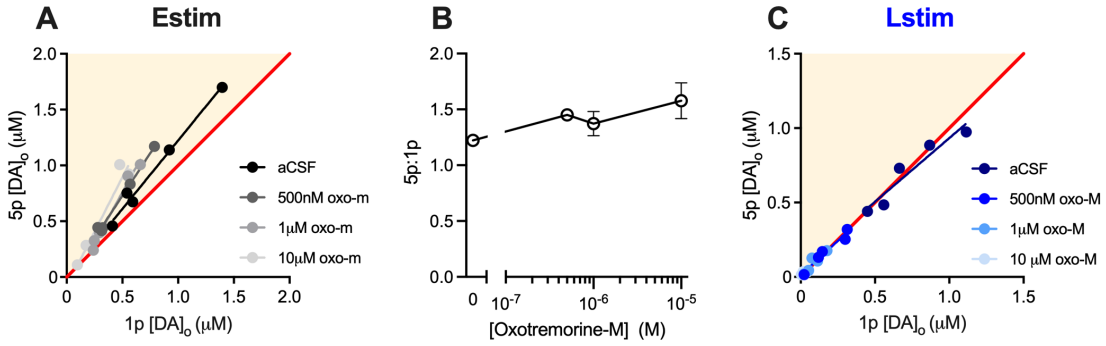


Figure 4.6. In dorsolateral striatum, agonism of mAChRs failed to promote additional sensitivity to stimulation frequency in light and electrically-evoked DA.
(A) *Peak 5p-driven $[DA]_o$ plotted against peak 1p-driven $[DA]_o$ in drug-free and oxotremorine-M. Linear regression analysis and comparison with x = y perfect line (red) was performed to test whether release driven by 5p and 1p was analogous. Linear regression and slope comparison with x = y line: aCSF: R^2 = 0.98; 500 nM: R^2 = 0.99; 1 μM: R^2 = 0.98; 10 μM: R^2 = 0.92, p < 0.0001, n = 5 slices in N = 4 mice.*
(B) *Mean (± SEM) 5p:1p peak $[DA]_o$ plotted against oxotremorine-M concentration. Ratios did not increase significantly upon oxotremorine wash on at progressively higher concentrations. Linear regression analysis and slope significantly non-zero: R^2 = 0.64, p = 0.19, n = 5 slices in N = 4 mice. (Line not shown on logarithmic scale).*
(C) *Peak 5p-driven $[DA]_o$ plotted against peak 1p-driven $[DA]_o$ in drug-free (aCSF) and oxotremorine-M, for light-evoked DA release. Linear regression analysis and comparison with x = y perfect line (red) was performed to test whether release driven by 5p and 1p was analogous. Linear regression and comparison with x = y line: aCSF: R^2 = 0.90; 500 nM: R^2 = 0.95; 1 μM: R^2 = 0.83; 10 μM: R^2 = 0.46, p = 0.56, n = 5 slices in N = 4 mice.*

In the NAcC, electrically-evoked DA release was progressively decreased upon wash on of oxotremorine at increasing concentrations (**Figure 4.7A-B**. Two-way ANOVA, concentration x frequency interaction: F(3,18) = 0.10, p = 0.95; frequency effect: F (1,6) = 17.42, p = 0.0059; concentration effect: F (3,18) = 6.68, p = 0.0032, n = 4 slices in N = 4 mice). Light-evoked DA was also decreased (**Figure 4.7C-D**. Two-way ANOVA, concentration x frequency interaction: F (3,18) = 0.028, p = 0.99; frequency effect: F (1,6) = 0.18, p = 0.67; concentration effect: F (3,18) = 39.34, p < 0.0001, n = 4 slices in N = 4 mice).

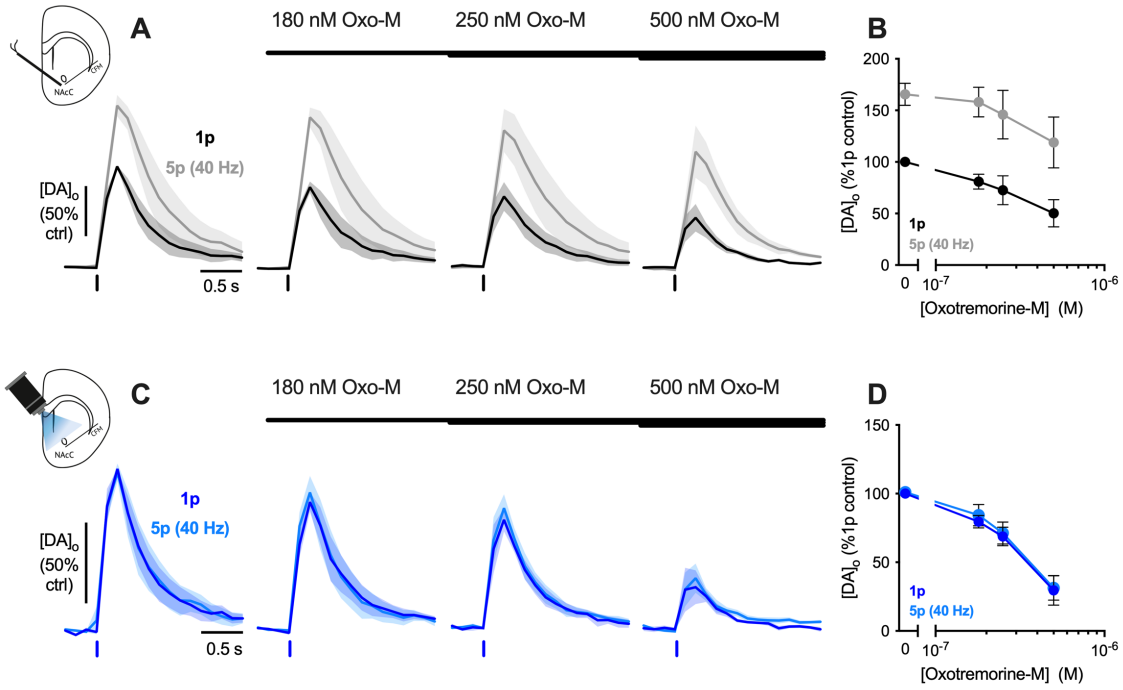


Figure 4.7. In ventral striatum, agonism of mAChRs reduced electrically and light-evoked DA release.
(A) *Mean $[DA]_o$ transients (± SEM) against time in different oxotremorine-M concentrations evoked by single electrical pulses (1p) or trains of 5 pulses (5p) at 40 Hz in ventral striatum (NAcC). Transients are normalised to 1p in control conditions (drug-free). Oxotremorine decreased electrically-evoked DA release (quantified in B), n = 4 slices in N = 4 mice.*
(B) *Mean peak $[DA]_o$ electrically-evoked by 1p or 5p plotted against oxotremorine-M concentration. Agonism of mAChRs reduced electrically-evoked DA release. Two-way ANOVA: concentration x frequency interaction: F(3,18) = 0.10, p = 0.95; frequency effect: F (1,6) = 17.42, p = 0.0059; concentration effect: F (3,18) = 6.68, p = 0.0032, n = 4 slices in N = 4 mice.*
(C) *Mean $[DA]_o$ transients (± SEM) against time in different oxotremorine-M concentrations evoked single light pulses (1p) trains of 5p at 40 Hz in ventral striatum. Transients are normalised to 1p in control conditions (drug-free). Oxotremorine decreases light evoked DA release (quantified in D), n = 4 slices in N = 4 mice.*
(D) *Mean peak $[DA]_o$ light-evoked by 1p or 5p plotted against oxotremorine-M concentration. Agonism of mAChRs reduced light-evoked DA release. Two-way ANOVA: concentration x frequency interaction: F (3,18) = 0.028, p = 0.99; frequency effect: F (1,6) = 0.18, p = 0.67; concentration effect: F (3,18) = 39.34, p < 0.0001, n = 4 slices in N = 4 mice*

Decreasing ACh levels by agonising mAChRs with oxotremorine promoted stimulation sensitivity of electrically-evoked DA release, as shown by higher DA release driven by bursts of 5p (**Figure 4.8A.** Linear regression and comparison with x = y line, aCSF: R^2 = 0.94; 180 nM: R^2 = 0.98; 250 nM: R^2 = 0.99; 500 nM: R^2 = 0.99, p = 0.0004, n = 4 slices in N = 4 mice) and a concentration-dependent increase in the 5p:1p ratios (**Figure 4.8B.** Linear regression and slope significantly non-zero: R^2 = 0.58, p = 0.0005, n = 4 slices in N = 4 mice). However, oxotremorine failed to promote light-driven DA release sensitivity to ChI activation (**Figure 4.8C.** Linear regression and comparison with x = y line, aCSF: R^2 = 0.99; 180 nM: R^2 = 0.98; 250 nM: R^2 = 0.99; 500 nM: R^2 = 0.99, p = 0.26, n = 4 slices in N = 4 mice). Overall, these results suggest

that lower ACh release levels driven by agonism of mAChRs in NAcC and consequent reduction of ACh tone at nAChRs promotes DA release sensitivity to DA neuron activity (electrical stimulation), but not ChIs (light stimulation).

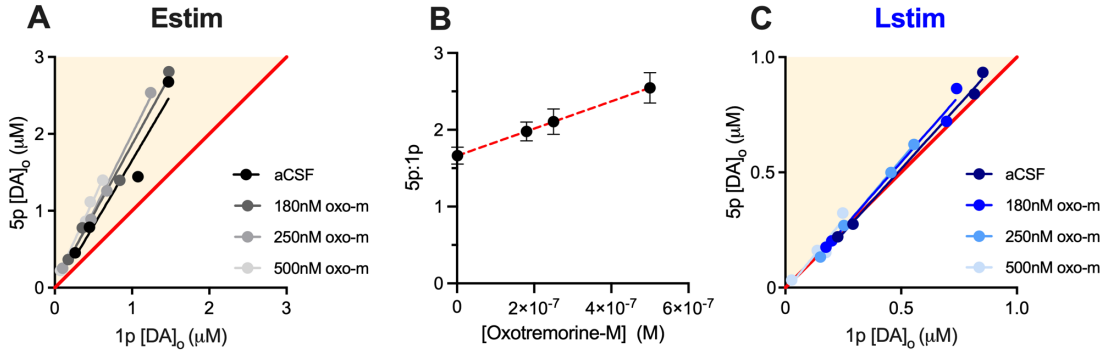


Figure 4.8. Agonism of mAChRs promoted sensitivity to stimulation frequency of electrically but not light-evoked DA release in ventral striatum.
(A) *Peak 5p-driven $[DA]_o$ plotted against peak 1p-driven $[DA]_o$ in drug-free and oxotremorine-M. Linear regression analysis and comparison with x = y perfect line (red) was performed to test whether release driven by 5p and 1p was analogous. Linear regression and comparison with x = y line: aCSF: $R^2 = 0.94$; 180 nM: $R^2 = 0.98$; 250 nM: $R^2 = 0.99$; 500 nM: $R^2 = 0.99$, p = 0.0004, n = 4 slices in N = 4 mice.*
(B) *Mean (± SEM) 5p:1p peak $[DA]_o$ plotted against oxotremorine-M concentration. Ratios were increased upon oxotremorine wash on. Linear regression analysis and slope significantly non-zero: $R^2 = 0.58$, p = 0.0005, n = 4 slices in N = 4 mice.*
(C) *Peak 5p-driven $[DA]_o$ plotted against peak 1p-driven $[DA]_o$ in drug-free (aCSF) and oxotremorine-M, for light-evoked DA release. Linear regression analysis and comparison with x = y perfect line (red) was performed to test whether release driven by 5p and 1p was analogous. Linear regression and comparison with x = y line: aCSF: $R^2 = 0.99$; 180 nM: $R^2 = 0.98$; 250 nM: $R^2 = 0.99$; 500 nM: $R^2 = 0.99$, p = 0.26, n = 4 slices in N = 4 mice.*

Taken together, these findings show that levels of ACh release are significant in determining the magnitude of ChI-driven DA release but do not correspond to a dynamic response of DA release to ChI activation.

4.3.3. Putative increase in ACh levels driven by antagonism of mAChRs promotes DA release sensitivity to stimulation of DA neurons but not ChIs

In this section, I used the broad spectrum mAChR antagonist atropine to block mAChRs and putatively enhance ACh release from ChIs. As for experiments using mAChR agonists, it is difficult to directly test the effect of such compounds on ACh release measured with $GRAB_{ACh}$ sensors, given that the $GRAB_{ACh}$ itself is a mAChR.

Indeed, oxotremorine and atropine directly act at $GRAB_{ACh}$ sensors to respectively increase or decrease fluorescent signals (Jing et al., 2018).

To test whether a potential increase in ACh levels mediated by antagonism of mAChRs unveiled sensitivity of DA release to stimulation of ChI or DA axons, I combined electrical (ChIs + DA axons) and light stimulation (ChIs only, **Figure 4.1**), FCV to detect DA release and washed on the mAChR antagonist atropine at increasing concentrations. I adopted the same stimulation protocol described above in **Section 4.3.2**, consisting of 1p or a train of 5p at 40 Hz. In the study conducted by Threlfell et al. (2010), mAChR inhibition with atropine (2 μM) did not alter the frequency responsiveness of electrically-evoked DA release. Nonetheless, such concentration might be too low and not provide full inhibition. To test this, I measured ChI activation in dorsal striatal slices from mice expressing GCaMP6f selectively in ChIs (ChAT-Cre;Ai95D) upon wash on of the mAChR antagonist atropine at 2 μM. Atropine did not alter ChI activation upon stimulation with single electrical pulses (**Figure 4.9A-B**. Two-tailed paired Student's t-test, $p = 0.54$, $n = 4$ slices in $N = 4$ mice), or trains of 5p at 2 Hz (**Figure 4.9A-C**. Two-way ANOVA, stim number x drug interaction: $F(4,15) = 3.15$, $p = 0.045$; stim number effect: $F(4,15) = 1.88$, $p = 0.16$; drug effect: $F(1,15) = 1.58$, $p = 0.22$. Bonferroni multiple comparisons, stim 1: $p = 0.44$; stim 2: $p > 0.99$; stim 3: $p > 0.99$; stim 4: $p = 0.21$; stim 5: $p = 0.19$, $n = 4$ slices in $N = 4$ mice), suggesting that this atropine concentration might be too low to provide significant inhibition.

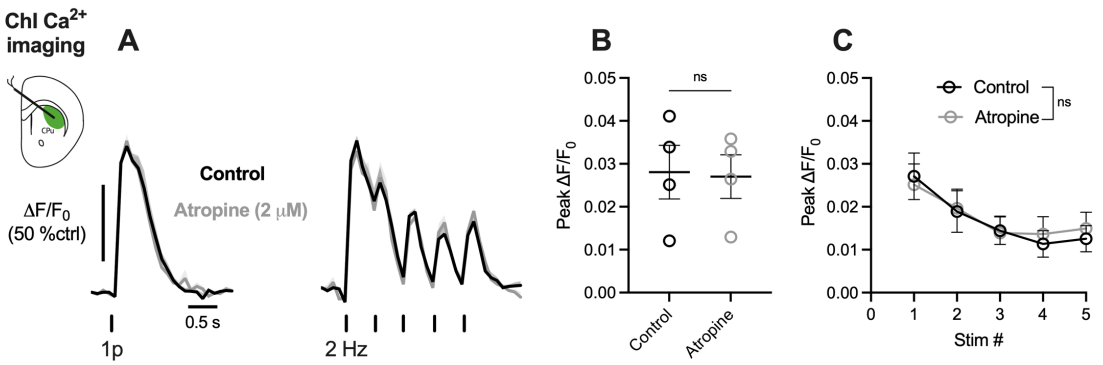


Figure 4.9. Antagonism of mAChRs with 2 μM atropine did not alter ChI activation measured with calcium imaging. ***(A)*** *Mean (± SEM) Ca^{2+} transients evoked by single electrical pulses (1p) or trains of 5 pulses at 2 Hz in dorsolateral striatum (CPu). Data are normalised to single pulse in control conditions (drug-free), n = 4 slices in N = 4 mice.* ***(B)*** *Mean peak $\Delta F/F_0$ (± SEM) evoked by 1p in control and atropine. Antagonism of mAChRs with 2 μM atropine did not alter Ca^{2+} responses evoked by 1p. Two-tailed paired Student's t-test: p = 0.54, n = 4 slices in N = 4 mice.* ***(C)*** *Mean peak $\Delta F/F_0$ (± SEM) plotted against stimulus number (stim #) in 2 Hz trains in control and atropine. Atropine did not alter Ca^{2+} responses evoked by 2 Hz trains. Two-way ANOVA, stim number x drug interaction: F (4,15) = 3.15, p = 0.045; stim number effect: F (4,15) = 1.88, p = 0.16; drug effect: F (1,15) = 1.58, p = 0.22. Bonferroni multiple comparisons, stim 1: p = 0.44; stim 2: p > 0.99; stim 3: p > 0.99; stim 4: p = 0.21; stim 5: p = 0.19, n = 4 slices in N = 4 mice.*

Therefore, for experiments investigating the contribution of mAChR antagonism on the dual component of DA release I started at 2 μM atropine to replicate previous findings and subsequently washed on higher concentrations (10-50 μM).

In the dorsolateral striatum, wash on of atropine at progressively higher concentrations did not significantly alter electrically-evoked DA release (**Figure 4.10A-B**. Two-way ANOVA, drug x stimulation interaction: F (3,24) = 0.050, p = 0.98; drug effect: F (3,24) = 0.79, p = 0.50; stimulation effect: F (1,8) = 5.51, p = 0.046, n = 5 slices in N = 5 mice). On the other hand, atropine significantly reduced light-driven DA release at high concentration (**Figure 4.10C-D**. Two-way ANOVA. Drug x stimulation interaction: F (3,24) = 0.43, p = 0.73; drug effect: F (1.92,14.40) = 94.84, p < 0.0001; stimulation effect: F (1,8) = 0.33, p = 0.57, n = 5 slices in N = 5 mice). These results suggest that inhibition of mAChRs enhanced ACh release and partially decreased ACh-driven DA release, through a potential partial desensitisation of nAChRs on DA axons. The fact that an effect is only seen at high concentration further suggests the need to increase atropine concentration to fully antagonise the receptors.

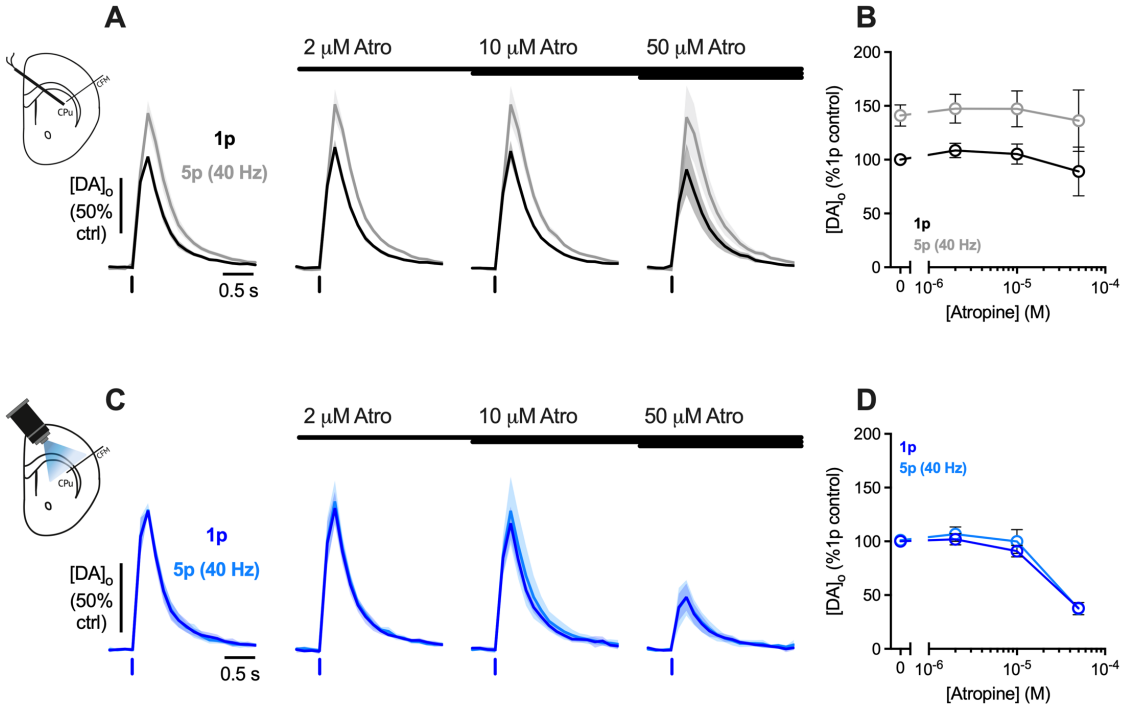


Figure 4.10. Antagonism of mAChRs reduced light-evoked DA release but not electrically-evoked DA in dorsolateral striatum.
(A) *Mean $[DA]_o$ transients (± SEM) plotted against time in different atropine concentrations evoked by single electrical pulses (1p) trains of 5 pulses (5p) at 40 Hz in dorsolateral striatum (CPu). Transients are normalised to 1p in control conditions (drug-free). Atropine did not significantly alter electrically-evoked DA release (quantified in B), n = 5 slices in N = 5 mice.*
(B) *Mean peak $[DA]_o$ evoked by 1p or 5p (electrical stimuli) plotted against atropine concentration. Two-way ANOVA: drug x stimulation interaction: F (3,24) = 0.050, p = 0.98; drug effect: F (3,24) = 0.79, p = 0.50; stimulation effect: F (1,8) = 5.51, p = 0.046, n = 5 slices in N = 5 mice.*
(C) *Mean $[DA]_o$ transients (±SEM) plotted against time in different atropine concentrations evoked by single light pulses (1p) trains of 5p at 40 Hz in dorsolateral striatum. Transients are normalised to 1p in control conditions (drug-free). Atropine decreased light evoked DA release at high concentration (quantified in D), n=5 slices in N=5 mice.*
(D) *Mean peak $[DA]_o$ evoked by 1p or 5p (light pulses) plotted against atropine concentration. Antagonism of mAChRs reduced light evoked DA release. Two-way ANOVA: drug x stimulation interaction: F (3,24) = 0.43, p = 0.73; drug effect: F (1.92,14.40) = 94.84, p < 0.0001; stimulation effect: F (1,8) = 0.33, p = 0.57, n = 5 slices in N = 5 mice.*

To test whether changes in ACh release levels driven by wash on of atropine at increasing concentration unmasked a stimulation sensitivity in electrically and light-evoked DA release, I looked at 5p:1p ratios. Ratios are increased for electrically-evoked DA but not light-driven DA (**Figure 4.12A**. Linear regression and slope significantly non-zero, Estim: $R^2 = 0.19$, p = 0.048; Lstim: $R^2 = 0.02$, p = 0.51. Slopes differ between stimulation modalities, p = 0.038, n = 5 slices in N = 5 mice). Overall, these results suggest that high concentration of atropine might promote ACh release, increasing ACh tone at nAChRs and promoting partial desensitisation, leading to an

increase in the frequency sensitivity of electrically-evoked DA and a decrease of light-evoked DA.

In the ventral striatum, wash on of progressively higher concentrations of atropine promoted DA release driven by trains of electrical stimuli (**Figure 4.11A-B**. Two-way ANOVA, drug x stimulation interaction: $F(3,12) = 3.31$, $p = 0.056$; drug effect: $F(1.76,7.05) = 6.09$, $p = 0.031$; stimulation effect: $F(1,4) = 86.30$, $p = 0.0007$, n = 3 slices in N = 3 mice), as also shown by an increase in the 5p:1p ratios (**Figure 4.12B**. Simple linear regression and slope significantly non-zero, Estim: $R^2 = 0.75$, $p = 0.0002$; Lstim: $R^2 = 0.27$, $p = 0.081$. Slopes differ between stimulation modalities, $p = 0.0078$, n = 3 slices in N = 3 mice). On the other hand, atropine wash on decreased light-evoked DA release at high concentrations (**Figure 4.11C-D**. Two-way ANOVA, drug x stimulation interaction: $F(3,12) = 0.10$, $p = 0.95$; drug effect: $F(1.31,5.26) = 31.51$, $p = 0.0017$; stimulation effect: $F(1,4) = 0.16$, $p = 0.70$, n = 3 slices in N = 3 mice) and did not alter frequency sensitivity of ACh-driven DA, as shown by no change in the 5p:1p ratios (**Figure 4.12B.** Simple linear regression and slope significantly non-zero, Lstim: $R^2 = 0.27$, $p = 0.081$, n = 3 slices in N = 3 mice).

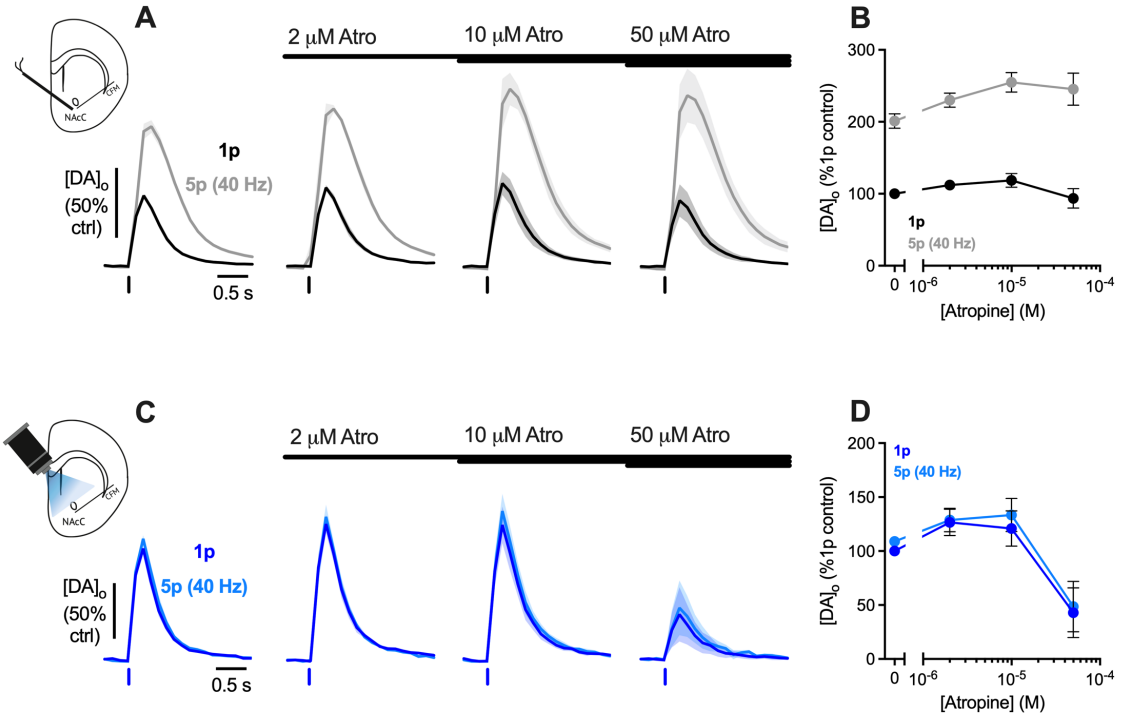


Figure 4.11. Antagonism of mAChRs reduced light-evoked DA release but not electrically-evoked DA in ventral striatum.

(A) *Mean $[DA]_o$ transients (± SEM) against time in different atropine concentrations evoked by single electrical pulses (1p) trains of 5p at 40 Hz in ventral striatum. Transients are normalised to 1p in control conditions (drug-free), n = 3 slices in N = 3 mice.*

(B) *Mean peak $[DA]_o$ evoked by 1p or 5p (electrical) plotted against atropine concentration. Two-way ANOVA: drug x stimulation interaction: F (3,12) = 3.31, p = 0.056; drug effect: F (1.76,7.05) = 6.09, p = 0.031; stimulation effect: F (1,4) = 86.30, p = 0.0007, n = 3 slices in N = 3 mice.*

(C) *Mean $[DA]_o$ transients (± SEM) against time in different atropine concentrations evoked single light pulses (1p) trains of 5p at 40 Hz in ventral striatum. Transients are normalised to 1p in control conditions (drug-free). Atropine decreases light evoked DA release at high concentration (quantified in D), n=3 slices in N=3 mice.*

(D) *Mean peak $[DA]_o$ evoked by 1p or 5p (light) plotted against atropine concentration. Antagonism of mAChRs reduces light evoked DA release. Two-way ANOVA: drug x stimulation interaction: F (3,12) = 0.10, p = 0.95; drug effect: F (1.31,5.26) = 31.51, p = 0.0017; stimulation effect: F (1,4) = 0.16, p = 0.70, n = 3 slices in N = 3 mice.*

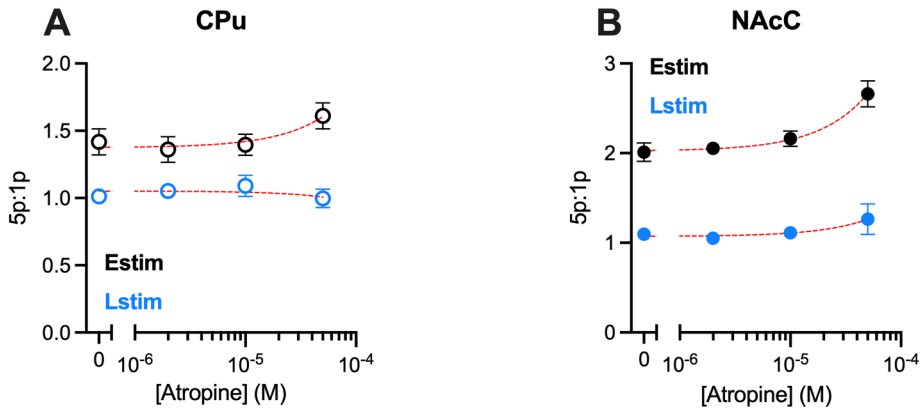


Figure 4.12. Antagonism of mAChRs promotes frequency sensitivity of electrically-evoked but not light-evoked DA release.
(A) *Mean (± SEM) 5p:1p ratios for electrical (Estim) and light (Lstim) evoked DA plotted against atropine concentration in dorsolateral striatum (CPu). Estim: simple linear regression: $R^2 = 0.19$, slope significantly non-zero: $p = 0.048$; Lstim: simple linear regression: $R^2 = 0.02$, slope significantly non-zero: $p = 0.51$. Slopes differ between stimulations, $p = 0.038$, $n = 5$ slices in $N = 5$ mice.*
(B) *Mean (± SEM) 5p:1p ratios for electrical (Estim) and light (Lstim) evoked DA plotted against atropine concentration in ventral striatum (NAcC). Estim: simple linear regression: $R^2 = 0.75$, slope significantly non-zero: $p = 0.0002$; Lstim: simple linear regression: $R^2 = 0.27$, slope significantly non-zero: $p = 0.081$. Slopes differ between stimulations, $p = 0.0078$, $n = 3$ slices in $N = 3$ mice. Data are represented on a logarithmic scale, but linear fits were performed on actual data.*

Overall, these data suggest that increase in ACh levels altered ACh-driven DA release in a way insensitive to ChI activation. However, said increase in ACh driven by antagonism of mAChRs partially promoted DA release sensitivity to activation of DA axons, recruited by electrical stimulation.

4.3.4. nAChRs regulate short-term plasticity of DA release but not ACh release

NAChRs are localised on DA axons (Jones et al., 2001) and strongly modulate DA release STP. Indeed, activation of nAChRs drives DA release by single pulse and promotes STD of DA release in train stimulation, limiting how action potential firing in DA neurons is converted into DA release (Zhou et al., 2001; Rice and Cragg, 2004). Conversely, block of nAChRs reduces 1p-driven release and relieves STD, promoting DA release according to stimulation frequency and pulse number (Rice and Cragg, 2004; Threlfell and Cragg, 2011). It is still incompletely characterised how new generation fluorescent DA sensors report these effects, well established with FCV.

To test nAChR-mediated regulation of DA release measured with the new-generation fluorescent sensor $GRAB_{DA}2m$ (Sun et al., 2020), I electrically evoked DA release in dorsal striatal slices with either single pulses or trains of 5p at different frequencies (25-100 Hz) in presence or absence of the β2-nAChR antagonist DHβE. In control conditions (nAChRs on), DA released by single pulses and trains at increasing frequencies was similar, however when DHβE was washed on, DA was released according to frequency, as showed by an increase in the 5p:1p ratios (**Figure 4.13**. Two-way ANOVA, frequency x drug interaction: F (3,24) = 5.91, p = 0.0036; frequency effect: F (3,24) = 17.76, p < 0.0001; drug effect: F (1,24) = 35.43, p < 0.0001. Bonferroni multiple comparisons, 1p: p > 0.99; 25 Hz: p = 0.045; 40 Hz: p = 0.016; 100 Hz: p < 0.0001, n = 7 slices in N = 6 mice). Overall, these results are consistent with previous reports that nAChRs modulate DA release STP and limit DA release sensitivity to stimulation frequency.

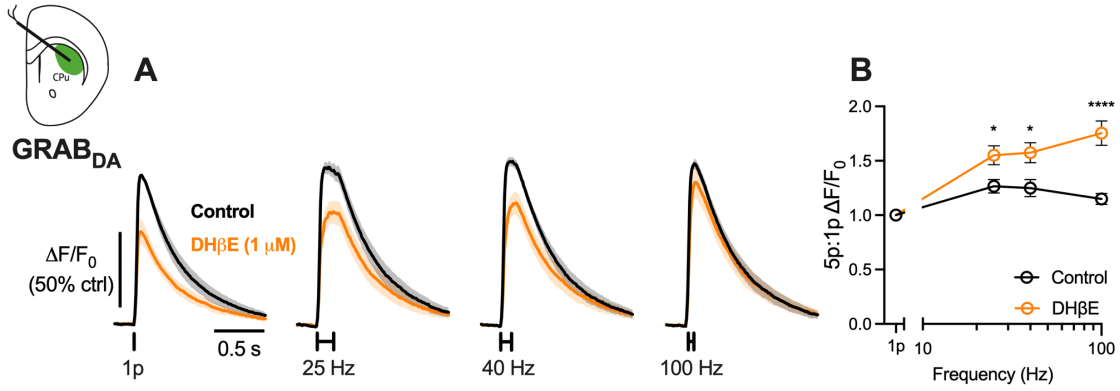


Figure 4.13. nAChRs regulate the frequency response of DA release measured with GRAB$_{DA}$ sensors.
(A) *Mean (± SEM) DA transients in dorsolateral striatum (CPu) evoked by 1p or trains of 5p (25-100 Hz) in control (drug-free, black) or in presence of the β2-nAChR antagonist DHβE (1 μM, orange), n = 7 slices in N = 6 mice.*
(B) *5p:1p ratios ΔF/F$_0$ plotted against stimulation frequency in control and DHβE. Antagonism of β2-nAChR promotes frequency sensitivity of DA release. Two-way ANOVA: frequency x drug interaction: F (3,24) = 5.91, p = 0.0036; frequency effect: F (3,24) = 17.76, p < 0.0001; drug effect: F (1,24) = 35.43, p < 0.0001. Bonferroni multiple comparisons: 1p: p > 0.99; 25 Hz: p = 0.045; 40 Hz: p = 0.016; 100 Hz: p < 0.0001, n = 7 slices in N = 6 mice.*

Striatal ChIs express mRNA for the β2 subunit of nAChRs (Azam et al., 2003; Lim et al., 2014) but the role of nAChRs in modulating ACh release is incompletely characterised. To test whether nAChRs can modulate striatal ACh release, I used a selective antagonist (DHβE) and stimulated with either single pulses or trains of electrical stimuli mimicking tonic/phasic firing frequencies (2-25Hz). In both

dorsolateral and ventral striatum, antagonism of nAChRs did not alter ACh release driven by single electrical pulses (**Figure 4.14B**. Two-tailed paired Student's t-test, p = 0.33, n = 6 slices in N = 6 mice; **4.14F**. Two-tailed paired Student's t-test, p = 0.42, n = 5 slices in N = 5 mice), 5p at 25 Hz (**Figure 4.14D**. Two-tailed paired Student's t-test, p = 0.30, n = 6 slices in N = 6 mice; **4.14H.** Two-tailed paired Student's t-test, p = 0.19, n = 5 slices in N = 5 mice) and 2 Hz (**Figure 4.14C**. Two-way ANOVA, drug x stim number interaction: $F(4,25) = 2.30$, $p = 0.086$; stim number effect: $F(4,25) = 13.90$, $p < 0.0001$; drug effect: $F(1,25) = 0.87$, $p = 0.36$, n = 6 slices in N = 6 mice; **4.14G**. Two-way ANOVA, drug x stim number interaction: $F(4,20) = 0.74$, $p = 0.57$; stim number effect: $F(4,20) = 10.27$, $p = 0.0001$; drug effect: $F(1,20) = 3.18$, $p = 0.09$, n = 5 slices in N = 5 mice). The differences in the kinetics of ACh transients in the NAcC are due to sensor expression with AAV9 instead of AAV5 vectors (**Chapter 2, Section 2.3.6**).

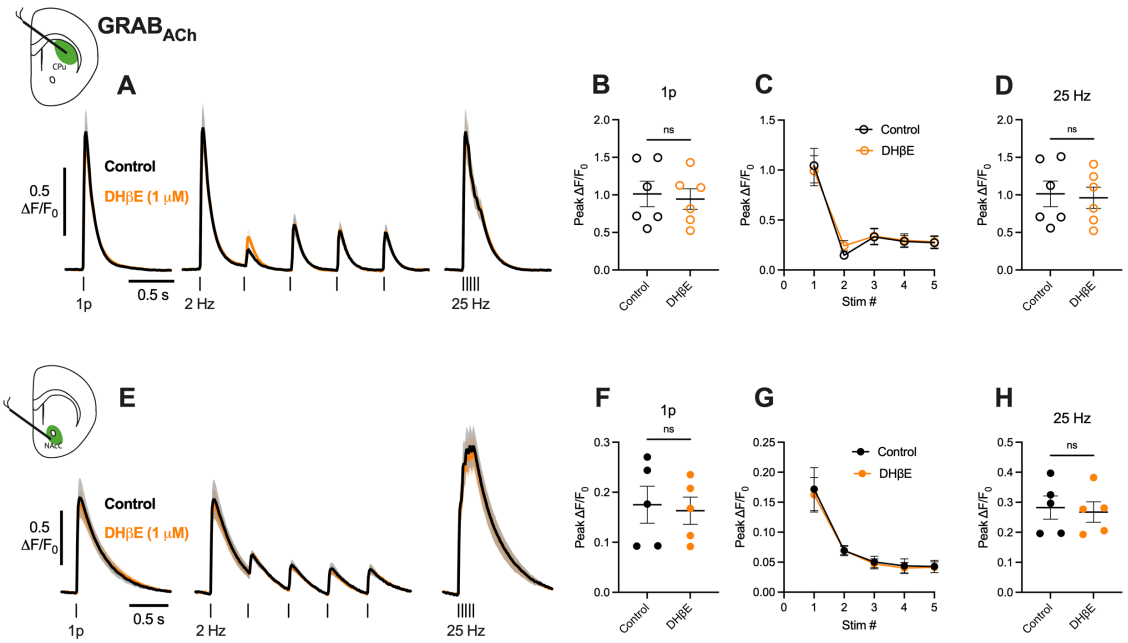


Figure 4.14. nAChRs do not regulate ACh release plasticity in dorsolateral and ventral striatum.
(A) *Mean (± SEM) ACh transients in dorsolateral striatum (CPu) evoked by single electrical pulses or trains of 5 pulses at 2-25 Hz in control (drug-free, black) and in presence of DHβE (1 μM, orange), n = 6 slices in N = 6 mice.*
(B) *Peak ΔF/F₀ in control or DHβE. DHβE does not alter ACh released by single electrical pulses. Two-tailed paired Student's t-test: p = 0.33, n = 6 slices in N = 6 mice.*
(C) *Mean peak ΔF/F₀ (± SEM) plotted against stimulus number (stim #) in 2 Hz trains for control and DHβE in dorsolateral striatum (CPu). When nAChRs are antagonised with DHβE, ACh release is unaltered. Two-way ANOVA: drug x stim number interaction: F (4,25) = 2.30, p = 0.085; stim number effect: F (4,25) = 13.90, p < 0.0001; drug effect: F (1,25) = 0.86, p = 0.36, n = 6 slices in N = 6 mice.*
(D) *Peak ΔF/F₀ in control or DHβE in dorsolateral striatum (CPu). DHβE does not alter ACh released by trains of 5 pulses at 25 Hz. Two-tailed paired Student's t-test: p = 0.30, n = 6 slices in N = 6 mice.*
(E) *Mean (± SEM) ACh transients in NAcC evoked by 1p or trains of 5p at 2-25 Hz in control (drug-free, black) and in presence of DHβE (1 μM, orange), n = 5 slices in N = 5 mice. GRABs were expressed via AAV9.*
(F) *Peak ΔF/F₀ in control or DHβE in NAcC. DHβE does not alter ACh released by 1p. Two-tailed paired Student's t-test: p = 0.42, n = 5 slices in N = 5 mice.*
(G) *Mean peak ΔF/F₀ (± SEM) plotted against stimulus number (stim #) in 2 Hz trains for control and DHβE. When nAChRs are antagonised with DHβE, ACh release is unchanged. Two-way ANOVA: drug x stim number interaction: F (4,20) = 0.74, p = 0.57; stim number effect: F (4,20) = 10.27, p = 0.0001; drug effect: F (1,20) = 3.18, p = 0.74, n = 5 slices in N = 5 mice.*
(H) *Peak ΔF/F₀ in control or DHβE in NAcC. DHβE does not alter ACh released by trains of 5p at 25 Hz. Two-tailed paired Student's t-test: p = 0.19, n = 5 slices in N = 5 mice. The data in panel (A-D) were collected using AAV5.hSyn.ACh3.0, while those in panel (E-H) using AAV9.hSyn.ACh3.0.*

Overall, these data suggest that nAChRs do not regulate ACh release STP in response to stimulation frequency. Antagonism of nAChRs will nonetheless impact on DA release levels, which might in turn act at D2Rs on ChIs to inhibit ACh release. To test if the changes in DA release levels driven by antagonism of nAChRs regulate ACh release response to DHβE, I blocked D2Rs with the selective antagonist L-741,626 (1 μM) and subsequently washed on DHβE, while measuring ACh release with $GRAB_{ACh}$. Preliminary observations showed no effect of DHβE on ACh release

driven by single electrical pulses (**Figure 4.15B**. Two-tailed paired Student's t-test, p = 0.50, n = 3 slices in N = 2 mice), trains of 5p at 2 Hz (**Figure 4.15C**. Two-way ANOVA, stim number x drug interaction: F (4,10) = 0.25, p = 0.90; stim number effect: F (4,10) = 4.15, p = 0.030; drug effect: F (1,10) = 2.25, p = 0.16, n = 3 slices in N = 2 mice) or 25 Hz (**Figure 4.15D**. Two-tailed paired Student's t-test, p = 0.74, n = 3 slices in N = 2 mice) in presence of the D2R antagonist L-741,626 in dorsolateral striatum.

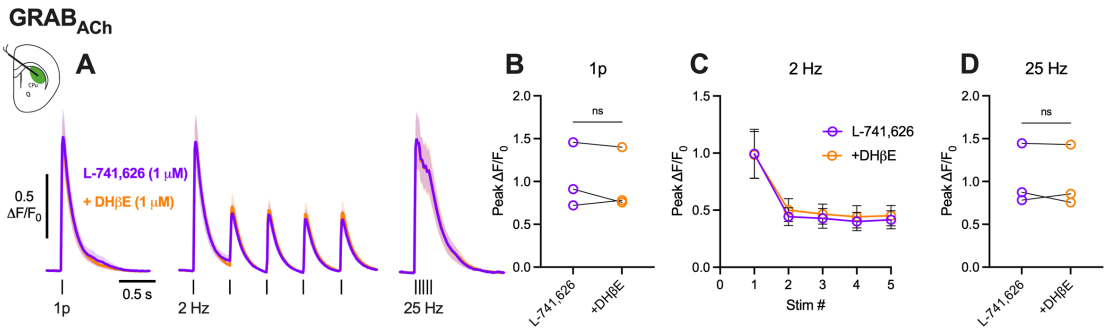


Figure 4.15. nAChRs do not regulate ACh release plasticity upon antagonism of D2Rs in dorsolateral striatum.
(A) *Mean (± SEM) ACh transients in dorsolateral striatum (CPu) evoked by single electrical pulses or trains of 5 pulses at 2-25 Hz in presence of the D2R antagonist L-741,626 (1 μM, purple) and after washing on DHβE (1 μM, orange). These data are preliminary observations, n = 3 slices in N = 2 mice.*
(B) *Peak ΔF/F$_0$ in D2R antagonism or after DHβE wash on. ACh release evoked by 1p is not altered by nAChR antagonism when D2R are blocked. Two-tailed paired Student's t-test: p = 0.50, n = 3 slices in N = 2 mice.*
(C) *Mean peak ΔF/F$_0$ (± SEM) plotted against stimulus number (stim #) in 2 Hz trains for L-741,626 and DHβE in dorsolateral striatum (CPu). When D2R are antagonised, wash on of DHβE does not alter ACh release. Two-way ANOVA: drug x stim number interaction: F (4,10) = 0.25, p = 0.90; stim number effect: F (4,10) = 4.15, p = 0.030; drug effect: F(1,10) = 2.25, p = 0.16, n = 3 slices in N = 2 mice.*
(D) *Peak ΔF/F$_0$ in D2R antagonism or after DHβE wash on. ACh release evoked by 5p at 40 Hz is not altered by nAChR antagonism when D2R are blocked. Two-tailed paired Student's t-test: p = 0.74, n = 3 slices in N = 2 mice. The data here represented were collected with AAV5.hSyn.ACh3.0.*

4.3.5. Probing evidence for nAChR desensitisation by endogenous ACh

When nAChRs are on, they promote STD of DA release by train stimuli and limit DA release responsiveness to stimulation frequency, which is re-established when they are turned off. Looking at the burst to 1p ratio could be used to infer about nAChR state. Hence, to define the time course of nAChR activation on DA axons and probe potential desensitisation by endogenous ACh, I used a stimulation paradigm comprising a single electrical pulse (1p) followed by either 1p or a burst of 3 pulses at high frequency (3p, 100 Hz) at different inter-pulse intervals (IPIs) and measured resulting DA release with FCV. When nAChRs are on, they promote high release

probability by single pulse and STD of DA released by trains of stimuli. Therefore, I hypothesised that if nAChRs are on DA release driven by 1p is equal to DA release driven by burst stimulation. On the other hand, when nAChRs are off (either inactive, antagonised, or desensitised), STD is relived, and DA release is proportional to stimulation. I then expected that if nAChRs are off, DA release driven by trains at 100 Hz would be higher than release driven by 1p.

In the dorsolateral striatum, burst-driven DA release is enhanced 100 ms to 300 ms after the first stimulus (**Figure 4.16A.** Two-way ANOVA, time x stimulation interaction: $F(4,56) = 5.30$, $p = 0.001$; time effect $F(4,56) = 11.32$, $p < 0.0001$; stimulation effect: $F(1,56) = 54.64$, $p < 0.0001$. Bonferroni multiple comparisons, 100 ms: $p < 0.0001$; 200 ms: $p < 0.0001$; 300ms: $p < 0.0001$. IPI 10-300-2000 ms: n = 5 slices in N = 3 mice, IPI 100-200-300 ms: n = 6 slices in N = 3 mice), suggesting that nAChRs were turned off (inactive or desensitised). When stimuli were delivered after 10 ms or 2 s, DA release by 1p or 3p was analogous, suggesting that nAChRs were on (**Figure 4.16A**. Bonferroni multiple comparisons, 10ms: $p > 0.99$; 2 s: $p > 0.99$).

In the NAcC, preliminary observations show that DA released by bursts is higher than DA released by single pulses at 10-100-300 ms, suggesting a less strong regulation than that seen in the CPu (**Figure 4.16B**. Two-way ANOVA, time x stimulation interaction: $F(3,32) = 4.06$, $p = 0.014$; time effect $F(3,32) = 20.81$, $p < 0.0001$; stimulation effect: $F(1,32) = 63.86$, $p < 0.0001$. Bonferroni multiple comparisons, 10 ms: $p = 0.015$; 100 ms: $p < 0.0001$; 300ms: $p = 0.0011$; 2 s: $p = 0.081$ IPI 10-100 ms: n = 4 slices in N = 2 mice, IPI 10-300-2000 ms: n = 4 slices in N = 2 mice).

Overall, these findings suggest that nAChRs might be desensitised by endogenous ACh on short timescales, with regional differences. However, this protocol is unable to discriminate between the actual state of nAChRs, but only give information on whether the receptors are on or off. At the timepoints in which I reported facilitation of DA release by burst stimulation, nAChRs might not be desensitised but simply inactive. This underlines the importance to concurrently measure ACh release levels.

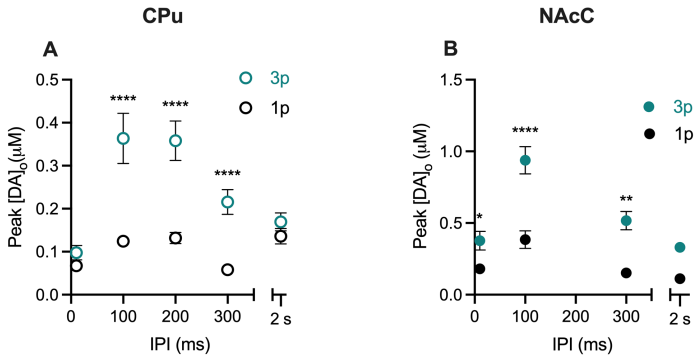


Figure 4.16. Probing potential nAChR desensitisation by endogenous ACh.
(A) *Mean peak $[DA]_o$ (± SEM) evoked by an initial single electrical stimulus (1p) followed by 1p or trains of 3 stimuli at 100 Hz in drug-free conditions plotted against inter-pulse interval (IPI) in dorsolateral striatum (CPu). DA release driven by the second stimulation was calculated by subtracting release driven by the first pulse. Two-way ANOVA: time x stimulation interaction: $F(4,56) = 5.30$, $p = 0.001$; time effect: $F(4,56) = 11.32$, $p < 0.0001$; stimulation effect: $F(1,56) = 54.64$, $p < 0.0001$. Bonferroni multiple comparisons: 10 ms: $p > 0.99$; 100 ms: $p < 0.0001$; 200 ms: $p < 0.0001$; 300ms: $p < 0.0001$; 2 s: $p > 0.99$. IPI 10-300-2000 ms: n = 5 slices in N = 3 mice, IPI 100-200-300 ms: n = 6 slices in N = 3 mice.*
(B) *Mean peak $[DA]_o$ (± SEM) evoked by single electrical pulses or trains of 3 stimuli at 100 Hz in drug-free conditions plotted against inter-pulse interval (IPI) in ventral striatum (NAcC). DA release driven by the second stimulation was calculated by subtracting release driven by the first pulse. Two-way ANOVA: time x stimulation interaction: $F(3,32) = 4.06$, $p = 0.014$; time effect: $F(3,32) = 20.81$, $p < 0.0001$; stimulation effect: $F(1,32) = 63.86$, $p < 0.0001$. Bonferroni multiple comparisons: 10 ms: $p = 0.015$; 100 ms: $p < 0.0001$; 300ms: $p = 0.0011$; 2 s: $p = 0.081$. IPI 10-100 ms: n = 4 slices in N = 2 mice, IPI 10-300-2000 ms: n = 4 slices in N = 2 mice.*

4.3.6. Calbindin D-28K does not interact with nAChRs in the ventral striatum

The intracellular mechanisms though which nAChRs operate to regulate DA release STP are currently poorly understood. These receptors are associated with a wide range of proteins, including proteins involved in intracellular Ca^{2+} signalling (McClure-Begley et al., 2013). The Ca^{2+} binding protein calbindin D-28K (calb1) is particularly enriched in VTA DA neurons (Greene et al., 2005) and regulates DA release in the NAcC by reducing intracellular Ca^{2+} availability and interacting with the DAT (Brimblecombe et al., 2019). Given this role, calb1 might potentially operate downstream of nAChRs to buffer intracellular Ca^{2+} and consequently limit Ca^{2+} summation and favour STD of DA release. I therefore explored a potential role for calb1 in mediating nAChR function in the NAcC. I used striatal slices from transgenic mice with knockdown of calb1 selectively in DA neurons (calbKD) and FCV to detect DA released by different stimulation frequencies in presence or absence of nAChR antagonism. If calb1 is associated with nAChRs to buffer intracellular Ca^{2+} and

promote STD, its removal should relief STD and promote DA release sensitivity to stimulation frequency. However, in control conditions (nAChRs on), knockdown of calb1 in DA axons did not alter DA release in response to trains of 5 electrical pulses at increasing frequencies compared to wild-type levels of calb1 (calbWT) (**Figure 4.17A-B**. Two-way ANOVA, frequency x genotype interaction: $F(4,15) = 0.22$, $p = 0.92$; frequency effect: $F(4,15) = 11.14$, $p = 0.0002$; genotype effect: $F(1,15) = 2.89$, $p = 0.11$, n = 4 slices in N = 4 mice). In presence of the β2-nAChR antagonist DHβE (1 μM), the frequency response of DA release was also not different between slices from calbKD and calbWT mice (**Figure 4.17C-D**. Two-way ANOVA, frequency x genotype interaction: $F(4,15) = 0.13$, $p = 0.96$; frequency effect: $F(4,15) = 35.65$, $p < 0.0001$; genotype effect: $F(1,15) = 0.0063$, $p = 0.93$, n = 4 slices in N = 4).

Overall, these data suggest that calb1 does not affect the relationship between stimulation frequency and DA release and has no functional interaction with nAChRs in the NAcC (Brimblecombe et al., 2019).

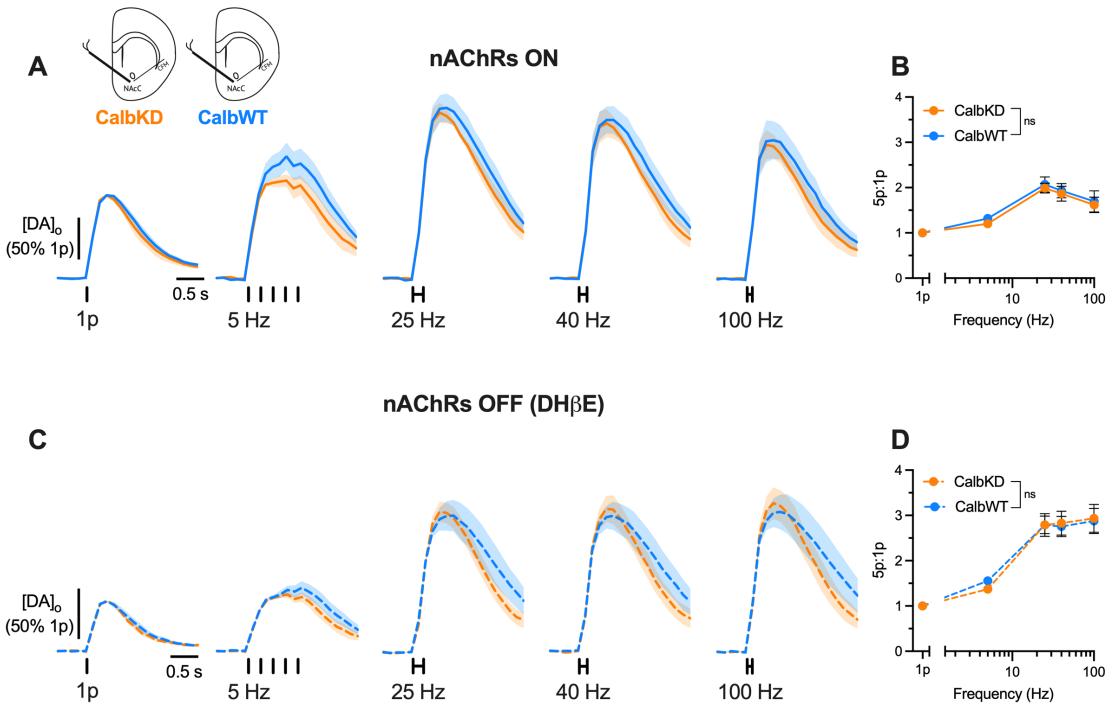


Figure 4.17. Calb1 has no role in mediating nAChR control of DA release in response to stimulation frequency (data published in Brimblecombe et al. (2019)).

(A) *Mean $[DA]_o$ transients (± SEM) against time in drug-free conditions in CalbKD and CalbWT slices evoked by single electrical pulses (1p) or trains of 5 pulses (5p) at a range of frequencies (5-100 Hz), n = 4 slices in N = 4 mice for each genotype.*

(B) *Mean 5p:1p (± SEM) ratios plotted against stimulation frequency in drug-free in CalbKD and CalbWT mice. Knock-down of calb1 does not alter the frequency sensitivity of DA release when nAChRs are active. Two-way ANOVA: frequency x genotype interaction: F (4,15) = 0.22, p = 0.92; frequency effect: F (4,15) = 11.14, p = 0.0002; genotype effect: F (1,15) = 2.89, p = 0.11, n = 4 slices in N = 4 mice for each genotype.*

(C) *Mean $[DA]_o$ transients (± SEM) against time in nAChR antagonism (DHβE, 1 μM) in CalbKD and CalbWT slices evoked by 1p or trains of 5p at a range of frequencies (5-100 Hz), n = 4 slices in N = 4 mice for each genotype.*

(D) *Mean 5p:1p (± SEM) ratios plotted against stimulation frequency in DHβE in CalbKD and CalbWT mice. Knock-down of calb1 does not alter the frequency sensitivity of DA release when nAChRs are antagonised. Two-way ANOVA: frequency x genotype interaction: F (4,15) = 0.13, p = 0.96; frequency effect: F (4,15) = 35.65, p < 0.0001; genotype effect: F (1,15) = 0.0063, p = 0.93, n = 4 slices in N = 4 mice per genotype.*

4.4 DISCUSSION

In this chapter, I've explored the relationship between dynamic changes in ACh release and the dual component of DA release, the role of nAChRs in modulating plasticity of DA and ACh release measured with GRAB sensors and finally a potential mechanism operating downstream of nAChRs. I found that ACh-driven DA release is proportional to changes in ACh release levels but not to differential activation of ChIs (**Section 4.3.1, 4.3.2, 4.3.3**). I also showed that nAChRs regulate DA but not ACh release STP, replicating FCV findings (**Section 4.3.4**). I showed that inferring nAChR state from their regulation of DA release sensitivity to stimulation frequency suggests that nAChRs might turn off (inactive or desensitised) with rapid timescales (**Section 4.3.5**). Finally, I reported that the fast Ca^{2+} buffer protein calbindin-D28K is not mediating nAChR effects on DA axons in the ventral striatum (**Section 4.3.6**).

4.4.1 Changes in ACh release levels resulting from activity in ChIs are not translated into changes in ACh-driven DA release

In **Sections 4.3.1, 4.3.2** and **4.3.3**, I investigated how dynamic changes in ACh release driven by changes in ChI activation and ACh release probability impact on cholinergic-driven DA release. In **Figure 4.2**, I showed that single light pulse-evoked ACh-driven DA was released according to stimulation light intensity. Therefore, higher levels of ACh can drive more DA release, assuming that increasing the light power that recruits ChIs will result in higher ACh release. Given the fact that both $GRAB_{ACh}$ sensors and ChR2 are excited by blue light, I was unable to directly test if changes in light power are proportional to changes in ACh release. Nonetheless, I previously showed that ACh driven by electrical pulses is released according to current intensity (**Chapter 3**, **Figure 3.1E**). Despite the differences in the two stimulation parameters, it is possible to assume that ACh released from ChIs is proportional to stimulation intensity. Furthermore, I found regional differences in the ChI-driven DA release response to changes in stimulation light intensity (**Figure 4.2**). Given that ACh is released according to stimulation intensity similarly in both ventral

and dorsolateral striatum (**Chapter 3**, **Figure 3.1E**), the mechanism underlying said differences in ACh-driven DA could be intrinsic to DA axons. Expression of different nAChR subtypes could underlie the reported regional differences. Indeed, nAChR subunit composition can affect substrate binding affinity, channel permeability and desensitisation kinetics (Dani and Bertrand, 2007). Furthermore, it is known that nAChRs composed by different $\alpha\beta$ subunit combinations regulate DA release plasticity in dorsal or ventral striatum (**Chapter 1**, **Figure 1.4**) (Exley et al., 2008, 2012). An alternative explanation for these regional differences could be different ACh hydrolysis leading to different levels of ACh reaching DA axons.

To investigate the relationship between ACh release and the dual component of DA release (DA-driven and ACh-driven) I've used a range of strategies to change ACh release probability, together with $GRAB_{ACh}$ sensor and FCV to measure resulting ACh and DA. The pharmacological manipulations used in these experiments ($\Delta[Ca^{2+}]_o$ and agonism/antagonism of mAChRs) are not restricted to ChIs but will also impact DA axons. However, it was previously reported that changes in $[Ca^{2+}]_o$ have little impact on STP of DA release, which is mainly regulated by K^+-dependent mechanisms and the DAT (Condon et al., 2019). DA neurons express M_5-mAChRs mRNA (despite the receptors have not directly been localised on DA axons) (Vilaró et al., 1990; Weiner et al., 1990), however it was previously reported that M_5-mAChR do not cover a role in modulating the frequency sensitivity of DA release upon changes in ACh release levels (Threlfell et al., 2010). The manipulations here adopted constitute therefore a good proxy for changes in ACh release probability. However, given that $GRAB_{ACh}$ sensors are mAChRs, I was unable to directly test how agonism/antagonism of mAChRs altered ACh release levels. Calcium imaging measuring activation of ChIs could be used in potential future experiments as an alternative approach.

The findings included in **Sections 4.3.1, 4.3.2** and **4.3.3** highlighted how the cholinergic component of DA release is insensitive to changes in stimulation frequency of ChIs, consistent with previous reports in dorsal and ventral striatum (Threlfell et al., 2012; Shin et al., 2017). I further showed that changes in ACh release levels driven by changes in $[Ca^{2+}]_o$ or mAChR activation impact on the magnitude of

ACh-driven DA release. Consistently, it was shown that application of vesamicol (inhibitor of the vesicular ACh transporter) decreased the amplitude of the ChI-driven DA current measured with continuous amperometry, suggesting a dependency upon the amount of ACh released from the presynaptic terminals (Wang et al., 2014b). However, once ACh has driven DA release, additional dynamic changes in ACh release levels do not drive any more or less DA release. Given that ACh has to bind to nAChRs on DA axons to drive DA release, potential underlying explanations include receptor desensitisation and nAChR-mediated STD. For instance, nAChRs might desensitise after exposure to endogenous ACh released after the first stimulus in the train. Indeed, in the NAcSh, where a small frequency sensitivity of ACh-driven DA release was reported, block of ACh clearance by inhibition of AChE prevented ACh-driven DA signal summation upon stimulation at different frequencies, suggesting that nAChR desensitisation is important in shaping ChI-driven DA release (Shin et al., 2017). However, recent evidence from mouse striatal slices expressing $GRAB_{ACh}$ sensors selectively in DA axons proposed a role for depression of ACh release after the first stimulus rather than nAChR desensitisation by endogenous ACh in regulating DA release plasticity (Kramer et al., 2022; Liu et al., 2022). Those studies reported that paired-pulse evoked ACh release reaching DA axons was depressed after the first stimulus and this effect was partly attenuated by nAChR or D2R antagonists and supply of ACh locally at DA axons via iontophoresis, suggesting feedback inhibition mediated by DA and lack of desensitisation by endogenous ACh (Kramer et al., 2022; Liu et al., 2022). Consistently with these findings, I showed that ACh released by low frequency trains is under D2R-mediated inhibition (**Chapter 3**, **Figure 3.10** and **3.11**). In **Chapter 3** (**Figure 3.5**), I also showed rundown of ACh release after the first stimulus in a train, which further supports the idea of STD of ACh release as a mechanism for the lack of frequency dependence of ACh-driven DA release. Despite ACh release depression after the first release event plays a major role in modulating ChI-driven DA release plasticity, unpublished observations from the lab seem to also suggest a role for nAChR-mediated STD of DA release. Indeed, subthreshold light activation of ChIs (which does not drive DA release) promotes depression of DA

release evoked by a subsequent electrical pulse, compared to DA evoked by an electrical pulse alone. These observations seem to suggest that activation of ChIs and nAChRs at levels lower than those required to drive DA release inhibits subsequent DA release. The intracellular mechanisms underlying nAChR action on DA axons are currently incompletely characterised and are further discussed in **Section 4.4.5**.

4.4.2. nAChRs as regulators of DA but not ACh release plasticity

ACh acting at nAChRs on DA axons strongly regulates DA release plasticity and the sensitivity of DA release to activity (Rice et al., 2011). The effect of nAChRs on DA release plasticity is well documented in striatal slices using FCV as a measurement of DA release. Antagonism of nAChRs reduces DA release evoked by a single pulse and relieves STD of DA re-release, rescuing the relationship between DA release and stimulation frequency and pulse number (Rice and Cragg, 2004). In **Figure 4.13**, I used next-generation $GRAB_{DA}$ sensors (Sun et al., 2020) to investigate nAChR regulation of DA release and replicated published FCV data. Indeed, antagonism of nAChRs reduced 1p-driven DA release and promoted DA release sensitivity to stimulation frequency. Therefore, the overall effect of nAChR antagonism is maintained when measuring DA release with different techniques. However, when DA release was measured with $GRAB_{DA}$, trains of pulses at high frequency in DHβE failed to promote additional release than in drug-free conditions. On the other hand, when measuring DA release with FCV, high frequency stimulation in nAChR antagonism drives DA release to a higher extent than in drug-free, supporting the notion that depletion of DA pool after the first stimulus is not sufficient to explain nAChR-mediated STD (**Section 4.4.5**). One potential explanation for these differences in signal detection is $GRAB_{DA}$ signal bleaching over time. In **Chapter 2** (**Figure 2.4**), I showed that fluorescence responses measured with $GRAB_{DA}$ are stable over a timespan of 30 minutes, in drug-free conditions. Given that DHβE was washed on after recording in drug-free conditions, prolonged exposure to excitation light might promote sensor bleaching. Another potential explanation could be saturation of the

$GRAB_{DA}$ sensor. Indeed, according to the affinity tuning curve of the published sensor (Sun et al., 2018, 2020) DA concentrations in the 1-10 μM range approach fluorescence response saturation. Given that these new tools are more frequently adopted in recent studies, it is important to evaluate how they report DA release dynamics and ponder the advantages and disadvantages of their use over electrochemical methods (see **Section 2.2** for a more detailed discussion).

In **Figure 4.14,** I looked at whether nAChRs can regulate ACh release plasticity. I found no effect of inhibiting nAChRs on ACh release in response to stimulation frequency. ChIs express the mRNA for the β2 subunit of nAChRs (Azam et al., 2003) and nicotine was found to induce ACh release measured by radioassay in rat striatal slices (Sandor et al., 1991). Notably, the effect of nicotine on ACh release was only seen in presence of D2R antagonists or upon pre-treatment with 6-hydroxydopamine (6-OHDA) to induce DA denervation (Sandor et al., 1991). Pilot data suggest no effect of blocking D2Rs on nAChR-mediated regulation of ACh release measured with $GRAB_{ACh}$ (**Figure 4.15**). The discrepancies between these findings might be due to the different detection methods and species used and to looking at effect of endogenous versus exogenous agonists.

Recent evidence using fluorescent in situ hybridisation (FISH) and selective deletion of β2-nAChRs on striatal interneurons suggests a key role for these receptors in regulating several behaviours (Abbondanza et al., 2022). In that study, β2-nAChRs were found predominantly expressed by ChIs (Abbondanza et al., 2022). Given this apparent high expression profile, the lack of effect of nAChR block on ACh release might be due to a low antagonist concentration used. However, the purpose of this experiment was to evaluate changes in ACh release in our preparation under the conditions in which we routinely measure DA release, which was fulfilled.

These findings are in apparent contrast with recent evidence which reported an attenuation of paired-pulse depression of ACh release upon nAChR antagonism (Liu et al., 2022). These discrepancies could be due to the differential expression of $GRAB_{ACh}$. In this thesis, $GRAB_{ACh}$ was globally expressed in striatal neuropil to measure bulk extracellular ACh release. While in the work by Liu et al. (2022), $GRAB_{ACh}$

expression was confined to DA axons, potentially biasing ACh release sampling to regions where ChI terminals exist in proximity to DA axons and nAChRs.

4.4.3. Probing potential nAChR desensitisation by endogenous ACh

In **Section 4.3.5**, I explored evidence for desensitisation of nAChRs by endogenous ACh by looking at changes in nAChR-mediated regulation of DA release sensitivity to stimulation frequency. In CPu, nAChRs are active and mediate STD of DA release at short time scales (10 ms), while they rapidly turn off 100 ms to 300 ms after initial activation. In the NAcC, nAChR-mediated STD is less strong than in the CPu and DA released by bursts was promoted 10 to 300 ms after initial activation (**Figure 4.16**). One potential explanation for the reported regional differences is DA release regulation by nAChRs with different subunit composition in the ventral and dorsal striatum (Exley et al., 2008, 2012), which will impact on substrate binding and desensitisation kinetics (Dani and Bertrand, 2007). Regional differences in nAChR state could also be due to differences in ACh release levels. At 10 ms after initial activation nAChRs appear to promote DA STD more strongly in CPu than in the NAcC. Consistently, when ACh was released by pulses delivered every 10 ms, I reported regional differences in the extracellular summation of the evoked signal measured with $GRAB_{ACh}$ (**Chapter 3**, **Figure 3.5D-F**). Divergence in nAChR regulation of DA STD is also seen at IPI of 2 s, where nAChRs mediated stronger STD in CPu than in the NAcC (although this effect did not reach statistical significance). Notably, ACh release is also different at these timescales, with higher release of ACh in dorsolateral than ventral striatum (**Chapter 3**, **Figure 3.3H**). To better define the contribution of ACh release levels reaching DA axons in mediating nAChR activation state, future experiments could measure ACh release with $GRAB_{ACh}$ selectively expressed on DA axons in response to the same stimulation protocol.

Nonetheless, it is important to note that the protocol adopted for these experiments cannot discriminate between different nAChR states, but only give information on whether the receptors are on (STD) or off (relief of STD). At the timepoints in which I reported facilitation of DA release by burst stimulation, nAChRs

might not be desensitised by endogenous ACh but might be simply inactive. In **Chapter 3**, I showed how ACh release transients are fast and strongly modulated by AChE, so that it is plausible that AChE might clear ACh and leave the receptors inactive.

4.4.4 Role of Calbindin-D28K in mediating nAChR function

In **Figure 4.17**, I tested a potential role for calb1 in operating downstream of nAChRs. I found no effect of knocking down calb1 selectively in DA axons on the nAChR-mediated regulation of DA release response to stimulation frequency, suggesting no functional interaction between the two. However, nAChR might still operate via a different Ca^{2+}- related mechanism or Ca^{2+} buffer proteins (**Section 4.4.5**). Consistently, quantitative proteomics analysis has reported that several proteins involved in Ca^{2+} signalling are associated with mouse neuronal β2-nAChRs, such as calcium/calmodulin-dependent kinases (McClure-Begley et al., 2013).

Calb1 was chosen as a potential candidate to explore given its role in modulating Ca^{2+}-dependency and STP of neurotransmitter release (Blatow et al., 2003; Schmidt et al., 2005; Lee et al., 2006; Schmidt, 2012). In rat VTA neurons, calb1 buffers intracellular Ca^{2+} limiting release probability (Pan and Ryan, 2012). In the striatum, there are differences in the coupling between Ca^{2+} and DA release between dorsal and ventral regions, with a role for an endogenous fast Ca^{2+} buffer in the NAcC (Brimblecombe et al., 2015). The fast Ca^{2+} buffer calb1, which is expressed predominantly in the NAc, is indeed the candidate involved in modulating DA release (Brimblecombe et al., 2019). In the NAcC, calb1 limits DA release by reducing intracellular Ca^{2+} availability and interacting with the DAT (Brimblecombe et al., 2019). Hence, despite the lack of interaction with nAChRs, calb1 is nonetheless a major modulator of DA release dynamics in the ventral striatum.

4.4.5 Potential mechanisms operating downstream of nAChRs on DA axons

As discussed above in **Section 4.4.4**, in this chapter I tested whether calb1 was operating downstream of nAChRs to regulate DA release plasticity. Calb1 was chosen as a potential candidate given that nAChRs are associated to intracellular Ca^{2+}-binding proteins and calb1 is involved in neurotransmitter release plasticity (Blatow et al., 2003; Schmidt, 2012; McClure-Begley et al., 2013). However, calb1 was not functionally linked to nAChRs. The mechanisms via which nAChRs drive use-dependent STD of DA release are currently still incompletely defined.

One proposed mechanism for nAChR-mediated STD of DA release is depletion of the vesicle pool after the first stimulus. Work using continuous amperometry to measure DA release current found that the first pulse in a burst induced high percentage of DA release so that the vesicle pool was depleted, causing STD (Wang et al., 2014a). In the presence of nicotine, the vesicle pool was less depleted, and this permitted DA release response to stimulation frequency (Wang et al., 2014a). However, previous work showed that, when nAChRs are inhibited or desensitised, DA release by train of pulses at high frequency is higher than release when nAChRs are active (Rice and Cragg, 2004), proving that net DA release in response to nAChR activation is not simply limited by the size of the vesicle pool. Furthermore, short-term plasticity of DA release is weakly release-dependent (Condon et al., 2019). Indeed, lowering extracellular Ca^{2+} concentration, which should reduce initial release probability and potentially rescue depression due to depletion, is not sufficient to rescue STD of DA release (Condon et al., 2019).

Nicotinic receptors might operate though Ca^{2+}-related mechanisms, such as limiting intracellular Ca^{2+} summation or inactivating VGCCs. Indeed, in the SNc, β2-nAChRs on DA neurons operate in Ca^{2+} mobilization mechanisms that are followed by Na^{+} and T-type Ca^{2+} channels activation (Tsuneki et al., 2000). In striatal synaptosomes, β2-nAChRs on DA axons are associated to different types of VGCCs, recruited through local membrane depolarization (Soliakov and Wonnacott, 1996; Kulak et al., 2001). In cortical neurons, nicotine-mediated activation of β2-nAChRs underlies decrease in L-type Ca^{2+} channel activity which in turn protects from

excitotoxicity (Stevens et al., 2003). Unpublished observations from the lab using Ca^{2+} imaging of DA axons show that, when nAChRs are active, they limit increases in intracellular Ca^{2+} levels in response to burst-like stimuli, suggesting that activation of nAChRs limits intracellular Ca^{2+} summation.

Other potential mechanism via which nAChRs might operate include changes in membrane polarisation properties via regulation of Na^+ and K^+ conductance. For instance, nAChRs might promote Na^+ channel inactivation. Inactivation and rate of recovery of Na^+ channels are fundamental to regulate neurotransmitter release (Debanne et al., 2011) and Na^+ channel inactivation is involved in mediating short-term plasticity at hippocampal synapses. Indeed, Na^+ channel block by application of low concentration (nanomolar range) of tetrodotoxin (TTX) at hippocampal glutamatergic synapses enhanced STD of neurotransmitter release (Brody and Yue, 2000; Prakriya and Mennerick, 2000; He et al., 2002). Moreover, β2-nAChRs have potentially long channel opening times (Zeng et al., 1999; Kramer et al., 2022) that can result in prolonged axonal depolarization and promote Na^+ channel dependent refractoriness of action potentials, which consequently results in depression of re-release. Further candidate mechanisms through which nAChRs might mediate STD of DA release include hyperpolarisation or delayed repolarisation via interaction with K^+ channels. Indeed, DA release plasticity is strongly influenced by mechanisms governing axonal membrane polarisation (Condon et al., 2019). Increase in extracellular K^+ levels enhanced STD of DA release and decreased intracellular Ca^{2+} summation, when nAChRs are blocked (Condon et al., 2019). Future experiments combining the use of genetically encoded voltage indicators (GEVIs) with two-photon imaging can help to better understand how nAChRs might influence DA axon physiology. A subclass of GEVIs that combine a voltage sensing domain with a cpFP, allows to detect subthreshold events and individual spiking up to 100 Hz (Panzera and Hoppa, 2019), suitable to measure potential alterations in spike propagation driven by activation/inactivation of nAChRs.

Recently published work suggested that ACh release from ChIs induces action potential firing in distal DA axons as a physiological mechanism to regulate DA

signalling (Liu et al., 2022). Indeed, selective optogenetic activation of ChIs evoked action potentials in DA axons measured via perforated patch recordings, which were abolished by the nAChR antagonist DHβE (Liu et al., 2022). NAChR activation on DA axons initiated ectopic action potentials followed by opening of P/Q-type and N-type Ca^{2+} channels, as a mechanism for ACh-induced DA release (Liu et al., 2022). However, despite these recent advances, the mechanism via which nAChRs mediate STD of DA release is still unresolved. Future work could test whether failing of action potential initiation or propagation might underlie DA release depression mediated by nAChR activation.

Overall, in this chapter I've explored how dynamic changes in ACh release can modulate the dual component of DA release, together with assessing nAChR regulation of DA and ACh release plasticity and potential downstream mechanisms. After having explored mutual regulation of striatal DA and ACh release in healthy models, in the next chapter I will investigate maladaptive alterations in striatal ACh signalling in a mouse model of early Parkinson's disease.

5. Dysfunction in striatal acetylcholine release in a mouse model of early Parkinson's disease

5.1 INTRODUCTION

The work described in the previous chapters outlined major properties of striatal ACh release and its regulation of DA release plasticity in healthy mouse models. In this chapter, I will highlight maladaptive changes in striatal ACh release in a transgenic mouse model of early parkinsonism.

Parkinson's disease (PD) is a neurodegenerative disorder that results from loss of SNc DA neurons that innervate the dorsal striatum. Historically, PD has been considered as a hypodopaminergic and an hypercholinergic condition. Indeed, it has been proposed that DA and ACh in the striatum are in equilibrium to guarantee normal movement control and that this equilibrium is altered in PD, where a loss of DA results in a hypercholinergic state (Barbeau, 1962). Currently, levodopa (L-DOPA) is the gold standard therapy to alleviate PD motor symptoms (Tubert and Murer, 2021). Before this, anticholinergic drugs were the preferred therapy for PD (Barbeau, 1962). Anticholinergic drugs can effectively improve motor symptoms in PD patients, but they're less effective than L-DOPA and can lead to cognitive and autonomic side effects (Lim et al., 2014; Tubert and Murer, 2021). Alterations in striatal ACh transmission are therefore fundamental in the pathogenesis of PD.

A variety of animal models have been generated to study the pathogenesis and therapeutic development of PD (Chia et al., 2020). PD models can be generated either with neurotoxins (such as 6-hydroxydopamine, 6-OHDA), which lead to death of DA neurons, or with a genetic approach, by overexpressing or knocking out genes associated with PD (Chia et al., 2020). In particular, mutations and locus multiplications of the gene encoding for the protein α-synuclein (*SNCA*) are associated with sporadic and familial forms of PD (Singleton et al., 2003; Bekris et al., 2010; Venda et al., 2010). α-synuclein is an abundant presynaptic protein involved in regulating synaptic vesicle mobilisation and neurotransmitter release (Cabin et al., 2002; Nemani et al., 2010; Lautenschläger et al., 2018) . In PD, α-synuclein is the main component of the Lewy bodies, protein aggregates that underlie neuronal degeneration (Baba et al., 1998; Spillantini et al., 1998). Here, we used an α-synuclein

transgenic mouse model (*SNCA*-OVX) that overexpresses the human *SNCA* locus at disease relevant levels (Janezic et al., 2013). This mouse model does not express endogenous mouse α-synuclein and allows to investigate the pathological mechanisms triggered by progressive human α-synuclein accumulation. *SNCA*-OVX mice present early deficits in DA release, age-dependent loss of DA neurons and motor phenotypes characteristic of PD (Janezic et al., 2013). Mice not expressing endogenous α-synuclein nor human α-synuclein (*Snca -/-*) were used as controls since they avoid confounding interactions driven by expression of the endogenous protein. Synuclein null mice presented no differences in storage and release of DA compared to mice expressing moderate levels of human α-synuclein, suggesting that the reported deficits in DA neurotransmission are due to overexpression of α-synuclein rather than expression per se (Janezic et al., 2013). For the work included in this chapter, we adopted this progressive and highly physiological model of PD to investigate potential alterations in striatal ACh transmission occurring at the early stages of PD progression, preceding DA neuron degeneration.

Several studies in different PD rodent models have reported evidence for altered cholinergic transmission in the parkinsonian striatum. Microdialysis studies in the 6-OHDA model found elevated levels of extracellular ACh in the striatum (DeBoer et al., 1993; Ikarashi et al., 1997). Loss of striatal DA also leads to changes in ChI excitability. For instance, chronic loss of DA driven by 6-OHDA injections in rats drives a reduction of the slow afterhyperpolarisation current in ChIs which results in increased ChI excitability (Sanchez et al., 2011). On the other hand, in mice lesioned with 6-OHDA, DA loss was found to decrease ChI spontaneous firing (Choi et al., 2020). In an early-stage PD mouse model (partial lesions with low dose of 6-OHDA), ChI excitation mediated by glutamate co-release from DA axons is lost via downregulation of metabotropic glutamate receptors on ChIs and underlined parkinsonian motor impairments (Cai et al., 2021). Conversely, optogenetic inhibition of ChIs was found to improve motor deficits in the 6-OHDA PD model (Maurice et al., 2015; Ztaou et al., 2016). DA depletion with 6-OHDA also resulted in downregulation of M_4 muscarinic ACh receptors (M_4-mAChRs) signalling on ChIs, leading to a loss of

autoreceptors control of ChI firing (Ding et al., 2006). The discrepancies in the findings here described can be attributable to a number of reasons, including the use of different protocols or rodent species. Different adaptations in striatal cholinergic signalling might also occur at different stages of disease progression. Nonetheless, there's evidence for aberrant cholinergic transmission in the striatum following loss of DA in PD. However, most studies report alterations in ChI excitability and do not provide a direct measurement of ACh release dynamics at different stages of disease progression. To date, potential alterations in striatal cholinergic transmission in the *SNCA*-OVX mouse model remain uncharacterised. In particular, it is unclear whether this progressive model of PD presents a hypercholinergic phenotype. In **Section 5.3.1** and **5.3.2**, we used $GRAB_{ACh}$ sensors to examine changes in tonic regulation of ACh release and differences in levels of evoked ACh release in *SNCA*-OVX mice compared to *Snca* -/- controls.

Several properties of striatal and midbrain DA transmission are altered in *SNCA*-OVX mice. α-synuclein overexpression leads to an age-dependent loss of nigrostriatal DA neurons and a reduction in SNc DA neuron firing rates, with no changes in firing patterns (Janezic et al., 2013). Furthermore, evoked DA release in the dorsolateral striatum in *ex vivo* slices from *SNCA*-OVX mice was around 30% lower than in control mice (Janezic et al., 2013). These deficits in DA release were present in young adult mice (3-4 months old), preceded DA neuron loss and changes in firing activity, and persisted throughout the lifespan of adult mice (Janezic et al., 2013). It is currently undefined whether these early changes in DA release in *SNCA*-OVX mice can alter ACh release. In **Section 5.3.3**, we tested if DA regulation of ACh release via D2Rs was altered in young adult *SNCA*-OVX mice.

SNCA-OVX mice also present alterations in GABAergic regulation of DA release from young adulthood (3 months). In the dorsolateral striatum of healthy wild-type (WT) mice, DA release is under tonic GABAergic inhibition determined by the activity of the GABA transporters (GATs) (Lopes et al., 2019; Roberts et al., 2020). In the early PD model *SNCA*-OVX, GATs are downregulated, and tonic GABAergic inhibition of DA release is increased (Roberts et al., 2020). Moreover, GABA co-released from DA axons

is reduced in *SNCA*-OVX mice (Roberts et al., 2020). It is unresolved whether changes in GAT levels and in GABA tone in the dorsolateral striatum of *SNCA*-OVX mice impact on ACh release regulation. In **Section 5.3.4**, we examined potential changes in GABAergic tonic inhibition of ACh release in *SNCA*-OVX mice compared to their *Snca* -/- controls. Furthermore, we tested whether the increased GABAergic tonic inhibition of DA release seen in *SNCA*-OVX mice altered tonic inhibition of ACh release.

Overall, the work included in this chapter aimed at characterising maladaptive changes in ACh release dynamics in the α-synuclein overexpressing mouse model of early PD. To begin with, we calibrated $GRAB_{ACh}$ signal in both genotypes (**Section 5.3.1**). Then, we tested whether *SNCA*-OVX mice presented a hypercholinergic phenotype, by assessing evoked and tonic ACh release levels (**Section 5.3.1**, **5.3.2**). Moreover, we tested whether deficits in DA release reported in *SNCA*-OVX mice resulted in altered D2R-mediated regulation of ACh release (**Section 5.3.3**). Finally, we tested if changes in striatal GABA tone reported in *SNCA*-OVX mice resulted in altered tonic GABAergic inhibition of ACh release (**Section 5.3.4**).

5.2 METHODS

5.2.1 Animals and slice preparation

Mice overexpressing human α-synuclein (*SNCA*-OVX) at disease relevant levels were used as a model for early parkinsonism (Janezic et al., 2013). This mouse line was generated as described in **Chapter 2** (**Section 2.1.2**). Mice devoid of endogenous α-synuclein expression (*Snca* -/-) were chosen as controls (Janezic et al., 2013). Male and female sex and age matched littermates *SNCA*-OVX and *Snca* -/- were injected with AAV9.hSyn.ACh3.0 (with a titre of 0.7 x 10^{13} gc/ml) in the dorsal striatum as described in **Section 2.1.3**. Three weeks after injection, mice were sacrificed and acute *ex vivo* coronal slices containing striatum were prepared as described in **Section 2.2.1** and **2.3.3**.

All mice used were aged 3-4 months to probe early stage α-synuclein-driven impairments in striatal ACh transmission. At this age, *SNCA*-OVX mice present deficits in striatal dopaminergic and GABAergic transmission (Janezic et al., 2013; Roberts et al., 2020). Recordings were performed in the dorsolateral striatum, where previous deficits in DA and GABAergic transmission were identified (Janezic et al., 2013; Roberts et al., 2020).

5.2.2 $GRAB_{ACh}$ imaging

For experiments where ACh was electrically evoked, recordings were carried out as described in **Chapter 2** (**Section 2.3.3** and **2.3.4**). To achieve a sampling frequency of 100 Hz, a recording window of active pixels was defined, the camera exposure rate set to 10 ms and the pixels binned 2x2. A continuous blue LED (470 nm) light was used to excite the sensor fluorophore at an intensity of ~ 10-11 mW. Data were extracted and processed as described in **Section 2.3.5**. Electrical stimuli (0.6 mA, 200 μs) were delivered every 2.5 minutes, stimulation protocols were repeated in duplicates and the order of stimuli was randomised. Differences in the kinetics of electrically evoked ACh signals in this chapter, compared to signals in WT

mice described in **Chapter 3**, are due to the use of AAV9-packaged $GRAB_{ACh}$ and not the transgenic mouse lines. A description of the differences in ACh signals driven by the chosen viral serotype is found in **Section 2.3.6**.

For experiments investigating tonic ACh levels or calibration of the $GRAB_{ACh}$ signal measured in the two genotypes, we intermittently sampled fluorescence for 1 s every 30 s. The whole recording window was maintained, the camera exposure rate increased to 100 ms and the excitation light was lowered to ~ 2 mW. Data were extracted and processed as described in **Chapter 2** (**Section 2.3.5**). Wash on of ACh for signal calibration was performed after washing on the acetylcholinesterase (AChE) inhibitor ambenonium in experiments evaluating regulation of tonic ACh release levels (**Figure 5.1C-D**).

For each set of experiments the number of experimental animals was $N \geqslant 3$. Slices from either genotype were prepared in one experimental day, so that recording were performed only on one genotype at a time. We chose this approach to avoid increased exposure to excitation light while not recording that can result from having slices from both genotypes in the bath.

5.2.3 Drugs

Drugs were diluted in either dH_2O or DMSO (dymethil sulfoxide) to 1,000x stock aliquots and stored at -20°C. Final drug concentrations (**Table 5.1**) were prepared in aCSF saturated with 95% O_2/ 5% CO_2 right before use.

DRUG	SUPPLIER	ACTION	CONCENTRATION	REFERENCES
Acetylcholine	Bio-Techne	Endogenous ACh	50 µM	(Jing et al., 2018)
Ambenonium	Bio-Techne	AChE inhibitor	5 µM	(Exley et al., 2008)
Bicuculline	Abcam	$GABA_A$ receptor antagonist	10 µM	(Lopes et al., 2019)
CGP 55845	Abcam	$GABA_B$ receptor antagonist	4 µM	(Roberts et al., 2020)
L-741,626	Abcam	D2 receptor antagonist	1 µM	(Condon et al., 2019)

Table 5.1. List of drugs used in Chapter 5 with mode of action and references to clarify choice of concentration.

5.3 RESULTS

5.3.1 Acetylcholinesterase regulates tonic levels of ACh more efficiently in SNCA-OVX mice

To examine potential alterations in striatal ACh transmission in the α-synuclein overexpressing PD mouse model (*SNCA*-OVX), we used $GRAB_{ACh}$ sensors to monitor ACh release in the dorsolateral striatum of these mice and compared it to their synuclein null controls (*Snca* -/-, **Section 5.2.1**). First, we tested whether $GRAB_{ACh}$ sensors report ACh levels in a similar way in both genotypes. We calibrated the sensors with 50 µM ACh in presence of the AChE inhibitor ambenonium (5 µM). We found no differences in the readout of ACh in both genotypes (**Figure 5.1A**. Two-way ANOVA, time x genotype interaction: $F(14,150) = 1.13$, $p = 0.33$; time effect: $F(14,150) = 10.31$, $p < 0.0001$; genotype effect: $F(1,150) = 2.29$, $p = 0.13$. *SNCA*-OVX: n = 6 slices in N = 4 mice, *Snca* -/-: n = 6 slices in N = 5 mice). Peak fluorescence responses upon wash on of ACh were also analogous in both genotypes (**Figure 5.1B**. Two-tailed unpaired Student's t-test, $p = 0.42$. *SNCA*-OVX: n = 6 slices in N = 4 mice, *Snca* -/-: n = 6 slices in N = 5 mice).

Historically, the striatum in PD is thought to be in a hypercholinergic state, driven by loss of DA-ACh balance (Barbeau, 1962). In **Section 3.3.4**, I showed that AChE strongly modulates the spatiotemporal dynamics of tonic and evoked ACh release in a healthy mouse model. AChE could be a potential candidate contributing to ACh dysfunction in PD and its expression is altered in PD patients (Dong et al., 2021). Furthermore, anti-cholinesterase treatments have also been used to alleviate motor symptoms and cognitive impairments in PD patients (Poewe et al., 2006; Chung et al., 2010). Hence, we tested whether AChE regulation of tonic ACh levels was altered in the dorsolateral striatum of *SNCA*-OVX mice compared to control *Snca* -/- mice. In absence of stimulation, we intermittently sampled fluorescence change upon ambenonium (5 µM) wash on in presence/absence of TTX (1 µM), to determine action potential dependency. In slices from *SNCA*-OVX mice, AChE block significantly

increased fluorescence in a TTX-dependent way (**Figure 5.1C**. Two-way ANOVA, time x drug interaction: $F(49,450) = 2.26$, $p < 0.0001$; time effect: $F(49,450) = 16.76$, $p < 0.0001$; drug effect: $F(1,450) = 149.5$, $p < 0.0001$, n = 6 slices in N = 4 mice). In slices from *Snca* -/- mice, we found that AChE modestly increased fluorescence in a TTX-dependent manner (**Figure 5.1D**. Two-way ANOVA, time x drug interaction: $F(49,500) = 1.79$, $p = 0.0011$; time effect: $F(49,500) = 20.57$, $p < 0.0001$; drug effect: $F(1,500) = 41.74$, $p < 0.0001$, n = 6 slices in N = 5 mice). Overall, these data show that in both models AChE regulated ambient levels of striatal ACh. However, we found a difference in the size of the effect of AChE inhibition between genotypes. To compare the effect of AChE inhibition between genotypes, we averaged the fluorescence responses measured after ambenonium was fully washed on and a plateau was reached (last 10 minutes). Ambenonium effect is higher in *SNCA*-OVX mice (**Figure 5.1E**. Two-tailed unpaired Student's t-test, $p = 0.026$. *SNCA*-OVX: n = 6 slices in N = 4 mice, *Snca* -/-: n = 6 slices in N = 5 mice). These findings suggest that AChE regulates tonic ACh levels more strongly in *SNCA*-OVX mice compared to *Snca* -/- controls.

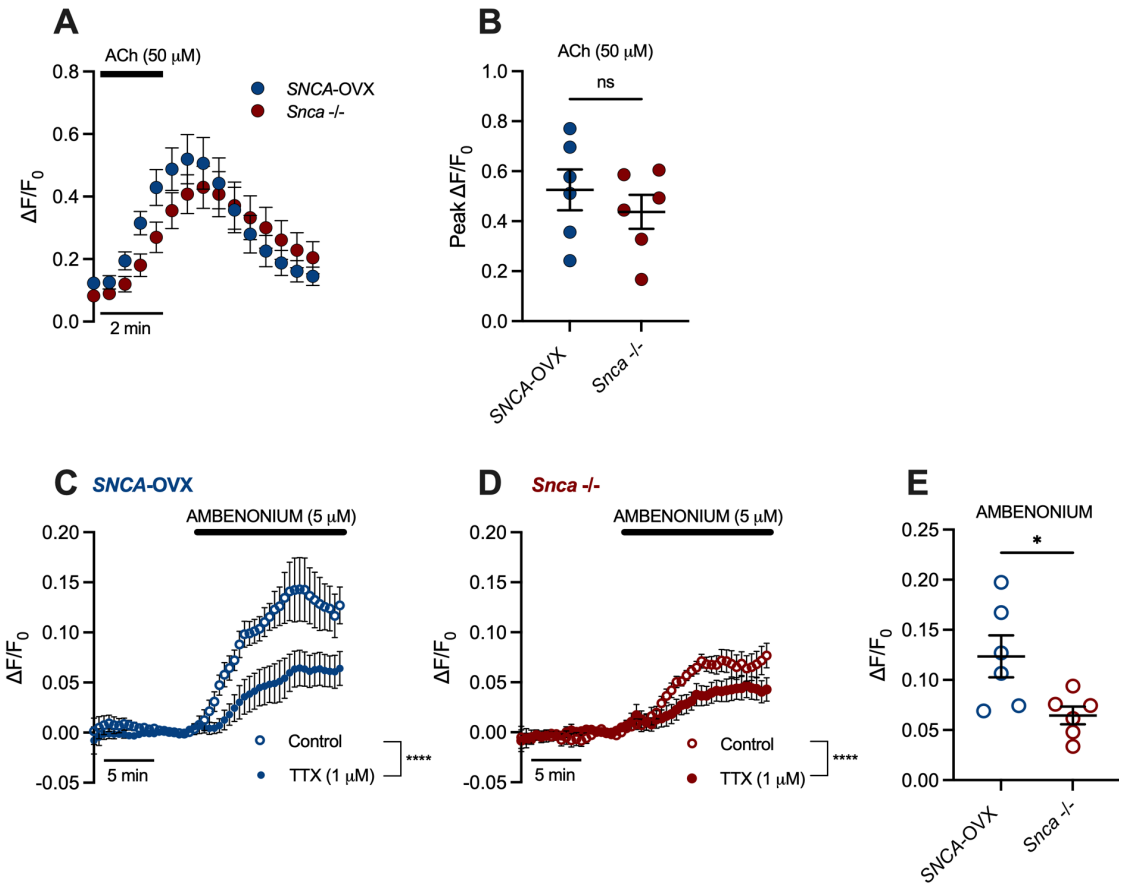


Figure 5.1. Inhibition of AChE leads to higher increase in tonic ACh levels in SNCA-OVX mice compared to Snca -/-.
(A) *Mean ΔF/F$_0$ (± SEM) in SNCA-OVX and Snca -/- slices upon wash on of ACh (50 µM) in presence of AChE antagonist ambenonium (5 µM) and in absence of stimulation. ACh was bath applied at the end of the tonic experiment described in panel C and D. There are no significant genotype-related differences in ACh signal readout by GRAB$_{ACh}$. Two-way ANOVA: time x genotype interaction: F (14,150) = 1.13, p = 0.33; time effect: F (14,150) = 10.31, p < 0.0001; genotype effect: F (1,150) = 2.29, p = 0.13. SNCA-OVX: n = 6 slices in N = 4 mice, Snca -/-: n = 6 slices in N = 5 mice.*
(B) *Peak ΔF/F$_0$ in presence of ACh in SNCA-OVX and Snca -/-. The size of fluorescence responses measured by GRAB$_{ACh}$ does not differ between genotypes. Two-tailed unpaired Student's t-test: p = 0.42. SNCA-OVX: n = 6 slices in N = 4 mice, Snca -/-: n = 6 slices in N = 5 mice.*
(C) *Mean (± SEM) ΔF/F$_0$ sampled every 30 s in presence/absence of TTX in the dorsolateral striatum of SNCA-OVX mice (in absence of stimulation). Inhibiting AChE with ambenonium (5 µM) increases ACh levels in a TTX-dependent way, suggesting that AChE limits tonic ACh levels arising from APs. Two-way ANOVA: time x drug interaction: F (49,450) = 2.26, p < 0.0001; time effect: F (49,450) = 16.76, p < 0.0001; drug effect: F (1,450) = 149.5, p < 0.0001, n = 6 slices in N = 4 mice.*
(D) *Mean (± SEM) ΔF/F$_0$ sampled every 30 s in presence/absence of TTX in the dorsolateral striatum of Snca -/- mice. Inhibition of AChE with ambenonium (5 µM) modestly but significantly increases ACh levels in a TTX-dependent way, suggesting that AChE partly limits tonic ACh levels arising from APs. Two-way ANOVA: time x drug interaction: F (49,500) = 1.79, p = 0.0011; time effect: F (49,500) = 20.57, p < 0.0001; drug effect: F (1,500) = 41.74, p < 0.0001, n = 6 slices in N = 5 mice.*
(E) *Effect of ambenonium wash on in SNCA-OVX and Snca -/- mice calculated as average ΔF/F$_0$ after ambenonium wash on (last 10 minutes). Inhibiting AChE increases ambient ACh more strongly in SNCA-OVX mice. Two-tailed unpaired Student's t test: p = 0.026. SNCA-OVX: n = 6 slices in N = 4 mice, Snca -/-: n = 6 slices in N = 5 mice.*

5.3.2 Evoked ACh release is lower in SNCA-OVX mice

Microdialysis studies reported elevated levels of ACh in the striatum of 6-OHDA PD models (DeBoer et al., 1993; Ikarashi et al., 1997). Here, to test whether levels of ACh release were altered in the *SNCA*-OVX PD model, we used $GRAB_{ACh}$ sensors to measure ACh release in real-time. We combined single pulse-evoked ACh release transients in drug-free conditions across multiple experiments and compared the size and duration of ACh responses between genotypes. Somewhat surprisingly, we found that ACh release was higher in *Snca* -/- mice compared to *SNCA*-OVX mice (**Figure 5.2A**). Indeed, the peak size of fluorescence responses was higher in *Snca* -/- mice (**Figure 5.2B**. Unpaired two-tailed Student's t-test: p = 0.0005. *SNCA*-OVX: n = 75 transients in N = 11 mice. *Snca* -/-: n = 76 transients in N = 11 mice). AUC of ACh transients was numerically increased in *Snca* -/- mice, but not significantly (**Figure 5.2C**. Unpaired two-tailed Student's t-test: p = 0.052. SNCA-OVX: n = 75 transients in N = 11 mice. *Snca* -/-: n = 76 transients in N = 11 mice). Half-lives were higher in *SNCA*-OVX mice (**Figure 5.2D**. Unpaired two-tailed Student's t-test: p=0.0086. *SNCA*-OVX: n = 75 transients in N = 11 mice. Snca -/-: n = 76 transients in N = 11 mice). Baseline fluorescence F_0 did not differ between genotypes (**Figure 5.2E**. Two-tailed unpaired Student's t-test, p = 0.69. SNCA-OVX: n = 75 transients in N = 11 mice. *Snca* -/-: n = 76 transients in N = 11 mice), suggesting similar expression of $GRAB_{ACh}$ sensors in both genotypes. Overall, these results suggest that evoked ACh release in the dorsolateral striatum of *SNCA*-OVX is smaller and has higher half-life.

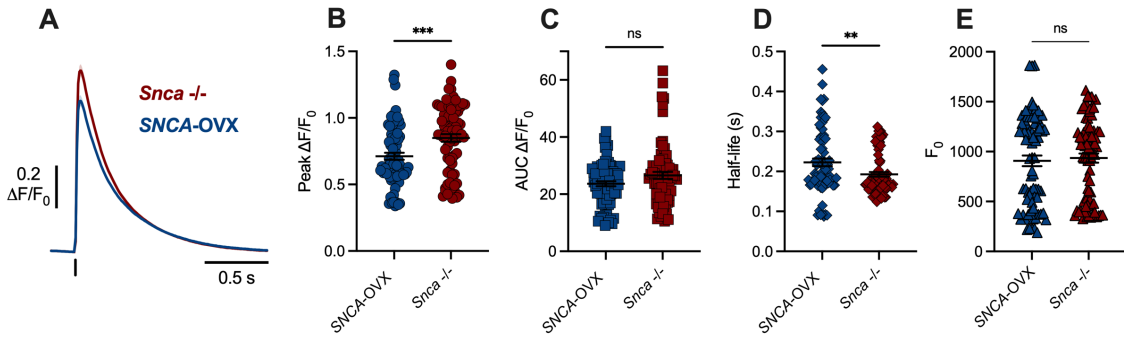


Figure 5.2 Peak size of electrically-evoked ACh release is smaller in SNCA-OVX while half-lives are higher compared to Snca -/-. (data collected by S.Vietti-Michelina and E.Lopes)

(A) *Mean (± SEM) ACh transients evoked by single electrical pulses in dorsolateral striatum of SNCA-OVX and Snca -/-. Stimulations were collated for single pulses across a range of experiments in drug-free conditions. ACh release is slightly enhanced in Snca -/- mice. SNCA-OVX: n = 75 transients in N = 11 mice, Snca -/-: n = 76 transients in N = 11 mice.*

(B) *Peak $\Delta F/F_0$ in SNCA-OVX and Snca -/-. ACh release measured by peak size is higher in Snca -/-. Two-tailed unpaired Student's t-test: p = 0.0005. SNCA-OVX: n = 75 transients in N = 11 mice, Snca -/-: n = 76 transients in N = 11 mice.*

(C) *Area under curve (AUC) $\Delta F/F_0$ in SNCA-OVX and Snca -/-. AUC is slightly higher in Snca -/- but not significantly. Two-tailed unpaired Student's t-test: p = 0.052. SNCA-OVX: n = 75 transients in N = 11 mice, Snca -/-: n = 76 transients in N = 11 mice.*

(D) *Half-lives of ACh transients in SNCA-OVX and Snca -/-. Half-lives were calculated from falling phases of ACh transients by fitting a one-phase decay function. Half-lives were higher in SNCA-OVX mice. Two-tailed unpaired Student's t-test: p = 0.0086. SNCA-OVX: n = 75 transients in N = 11 mice, Snca -/-: n = 76 transients in N = 11 mice.*

(E) *Baseline fluorescence F_0 in SNCA-OVX and Snca -/-. F_0 is similar for both genotypes. Two-tailed unpaired Student's t-test: p = 0.69. SNCA-OVX: n = 75 transients in N = 11 mice, Snca -/-: n = 76 transients in N = 11 mice.*

5.3.3 SNCA-OVX mice show stronger D2R regulation of ACh release

Levels of evoked DA release in *SNCA*-OVX mice are around 30% lower than in their littermate *Snca* -/- controls (Janezic et al., 2013). Given these deficits in DA release, we explored whether D2R regulation of ACh release was altered in *SNCA*-OVX compared to *Snca* -/- controls. First, we examined the effect of a D2R selective antagonist (L-741,626, 1 µM) on ACh release evoked by single electrical pulses (1p) or trains of 5 pulses (5p) at a range of frequencies mimicking tonic ChI firing (Wilson et al., 1990; Bennett and Wilson, 1999a). In *SNCA*-OVX mice, antagonism of D2Rs enhanced ACh release driven by 5p at all frequencies (**Figure 5.3A-B**. Two-way ANOVA, frequency x drug interaction: F (3,20) = 1.48, p = 0.24; frequency effect: F (3,20) = 25.19, p < 0.0001; drug effect: F (1,20) = 14.61, p = 0.0011. *SNCA*-OVX: n = 6 slices in N = 3 mice, *Snca* -/-: n = 5 slices in N = 3 mice). On the other hand, in *Snca* -/-, no effect of D2R blockade on ACh release was reported (**Figure 5.3C-D**. Two-way ANOVA, frequency x drug interaction: F (3,16) = 2.045, p = 0.14; frequency effect: F

(3,16) = 9.53, p = 0.0008; drug effect: F (1,16) = 0.40, p = 0.53. *SNCA*-OVX: n = 6 slices in N = 3 mice, *Snca* -/-: n = 5 slices in N = 3 mice). To better evaluate genotype-driven differences, we sought to directly compared the effect of D2R antagonism between early parkinsonian and control mice. To do so, we first performed a three-way analysis to evaluate the effects of genotype, treatment (D2R antagonist L-741,626) and stimulation frequency (**Figure 5.3E**). An overall effect of stimulation frequency ($F(3,36) = 30.37$, $p < 0.0001$), genotype ($F(1,36) = 6.62$, $p = 0.014$) and treatment ($F(1,36) = 10.93$, $p = 0.0022$) was seen. Furthermore, we found a significant interaction between genotype and treatment ($F(1,36) = 6.55$, $p = 0.014$), so we proceeded with two-way comparisons (**Figure 5.4**).

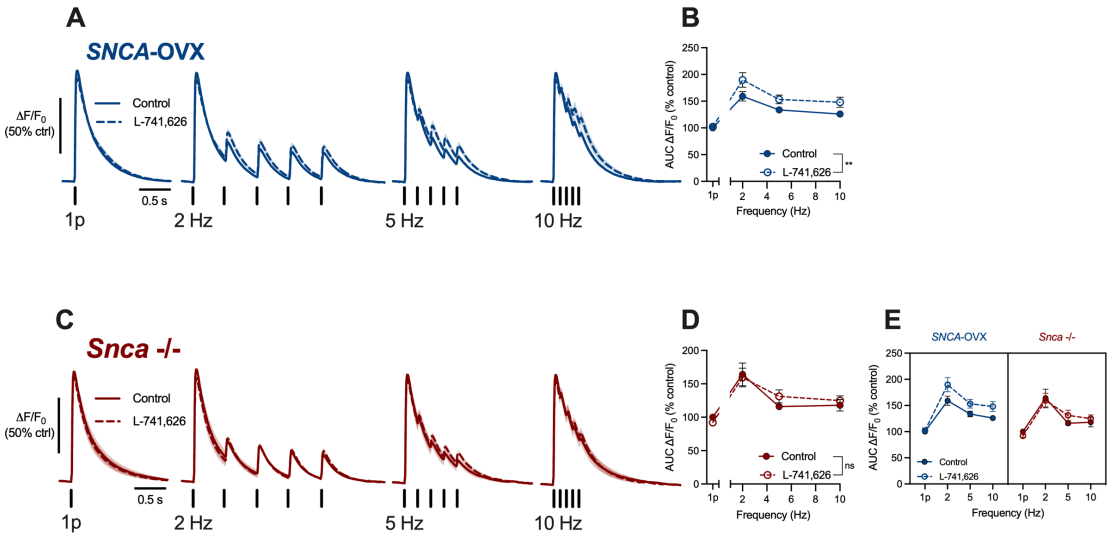


Figure 5.3. Antagonism of D2R promotes ACh release in the dorsolateral striatum of SNCA-OVX but not Snca -/- mice. (Data collected by S.Vietti-Michelina and E.Lopes)

(A) *Mean (± SEM) ACh transients evoked by single electrical pulses (1p) or trains of 5 pulses (5p) at 2-5-10 Hz in SNCA-OVX mice in drug-free or after washing on the D2R antagonist L-741,626 (1 μM). Data are normalised to single pulse in drug-free, n = 6 slices in N = 3 mice.*

(B) *Mean AUC $\Delta F/F_0$ (± SEM) plotted against stimulation frequency. Data are normalised to single pulses in control conditions. D2R block enhanced ACh released by trains of 5p. Two-way ANOVA: frequency x drug interaction: F (3,20) = 1.48, p = 0.24; frequency effect: F (3,20) = 25.19, p < 0.0001; drug effect: F (1,20) = 14.61, p = 0.0011, n = 6 slices in N = 3 mice.*

(C) *Mean (± SEM) ACh transients evoked by single electrical pulses or trains of 5p at 2-5-10 Hz in Snca -/- mice in presence/absence of the D2R antagonist L-741,626 (1 μM). Data are normalised to single pulse in drug-free conditions, n = 5 slices in N = 3 mice.*

(D) *Mean AUC $\Delta F/F_0$ (± SEM) plotted against stimulation frequency. Data are normalised to single pulses in control conditions. Block of D2R did not significanlty alter ACh released by trains of pulses. Two-way ANOVA: frequency x drug interaction: F (3,16) = 2.04, p = 0.14; frequency effect: F (3,16) = 9.53, p = 0.0008; genotype effect: F (1,16) = 0.40, p = 0.53, n = 5 slices in N = 3 mice.*

(E) *A three-way ANOVA was performed to determine the effect of frequency, genotype and D2R antagonism before directly compare drug effects in each genotype as shown in Figure 5.4. Three-way ANOVA: stim frequency effect: F(3,36) = 30.37, p < 0.0001; genotype (SNCA-OVX vs Snca -/-) effect: F(1,36) = 6.62, p = 0.014; treatment effect (control vs L-741,626): F(1,36) = 10.93, p = 0.0022; stim frequency x genotype interaction: F(3,36) = 0.362, p = 0.78; stim frequency x treatment interaction: F(3,36) = 2.04, p = 0.12; genotype x treatment interaction: F(1,36) = 6.55, p = 0.014; stim frequency x genotype x treatment interaction: F(3,36) = 1.11, p = 0.35, n = 5 slices in N = 3 mice.*

In control conditions (drug-free), ACh release evoked by trains of pulses at different frequencies did not differ between genotypes (**Figure 5.4A-B**. Two-way ANOVA, frequency x genotype interaction: F (3,36) = 0.87, p = 0.46; frequency effect: F (3,36) = 23.39, p < 0.0001; genotype effect: F (1,36) = 0.95, p = 0.33. *SNCA*-OVX: n = 6 slices in N = 3 mice, *Snca* -/-: n = 5 slices in N = 3 mice). In D2R block, ACh release was modestly but significantly enhanced in *SNCA*-OVX mice (**Figure 5.4C-D**. Two-way ANOVA, frequency x genotype interaction: F (3,36) = 0.37, p = 0.76; frequency effect: F (3,36) = 22.10, p < 0.0001; genotype effect: F (1,36) = 10.06, p = 0.0031. *SNCA*-OVX: n = 6 slices in N = 3 mice, *Snca* -/-: n = 5 slices in N = 3 mice). In summary, these

findings suggest that, despite a deficit in DA release, D2R-mediated inhibition of ACh release is higher in *SNCA*-OVX mice.

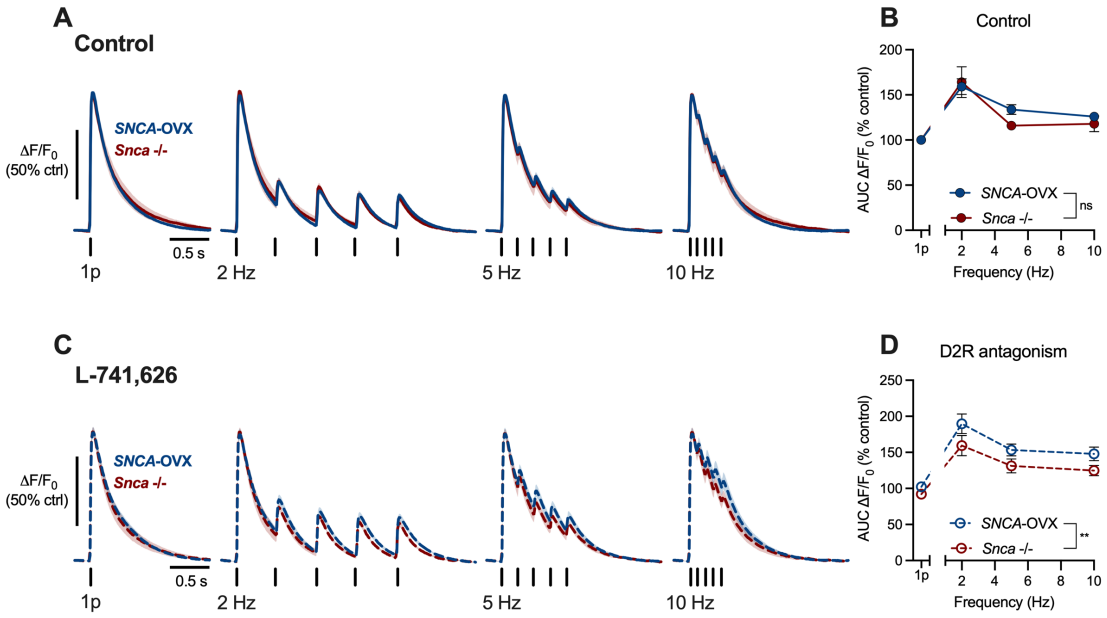


Figure 5.4. D2R-mediated inhibition of ACh release is stronger in the dorsolateral striatum of SNCA-OVX mice. (Data collected by S.Vietti-Michelina and E.Lopes)

(A) *Mean (± SEM) ACh transients evoked by single electrical pulses (1p) or trains of 5 pulses (5p) at 2-5-10 Hz in SNCA-OVX and Snca -/- mice in drug-free conditions (control). Data are normalised to single pulse in drug-free condition for each genotype. SNCA-OVX: n = 6 slices in N = 3 mice, Snca -/-: n = 5 slices in N = 3 mice.*

(B) *Mean AUC ΔF/F₀ (± SEM) plotted against stimulation frequency. Data are normalised to single pulses in control conditions for each genotype. When D2Rs are active, there are no significant differences in the frequency response of ACh release between genotypes. Two-way ANOVA: frequency x genotype interaction: F (3,36) = 0.87, p = 0.46; frequency effect: F (3,36) = 23.39, p < 0.0001; genotype effect: F (1,36) = 0.95, p = 0.33. SNCA-OVX: n = 6 slices in N = 3 mice, Snca -/-: n = 5 slices in N = 3 mice.*

(C) *Mean (± SEM) ACh transients evoked by single electrical pulses or trains of 5p at 2-5-10 Hz in SNCA-OVX and Snca -/- mice in presence of the D2R antagonist L-741,626 (1 μM). Data are normalised to single pulse in drug-free condition for each genotype. SNCA-OVX: n = 6 slices in N = 3 mice, Snca -/-: n = 5 slices in N = 3 mice.*

(D) *Mean AUC ΔF/F₀ (± SEM) plotted against stimulation frequency in D2R antagonism. Data are normalised to single pulses in control conditions for each genotype. When D2Rs are inhibited, ACh response to frequency is higher in SNCA-OVX mice. Two-way ANOVA: frequency x genotype interaction: F (3,36) = 0.37, p = 0.76; frequency effect: F (3,36) = 22.10, p < 0.0001; genotype effect: F (1,36) = 10.06, p = 0.0031. SNCA-OVX: n = 6 slices in N = 3 mice, Snca -/-: n = 5 slices in N = 3 mice.*

5.3.4 Presumed tonic GABAergic inhibition of ACh release does not differ between SNCA-OVX and Snca -/- mice

In the dorsolateral striatum of *SNCA*-OVX mice, tonic GABAergic inhibition of DA release is enhanced, due to reduced GAT expression (Roberts et al., 2020). In WT mice, AUC of single pulse electrically-evoked ACh transients is enhanced upon inhibition of GABA receptors (**Chapter 3**, **Section 3.3.5**), suggesting a potential tonic

inhibition of ACh release by GABA. Here, we tested whether GABAergic regulation of ACh release was altered in the *SNCA*-OVX model. To test this, we examined the effect of $GABA_{A/B}$ receptor antagonists (bicuculline, 10 µM, CGP 55845, 4 µM) on single pulse-evoked ACh release in slices from *SNCA*-OVX and *Snca* -/- mice. Wash on of GABA receptor antagonists increased the size (measured by AUC) of 1p-evoked ACh release similarly in both genotypes (**Figure 5.5A-B**. Two-way ANOVA, time x genotype interaction: $F(14, 205) = 0.63$, $p = 0.82$; time effect: $F(14,205) = 6.22$, $p<0.0001$; genotype effect: $F(1,205) = 1.86$, $p = 0.17$. *SNCA*-OVX: n = 8 slices in N = 4 mice, *Snca* -/-: n = 8 slices in N = 4 mice). Overall, these data suggest that changes in GABA tone in the *SNCA*-OVX mice do not impact on GABAergic regulation of ACh release.

GABA receptor antagonism enhanced 1p-evoked DA release to a greater degree in *SNCA*-OVX mice (Roberts et al., 2020). To test whether the effect of GABA receptor antagonism on ACh release was limited by the increase in DA levels in *SNCA*-OVX vs *Snca* -/-, we blocked D2Rs with a selective antagonist (L-741,626, 1 µM). In D2R block, single pulse-evoked ACh release is increased upon wash on of GABA receptor antagonists similarly in both genotypes (**Figure 5.5C-D**. Two-way ANOVA, time x genotype interaction: $F(14,223) = 0.37$, $p = 0.98$; time effect: $F(14, 223) = 10.21$, $p < 0.0001$; genotype effect: $F(1, 223) = 0.50$, $p = 0.48$. *SNCA*-OVX: n = 9 slices in N = 4 mice, *Snca* -/-: n = 8 slices in N = 4 mice). Overall, these results suggest that changes in DA levels driven by enhanced tonic GABAergic inhibition of DA release observed in *SNCA*-OVX mice did not impact on ACh release.

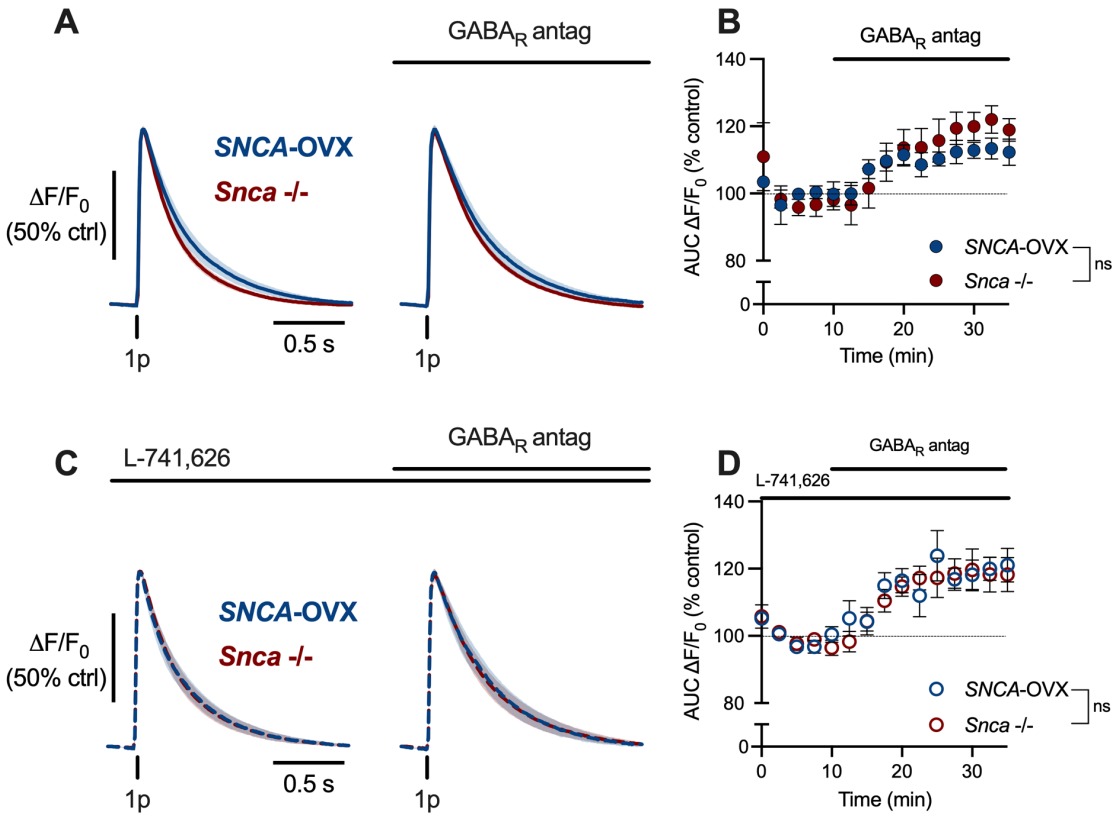


Figure 5.5. GABAergic modulation of ACh release does not differ between SNCA-OVX and Snca -/- mice. (Data collected by S.Vietti-Michelina and E.Lopes)

(A) *Mean (± SEM) ACh transients in drug-free (right) or after GABA receptor ($GABA_R$) antagonist (bicuculline, 10 μM, and CGP 55845, 4 μM, left) wash on. ACh release was evoked by single electrical pulses and normalised to pre-wash on baseline for each genotype. SNCA-OVX: n = 8 slices in N = 4 mice, Snca -/-: n = 8 slices in N = 4 mice.*

(B) *Mean AUC $\Delta F/F_0$ (± SEM) plotted against time. Data were normalised to pre-wash on baseline. ACh release is increased by GABA receptor block similarly in both genotypes, suggesting that tonic GABAergic inhibition of ACh release does not differ between genotypes. Two-way ANOVA: time x genotype interaction: F (14, 205) = 0.63, p = 0.82; time effect: F (14,205) = 6.22, p < 0.0001; genotype effect: F (1,205) = 1.86, p = 0.17. SNCA-OVX: n = 8 slices in N = 4 mice, Snca -/-: n = 8 slices in N = 4 mice.*

(C) *Mean (± SEM) ACh transients in presence of D2R antagonist (L-741,626, 1 μM) or after $GABA_R$ antagonists (bicuculline, 10 μM, and CGP 55845, 4 μM, left) wash on. ACh release was evoked by 1p and normalised to pre-wash on baseline for each genotype. SNCA-OVX: n = 9 slices in N = 4 mice, Snca -/-: n = 8 slices in N = 4 mice.*

(D) *Mean AUC $\Delta F/F_0$ (± SEM) plotted against time. Data were normalised to pre-wash on baseline. ACh is increased similarly by $GABA_R$ antagonists in both genotypes when D2Rs are blocked, suggesting that changes in DA release do not alter tonic GABAergic inhibition of ACh release. Two-way ANOVA: time x genotype interaction: F (14,223) = 0.37, p = 0.98; time effect: F (14, 223) = 10.21, p < 0.0001; genotype effect: F (1, 223) = 0.50, p = 0.48. SNCA-OVX: n = 9 slices in N = 4 mice, Snca -/-: n = 8 slices in N = 4 mice.*

5.4 DISCUSSION

In this chapter, we looked at adaptations in striatal ACh signalling in an α-synuclein-overexpressing model of early PD. Taken together, these findings show that AChE regulates tonic ACh levels more strongly in *SNCA*-OVX mice (**Figure 5.1**) and that evoked ACh levels are lower but have longer extracellular lifetime in *SNCA*-OVX mice (**Figure 5.2**). Furthermore, we reported a stronger regulation of ACh release by D2Rs in *SNCA*-OVX mice (**Figure 5.3** and **5.4**). Finally, there are no changes in GABA receptor-mediated modulation of ACh release in both genotypes (**Figure 5.5**).

5.4.1 Alterations in ACh tone regulation in the dorsolateral striatum of the early PD model SNCA-OVX

In **Section 5.3.1**, we showed that limiting ACh breakdown by inhibiting AChE had a stronger effect on tonic ACh release in *SNCA*-OVX mice. This effect suggested that AChE more efficiently inhibits tonic ambient ACh levels in the early PD mouse model, which appears to be in contrast with the long-standing idea of PD as a hypercholinergic disease (Barbeau, 1962). However, AChE inhibitors have been previously used clinically to improve motor symptoms and cognitive deficits of PD patients (Chung et al., 2010; Rolinski et al., 2012; Wang et al., 2015). Indeed, it has been proposed that the increase in ACh levels given by anti-cholisterase treatments might promote DA transmission through desensitisation of nAChRs or desensitise ACh autoreceptors and mimic an anticholinergic drug effect (Lim et al., 2014).

One potential explanation for this enhanced role of AChE in limiting tonic ACh levels in *SNCA*-OVX is an increase in its expression, at least at the early stages of disease progression. At later stages of the disease progression, AChE expression could be downregulated, potentially exacerbating the hypercholinergic phenotype. In line with this idea, proteomics and transcriptomics analysis of sequencing data from SNc of PD patients have revealed that AChE is downregulated in PD (Dong et al., 2021). In PD patients, AChE expression is also decreased in different organs in the peripheral system (Gjerløff et al., 2015; Fedorova et al., 2017). Besides changes in its expression,

an increase in AChE activity could also explain the reported results in the *SNCA*-OVX model. Indeed, the enhanced role of AChE in limiting tonic ACh levels in *SNCA*-OVX mice could be due to a compensatory increase in AChE activity in this model. For instance, work examining exosomal AChE in PD patients revealed a strong negative correlation between AChE activity and disease progression (Shim et al., 2021). It is therefore plausible that at the early stages of the disease examined in this model, AChE activity is enhanced due to compensatory mechanisms, while its activity could be subsequently reduced upon progression of the disease. To further support this idea, α-synuclein inclusions in ChIs of PD patients are only observed in late stages of PD progression, suggesting that α-synuclein overexpression-related dysfunction of ChI machinery might be observed at a later stage of the disease (Mori et al., 2008; Lim et al., 2014). A useful direction for future work aimed at better understanding whether AChE activity is altered at early stages of the disease progression would be to perform a colorimetric enzyme activity assay on striatal tissue punches of overexpressors and control mice.

In these experiments, we examined the role of AChE in spatiotemporally regulating ambient ACh in the PD model and healthy controls. One fundamental aspect of alterations in ACh signalling in PD is loss of autoinhibitory mechanism mediated by muscarinic autoreceptors on ChIs. Indeed, DA depletion with 6-OHDA-induced lesions resulted in an upregulation of the autoreceptor-associated GTPase-accelerating protein RGS4, which in turn reduced M_4-mAChR control of ChI firing (Ding et al., 2006). Testing the role of mAChRs on ACh release measured with $GRAB_{ACh}$ in a PD model is difficult because GRAB sensors themselves are muscarinic receptors and there is limited availability of subtype-selective antagonists, as discussed in **Chapter 3** (**Section 3.4.4**).

5.4.2 Alterations in evoked ACh release in the mouse model of early PD SNCA-OVX

In **Section 5.3.2**, we found differences in the profiles of evoked ACh release in *SNCA*-OVX versus control mice. We showed that peak ACh release is lower in *SNCA*-OVX mice compared to controls, while AUC is unaltered, and half-lives are increased

(**Figure 5.2**). The lower ACh release levels reported in *SNCA*-OVX mice appear to contrast with microdialysis studies which found elevated levels of ACh release in the striatum of PD models (DeBoer et al., 1993; Ikarashi et al., 1997). Said inconsistencies might arise from the different PD models in use and the different stages of PD progression that these models represent. Indeed, these studies used a toxin model of PD, by lesioning DA projections with 6-OHDA injections, while in this thesis we adopted a progressive genetic model of early parkinsonism. Consistently, a progressive model of DA deficiency showed reduction in ChI firing and ACh availability (McKinley et al., 2019). In that study, progressive death of DA neurons was achieved by injections of the diphtheria toxin in Slc6a3$^{DTR/+}$ mice, which express the diphtheria toxin receptor in DA neurons (McKinley et al., 2019). Progressive loss of DA reduced ChI firing and pacemaking activity via an inhibition of hyperpolarisation-activated cation (HCN) channel transcription (McKinley et al., 2019). Furthermore, this is consistent with unpublished data from our group that showed lower activation of ChIs in *SNCA*-OVX mice, by looking at phosphorylation of the ribosomal protein S6 (S6rp), a marker suggested to report ChI activity (Bertran-Gonzalez et al., 2012).

However, we also reported a small increase in the duration of extracellular ACh signals in *SNCA*-OVX mice, as measured by an increase in half-lives of the transients (**Figure 5.2D**). These findings are in contrast with the previous report of an augmented role of AChE in regulating the dynamics of extracellular ACh signals in *SNCA*-OVX mice (**Figure 5.1**). It is important to underline that ACh release signals measured with GPCR-based sensors are a function of binding and unbinding to the sensors, so that the duration of the signal might depend on GRAB$_{ACh}$ localisation in the two genotypes. Indeed, genetic alterations might drive GRAB$_{ACh}$ expression in different neuronal subtypes or different cellular compartments, so that GRABs could be localised closer or further away from ACh release sites and measure longer lasting or partially degraded faster ACh signals, respectively.

In **Figure 5.1A-B**, we showed that GRAB$_{ACh}$ measured similar fluorescence responses upon wash on of a known concentration of the agonist ACh. Furthermore,

we showed that basal fluorescence F_0 is similar in both genotypes (**Figure 5.2E**). These findings suggests that the sensors are expressed to a similar level in both genotypes. However, we have no information on where the sensors localise in the two genotypes, which can still drive small changes in the signal kinetics.

5.4.3 Compensatory changes in D2R regulation of ACh release in SNCA-OVX mice

In **Section 5.3.3**, we investigated the role of D2Rs in regulating ACh release in *SNCA*-OVX and *Snca -/-* mice. We found higher ACh re-release upon block of D2Rs in *SNCA*-OVX mice, suggesting that D2Rs more strongly inhibit ACh release in early parkinsonian mice. However, *SNCA*-OVX mice showed a 30% deficit in DA release in dorsolateral striatum compared to *Snca -/-* controls (Janezic et al., 2013). The increased D2R control of ACh release despite a deficit in DA release could be due to a compensatory mechanism, occurring at early stages of disease progression. Indeed, an upregulation of D2R signalling could compensate for a loss of DA, in line with the idea of an ACh-DA balance that is progressively lost in PD (Barbeau, 1962). Enhanced D2R-mediated regulation of ACh release might occur via an increase in receptor binding affinity, an upregulation of expression or changes in the receptor downstream signalling cascade. For instance, chronic depletion of DA with 6-OHDA was accompanied by an increase in sensitivity of D1Rs and D2Rs on MSNs in the dorsal striatum of rats (Hu et al., 1990). Furthermore, tomography studies of the CPu of PD patients reported higher binding and upregulation of D2Rs at the initial stages of the disease, followed by progressive loss of D2Rs around 4 years after motor symptoms onset (Kaasinen et al., 2021). However, it is important to note that the alterations in ACh release here reported might be due to α-synuclein and that the direct effects of α-synuclein overexpression (or lack of expression) on ACh release dynamics in this model and in the control mice are currently unresolved.

D2Rs are therefore fundamental in the regulation of ChI excitability upon progressive loss of DA during PD progression. ChIs also express D1 and D5 receptors, which increase neuronal firing (Lim et al., 2014), and are also implicated in PD-related dysfunction in ACh signalling. For instance, in the 6-OHDA mouse model treated with

L-DOPA, aberrant activation of D1/D5 receptors on ChIs causes pathological changes in ChI burst-pause firing activity (Paz et al., 2021).

5.4.4 No changes in GABA receptor modulation of ACh release in SNCA-OVX versus Snca -/-

In **Section 5.3.4**, we found that antagonism of GABA receptors increased AUC of single pulse-evoked ACh release to a similar extent in both genotypes, suggesting that GABA might tonically inhibits ACh release in both a healthy and early parkinsonian mouse model. This is consistent with observations in WT mice described in **Chapter 3** (**Section 3.3.5**).

However, previous studies showed alterations in GABAergic inhibition in models of PD. In the 6-OHDA model, loss of DA resulted in an impairment of GABAergic inhibition and an increase in excitability of dual-transmission cholinergic and GABAergic ChIs (Lozovaya et al., 2018b). On the other hand, in the *SNCA*-OVX model, tonic GABAergic inhibition of DA release was increased in the dorsolateral striatum of PD mice, as a result of downregulation of GABA transporters at least partially located on astrocytes (Roberts et al., 2020). These changes were reported at early stages of disease progression (3 months old), where no DA neuron loss occurred but DA release deficits were already observed (Janezic et al., 2013). These early changes in GABA tone and tonic inhibition of DA do not seem to impact on ACh release levels in *SNCA*-OVX mice. It is possible that progressive dysregulation of GABAergic regulation of ACh release might occur at later stages of the disease progression.

In early parkinsonian *SNCA*-OVX mice, GABA co-released from DA axons was attenuated (Roberts et al., 2020). GABA co-released from DA axons could be a potential source of GABA mediating tonic inhibition of ACh. Hence, despite an increase in GABA tone driven by downregulation of GATs, the decreased release of GABA from DA axons might contribute to a null impact on ACh release tonic regulation in *SNCA*-OVX mice.

Overall, in this chapter, we've examined maladaptive alterations in ACh transmission at the early stages of PD progression in a transgenic mouse model of PD. In apparent contrast with the long-lasting view of PD as a hypercholinergic disease, in the *SNCA*-OVX model we found lower ACh release, enhanced AChE control of tonic ACh levels and higher D2R-mediated regulation of ACh, together with no alterations in putative GABAergic tonic inhibition of ACh release. Taken together, these findings suggest that at the early stages of disease progression compensatory mechanisms might be at play to boost ACh release regulation and compensate for DA loss. At later stages of the disease, further dysregulation might occur resulting in a hypercholinergic state. Future work could investigate ACh release properties in this model at later stages of the disease progression, when DA neurons are lost, as further discussed in **Chapter 6**.

6. General Discussion

DA plays a critical role in regulating striatal transmission and downstream basal ganglia activity and disruptions to its signalling underlie several psychomotor disorders, including PD. DA neurons projecting to the striatum form extensive axonal arborisations which are subject to local neuromodulation, regulating how action potential firing at the level of DA cell bodies translates into striatal DA release. Understanding these mechanisms is therefore fundamental to better appreciate DA release dynamics and their impact on striatal output and behaviour. ACh covers a fundamental role in the modulation of striatal circuitry in health and disease and exerts a range of powerful effects on striatal DA release. The aim of this thesis was to explore the dynamic interplay between ACh and DA in the striatum. In **Chapter 3**, I've characterised the main properties of ACh release in dorsolateral and ventral striatum. Overall, I've showed that ACh is released according to activity in ChIs and is spatiotemporally regulated by AChE. I also reported that ACh release is under regulation by GABA and endogenous DA via D2Rs. In **Chapter 4**, I've expanded upon these findings to investigate how dynamic changes in striatal ACh release modulate DA release STP. I found that ACh-driven DA release is sensitive to changes in ACh release levels driven by extracellular manipulations which alter ACh release probability. However, ACh-driven DA release is insensitive to changes in ACh release levels arising from activity in ChIs. Furthermore, I showed that nAChRs modulate plasticity of DA but not ACh release and that calb1 does not operate downstream of nAChRs on DA axons to mediate their effects. Finally, in **Chapter 5** we explored maladaptive alterations in striatal ACh signalling in an α-synuclein overexpressing mouse model of early PD. Overall, we showed that in early parkinsonian mice ACh release is lower and AChE regulation of tonic ACh stronger. Despite a deficit in DA release, we show a compensatory stronger dopaminergic regulation of ACh release via D2Rs in the parkinsonian model. We also found no effect on ACh release driven by altered GABAergic tone in the dorsolateral striatum of early parkinsonian mice. In this chapter I will discuss the main findings of this thesis and their implications for understanding striatal function in health and disease.

6.1 Measuring striatal ACh release with $GRAB_{ACh}$

In this thesis, ACh release was detected using new generation $GRAB_{ACh}$ sensors (ACh3.0) (Jing et al., 2020). *In vitro*, $GRAB_{ACh}$ sensors exhibit negligible coupling with G protein-mediated downstream signalling pathways, minimal perturbation of cellular physiology and membrane properties and lack of internalisation upon prolonged agonist exposure (Jing et al., 2018, 2020). Given all these features, $GRAB_{ACh}$ sensors appear to be optimal for measuring ACh release in real-time, with minimal disruption of the native properties of the system in which they are expressed. Several other tools for detecting ACh release have been developed and a more detailed overview is provided in **Chapter 1** (**Section 1.3.6**).

Despite the numerous advantages of the use of these sensors, it's important to note that the signal readout is a function of binding and unbinding to the receptor, sensor localisation and its expression levels. Therefore, the measured ACh signal might not accurately reflect endogenous timescales of neurotransmitter release and clearance from the extracellular space or the levels of neurotransmitter to which endogenous receptors are exposed to. For instance, if $GRAB_{ACh}$ sensors localise close to ACh release sites, they will be exposed to higher ligand concentration which might result in higher receptor occupancy and a larger, longer lasting fluorescent signal. On the other hand, sensors expressed further away from release sites might report a faster and smaller signal, which has already been partially degraded or might not diffuse far enough. Knowledge of where ACh is sampled from can help better understanding ACh signalling modalities (volume transmission vs. point-to-point transmission) and estimating the sphere of influence of ACh once released. In **Chapter 3**, I showed that $GRAB_{ACh}$ sensors were expressed by the majority of striatal neurons (MSNs) and their projections, suitable for measuring bulk extracellular ACh signal, in accordance with the purpose of this work. Further spatial resolution can be achieved by targeting $GRAB_{ACh}$ sensor expression to specific neuronal subtypes using a Cre recombinase-dependent approach. Future work could use the floxed $GRAB_{ACh}$ (DIO-ACh3.0) injected in ChAT-Cre mice to achieve selective expression of the sensor on ChIs and therefore measure the most local signal, giving information on how receptor

localisation might impact on ACh signal readout. Using a similar approach to target $GRAB_{ACh}$ expression to DA axons (DIO-ACh3.0 injected in DAT-Cre mice) can give information on the levels of ACh to which DA axons are exposed to. Indeed, this approach has been adopted in recent studies investigating the nAChR-mediated effects of ACh release on DA axon physiology (Kramer et al., 2022; Liu et al., 2022). Despite targeted expression of fluorescent sensors is key to investigate the effects of neurotransmitter release on one specific neuronal subtype, global expression of these tools (pending more thorough anatomical characterisation) is highly valuable to better understand the overall signalling dynamics in a brain region. Furthermore, the use of globally expressed sensors is not constrained to a specific transgenic rodent line expressing Cre recombinase and allows for evaluation of neurotransmitter dynamics in native systems and potential comparisons across species. Indeed, the expression of Cre recombinase has been shown to alter protein expression and behaviour in rodents (Bäckman et al., 2006; Chen et al., 2018; Mantanona et al., 2019). A more careful consideration on targeting sensor expression is therefore needed for future experiments.

$GRAB_{ACh}$ sensors measure ACh release as a change in fluorescence from baseline and do not provide information on ACh concentration. However, to reliably compare between different regions or genotypes, the calibration of this signal is fundamental. Here, I calibrated the fluorescent signal measured with $GRAB_{ACh}$ by briefly washing on/off known concentrations of ACh, showing a linear relationship between the size of fluorescent responses and ACh concentration (**Chapter 3**, **Figure 3.1B-C**). These findings revealed that the signal measured with $GRAB_{ACh}$ is proportional to the concentration of ACh released extracellularly. For instance, this calibration approach is also useful to determine whether $GRAB_{ACh}$ sensor detection of ACh differs between two genotypes. Indeed, I adopted this approach in **Chapter 5** (**Figure 5.1A-B**) to verify that differences in ACh release reported between *SNCA*-OVX and *Snca* -/- mice were not due to the $GRAB_{ACh}$ sensors differently detecting ACh release levels in the two genotypes. To allow quantification of neurotransmitter release, future work should aim to develop ratiometric sensors. The potential use of

ratiometric sensors could also allow to measure neurotransmitter release independently from sensor expression, illumination intensity or bleaching. Furthermore, quantitative imaging could also provide information on baseline neurotransmitter levels. In **Chapter 3** (**Section 3.4.2**), I discussed whether dynamic changes in baseline fluorescence F_0 could indicate changes in ambient ACh tone. The potential future development of ratiometric $GRAB_{ACh}$ sensors could allow measurement of baseline ACh levels and comparison across regions or genotypes. For instance, ratiometric FRET calcium imaging has been used to monitor basal calcium levels and their changes upon onset of neurodegenerative processes (Kuchibhotla et al., 2008; Siffrin et al., 2010; Thestrup et al., 2014).

6.2 ACh release in the striatum

The striatum is one of the brain regions exhibiting the highest levels of cholinergic markers (Mesulam et al., 1992; Zhou et al., 2002). ChIs provide widespread innervation in the striatum via their highly branched axonal arbors and are tonically active, resulting in continuous exposure of all tissue elements to ambient levels of ACh (Contant et al., 1996; Descarries et al., 1997). Nonetheless, ACh release dynamics in the striatum are incompletely characterised. In **Chapter 3**, I provided a characterisation of striatal ACh release and its regulation by AChE, GABA and DA.

6.2.1 ChI activity and AChE in the regulation of ACh release dynamics

ChIs display multiple firing patterns *in vivo*, from tonic activity to bursts and pauses (Wilson et al., 1990; Bennett and Wilson, 1999b; Morris et al., 2004). Stimulating at low tonic-like or high burst-like frequencies, I found that ACh is released according to stimulation across striatal regions. However, these dynamic changes in ACh release in response to ChI activation do not seem to impact on ACh-driven DA release (as shown in **Chapter 4**), which raises the question on the potential significance of ChI signalling for DA release regulation *in vivo* (**Section 6.3.1**).

AChE is one of the fastest known enzymes (Descarries et al., 1997), is enriched in striatum (Bernard et al., 1995) and has been proposed as a key player to maintain extracellular ACh levels within physiological limits (Contant et al., 1996; Descarries et al., 1997). Here, I found that AChE regulates the spatiotemporal dynamics of evoked ACh release and its frequency sensitivity, together with limiting tonic striatal ACh levels. This is consistent with microdialysis studies which reported a steady-state basal level of ACh in the extracellular space, which is increased by anti-AChE treatment (Xu et al., 1991; Messamore et al., 1993; Descarries et al., 1997). The role of AChE described in this body of work is also consistent with findings from a recent in silico study investigating ACh signalling modalities (Nosaka and Wickens, 2022). In that mathematical model, the authors reported lack of effect of AChE on fast, point-to-point synaptic ACh signalling, but that AChE shaped the diffusion profile of ACh

release further away from release sites (distances >5 μm) (Nosaka and Wickens, 2022). Here, I sampled from ROIs large enough (100 μm) to detect *ex vivo* this role of AChE in regulating ACh diffusion and signal summation upon differential activation of ChIs. Overall, the findings here discussed suggest that ACh might signal as a volume transmitter whose sphere of influence is shaped by AChE. Work using fluorescent sensors to measure ACh volume transmission and its spread-length constant revealed contrasting results (Jing et al., 2018; Zhu et al., 2020). A fundamental factor to consider when assessing the spread of ACh release measured with fluorescent sensors is their localisation and distance from release sites, which might result in bias in sampling (**Section 6.1**). Future work could characterise $GRAB_{ACh}$ expression in different neuronal compartments in intact tissue to verify that GRABs localise evenly on the membrane of the cells that express them. Future work could also use Cre-dependent expression of $GRAB_{ACh}$ on selective striatal subtypes to investigate the levels of ACh reaching these neurons and the role of AChE in limiting these signals. Indeed, recent evidence from mouse striatal slices expressing $GRAB_{ACh}$ in DA axons reported a role for AChE in regulating the spatiotemporal dynamics of ACh release onto DA axons (Kramer et al., 2022). Indeed, AChE inhibition led to a transient increase in the frequency of spontaneous nAChR-mediated excitatory postsynaptic potentials in DA axons (axEPSPs) and a change in their decay kinetics (Kramer et al., 2022). Notably, AChE inhibition did not impact on axEPSPs peak amplitude, suggesting that a fraction of ChI terminals exist in proximity to nAChRs on DA axons and that ACh might also mediate a fast, synaptic-like axo-axonal neurotransmission onto DA axons (Kramer et al., 2022). Evidence from mathematical modelling of ChI activity and ACh release also supports the view of ACh mediating short-range point-to-point transmission together with ambient ACh tone originating from ChI tonic activity (Nosaka and Wickens, 2022).

Differences in ACh release levels and summation of ACh upon differential stimulation in ChIs in dorsolateral and ventral striatum were also reported (**Chapter 3**, **Section 3.3.2** and **3.3.3**), consistently with a dorsoventral gradient in ChI count and activity (Matamales et al., 2016). These differences could potentially arise from

regional discrepancies in AChE form (membrane-bound or secreted) or levels of activity. Future experiments using a colorimetric assay to determine AChE activity (Ellman et al., 1961) in striatal tissue punches from WT mice containing either dorsal or ventral striatum could reveal potential regional differences in AChE activity. Differences in extracellular summation of ACh signal upon high frequency stimulation could also reveal a potential contribution of synchronous and asynchronous release (AR). To test this, future experiments could use EGTA or substitute extracellular Ca^{2+} with Sr^{2+}, found to abolish or enhance AR respectively (Kaeser and Regehr, 2014; Rozov et al., 2019).

Autoreceptor regulation of ACh release is a fundamental aspect of ACh signalling which remains unexplored. ChIs express M_2 and M_4-mAChRs which act as autoreceptors to modulate ChI activation and prevent excessive ACh release (Bernard et al., 1992; Yan and Surmeier, 1996; Calabresi et al., 1998b; Lim et al., 2014). Investigating their contribution is difficult since $GRAB_{ACh}$ are mAChRs and can be agonised/antagonised by mAChR agonist/antagonists. Indeed, all mAChR subtypes have a high degree of similarity in the ligand-binding site, limiting the availability of subtype-selective ligands (Eglen, 2006; Abudukeyoumu et al., 2019). I piloted the use of two alleged M_2 and M_4-mAChRs selective antagonists (AF-DX116 and PD102807, respectively) in striatal slices expressing $GRAB_{ACh}$ and found a concentration-dependent decrease in the measured ACh signal. Given that blockade of autoreceptors should promote ACh release, these findings suggested a non-specific effect of the antagonists on the $GRAB_{ACh}$ itself. Future experiments aimed at investigating the role of autoreceptors in regulating ACh release measured with $GRAB_{ACh}$ should be carried out using transgenic mouse lines with selective knockout of mAChRs subtypes.

6.2.2 Potential tonic GABAergic inhibition of ACh release

The majority of neurons in the striatum use GABA as their neurotransmitter and there is striatal ambient GABA tone which mediates tonic inhibition of DA release (Lopes et al., 2019; Roberts et al., 2020, 2021). Here, I found that size of ACh

transients measured by AUC is increased upon antagonism of GABA receptors in the dorsolateral and ventral striatum (**Chapter 3**, **Section 3.3.5**). These findings seem to suggest that ACh release in the dorsolateral and ventral striatum might be under tonic GABAergic inhibition consistently with previous microdialysis findings (DeBoer and Westerink, 1994). Notably, the findings here reported consider compound effects of both GABA receptor subtypes. Future work could investigate the contribution of each receptor separately and help discriminate between direct and indirect effects of GABA on ACh release. Furthermore, the increase in DA release following GABA receptor antagonism was found to feebly limit the effects of GABA receptor antagonists on ACh release via activation of D2Rs (**Chapter 3**, **Section 3.3.5**). Future experiments could use a stimulation paradigm better reflecting the time course of D2R activation to further assess the contribution of a relief in tonic DA inhibition on ACh release. GABA receptor activation has also been found to enhance the contrast in DA released by bursts of stimuli at high frequencies (Lopes et al., 2019). Future work could investigate whether GABA cover a similar role in modulating ACh release short-term plasticity upon differential activation of ChIs when D2Rs are antagonised, to avoid confounding effects on ACh release driven by changes in DA release.

The sources of GABA mediating these effects on ACh release have not been fully elucidated and a discussion of the different GABAergic input to ChIs is provided in **Chapter 3** (**Section 3.4.5**). Notably, DA axons co-release GABA (Tritsch et al., 2012), which might regulate ACh release. Future work could test GABA receptor-mediated IPSCs on ChIs driven by selective optogenetic activation of DA axons. Experiments should be performed in presence of D2R and glutamate receptor antagonists, to avoid confounding effects of DA and glutamate co-release.

6.2.3 Dopaminergic modulation of ACh release

DA is another powerful modulator of ACh release. I found that ACh release is inhibited by endogenous DA acting at D2Rs (**Chapter 3**, **Section 3.3.6**), consistent with electrophysiology studies reporting D2R-mediated inhibition in ChI firing (Maurice et al., 2004; Deng et al., 2007a; Chuhma et al., 2014). Agonism of D2Rs more

pronouncedly inhibited ACh release in the dorsolateral than ventral striatum, consistently with older findings monitoring radiolabelled ACh release (Henselmans and Stoof, 1991). These differences might be due to ChIs expressing different levels of D2Rs or receptors with different affinity along a dorsoventral axis. Indeed, RNAseq of D2R-expressing striatal neurons revealed lower expression of cholinergic markers along the dorsoventral axis (Puighermanal et al., 2020). Future work characterising D2R expression profiles in ChIs across striatal subregions could help better understand regional differences in dopaminergic regulation of ACh release. Furthermore, future experiments evaluating the effects of D2R agonism in presence of antagonists of D1/D5 receptors can help better discriminate between the excitatory and inhibitory effects of DA on ACh release across striatal regions. I also found no effect of antagonising D2Rs on single pulse-evoked ACh release, suggesting no striatal basal tone of DA, consistent with previous findings on DA release (Rice et al., 2011). Furthermore, the maximal effect of D2R-mediated inhibition of ACh release was at 500 ms, with an effect sustained for at least 2 s, consistently with previous reports in rodent slices (Lee et al., 2002; Phillips et al., 2002; Rice et al., 2011; Sulzer et al., 2016). Recent findings in mouse striatal slices expressing $GRAB_{ACh}$ selectively in DA axons also showed an increase in the paired-pulse ratios of ACh release evoked by pairs of electrical stimuli in presence of the D2R antagonist sulpiride (Liu et al., 2022), consistent with the findings reported in this thesis. However, in that study they also showed a significant increase in ACh release evoked by the first electrical stimulus upon D2R blockade, suggesting that ACh release might be tonically inhibited by DA (Liu et al., 2022) and in contrast with the findings presented in this thesis. Discrepancies in the findings might be driven by differential expression of the $GRAB_{ACh}$ sensors. An effect on single pulse-evoked ACh release might have been overlooked in this work because global expression of the sensor might lead to sampling from regions distal from release sites or with higher AChE activity than on the membrane of DA axons. Nonetheless, expression restricted to DA axons could potentially bias ACh release sampling to regions where ChI terminals exist near DA axons and nAChRs.

Increasing DA levels with cocaine unveiled remarkably different effects on ACh release in dorsolateral and ventral striatum (**Chapter 3**, **Section 3.3.6**). In dorsolateral striatum, cocaine inhibited ACh release in a D2R-dependent manner. Therefore, these findings support the notion that higher DA levels given by cocaine act at D2Rs on ChIs to inhibit ACh release. It is then plausible that this reduction in ACh levels might result in reduced ACh tone at nAChRs on DA axons, lower activation these receptors and consequent relief nAChR-mediated STD of DA release. Unpublished observations from the lab monitoring DA release with FCV seem to support this hypothesis in CPu. On the other hand, the cocaine-D2R-mediated inhibition of ACh release was less pronounced in the ventral striatum. These findings suggest that, in the ventral striatum, increased DA levels in cocaine act at D2Rs on ChIs to modestly reduce ACh release, which will in turn partially reduce nAChR activation on DA axons and contribute to a small relief of nAChR-mediated STD of DA release. Unpublished observations from the lab seem to support this hypothesis and to suggest an additional mechanism intrinsic to DA axons mediated by D2Rs to further enhance DA release in presence of cocaine. Future work could implement a dual color fluorescence approach, using $GRAB_{ACh}$ (cpGFP,green) together with $GRAB_{DA}$ (rDA, cmpApple, red) (Sun et al., 2020) for simultaneous measurement of ACh and DA. This approach could help better understand the mechanisms underlying the changes in the DA-ACh regulatory axis in presence of cocaine. Furthermore, an *in vivo* validation is fundamental to understand the significance of this mutual regulation in behaviour.

6.3 Cholinergic modulation of DA release

ACh can modulate DA release in a multiplicity of ways. For instance, ACh released following synchronous activation of ChIs can directly evoke DA release via β2-nAChRs, in absence of action potential firing at the level of DA neuron cell bodies (Cachope et al., 2012; Threlfell et al., 2012). Measurement of electrically-evoked DA release with continuous amperometry showed a biphasic profile, characterised by an initial dopaminergic component and a subsequent cholinergic component (Wang et al., 2014a, 2014b). In **Chapter 4**, I investigated this complex relationship between dynamic changes in ACh release and the dual component of DA release.

6.3.1 Complexity of investigating cholinergic modulation of DA release short-term plasticity

ACh-driven DA release is not sensitive to differential activation of ChIs (Threlfell et al., 2012). It was previously poorly defined whether changes in ChI stimulation frequency or pulse number would result in changes in ACh release levels. Here, I showed that ACh is released dynamically according to ChI stimulation (**Chapter 3**, **Section 3.3.3**). Furthermore, I showed that manipulations that alter ACh release probability are positively correlated to the amount of ACh-driven DA that is released from DA axons, that is more ACh release drives more DA release (**Chapter 4**, **Section 4.3.1**). However, once nAChRs have been activated by ACh and driven DA release, additional ACh released from ChIs stimulated with trains of pulses at different frequencies failed to alter ChI-driven DA release. Hence, I revealed a dynamic component in ChI-driven DA release but confirmed unresponsiveness to activity in ChIs. Changes in ACh release levels should result in changes in ACh tone at nAChRs on DA axons and result in more or less activation of nAChRs. It is well documented that nAChRs promote STD of DA release and that lack of activation, desensitisation or antagonism of the receptors relieves the depression and re-establishes DA release sensitivity to stimulation (Rice and Cragg, 2004). The effect of differential nAChR activation on DA release only occurs with concurrent activity in DA neurons, that is

when providing global tissue depolarisation via electrical stimulation. Therefore, it appears that nAChRs report a digital all-or-nothing signal when mediating ACh-driven DA release in isolation. ACh can also directly drive DA release *in vivo* (Cachope et al., 2012), therefore it is important to reflect on the significance of these properties in a behavioural context. It has been proposed that ACh-driven DA release might signal activity in a population of ChIs as a coincidence detector (Threlfell et al., 2012). *In vivo*, DA neurons are tonically active and burst fire when signalling reward-related information, while, on a similar timescale, ChIs pause their tonic firing, flanked by brief burst firing. Given that there is concurrent activity in DA neurons, potential reduction in ACh levels driven by ChI pause and consequent lower nAChR activation might still promote relief of nAChR-mediated STD of DA release. Indeed, cue-evoked NAcC DA release in a Pavlovian-to-instrumental transfer task (PIT) in rats was enhanced upon administration of the nAChR antagonist mecamylamine (Collins et al., 2016). Those findings support the idea that activation of nAChRs on DA axons promotes depression of DA release upon burst firing of DA neurons, which can be alleviated by decreasing activity at the receptors (Collins et al., 2016). Initial and rebound excitation of ChI before and after the pause might then trigger ACh-driven DA release and summate to this signal to overall promote DA release in a reward-related context.

One major complication in understanding the relationship between ACh and DA release arises from the fact that manipulations that will impact on one neurotransmitter will also impact on the other. Future work aimed at investigating the individual contributions of ACh and DA-driven DA release could implement a dual opsin (e.g., ChR2 and Chrimson) optogenetic approach to achieve selective activation of ChIs and DA neurons. However, this will preclude the use of $GRAB_{ACh}$ sensors for direct measurement of ACh release. Future experiments could also use Cre-dependent GRAB sensors in DAT-Cre mice to achieve selective expression of $GRAB_{ACh}$ on DA axons and measure the levels of ACh reaching DA axons, to directly test whether dynamic changes in ACh release are reported at the level of DA axons. Recent evidence using this approach suggested that depression of ACh release after

the first stimulus in a paired-pulse stimulation might be underlying STD of DA release (Kramer et al., 2022; Liu et al., 2022). Data included in **Chapter 3** (**Figure 3.5**) measuring ACh release with the globally expressed $GRAB_{ACh}$ also showed that ACh released by successive stimuli in low frequency trains is lower than ACh released by the first stimulus. It is unclear what are the levels of ACh at DA axons necessary to activate nAChRs and trigger ACh release. Work measuring axEPSPs on DA axons following light activation of ChIs with pairs of pulses reported that paired-pulse ratios (PPR) between the second and first pulse were depressing (PPR < 1) at all inter-stimulus intervals tested (Kramer et al., 2022). Similar profiles were obtained when measuring ACh release onto DA axons with $GRAB_{ACh}$ expressed on DA axons. Nonetheless, axEPSPs were still triggered by the second pulse (Kramer et al., 2022), suggesting that enough ACh is released onto DA axons to activate nAChRs and trigger their downstream effects. However, this might not be sufficient to drive a subsequent DA release event supporting the idea that depression of ACh release in train stimulation is a strong component of insensitivity of ACh-driven DA release to activation of ChIs. Besides the role of ACh release rundown in train stimulation, unpublished observations from the lab seem to also suggest a nAChR-mediated STD component as discussed in **Section 4.4.1**.

6.3.2 Potential mechanisms operating downstream of nAChRs

The mechanisms operating downstream of nAChRs via which they regulate shot-term plasticity of DA release are currently incompletely characterised. NAChRs might operate though Ca^{2+}-related mechanisms, such as limiting intracellular Ca^{2+} summation, interacting with intracellular Ca^{2+} buffer proteins and inactivating VGCCs. Indeed, previous studies in midbrain and cortical neurons found that nAChRs modulate the activation of different VGCCs (Tsuneki et al., 2000; Stevens et al., 2003) and quantitative proteomics analysis has shown that several proteins involved in Ca^{2+} signalling are associated with mouse neuronal β2-nAChRs (McClure-Begley et al., 2013). In this thesis, I tested a potential role for the Ca^{2+} buffer protein calb1 in operating downstream of nAChRs, possibly buffering intracellular Ca^{2+} and limiting

Ca^{2+} summation to favour STD of DA release during train stimulation. I found no effect of knocking-down calb1 selectively in DA neurons on the nAChR-mediated STD of DA release in response to changes in stimulation frequency, suggesting no functional association between the two. Nonetheless, nAChRs might still operate through Ca^{2+}-related mechanisms. For instance, unpublished observations from the lab imaging Ca^{2+} in DA axons show that when nAChRs are active, they limit increases in intracellular Ca^{2+} levels in response to burst-like stimuli, suggesting that activation of nAChRs limits intracellular Ca^{2+} summation. Future work should determine whether this effect is mediated by inactivation of VGCCs, combining Ca^{2+} imaging of DA axons in slices from DAT-Cre;Ai95D mice (expressing GCaMP6f selectively in DA axons), selective VGCCs antagonists and the β2-nAChRs antagonist DHβE.

Other potential mechanisms operating downstream of nAChRs might include changes in membrane polarisation properties via regulation of Na^{+} and K^{+} conductance. To better understand how nAChRs might influence DA axon physiology, future work could use voltage indicators selectively expressed in DA axons with a Cre-recombinase approach and two-photon imaging to detect whether activation of nAChRs might alter action potential duration and propagation following train stimulation. Recent evidence suggests that ACh released from ChIs induces action potential firing in distal DA axons through the activation of nAChRs as a mechanism to regulate DA signalling (Liu et al., 2022). Ectopic action potentials initiated on DA axons by nAChR activation were followed by opening of P/Q-type and N-type Ca^{2+} channels (Liu et al., 2022). Furthermore, ChI-mediated activation of nAChRs on DA axons results in excitatory postsynaptic potentials in DA axons (axEPSPs) and summation of these axEPSPs can trigger spontaneous action potentials locally in a subset of DA axons (Kramer et al., 2022). Despite these fundamental advances, the mechanisms via which nAChRs mediate STD of DA release remain undefined. Future experiments could potentially test whether failing of action potential initiation or propagation might underlie DA release depression mediated by nAChR activation, as suggested above.

6.4 Striatal ACh signalling in a model of early PD

Historically, PD has been considered as a hypodopaminergic and an hypercholinergic condition and several alterations in ChI signalling have been reported in different animal models of PD. Discrepancies between the studies might arise from the use of models recapitulating different stages of disease progression, suggesting that alterations in striatal cholinergic signalling might undergo different adaptations at different stages of the disease.

In **Chapter 5**, we used a progressive and highly physiological transgenic mouse model of PD that overexpresses human α-synuclein (*SNCA*-OVX) at disease relevant levels to investigate ACh signalling at early stages of PD progression. **Figure 6.1** summarises the findings included in this thesis, together with previously published observations in this same model.

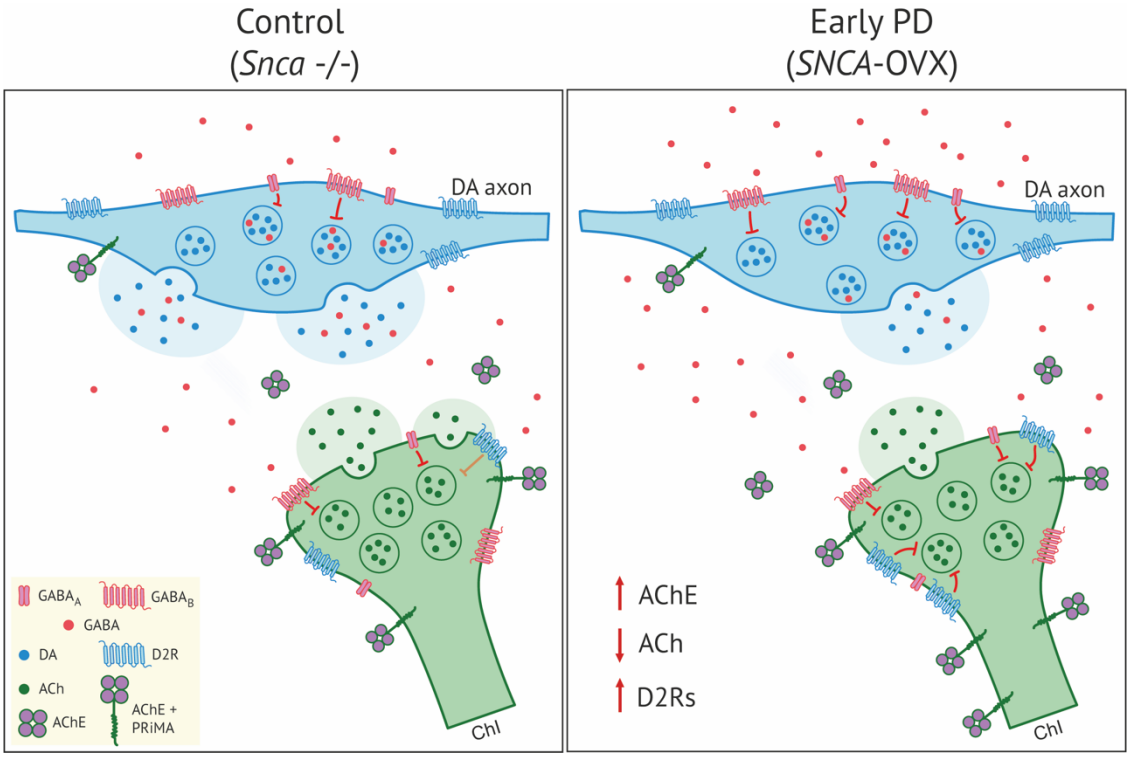


Figure 6.1. Dysfunction in dorsal striatal cholinergic signalling in a mouse model of early PD. *In early parkinsonian SNCA-OVX (3-4 months old), published studies have reported a decrease in striatal DA release that precedes DA neuron loss, augmented tonic GABAergic inhibition of DA release and a reduction in GABA co-release from DA axons. We found that, despite a deficit in DA release, D2R-mediated inhibition of ACh release is enhanced in SNCA-OVX. Despite an increase in GABA tonic inhibition of DA release, we found no changes in GABAergic regulation of ACh. In SNCA-OVX mice, we also reported stronger regulation of tonic ACh levels by AChE (found either membrane-bound through a PRiMA anchor or secreted) and smaller electrically-evoked ACh release.*

SNCA-OVX mice present early deficits (3-4 months of age) in DA release, which precede DA neuron loss in the SNc (Janezic et al., 2013). Despite this reduction in DA release levels, we reported a stronger D2R-mediated inhibition of ACh release in the early parkinsonian model (**Section 5.3.3**). This effect could be due to a compensatory mechanism resulting in increased expression, binding affinity, or changes in the downstream signalling cascade of D2Rs on ChIs. An increase in D2R regulation of ACh release at early stages of PD progression might therefore compensate for the deficits in DA release, in line with the idea of an ACh-DA balance that is progressively lost in PD (Barbeau, 1962). Consistently, studies in PD patients have reported upregulation of D2Rs in at the early stages of the disease (Kaasinen et al., 2021). Future experiments could monitor ACh release in aged *SNCA*-OVX mice (12 months and 18 months) to assess whether these compensatory mechanisms are lost at later stages of the disease, when SNc DA neuron loss and a motor phenotype have been reported (Janezic et al., 2013). Furthermore, future work could also investigate the role of DA release deficits on ACh release mediated by D1 and D5 receptors, which have been implicated in pathological changes in ChI firing patterns in a toxin model of PD (Paz et al., 2021).

In early parkinsonian *SNCA*-OVX mice, GABA tonic inhibition of DA release is increased and GABA co-release from DA axons is attenuated (Roberts et al., 2020). However, we found no alterations in alleged GABA tonic inhibition of ACh release in this same model (**Chapter 5**, **Section 5.3.4**). Dysregulation of tonic GABAergic modulation of ACh release might occur later in the disease progression. Future experiments in aged *SNCA*-OVX mice could therefore help to assess whether GABAergic tonic regulation of ACh release is dysregulated upon disease progression. The effect of higher GABA tonic inhibition in *SNCA*-OVX mice could also potentially be seen using a different stimulation paradigm. Indeed, pilot observations measuring ACh release with $GRAB_{ACh}$ in *SNCA*-OVX and *Snca -/-* upon stimulation with "tonic-like" frequency trains (2-10 Hz) suggest a stronger effect of GABA receptor blockade on ACh release in *SNCA*-OVX mice. Future work could extend on these findings and evaluate the contribution of changes in DA release acting at D2Rs on ChIs.

Furthermore, in early parkinsonian *SNCA*-OVX mice, GABA co-released from DA axons was attenuated (Roberts et al., 2020). Further work to investigate the role of GABA co-release from DA axons in regulating ACh release is needed, first in healthy controls (**Section 6.2.2**), then in the disease model.

In early parkinsonian *SNCA*-OVX mice, we found that AChE more efficiently limited tonic levels of ACh release and that evoked ACh release was smaller (**Chapter 5**, **Section 5.3.1** and **5.3.2**). These findings appear to be in contrast with the long-standing hypothesis of PD as a hypercholinergic disease (Barbeau, 1962). However, this view is not taking into account the progressive nature of the disease. Indeed, at early stages of the disease, adaptations in cholinergic signalling might lead to higher AChE expression or to an increase in its activity. Future experiments could for instance test activity levels of AChE in early parkinsonian and control mice using a colorimetric enzyme activity assay (Ellman et al., 1961).

Overall, these findings suggest that, at early stages of PD progression, deficits in DA transmission lead to a range of compensatory mechanisms in ACh signalling, namely enhanced D2R-mediated inhibition of ACh release and AChE regulation of tonic ACh release, which could contribute to exacerbate the deficits in DA transmission. As previously mentioned, future work in aged *SNCA*-OVX mice would be fundamental to better understand the molecular basis of disease progression towards a potential hypercholinergic phenotype. To avoid performing surgeries in old parkinsonian mice for expression of $GRAB_{ACh}$ sensors, the 6-OHDA toxin model could be used to model late stages of disease progression. This model lacks formation of Lewy bodies and the progressive nature of the α-synuclein overexpressing one, nonetheless it provides rapid degeneration of nigrostriatal neurons recapitulating later stages of PD progression. Alternatively, intrastriatal injection of α-synuclein pre-formed fibrils (PFF) has been reported to promote Lewy bodies formation and nigrostriatal degeneration in rodents (Paumier et al., 2015; Visanji et al., 2016). Injection of α-synuclein fibrils could be followed by injection of $GRAB_{ACh}$ sensors at early stages (~3 months) and later stages (~6 months) of disease progression and neuronal degeneration to evaluate alterations in striatal cholinergic signalling.

The considerations on $GRAB_{ACh}$ readout discussed in **Section 6.1** are particularly relevant when comparing between different genotypes. One approach we adopted to allow for direct comparison was to calibrate the signal measured with $GRAB_{ACh}$, for which we reported no inter-genotype differences. However, differential sensor localisation or transfection efficacy might underlie a bias in ACh sampling. Future work could use a *SNCA*-OVX;ChAT-Cre line, which presents selective expression of Cre recombinase in ChIs, together with a Cre-dependent $GRAB_{ACh}$, to achieve selective expression of the sensor in ChIs.

6.5 Conclusion

Overall, the data presented in this thesis outlined major properties of striatal ACh transmission, supporting a role for AChE, GABA and DA in modulating striatal ACh release. Furthermore, these dynamic changes in ACh release are not reflected by changes in ACh-driven DA release due to unresolved mechanisms operating downstream of nAChRs on DA axons. Finally, the findings included in this thesis provided evidence for maladaptive alterations in ACh signalling in a model of early PD.

REFERENCES

Abbondanza A, Bas IR, Modrak M, Capek M, Minich J, Tyshkevich A, Naser S, Rangotis R, Houdek P, Sumova A, Dumas S, Bernard V, Janickova H (2022) Nicotinic acetylcholine receptors expressed by striatal interneurons inhibit striatal activity and control striatal-dependent behaviors. J Neurosci:JN-RM-1627-21.

Abeliovich A, Schmitz Y, Farinas I, Choi-Lundberg D, Ho WH, Castillo PE, Shinsky N, Verdugo JMG, Armanini M, Ryan A, al. et (2000) Mice lacking a-synuclein display functional deficits in the nigrostriatal dopamine system. Neuron:239–252.

Abudukeyoumu N, Hernandez-Flores T, Garcia-Munoz M, Arbuthnott GW (2019) Cholinergic modulation of striatal microcircuits. Eur J Neurosci 49:604–622.

Ade KK, Janssen MJ, Ortinski PI, Vicini S (2008) Differential Tonic GABA Conductances in Striatal Medium Spiny Neurons. J Neurosci 28:1185–1197.

Albin RL, Young AB, Penney JB (1989) The functional anatomy of basal ganglia disorders. Trends Neurosci 12:366–375.

Alcantara AA, Chen V, Herring BE, Mendenhall JM, Berlanga ML (2003) Localization of dopamine D2 receptors on cholinergic interneurons of the dorsal striatum and nucleus accumbens of the rat. Brain Res 986:22–29.

Alcantara AA, Mrzljak L, Jakab RL, Levey AI, Hersch SM, Goldman-Rakic PS (2001) Muscarinic m1 and m2 receptor proteins in local circuit and projection neurons of the primate striatum: Anatomical evidence for cholinergic modulation of glutamatergic prefronto-striatal pathways. J Comp Neurol 434:445–460.

Anwar S, Peters O, Millership S, Ninkina N, Doig N, Connor-Robson N, Threlfell S, Kooner G, Deacon RM, Bannerman DM, Bolam JP, Chandra SS, Cragg SJ, Wade-Martins R, Buchman VL (2011) Functional Alterations to the Nigrostriatal System in Mice Lacking All Three Members of the Synuclein Family. J Neurosci 31:7264–7274.

Aosaki T, Graybiel AM, Kimura M (1994a) Effect of the Nigrostriatal Dopamine System on Acquired Neural Responses in the Striatum of Behaving Monkeys. Science 265:412–415.

Aosaki T, Kiuchi K, Kawaguchi Y (1998) Dopamine D1-Like Receptor Activation Excites Rat Striatal Large Aspiny Neurons In Vitro. J Neurosci 18:5180–5190.

Aosaki T, Tsubokawa H, Ishida A, Watanabe K, Graybiel A, Kimura M (1994b) Responses of tonically active neurons in the primate's striatum undergo

systematic changes during behavioral sensorimotor conditioning. J Neurosci 14:3969–3984.

Apicella P (2002) Tonically active neurons in the primate striatum and their role in the processing of information about motivationally relevant events. Eur J Neurosci 16:2017–2026.

Apicella P (2017) The role of the intrinsic cholinergic system of the striatum: What have we learned from TAN recordings in behaving animals? Neuroscience 360:81–94.

Apicella P, Deffains M, Ravel S, Legallet E (2009) Tonically active neurons in the striatum differentiate between delivery and omission of expected reward in a probabilistic task context. Eur J Neurosci 30:515–526.

Apicella P, Legallet E, Trouche E (1997) Responses of tonically discharging neurons in the monkey striatum to primary rewards delivered during different behavioral states. Exp Brain Res 116:456–466.

Apicella P, Ravel S, Deffains M, Legallet E (2011) The Role of Striatal Tonically Active Neurons in Reward Prediction Error Signaling during Instrumental Task Performance. J Neurosci 31:1507–1515.

Aschauer DF, Kreuz S, Rumpel S (2013) Analysis of Transduction Efficiency, Tropism and Axonal Transport of AAV Serotypes 1, 2, 5, 6, 8 and 9 in the Mouse Brain. Plos One 8:e76310.

Asri R, O'Neill B, Patel JC, Siletti KA, Rice ME (2016) Detection of evoked acetylcholine release in mouse brain slices. Analyst 141:6416–6421.

Assous M (2021) Striatal cholinergic transmission. Focus on nicotinic receptors' influence in striatal circuits. Eur J Neurosci 53:2421–2442.

Assous M, Kaminer J, Shah F, Garg A, Koós T, Tepper JM (2017) Differential processing of thalamic information via distinct striatal interneuron circuits. Nat Commun 8:15860.

Assous M, Tepper JM (2019) Excitatory extrinsic afferents to striatal interneurons and interactions with striatal microcircuitry. Eur J Neurosci 49:593–603.

Atallah HE, McCool AD, Howe MW, Graybiel AM (2014) Neurons in the Ventral Striatum Exhibit Cell-Type-Specific Representations of Outcome during Learning. Neuron 82:1145–1156.

Avshalumov MV, Chen BT, Marshall SP, Peña DM, Rice ME (2003) Glutamate-Dependent Inhibition of Dopamine Release in Striatum Is Mediated by a New Diffusible Messenger, H 2 O 2. J Neurosci 23:2744–2750.

Azam L, Winzer-Serhan U, Leslie FM (2003) Co-expression of α7 and β2 nicotinic acetylcholine receptor subunit mRNAs within rat brain cholinergic neurons. Neuroscience 119:965–977.

Azam L, Winzer-Serhan UH, Chen Y, Leslie FM (2002) Expression of neuronal nicotinic acetylcholine receptor subunit mRNAs within midbrain dopamine neurons. J Comp Neurol 444:260–274.

Baba M, Nakajo S, Tu PH, Tomita T, Nakaya K, Lee VM, Trojanowski JQ, Iwatsubo T (1998) Aggregation of alpha-synuclein in Lewy bodies of sporadic Parkinson's disease and dementia with Lewy bodies. Am J Pathology 152:879–884.

Bach J-P, Ziegler U, Deuschl G, Dodel R, Doblhammer-Reiter G (2011) Projected numbers of people with movement disorders in the years 2030 and 2050. Mov Disord Official J Mov Disord Soc 26:2286–2290.

Bäckman CM, Malik N, Zhang Y, Shan L, Grinberg A, Hoffer BJ, Westphal H, Tomac AC (2006) Characterization of a mouse strain expressing Cre recombinase from the 3′ untranslated region of the dopamine transporter locus. Genesis 44:383–390.

Baird GS, Zacharias DA, Tsien RY (1999) Circular permutation and receptor insertion within green fluorescent proteins. Proc National Acad Sci 96:11241–11246.

Baker KL, Bolger FB, Lowry JP (2014) A microelectrochemical biosensor for real-time in vivo monitoring of brain extracellular choline. Analyst 140:3738–3745.

Baker KL, Bolger FB, Lowry JP (2017) Development of a microelectrochemical biosensor for the real-time detection of choline. Sensors Actuators B Chem 243:412–420.

Balkenius A, Johansson AJ, Balkenius C (2015) Comparing Analysis Methods in Functional Calcium Imaging of the Insect Brain. Plos One 10:e0129614.

Barbeau A (1962) The pathogenesis of Parkinson's Disease: a new hypothesis. Can Med Assoc J:802–807.

Bassareo V, Chiara GD (1999) Modulation of feeding-induced activation of mesolimbic dopamine transmission by appetitive stimuli and its relation to motivational state. Eur J Neurosci 11:4389–4397.

Beaulieu J-M, Gainetdinov RR (2011) The Physiology, Signaling, and Pharmacology of Dopamine Receptors. Pharmacol Rev 63:182–217.

Beckstead MJ, Grandy DK, Wickman K, Williams JT (2004) Vesicular Dopamine Release Elicits an Inhibitory Postsynaptic Current in Midbrain Dopamine Neurons. Neuron 42:939–946.

Beery AK (2018) Inclusion of females does not increase variability in rodent research studies. Curr Opin Behav Sci 23:143–149.

Bekris LM, Mata IF, Zabetian CP (2010) The Genetics of Parkinson Disease. J Geriatr Psych Neur 23:228–242.

Bell MI, Richardson PJ, Lee K (2002) Functional and molecular characterization of metabotropic glutamate receptors expressed in rat striatal cholinergic interneurones. J Neurochem 81:142–149.

Benhamou L, Kehat O, Cohen D (2014) Firing Pattern Characteristics of Tonically Active Neurons in Rat Striatum: Context Dependent or Species Divergent? J Neurosci 34:2299–2304.

Bennett BD, Wilson CJ (1999a) Spontaneous Activity of Neostriatal Cholinergic Interneurons In Vitro. J Neurosci 19:5586–5596.

Bennett BD, Wilson CJ (1999b) Spontaneous activity of neostriatal cholinergic interneurons in vitro. J Neurosci.

Benoit-Marand M, Borrelli E, Gonon F (2001) Inhibition of Dopamine Release Via Presynaptic D2 Receptors: Time Course and Functional Characteristics In Vivo. J Neurosci 21:9134–9141.

Bergson C, Mrzljak L, Smiley J, Pappy M, Levenson R, Goldman-Rakic P (1995) Regional, cellular, and subcellular variations in the distribution of D1 and D5 dopamine receptors in primate brain. J Neurosci 15:7821–7836.

Bernard, Legay, Massoulie, Bloch (1995) Anatomical analysis of the neurons expressing the acetylcholinesterase gene in the rat brain, with special reference to the striatum. Neuroscience 64:995–1005.

Bernard V, Normand E, Bloch B (1992) Phenotypical characterization of the rat striatal neurons expressing muscarinic receptor genes. J Neurosci 12:3591–3600.

Bertran-Gonzalez J, Chieng BC, Laurent V, Valjent E, Balleine BW (2012) Striatal Cholinergic Interneurons Display Activity-Related Phosphorylation of Ribosomal Protein S6. Plos One 7:e53195.

Besson M-J, Graybiel AM, Nastuk MA (1988) [3H]SCH 23390 binding to D1 dopamine receptors in the basal ganglia of the cat and primate: Delineation of striosomal compartments and pallidal and nigral subdivisions. Neuroscience 26:101–119.

Bevan MD, Booth PAC, Eaton SA, Bolam JP (1998) Selective Innervation of Neostriatal Interneurons by a Subclass of Neuron in the Globus Pallidus of the Rat. J Neurosci 18:9438–9452.

Bianco CL, Ridet J-L, Schneider BL, Déglon N, Aebischer P (2002) α-Synucleinopathy and selective dopaminergic neuron loss in a rat lentiviral-based model of Parkinson's disease. Proc National Acad Sci 99:10813–10818.

Björklund A, Dunnett SB (2007) Dopamine neuron systems in the brain: an update. Trends Neurosci 30:194–202.

Blatow M, Caputi A, Burnashev N, Monyer H, Rozov A (2003) Ca2+ Buffer Saturation Underlies Paired Pulse Facilitation in Calbindin-D28k-Containing Terminals. Neuron 38:79–88.

Bolam JP, Hanley JJ, Booth PAC, Bevan MD (2000) Synaptic organisation of the basal ganglia. J Anat 196:527–542.

Bolam JP, Pissadaki EK (2012) Living on the edge with too many mouths to feed: Why dopamine neurons die. Movement Disord 27:1478–1483.

Bolam JP, Wainer BH, Smith AD (1984) Characterization of cholinergic neurons in the rat neostriatum. A combination of choline acetyltransferase immunocytochemistry, Golgi-impregnation and electron microscopy. Neuroscience.

Bonsi P, Martella G, Cuomo D, Platania P, Sciamanna G, Bernardi G, Wess J, Pisani A (2008) Loss of Muscarinic Autoreceptor Function Impairs Long-Term Depression But Not Long-Term Potentiation in the Striatum. J Neurosci 28:6258–6263.

Borden PM et al. (2020) A fast genetically encoded fluorescent sensor for faithful in vivo acetylcholine detection in mice, fish, worms and flies. Biorxiv:2020.02.07.939504.

Bracci E, Centonze D, Bernardi G, Calabresi P (2002) Dopamine Excites Fast-Spiking Interneurons in the Striatum. J Neurophysiol 87:2190–2194.

Bradfield LA, Bertran-Gonzalez J, Chieng B, Balleine BW (2013) The Thalamostriatal Pathway and Cholinergic Control of Goal-Directed Action: Interlacing New with Existing Learning in the Striatum. Neuron 79:153–166.

Brann MR, Buckley NJ, Bonner TI (1988) The striatum and cerebral cortex express different muscarinic receptor mRNAs. Febs Lett 230:90–94.

Brimblecombe KR, Cragg SJ (2015) Substance P Weights Striatal Dopamine Transmission Differently within the Striosome-Matrix Axis. J Neurosci 35:9017–9023.

Brimblecombe KR, Cragg SJ (2017) The Striosome and Matrix Compartments of the Striatum: A Path through the Labyrinth from Neurochemistry toward Function. Acs Chem Neurosci 8:235–242.

Brimblecombe KR, Gracie CJ, Platt NJ, Cragg SJ (2015) Gating of dopamine transmission by calcium and axonal N-, Q-, T- and L-type voltage-gated calcium channels differs between striatal domains. J Physiology 593:929–946.

Brimblecombe KR, Threlfell S, Dautan D, Kosillo P, Mena-Segovia J, Cragg SJ (2018) Targeted Activation of Cholinergic Interneurons Accounts for the Modulation of Dopamine by Striatal Nicotinic Receptors. Eneuro 5:ENEURO.0397-17.2018.

Brimblecombe KR, Vietti-Michelina S, Platt NJ, Kastli R, Hnieno A, Gracie CJ, Cragg SJ (2019) Calbindin-D28K Limits Dopamine Release in Ventral but Not Dorsal Striatum by Regulating Ca2+ Availability and Dopamine Transporter Function. Acs Chem Neurosci.

Britt JP, McGehee DS (2008) Presynaptic Opioid and Nicotinic Receptor Modulation of Dopamine Overflow in the Nucleus Accumbens. J Neurosci 28:1672–1681.

Brody DL, Yue DT (2000) Release-Independent Short-Term Synaptic Depression in Cultured Hippocampal Neurons. J Neurosci 20:2480–2494.

Bull DR, Sheehan MJ (1991) Presynaptic regulation of electrically evoked dopamine overflow in nucleus accumbens: a pharmacological study using fast cyclic voltammetry in vitro. Naunyn-schmiedeberg's Archives Pharmacol 343:260–265.

Burré J (2015) The Synaptic Function of α-Synuclein. J Park Dis 5:699–713.

Cabin DE, Shimazu K, Murphy D, Cole NB, Gottschalk W, McIlwain KL, Orrison B, Chen A, Ellis CE, Paylor R, Lu B, Nussbaum RL (2002) Synaptic Vesicle Depletion Correlates with Attenuated Synaptic Responses to Prolonged Repetitive Stimulation in Mice Lacking α-Synuclein. J Neurosci 22:8797–8807.

Cachope R, Mateo Y, Mathur BN, Irving J, Wang H-L, Morales M, Lovinger DM, Cheer JF (2012) Selective Activation of Cholinergic Interneurons Enhances Accumbal Phasic Dopamine Release: Setting the Tone for Reward Processing. Cell Reports 2:33–41.

Cai Y, Ford CP (2018) Dopamine Cells Differentially Regulate Striatal Cholinergic Transmission across Regions through Corelease of Dopamine and Glutamate. Cell Reports 25:3148-3157.e3.

Cai Y, Nielsen BE, Boxer EE, Aoto J, Ford CP (2021) Loss of nigral excitation of cholinergic interneurons contributes to parkinsonian motor impairments. Neuron 109:1137-1149.e5.

Caillé I, Dumartin B, Bloch B (1996) Ultrastructural localization of D1 dopamine receptor immunoreactivity in rat striatonigral neurons and its relation with dopaminergic innervation. Brain Res 730:17–31.

Calabresi P, Centonze D, Gubellini P, Pisani A, Bernardi G (1998a) Blockade of M2-like muscarinic receptors enhances long-term potentiation at corticostriatal synapses. Eur J Neurosci 10:3020–3023.

Calabresi P, Centonze D, Gubellini P, Pisani A, Bernardi G (2000) Acetylcholine-mediated modulation of stratal function. Trends Neurosci.

Calabresi P, Centonze D, Pisani A, Sancesario G, North RA, Bernardi G (1998b) Muscarinic IPSPs in rat striatal cholinergic interneurones. J Physiology 510:421–427.

Campos F, Alfonso M, Durán R (2010) In vivo modulation of α7 nicotinic receptors on striatal glutamate release induced by anatoxin-A. Neurochem Int 56:850–855.

Cao F, Luo F, Chen L, Chen H, Wei G, Cai J, Xu H, Tong E (2012) Experimental study on dynamic regulation of acetylcholine in striatum of rat parkinson disease model and behavior observation. J Huazhong Univ Sci Technology Medical Sci 32:732–736.

Carboni E, Imperato A, Perezzani L, Chiara GD (1989) Amphetamine, cocaine, phencyclidine and nomifensine increase extracellular dopamine concentrations preferentially in the nucleus accumbens of freely moving rats. Neuroscience 28:653–661.

Cardinal RN, Parkinson JA, Hall J, Everitt BJ (2002) Emotion and motivation: the role of the amygdala, ventral striatum, and prefrontal cortex. Neurosci Biobehav Rev 26:321–352.

Centonze D, Bracci E, Pisani A, Gubellini P, Bernardi G, Calabresi P (2002) Activation of dopamine D1-like receptors excites LTS interneurons of the striatum. Eur J Neurosci 15:2049–2052.

Centonze D, Grande C, Usiello A, Gubellini P, Erbs E, Martín AB, Pisani A, Tognazzi N, Bernardi G, Moratalla R, Borrelli E, Calabresi P (2003) Receptor Subtypes Involved in the Presynaptic and Postsynaptic Actions of Dopamine on Striatal Interneurons. J Neurosci 23:6245–6254.

Champtiaux N, Gotti C, Cordero-Erausquin M, David DJ, Przybylski C, Léna C, Clementi F, Moretti M, Rossi FM, Novère NL, McIntosh JM, Gardier AM, Changeux J-P (2003) Subunit Composition of Functional Nicotinic Receptors in Dopaminergic Neurons Investigated with Knock-Out Mice. J Neurosci 23:7820–7829.

Chang HT, Kita H (1992) Interneurons in the rat striatum: relationships between parvalbumin neurons and cholinergic neurons. Brain Res 574:307–311.

Chartier-Harlin M-C, Kachergus J, Roumier C, Mouroux V, Douay X, Lincoln S, Levecque C, Larvor L, Andrieux J, Hulihan M, Waucquier N, Defebvre L, Amouyel P,

Farrer M, Destée A (2004) Alpha-synuclein locus duplication as a cause of familial Parkison's disease. Lancet 364:1167–1169.

Chen E, Lallai V, Sherafat Y, Grimes NP, Pushkin AN, Fowler J, Fowler CD (2018) Altered Baseline and Nicotine-Mediated Behavioral and Cholinergic Profiles in ChAT-Cre Mouse Lines. J Neurosci 38:2177–2188.

Chen T-W, Lin B-J, Brunner E, Schild D (2006) In Situ Background Estimation in Quantitative Fluorescence Imaging. Biophys J 90:2534–2547.

Chen T-W, Wardill TJ, Sun Y, Pulver SR, Renninger SL, Baohan A, Schreiter ER, Kerr RA, Orger MB, Jayaraman V, Looger LL, Svoboda K, Kim DS (2013) Ultra-sensitive fluorescent proteins for imaging neuronal activity. Nature 499:295–300.

Chia SJ, Tan E-K, Chao Y-X (2020) Historical Perspective: Models of Parkinson's Disease. Int J Mol Sci 21:2464.

Choi SJ, Ma TC, Ding Y, Cheung T, Joshi N, Sulzer D, Mosharov EV, Kang UJ (2020) Alterations in the intrinsic properties of striatal cholinergic interneurons after dopamine lesion and chronic L-DOPA. Elife 9:e56920.

Chuhma N, Mingote S, Moore H, Rayport S (2014) Dopamine Neurons Control Striatal Cholinergic Neurons via Regionally Heterogeneous Dopamine and Glutamate Signaling. Neuron 81:901–912.

Chuhma N, Mingote S, Yetnikoff L, Kalmbach A, Ma T, Ztaou S, Sienna A-C, Tepler S, Poulin J-F, Ansorge M, Awatramani R, Kang UJ, Rayport S (2018) Dopamine neuron glutamate cotransmission evokes a delayed excitation in lateral dorsal striatal cholinergic interneurons. Elife 7:e39786.

Chuhma N, Tanaka KF, Hen R, Rayport S (2011) Functional Connectome of the Striatal Medium Spiny Neuron. J Neurosci 31:1183–1192.

Chung KA, Lobb BM, Nutt JG, Horak FB (2010) Effects of a central cholinesterase inhibitor on reducing falls in Parkinson disease(Podcast)(e–Pub ahead of print)(LOE Classification). Neurology 75:1263–1269.

Clayton JA (2016) Studying both sexes: a guiding principle for biomedicine. Faseb J 30:519–524.

Cohen JY, Haesler S, Vong L, Lowell BB, Uchida N (2012) Neuron-type specific signals for reward and punishment in the ventral tegmental area. Nature 482:85–88.

Collins AL, Aitken TJ, Greenfield VY, Ostlund SB, Wassum KM (2016) Nucleus Accumbens Acetylcholine Receptors Modulate Dopamine and Motivation. Neuropsychopharmacol 41:2830–2838.

Condon MD, Platt NJ, Zhang Y-F, Roberts BM, Clements MA, Vietti-Michelina S, Tseu M-Y, Brimblecombe KR, Threlfell S, Mann EO, Cragg SJ (2019) Plasticity in striatal dopamine release is governed by release-independent depression and the dopamine transporter. Nat Commun 10:4263.

Consolo S, Caltavuturo C, Colli E, Recchia M, Chiara GD (1999) Different sensitivity of in vivo acetylcholine transmission to D1 receptor stimulation in shell and core of nucleus accumbens. Neuroscience 89:1209–1217.

Contant C, Umbriaco D, Garcia S, Watkins KC, Descarries L (1996) Ultrastructural characterization of the acetylcholine innervation in adult rat neostriatum. Neuroscience 71:937–947.

Cragg SJ (2003) Variable Dopamine Release Probability and Short-TermPlasticity between Functional Domains of the Primate Striatum. The Journal of Neuroscience.

Cragg SJ (2006) Meaningful silences: how dopamine listens to the ACh pause. Trends Neurosci 29:125–131.

Cragg SJ, Greenfield SA (1997) Differential Autoreceptor Control of Somatodendritic and Axon Terminal Dopamine Release in Substantia Nigra, Ventral Tegmental Area, and Striatum. J Neurosci 17:5738–5746.

Crittenden JR, Graybiel AM (2011) Basal Ganglia Disorders Associated with Imbalances in the Striatal Striosome and Matrix Compartments. Front Neuroanat 5:59.

Crittenden JR, Lacey CJ, Lee T, Bowden HA, Graybiel AM (2014) Severe drug-induced repetitive behaviors and striatal overexpression of VAChT in ChAT-ChR2-EYFP BAC transgenic mice. Front Neural Circuit 8:57.

Crivici A, Ikura M (1995) MOLECULAR AND STRUCTURAL BASIS OF TARGET RECOGNITION BY CALMODULIN. Annu Rev Biophys Biomol Struct:85–166.

Dajas-Bailador F, Wonnacott S (2004) Nicotinic acetylcholine receptors and the regulation of neuronal signalling. Trends Pharmacol Sci 25:317–324.

Dajas-Bailador FA, Mogg AJ, Wonnacott S (2002) Intracellular Ca2+ signals evoked by stimulation of nicotinic acetylcholine receptors in SH-SY5Y cells: contribution of voltage-operated Ca2+ channels and Ca2+ stores. J Neurochem.

Dani JA, Bertrand D (2007) Nicotinic Acetylcholine Receptors and Nicotinic Cholinergic Mechanisms of the Central Nervous System. Annu Rev Pharmacol 47:699–729.

D'Ardenne K, McClure SM, Nystrom LE, Cohen JD (2008) BOLD Responses Reflecting Dopaminergic Signals in the Human Ventral Tegmental Area. Science 319:1264–1267.

Dautan D, Huerta-Ocampo I, Gut NK, Valencia M, Kondabolu K, Kim Y, Gerdjikov TV, Mena-Segovia J (2020) Cholinergic midbrain afferents modulate striatal circuits and shape encoding of action strategies. Nat Commun 11:1739.

Dautan D, Huerta-Ocampo I, Witten IB, Deisseroth K, Bolam JP, Gerdjikov T, Mena-Segovia J (2014) A Major External Source of Cholinergic Innervation of the Striatum and Nucleus Accumbens Originates in the Brainstem. J Neurosci 34:4509–4518.

Dawson VL, Dawson TM, Filloux FM, Wamsley JK (1988) Evidence for dopamine D-2 receptors on cholinergic interneurons in the rat caudate-putamen. Life Sci 42:1933–1939.

Day JJ, Roitman MF, Wightman RM, Carelli RM (2007) Associative learning mediates dynamic shifts in dopamine signaling in the nucleus accumbens. Nat Neurosci 10:1020–1028.

Debanne D, Campanac E, Bialowas A, Carlier E, Alcaraz G (2011) Axon Physiology. Physiol Rev 91:555–602.

DeBoer P, Abercrombie ED, Heeringa M, Westerink BHC (1993) differential effect of systemic administration of bromocriptine andl-DOPA on the release of acetylcholine from striatum of intact and 6-OHDA-treated rats. Brain Res 608:198–203.

DeBoer P, Westerink BHC (1994) GABAergic modulation of striatal cholinergic interneurons: an in vivo microdialysis study. J Neurochem 62:70–75.

DeLong MR (1990) Primate models of movement disorders of basal ganglia origin. Trends Neurosci 13:281–285.

Deng P, Zhang Y, Xu ZC (2007a) Involvement of Ih in Dopamine Modulation of Tonic Firing in Striatal Cholinergic Interneurons. J Neurosci 27:3148–3156.

Deng YP, Xie JP, Wang HB, Lei WL, Chen Q, Reiner A (2007b) Differential localization of the GluR1 and GluR2 subunits of the AMPA-type glutamate receptor among striatal neuron types in rats. J Chem Neuroanat 33:167–192.

Descarries L, Gisiger V, Steriade M (1997) Diffuse transmission by acetylcholine in the CNS. Prog Neurobiol 53:603–625.

Descarries L, Watkins KC, Garcia S, Bosler O, Doucet G (1996) Dual character, asynaptic and synaptic, of the dopamine innervation in adult rat neostriatum: A quantitative autoradiographic and immunocytochemical analysis. J Comp Neurol 375:167–186.

Dickinson JA, Hanrott KE, Mok MHS, Kew JNC, Wonnacott S (2007) Differential coupling of α7 and non-α7 nicotinic acetylcholine receptors to calcium-induced calcium release and voltage-operated calcium channels in PC12 cells. J Neurochem 100:1089–1096.

DiFiglia M, Aronin N (1982) Ultrastructural features of immunoreactive somatostatin neurons in the rat caudate nucleus. J Neurosci 2:1267–1274.

Dimova R, Vuillet J, Nieoullon A, Goff LK-L (1993) Ultrastructural features of the choline acetyltransferase-containing neurons and relationships with nigral dopaminergic and cortical afferent pathways in the rat striatum. Neuroscience 53:1059–1071.

Ding J, Guzman JN, Tkatch T, Chen S, Goldberg JA, Ebert PJ, Levitt P, Wilson CJ, Hamm HE, Surmeier DJ (2006) RGS4-dependent attenuation of M4 autoreceptor function in striatal cholinergic interneurons following dopamine depletion. Nat Neurosci 9:nn1700.

Dobbertin A, Hrabovska A, Dembele K, Camp S, Taylor P, Krejci E, Bernard V (2009) Targeting of Acetylcholinesterase in Neurons In Vivo: A Dual Processing Function for the Proline-Rich Membrane Anchor Subunit and the Attachment Domain on the Catalytic Subunit. J Neurosci 29:4519–4530.

Dodson PD, Dreyer JK, Jennings KA, Syed ECJ, Wade-Martins R, Cragg SJ, Bolam JP, Magill PJ (2016) Representation of spontaneous movement by dopaminergic neurons is cell-type selective and disrupted in parkinsonism. Proc National Acad Sci 113:E2180–E2188.

Doig NM, Moss J, Bolam JP (2010) Cortical and Thalamic Innervation of Direct and Indirect Pathway Medium-Sized Spiny Neurons in Mouse Striatum. J Neurosci 30:14610–14618.

Dong B, Niu Z, Zhang J, Zhou Y, Meng F, Dong A (2021) Complementary Transcriptomic and Proteomic Analysis in the Substantia Nigra of Parkinson's Disease. Dis Markers 2021:2148820.

Dorsey ER et al. (2018) Global, regional, and national burden of Parkinson's disease, 1990–2016: a systematic analysis for the Global Burden of Disease Study 2016. Lancet Neurology 17:939–953.

Dorst MC, Tokarska A, Zhou M, Lee K, Stagkourakis S, Broberger C, Masmanidis S, Silberberg G (2020) Polysynaptic inhibition between striatal cholinergic

interneurons shapes their network activity patterns in a dopamine-dependent manner. Nat Commun 11:5113.

Dunant Y, Gisiger V (2017) Ultrafast and Slow Cholinergic Transmission. Different Involvement of Acetylcholinesterase Molecular Forms. Molecules 22:1300.

Eglen RM (2006) Muscarinic receptor subtypes in neuronal and non-neuronal cholinergic function. Autonomic Autacoid Pharmacol 26:219–233.

Elghaba R, Vautrelle N, Bracci E (2016) Mutual Control of Cholinergic and Low-Threshold Spike Interneurons in the Striatum. Front Cell Neurosci 10:111.

Ellman GL, Courtney KD, Andres V, Featherstone RM (1961) A new and rapid colorimetric determination of acetylcholinesterase activity. Biochem Pharmacol 7:88–95.

English DF, Ibanez-Sandoval O, Stark E, Tecuapetla F, Buzsáki G, Deisseroth K, Tepper JM, Koos T (2012) GABAergic circuits mediate the reinforcement-related signals of striatal cholinergic interneurons. Nat Neurosci 15:123–130.

Exley R, Clements MA, Hartung H, McIntosh JM, Cragg SJ (2008) α6-Containing Nicotinic Acetylcholine Receptors Dominate the Nicotine Control of Dopamine Neurotransmission in Nucleus Accumbens. Neuropsychopharmacol 33:2158.

Exley R, Clements MA, Hartung H, McIntosh JM, Franklin M, Bermudez I, Cragg SJ (2013) Striatal dopamine transmission is reduced after chronic nicotine with a decrease in α6-nicotinic receptor control in nucleus accumbens. Eur J Neurosci 38:3036–3043.

Exley R, Cragg SJ (2008) Presynaptic nicotinic receptors: a dynamic and diverse cholinergic filter of striatal dopamine neurotransmission. Brit J Pharmacol 153:S283–S297.

Exley R, Maubourguet N, David V, Eddine R, Evrard A, Pons S, Marti F, Threlfell S, Cazala P, McIntosh JM, Changeux J-P, Maskos U, Cragg SJ, Faure P (2011) Distinct contributions of nicotinic acetylcholine receptor subunit α4 and subunit α6 to the reinforcing effects of nicotine. Proc National Acad Sci 108:7577–7582.

Exley R, McIntosh JM, Marks MJ, Maskos U, Cragg SJ (2012) Striatal α5 Nicotinic Receptor Subunit Regulates Dopamine Transmission in Dorsal Striatum. J Neurosci 32:2352–2356.

Farar V, Mohr F, Legrand M, d'Incamps BL, Cendelin J, Leroy J, Abitbol M, Bernard V, Baud F, Fournet V, Houze P, Klein J, Plaud B, Tuma J, Zimmermann M, Ascher P, Hrabovska A, Myslivecek J, Krejci E (2012) Near-complete adaptation of the PRiMA knockout to the lack of central acetylcholinesterase. J Neurochem 122:1065–1080.

Fedorova TD, Seidelin LB, Knudsen K, Schacht AC, Geday J, Pavese N, Brooks DJ, Borghammer P (2017) Decreased intestinal acetylcholinesterase in early Parkinson disease. Neurology 88:775–781.

Fiorillo CD, Tobler PN, Schultz W (2003) Discrete Coding of Reward Probability and Uncertainty by Dopamine Neurons. Science 299:1898–1902.

Freeze BS, Kravitz AV, Hammack N, Berke JD, Kreitzer AC (2013) Control of Basal Ganglia Output by Direct and Indirect Pathway Projection Neurons. J Neurosci 33:18531–18539.

Galarraga E, Hernández-López S, Reyes A, Miranda I, Bermudez-Rattoni F, Vilchis C, Bargas J (1999) Cholinergic Modulation of Neostriatal Output: A Functional Antagonism between Different Types of Muscarinic Receptors. J Neurosci 19:3629–3638.

Gallo EF, Greenwald J, Yeisley J, Teboul E, Martyniuk KM, Villarin JM, Li Y, Javitch JA, Balsam PD, Kellendonk C (2021) Dopamine D2 receptors modulate the cholinergic pause and inhibitory learning. Mol Psychiatr:1–13.

Gerfen C, Baimbridge K, Thibault J (1987) The neostriatal mosaic: III. Biochemical and developmental dissociation of patch-matrix mesostriatal systems. J Neurosci 7:3935–3944.

Gerfen CR (1985) The neostriatal mosaic. I. compartmental organization of projections from the striatum to the substantia nigra in the rat. J Comp Neurol 236:454–476.

Gerfen CR (1989) The Neostriatal Mosaic: Striatal Patch-Matrix Organization Is Related to Cortical Lamination. Science 246:385–388.

Gerfen CR, Baimbridge KG, Miller JJ (1985) The neostriatal mosaic: compartmental distribution of calcium-binding protein and parvalbumin in the basal ganglia of the rat and monkey. Proc National Acad Sci 82:8780–8784.

Gerfen CR, Engber TM, Mahan LC, Susel Z, Chase TN, Jr. FJM, Sibley DR (1990) D1 and D2 Dopamine Receptor-regulated Gene Expression of Striatonigral and Striatopallidal Neurons. Science 250:1429–1432.

Giniatullin R, Nistri A, Yakel JL (2005) Desensitization of nicotinic ACh receptors: shaping cholinergic signaling. Trends Neurosci 28:371–378.

Giros B, Sokoloff P, Martres M-P, Riou J-F, Emorine LJ, Schwartz J-C (1989) Alternative splicing directs the expression of two D2 dopamine receptor isoforms. Nature 342:923–926.

Gittis AH, Nelson AB, Thwin MT, Palop JJ, Kreitzer AC (2010) Distinct Roles of GABAergic Interneurons in the Regulation of Striatal Output Pathways. J Neurosci 30:2223–2234.

Gjerløff T, Fedorova T, Knudsen K, Munk OL, Nahimi A, Jacobsen S, Danielsen EH, Terkelsen AJ, Hansen J, Pavese N, Brooks DJ, Borghammer P (2015) Imaging acetylcholinesterase density in peripheral organs in Parkinson's disease with 11C-donepezil PET. Brain 138:653–663.

Goldberg JA, Ding JB, Surmeier DJ (2011) Muscarinic Receptors. Handb Exp Pharmacol:223–241.

Goldberg JA, Reynolds JNJ (2011) Spontaneous firing and evoked pauses in the tonically active cholinergic interneurons of the striatum. Neuroscience 198:27–43.

Gonzales KK, Pare J, Wichmann T, Smith Y (2013) GABAergic inputs from direct and indirect striatal projection neurons onto cholinergic interneurons in the primate putamen. J Comp Neurol 521:2502–2522.

Gonzales KK, Smith Y (2015) Cholinergic interneurons in the dorsal and ventral striatum: anatomical and functional considerations in normal and diseased conditions. Ann Ny Acad Sci 1349:1–45.

Grace A, Bunney B (1984a) The control of firing pattern in nigral dopamine neurons: single spike firing. J Neurosci 4:2866–2876.

Grace AA, Bunney BS (1984b) The control of firing pattern in nigral dopamine neurons: burst firing. The Journal of Neuroscience.

Grady SR, Salminen O, Laverty DC, Whiteaker P, McIntosh JM, Collins AC, Marks MJ (2007) The subtypes of nicotinic acetylcholine receptors on dopaminergic terminals of mouse striatum. Biochem Pharmacol 74:1235–1246.

Gray R, Rajan AS, Radcliffe KA, Yakehiro M, Dani JA (1996) Hippocampal synaptic transmission enhanced by low concentrations of nicotine. Nature 383:383713a0.

Graybiel AM, Ragsdale CW (1978) Histochemically distinct compartments in the striatum of human, monkeys, and cat demonstrated by acetylthiocholinesterase staining. Proc National Acad Sci 75:5723–5726.

Greene JG, Dingledine R, Greenamyre JT (2005) Gene expression profiling of rat midbrain dopamine neurons: implications for selective vulnerability in parkinsonism. Neurobiol Dis 18:19–31.

Grienberger C, Konnerth A (2012) Imaging Calcium in Neurons. Neuron 73:862–885.

Group G 2015 NDC et al. (2017) Global, regional, and national burden of neurological disorders during 1990–2015: a systematic analysis for the Global Burden of Disease Study 2015. Lancet Neurology 16:877–897.

Guo Q, Wang D, He X, Feng Q, Lin R, Xu F, Fu L, Luo M (2015) Whole-Brain Mapping of Inputs to Projection Neurons and Cholinergic Interneurons in the Dorsal Striatum. Plos One 10:e0123381.

Haery L, Deverman BE, Matho KS, Cetin A, Woodard K, Cepko C, Guerin KI, Rego MA, Ersing I, Bachle SM, Kamens J, Fan M (2019) Adeno-Associated Virus Technologies and Methods for Targeted Neuronal Manipulation. Front Neuroanat 13:93.

Hartung H, Threlfell S, Cragg SJ (2011) Nitric Oxide Donors Enhance the Frequency Dependence of Dopamine Release in Nucleus Accumbens. Neuropsychopharmacol 36:1811–1822.

Hattori T, Singh VK, McGeer EG, McGeer PL (1976) Immunohistochemical localization of choline acetyltransferase containing neostriatal neurons and their relationship with dopaminergic synapses. Brain Res 102:164–173.

He Y, Zorumski CF, Mennerick S (2002) Contribution of Presynaptic Na+ Channel Inactivation to Paired-Pulse Synaptic Depression in Cultured Hippocampal Neurons. J Neurophysiol 87:925–936.

Henselmans JML, Stoof JC (1991) Regional differences in the regulation of acetylcholine release upon D2 dopamine and N-methyl-d-aspartate receptor activation in rat nucleus accumbens and neostriatum. Brain Res 566:1–7.

Hermans A, Keithley RB, Kita JM, Sombers LA, Wightman RM (2008) Dopamine Detection with Fast-Scan Cyclic Voltammetry Used with Analog Background Subtraction. Anal Chem 80:4040–4048.

Hersch S, Gutekunst C, Rees H, Heilman C, Levey A (1994a) Distribution of m1-m4 muscarinic receptor proteins in the rat striatum: light and electron microscopic immunocytochemistry using subtype- specific antibodies. J Neurosci 14:3351–3363.

Hersch S, Gutekunst C, Rees H, Heilman C, Levey A (1994b) Distribution of m1-m4 muscarinic receptor proteins in the rat striatum: light and electron microscopic immunocytochemistry using subtype- specific antibodies. J Neurosci 14:3351–3363.

Hersch SM, Yi H, Heilman CJ, Edwards RH, Levey AI (1997) Subcellular localization and molecular topology of the dopamine transporter in the striatum and substantia nigra. J Comp Neurol 388:211–227.

Higley MJ, Gittis AH, Oldenburg IA, Balthasar N, Seal RP, Edwards RH, Lowell BB, Kreitzer AC, Sabatini BL (2011) Cholinergic Interneurons Mediate Fast VGluT3-Dependent Glutamatergic Transmission in the Striatum. Plos One 6:e19155.

Hikima T, Lee CR, Witkovsky P, Chesler J, Ichtchenko K, Rice ME (2021) Activity-dependent somatodendritic dopamine release in the substantia nigra autoinhibits the releasing neuron. Cell Reports 35:108951–108951.

Hnasko TS, Chuhma N, Zhang H, Goh GY, Sulzer D, Palmiter RD, Rayport S, Edwards RH (2010) Vesicular Glutamate Transport Promotes Dopamine Storage and Glutamate Corelease In Vivo. Neuron 65:643–656.

Holly EN, Davatolhagh MF, Choi K, Alabi OO, Cifuentes LV, Fuccillo MV (2019) Striatal Low-Threshold Spiking Interneurons Regulate Goal-Directed Learning. Neuron 103:92-101.e6.

Howe M, Ridouh I, Mascaro ALA, Larios A, Azcorra M, Dombeck DA (2019) Coordination of rapid cholinergic and dopaminergic signaling in striatum during spontaneous movement. Elife 8:e44903.

Howe MW, Dombeck DA (2016) Rapid signalling in distinct dopaminergic axons during locomotion and reward. Nature 535:505–510.

Howe WM, Young DA, Bekheet G, Kozak R (2016) Nicotinic receptor subtypes differentially modulate glutamate release in the dorsal medial striatum. Neurochem Int 100:30–34.

Hu X, Wachtel S, Galloway M, White F (1990) Lesions of the nigrostriatal dopamine projection increase the inhibitory effects of D1 and D2 dopamine agonists on caudate-putamen neurons and relieve D2 receptors from the necessity of D1 receptor stimulation. J Neurosci 10:2318–2329.

Hyland BI, Reynolds JNJ, Hay J, Perk CG, Miller R (2002) Firing modes of midbrain dopamine cells in the freely moving rat. Neuroscience 114:475–492.

Iacopino A, Christakos S, German D, Sonsalla PK, Altar CA (1992) Calbindin-D28K-containing neurons in animal models of neurodegeneration: possible protection from excitotoxicity. Mol Brain Res 13:251–261.

Ibanez-Sandoval O, Tecuapetla F, Unal B, Shah F, Koos T, Tepper JM (2010) Electrophysiological and Morphological Characteristics and Synaptic Connectivity of Tyrosine Hydroxylase-Expressing Neurons in Adult Mouse Striatum. J Neurosci 30:6999–7016.

Ibáñez-Sandoval O, Xenias HS, Tepper JM, Koós T (2015) Dopaminergic and cholinergic modulation of striatal tyrosine hydroxylase interneurons. Neuropharmacology 95:468–476.

Ikarashi Y, Takahashi A, Ishimaru H, Arai T, Maruyama Y (1997) Regulation of Dopamine D1 and D2 Receptors on Striatal Acetylcholine Release in Rats. Brain Res Bull 43:107–115.

Ikemoto S (2007) Dopamine reward circuitry: Two projection systems from the ventral midbrain to the nucleus accumbens–olfactory tubercle complex. Brain Res Rev 56:27–78.

Imperato A, Obinu MC, Demontis MV, Gessa GL (1992) Cocaine releases limbic acetylcholine through endogenous dopamine action on D1 receptors. Eur J Pharmacol 229:265–267.

Jakubík J, Bačáková L, El-Fakahany EE, Tuček S (1997) Positive Cooperativity of Acetylcholine and Other Agonists with Allosteric Ligands on Muscarinic Acetylcholine Receptors. Mol Pharmacol 52:172–179.

Janezic S et al. (2013) Deficits in dopaminergic transmission precede neuron loss and dysfunction in a new Parkinson model. Proc National Acad Sci 110:E4016–E4025.

Jimenez-Castellanos J, Graybiel AM (1987) Subdivisions of the dopamine-containing A8-A9-A10 complex identified by their differential mesostriatal innervation of striosomes and extrastriosomal matrix. Neuroscience 23:223–242.

Jing M et al. (2018) A genetically encoded fluorescent acetylcholine indicator for in vitro and in vivo studies. Nat Biotechnol 36:726.

Jing M et al. (2020) An optimized acetylcholine sensor for monitoring in vivo cholinergic activity. Nat Methods 17:1139–1146.

Jones IW, Bolam JPaul, Wonnacott S (2001) Presynaptic localisation of the nicotinic acetylcholine receptor β2 subunit immunoreactivity in rat nigrostriatal dopaminergic neurones. J Comp Neurol 439:235–247.

Joshua M, Adler A, Mitelman R, Vaadia E, Bergman H (2008) Midbrain Dopaminergic Neurons and Striatal Cholinergic Interneurons Encode the Difference between Reward and Aversive Events at Different Epochs of Probabilistic Classical Conditioning Trials. J Neurosci 28:11673–11684.

Kaasinen V, Vahlberg T, Stoessl AJ, Strafella AP, Antonini A (2021) Dopamine Receptors in Parkinson's Disease: A Meta-Analysis of Imaging Studies. Movement Disord 36:1781–1791.

Kaeser PS, Regehr WG (2014) Molecular Mechanisms for Synchronous, Asynchronous, and Spontaneous Neurotransmitter Release. Physiology 76:333–363.

Kaiser S, Wonnacott S (2000) α-Bungarotoxin-Sensitive Nicotinic Receptors Indirectly Modulate [3H]Dopamine Release in Rat Striatal Slices via Glutamate Release. Mol Pharmacol 58:312–318.

Kalivas PW, McFarland K (2003) Brain circuitry and the reinstatement of cocaine-seeking behavior. Psychopharmacology 168:44–56.

Kammer H von der, Demiralay C, Andresen B, Albrecht C, Mayhaus M, Nitsch RM (2001) Regulation of gene expression by muscarinic acetylcholine receptors. Biochem Soc Symp 67:131–140.

Kawaguchi Y (1993) Physiological, morphological and histochemical characterisation of three classes of interneurons in rat neostriatum. j Neurosci.

Kawaguchi Y, Wilson C, Emson P (1990) Projection subtypes of rat neostriatal matrix cells revealed by intracellular injection of biocytin. J Neurosci 10:3421–3438.

Kawaguchi Y, Wilson CJ, Augood SJ, Emson PC (1995) Striatal interneurones: chemical, physiological and morphological characterization. Trends Neurosci 18:527–535.

Kelley AE (2004) Ventral striatal control of appetitive motivation: role in ingestive behavior and reward-related learning. Neurosci Biobehav Rev 27:765–776.

Kemp JM, Powell TPS (1971) The structure of the caudate nucleus of the cat: light and electron microscopy. Philosophical Transactions Royal Soc Lond B Biological Sci 262:383–401.

Kennedy RT, Jones SR, Wightman RM (1992) Dynamic Observation of Dopamine Autoreceptor Effects in Rat Striatal Slices. J Neurochem 59:449–455.

Kimura M, Rajkowski J, Evarts E (1984) Tonically discharging putamen neurons exhibit set-dependent responses. Proc National Acad Sci 81:4998–5001.

Kirik D, Rosenblad C, Burger C, Lundberg C, Johansen TE, Muzyczka N, Mandel RJ, Björklund A (2002) Parkinson-Like Neurodegeneration Induced by Targeted Overexpression of α-Synuclein in the Nigrostriatal System. J Neurosci 22:2780–2791.

Kirmse K, Dvorzhak A, Kirischuk S, Grantyn R (2008) GABA transporter 1 tunes GABAergic synaptic transmission at output neurons of the mouse neostriatum. J Physiology 586:5665–5678.

Kirmse K, Kirischuk S, Grantyn R (2009) Role of GABA transporter 3 in GABAergic synaptic transmission at striatal output neurons. Synapse 63:921–929.

Kish SJ, Shannak K, Hornykiewicz O (1988) Uneven pattern of dopamine loss in the striatum of patients with idiopathic Parkinson's Disease. The New England Journal of medicine.

Kita H (1993) Chapter 4 GABAergic circuits of the striatum. Prog Brain Res 99:51–72.

Kita H, Kosaka T, Heizmann CW (1990) Parvalbumin-immunoreactive neurons in the rat neostriatum: a light and electron microscopic study. Brain Res 536:1–15.

Klug JR, Engelhardt MD, Cadman CN, Li H, Smith JB, Ayala S, Williams EW, Hoffman H, Jin X (2018) Differential inputs to striatal cholinergic and parvalbumin interneurons imply functional distinctions. Elife 7:e35657.

Knowlton BJ, Mangels JA, Squire LR (1996) A Neostriatal Habit Learning System in Humans. Science 273:1399–1402.

Koós T, Tepper JM (1999) Inhibitory control of neostriatal projection neurons by GABAergic interneurons. Nat Neurosci 2:467–472.

Koós T, Tepper JM (2002) Dual Cholinergic Control of Fast-Spiking Interneurons in the Neostriatum. J Neurosci 22:529–535.

Kordower JH, Olanow CW, Dodiya HB, Chu Y, Beach TG, Adler CH, Halliday GM, Bartus RT (2013) Disease duration and the integrity of the nigrostriatal system in Parkinson's disease. Brain 136:2419–2431.

Kosillo P, Zhang Y-F, Threlfell S, Cragg SJ (2016) Cortical Control of Striatal Dopamine Transmission via Striatal Cholinergic Interneurons. Cereb Cortex 26:4160–4169.

Kramer PF, Brill-Weil S, Cummins AC, Zhang R, Camacho-Hernandez GA, Newman AH, Eldridge MA, Averbeck BB, Khaliq ZM (2022) Fast synaptic-like axo-axonal transmission from striatal cholinergic interneurons onto dopaminergic fibers. Biorxiv:2022.03.25.485828.

Kravitz AV, Freeze BS, Parker PRL, Kay K, Thwin MT, Deisseroth K, Kreitzer AC (2010) Regulation of parkinsonian motor behaviours by optogenetic control of basal ganglia circuitry. Nature 466:622–626.

Kravitz AV, Tye LD, Kreitzer AC (2012) Distinct roles for direct and indirect pathway striatal neurons in reinforcement. Nat Neurosci 15:816–818.

Kubota Y, Inagaki S, Kito S, Wu J-Y (1987) Dopaminergic axons directly make synapses with GABAergic neurons in the rat neostriatum. Brain Res 406:147–156.

Kuchibhotla KV, Goldman ST, Lattarulo CR, Wu H-Y, Hyman BT, Bacskai BJ (2008) Aβ Plaques Lead to Aberrant Regulation of Calcium Homeostasis In Vivo Resulting in Structural and Functional Disruption of Neuronal Networks. Neuron 59:214–225.

Kügler S, Kilic E, Bähr M (2003) Human synapsin 1 gene promoter confers highly neuron-specific long-term transgene expression from an adenoviral vector in the adult rat brain depending on the transduced area. Gene Ther 10:337–347.

Kulak JM, McIntosh JM, Yoshikami D, Olivera BM (2001) Nicotine-evoked transmitter release from synaptosomes: functional association of specific presynaptic acetylcholine receptors and voltage-gated calcium channels. J Neurochem 77:1581–1589.

Labouesse MA, Cola RB, Patriarchi T (2020) GPCR-Based Dopamine Sensors—A Detailed Guide to Inform Sensor Choice for In Vivo Imaging. Int J Mol Sci 21:8048.

Lak A, Stauffer WR, Schultz W (2014) Dopamine prediction error responses integrate subjective value from different reward dimensions. Proc National Acad Sci 111:2343–2348.

Lanciego JL, Luquin N, Obeso JA (2012) Functional Neuroanatomy of the Basal Ganglia. Csh Perspect Med 2:a009621.

Lautenschläger J et al. (2018) C-terminal calcium binding of α-synuclein modulates synaptic vesicle interaction. Nat Commun 9:712.

Lazic SE, Clarke-Williams CJ, Munafò MR (2018) What exactly is 'N' in cell culture and animal experiments? Plos Biol 16:e2005282.

Lee D, Obukhov AG, Shen Q, Liu Y, Dhawan P, Nowycky MC, Christakos S (2006) Calbindin-D28k decreases L-type calcium channel activity and modulates intracellular calcium homeostasis in response to K+ depolarization in a rat beta cell line RINr1046-38. Cell Calcium 39:475–485.

Lee K, Dixon AK, Freeman TC, Richardson PJ (1998) Identification of an ATP-sensitive potassium channel current in rat striatal cholinergic interneurones. J Physiology 510:441–453.

Lee K, Holley SM, Shobe JL, Chong NC, Cepeda C, Levine MS, Masmanidis SC (2017) Parvalbumin Interneurons Modulate Striatal Output and Enhance Performance during Associative Learning. Neuron 93:1451-1463.e4.

Lee TH, Gee KR, Davidson C, Ellinwood EH (2002) Direct, real-time assessment of dopamine release autoinhibition in the rat caudate–putamen. Neuroscience 112:647–654.

Levey A, Kitt C, Simonds W, Price D, Brann M (1991) Identification and localization of muscarinic acetylcholine receptor proteins in brain with subtype-specific antibodies. J Neurosci 11:3218–3226.

Levey AI, Hersch SM, Rye DB, Sunahara RK, Niznik HB, Kitt CA, Price DL, Maggio R, Brann MR, Ciliax BJ (1993) Localization of D1 and D2 dopamine receptors in brain with subtype-specific antibodies. Proc National Acad Sci 90:8861–8865.

Lewis RG, Serra M, Radl D, Gori M, Tran C, Michalak SE, Vanderwal CD, Borrelli E (2020) Dopaminergic Control of Striatal Cholinergic Interneurons Underlies Cocaine-Induced Psychostimulation. Cell Reports 31:107527.

Li J-L, Kaneko T, Mizuno N (2002) Synaptic association of dopaminergic axon terminals and neurokinin-1 receptor-expressing intrinsic neurons in the striatum of the rat. Neurosci Lett 324:9–12.

Lim SAO, Kang UJ, McGehee DS (2014) Striatal cholinergic interneuron regulation and circuit effects. Frontiers Synaptic Neurosci 6:22.

Limberger N, Trout SJ, Kruk ZL, Starke K (1991) "Real time" measurement of endogenous dopamine release during short trains of pulses in slices of rat neostriatum and nucleus accumbens : role of autoinhibition. Naunyn-schmiedeberg's Archives Pharmacol 344:623–629.

Lin JY, Chung KKH, Castro DD, Funk GD, Lipski J (2004) Effects of muscarinic acetylcholine receptor activation on membrane currents and intracellular messengers in medium spiny neurones of the rat striatum. Eur J Neurosci 20:1219–1230.

Liu C, Cai X, Ritzau-Jost A, Kramer PF, Li Y, Khaliq ZM, Hallermann S, Kaeser PS (2022) An action potential initiation mechanism in distal axons for the control of dopamine release. Science 375:1378–1385.

Lobo MK, III HEC, Chaudhury D, Friedman AK, Sun H, Damez-Werno D, Dietz DM, Zaman S, Koo JW, Kennedy PJ, Mouzon E, Mogri M, Neve RL, Deisseroth K, Han M-H, Nestler EJ (2010) Cell Type–Specific Loss of BDNF Signaling Mimics Optogenetic Control of Cocaine Reward. Science 330:385–390.

Lopes EF, Roberts BM, Siddorn RE, Clements MA, Cragg SJ (2019) Inhibition of Nigrostriatal Dopamine Release by Striatal GABAA and GABAB Receptors. J Neurosci 39:1058–1065.

Lozovaya N, Ben-Ari Y, Hammond C (2018a) Striatal dual cholinergic /GABAergic transmission in Parkinson disease: friends or foes? Cell Stress 2:147–149.

Lozovaya N, Eftekhari S, Cloarec R, Gouty-Colomer LA, Dufour A, Riffault B, Billon-Grand M, Pons-Bennaceur A, Oumar N, Burnashev N, Ben-Ari Y, Hammond C (2018b) GABAergic inhibition in dual-transmission cholinergic and GABAergic striatal interneurons is abolished in Parkinson disease. Nat Commun 9:1422.

Lundblad M, Decressac M, Mattsson B, Björklund A (2012) Impaired neurotransmission caused by overexpression of α-synuclein in nigral dopamine neurons. Proc National Acad Sci 109:3213–3219.

Luo F, Wei Y, Wang Z, Luo M, Hu J (2018) Genetically Encoded Neural Activity Indicators. Brain Sci Adv 4:1–15.

Luo R, Janssen MJ, Partridge JG, Vicini S (2013a) Direct and GABA-mediated indirect effects of nicotinic ACh receptor agonists on striatal neurones. J Physiology 591:203–217.

Luo R, Partridge JG, Vicini S (2013b) Distinct roles of synaptic and extrasynaptic GABAAreceptors in striatal inhibition dynamics. Front Neural Circuit 7:186.

Ma L, Chen W, Yu D, Han Y (2020) Brain-Wide Mapping of Afferent Inputs to Accumbens Nucleus Core Subdomains and Accumbens Nucleus Subnuclei. Frontiers Syst Neurosci 14:15.

Maier-Peuschel M, Frölich N, Dees C, Hommers LG, Hoffmann C, Nikolaev VO, Lohse MJ (2010) A Fluorescence Resonance Energy Transfer-based M2 Muscarinic Receptor Sensor Reveals Rapid Kinetics of Allosteric Modulation*. J Biol Chem 285:8793–8800.

Mamaligas AA, Barcomb K, Ford CP (2019) Cholinergic Transmission at Muscarinic Synapses in the Striatum Is Driven Equally by Cortical and Thalamic Inputs. Cell Reports 28:1003-1014.e3.

Mamaligas AA, Ford CP (2016) Spontaneous Synaptic Activation of Muscarinic Receptors by Striatal Cholinergic Neuron Firing. Neuron 91:574–586.

Mansvelder HD, McGehee DS (2000) Long-Term Potentiation of Excitatory Inputs to Brain Reward Areas by Nicotine. Neuron 27:349–357.

Mansvelder HD, McGehee DS (2002) Cellular and synaptic mechanisms of nicotine addiction. J Neurobiol 53:606–617.

Mantanona CP, Alsiö J, Elson JL, Fisher BM, Dalley JW, Bussey T, Pienaar IS (2019) Altered motor, anxiety-related and attentional task performance at baseline associate with multiple gene copies of the vesicular acetylcholine transporter and related protein overexpression in ChAT::Cre+ rats. Brain Struct Funct 224:3095–3116.

Marcott PF, Gong S, Donthamsetti P, Grinnell SG, Nelson MN, Newman AH, Birnbaumer L, Martemyanov KA, Javitch JA, Ford CP (2018) Regional Heterogeneity of D2-Receptor Signaling in the Dorsal Striatum and Nucleus Accumbens. Neuron 98:575-587.e4.

Mark GP, Hajnal A, Kinney AE, Keys AS (1999) Self-administration of cocaine increases the release of acetylcholine to a greater extent than response-independent cocaine in the nucleus accumbens of rats. Psychopharmacology 143:47–53.

Markovic D, Holdich J, Al-Sabah S, Mistry R, Krasel C, Mahaut-Smith MP, Challiss RAJ (2012) FRET-Based Detection of M1 Muscarinic Acetylcholine Receptor Activation by Orthosteric and Allosteric Agonists. Plos One 7:e29946.

Martyniuk KM, Torres-Herraez A, Rubinstein M, Labouesse MA, Kellendonk C (2021) Dopamine D2Rs Coordinate Cue-Evoked Changes in Striatal Acetylcholine Levels. Biorxiv:2021.12.08.471871.

Matamales M, Götz J, Bertran-Gonzalez J (2016) Quantitative Imaging of Cholinergic Interneurons Reveals a Distinctive Spatial Organization and a Functional Gradient across the Mouse Striatum. Plos One 11:e0157682.

Matsuda W, Furuta T, Nakamura KC, Hioki H, Fujiyama F, Arai R, Kaneko T (2009) Single Nigrostriatal Dopaminergic Neurons Form Widely Spread and Highly Dense Axonal Arborizations in the Neostriatum. J Neurosci 29:444–453.

Maurice N, Liberge M, Jaouen F, Ztaou S, Hanini M, Camon J, Deisseroth K, Amalric M, Kerkerian-Le Goff L, Beurrier C (2015) Striatal Cholinergic Interneurons Control Motor Behavior and Basal Ganglia Function in Experimental Parkinsonism. Cell Reports 13:657–666.

Maurice N, Mercer J, Chan CS, Hernandez-Lopez S, Held J, Tkatch T, Surmeier DJ (2004) D2 Dopamine Receptor-Mediated Modulation of Voltage-Dependent Na+ Channels Reduces Autonomous Activity in Striatal Cholinergic Interneurons. J Neurosci 24:10289–10301.

May LJ, Wightman RM (1989) Effects of D-2 Antagonists on Frequency-Dependent Stimulated Dopamine Overflow in Nucleus Accumbens and Caudate-Putamen. J Neurochem 53:898–906.

McBride WJ, Murphy JM, Ikemoto S (1999) Localization of brain reinforcement mechanisms: intracranial self-administration and intracranial place-conditioning studies. Behav Brain Res 101:129–152.

McClure-Begley TD, Stone KL, Marks MJ, Grady SR, Colangelo CM, Lindstrom JM, Picciotto MR (2013) Exploring the Nicotinic Acetylcholine Receptor-associated Proteome with iTRAQ and Transgenic Mice. Genom Proteom Bioinform 11:207–218.

McKay BE, Placzek AN, Dani JA (2007) Regulation of synaptic transmission and plasticity by neuronal nicotinic acetylcholine receptors. Biochem Pharmacol 74:1120–1133.

McKinley JW, Shi Z, Kawikova I, Hur M, Bamford IJ, Devi SPS, Vahedipour A, Darvas M, Bamford NS (2019) Dopamine Deficiency Reduces Striatal Cholinergic Interneuron Function in Models of Parkinson's Disease. Neuron 103:1056-1072.e6.

Messamore E, Ogane N, Giacobini E (1993) Cholinesterase inhibitor effects on extracellular acetylcholine in rat striatum. Neuropharmacology 32:291–296.

Mesulam M -Marsel, Mash D, Hersh L, Bothwell M, Geula C (1992) Cholinergic innervation of the human striatum, globus pallidus, subthalamic nucleus, substantia nigra, and red nucleus. J Comp Neurol 323:252–268.

Mirenowicz J, Schultz W (1996) Preferential activation of midbrain dopamine neurons by appetitive rather than aversive stimuli. Nature 379:449–451.

Missale C, NASH SR, ROBINSON SW, JABER M, CARON MG (1998) Dopamine Receptors: From Structure to Function. Physiol Rev 78:189–225.

Moine CL, Normand E, Bloch B (1991) Phenotypical characterization of the rat striatal neurons expressing the D1 dopamine receptor gene. Proc National Acad Sci 88:4205–4209.

Monsma FJ, McVittie LD, Gerfen CR, Mahan LC, Sibley DR (1989) Multiple D2 dopamine receptors produced by alternative RNA splicing. Nature 342:926–929.

Mori F, Tanji K, Zhang H, Kakita A, Takahashi H, Wakabayashi K (2008) α-Synuclein pathology in the neostriatum in Parkinson's disease. Acta Neuropathol 115:453–459.

Morris G, Arkadir D, Nevet A, Vaadia E, Bergman H (2004) Coincident but Distinct Messages of Midbrain Dopamine and Striatal Tonically Active Neurons. Neuron 43:133–143.

Nakai J, Ohkura M, Imoto K (2001) A high signal-to-noise Ca2+ probe composed of a single green fluorescent protein. Nat Biotechnol 19:137–141.

Nemani VM, Lu W, Berge V, Nakamura K, Onoa B, Lee MK, Chaudhry FA, Nicoll RA, Edwards RH (2010) Increased Expression of α-Synuclein Reduces Neurotransmitter Release by Inhibiting Synaptic Vesicle Reclustering after Endocytosis. Neuron 65:66–79.

Nguyen Q-T, Schroeder LF, Mank M, Muller A, Taylor P, Griesbeck O, Kleinfeld D (2010) An in vivo biosensor for neurotransmitter release and in situ receptor activity. Nat Neurosci 13:127–132.

Nitsch RM, Rossner S, Albrecht C, Mayhaus M, Enderich J, Schliebs R, Wegner M, Arendt T, Kammer H von der (1998) Muscarinic acetylcholine receptors activate the acetylcholinesterase gene promoter. J Physiology-paris 92:257–264.

Nosaka D, Wickens JR (2022) Striatal Cholinergic Signaling in Time and Space. Molecules 27:1202.

Nowak L, Bregestovski P, Ascher P (1984) Magnesium gates glutamate-activated channels in mouse central neurones. Nature.

Obeso JA, Rodriguez-Oroz MC, Stamelou M, Bhatia KP, Burn DJ (2014) The expanding universe of disorders of the basal ganglia. Lancet 384:523–531.

O'Hare JK, Li H, Kim N, Gaidis E, Ade K, Beck J, Yin H, Calakos N (2017) Striatal fast-spiking interneurons selectively modulate circuit output and are required for habitual behavior. Elife 6:e26231.

Owen SF, Berke JD, Kreitzer AC (2018) Fast-Spiking Interneurons Supply Feedforward Control of Bursting, Calcium, and Plasticity for Efficient Learning. Cell 172:683-695.e15.

Pablo-Fernandez ED, Goldacre R, Pakpoor J, Noyce AJ, Warner TT (2018) Association between diabetes and subsequent Parkinson disease. Neurology 91:e139–e142.

Packard MG (1999) Glutamate infused posttraining into the hippocampus or caudate-putamen differentially strengthens place and response learning. Proc National Acad Sci 96:12881–12886.

Pagano G, Polychronis S, Wilson H, Giordano B, Ferrara N, Niccolini F, Politis M (2018) Diabetes mellitus and Parkinson disease. Neurology 90:e1654–e1662.

Pakhotin P, Bracci E (2007) Cholinergic Interneurons Control the Excitatory Input to the Striatum. J Neurosci 27:391–400.

Palij P, Bull DR, Sheehan MJ, Millar J, Stamford J, Kruk ZL, Humphrey PPA (1990) Presynaptic regulation of dopamine release in corpus striatum monitored in vitro in real time by fast cyclic voltammetry. Brain Res 509:172–174.

Pan P-Y, Ryan TA (2012) Calbindin controls release probability in ventral tegmental area dopamine neurons. Nat Neurosci 15:813–815.

Pan W-X (2005) Dopamine Cells Respond to Predicted Events during Classical Conditioning: Evidence for Eligibility Traces in the Reward-Learning Network. J Neurosci 25:6235–6242.

Pancani T, Bolarinwa C, Smith Y, Lindsley CW, Conn PJ, Xiang Z (2014) M4 mAChR-Mediated Modulation of Glutamatergic Transmission at Corticostriatal Synapses. Acs Chem Neurosci 5:318–324.

Panzera LC, Hoppa MB (2019) Genetically Encoded Voltage Indicators Are Illuminating Subcellular Physiology of the Axon. Front Cell Neurosci 13:52.

Papageorgiou GK, Baudonnat M, Cucca F, Walton ME (2016) Mesolimbic Dopamine Encodes Prediction Errors in a State-Dependent Manner. Cell Reports 15:221–228.

Paradiso KG, Steinbach JH (2003) Nicotine is Highly Effective at Producing Desensitization of Rat α4β2 Neuronal Nicotinic Receptors. J Physiology 553:857–871.

Patel J, Trout SJ, Kruk ZL (1992) Regional differences in evoked dopamine efflux in brain slices of rat anterior and posterior caudate putamen. Naunyn-schmiedeberg's Archives Pharmacol 346:267–276.

Patel JC, Rossignol E, Rice ME, Machold RP (2012) Opposing regulation of dopaminergic activity and exploratory motor behavior by forebrain and brainstem cholinergic circuits. Nat Commun 3:1172.

Patriarchi T, Cho JR, Merten K, Howe MW, Marley A, Xiong W-H, Folk RW, Broussard GJ, Liang R, Jang MJ, Zhong H, Dombeck D, Zastrow M von, Nimmerjahn A, Gradinaru V, Williams JT, Tian L (2018) Ultrafast neuronal imaging of dopamine dynamics with designed genetically encoded sensors. Science 360:eaat4422.

Patriarchi T, Mohebi A, Sun J, Marley A, Liang R, Dong C, Puhger K, Mizuno GO, Davis CM, Wiltgen B, Zastrow M von, Berke JD, Tian L (2020) An expanded palette of dopamine sensors for multiplex imaging in vivo. Nat Methods 17:1147–1155.

Paumier KL, Luk KC, Manfredsson FP, Kanaan NM, Lipton JW, Collier TJ, Steece-Collier K, Kemp CJ, Celano S, Schulz E, Sandoval IM, Fleming S, Dirr E, Polinski NK, Trojanowski JQ, Lee VM, Sortwell CE (2015) Intrastriatal injection of pre-formed mouse α-synuclein fibrils into rats triggers α-synuclein pathology and bilateral nigrostriatal degeneration. Neurobiol Dis 82:185–199.

Paz RM, Tubert C, Stahl AM, Amarillo Y, Rela L, Murer MG (2021) Levodopa Causes Striatal Cholinergic Interneuron Burst-Pause Activity in Parkinsonian Mice. Movement Disord 36:1578–1591.

Perese DA, Ulman J, Viola J, Ewing SE, Bankiewicz KS (1989) A 6-hydroxydopamine-induced selective parkinsonian rat model. Brain Res 494:285–293.

Perez-Rosello T, Figueroa A, Salgado H, Vilchis C, Tecuapetla F, Guzman JN, Galarraga E, Bargas J (2005) Cholinergic Control of Firing Pattern and Neurotransmission in Rat Neostriatal Projection Neurons: Role of CaV2.1 and CaV2.2 Ca2+ Channels. J Neurophysiol 93:2507–2519.

Pérez-Taboada I, Alberquilla S, Martín ED, Anand R, Vietti-Michelina S, Tebeka NN, Cantley J, Cragg SJ, Moratalla R, Vallejo M (2020) Diabetes Causes Dysfunctional Dopamine Neurotransmission Favoring Nigrostriatal Degeneration in Mice. Movement Disord 35:1636–1648.

Perrier AL, Massoulié J, Krejci E (2002) PRiMA The Membrane Anchor of Acetylcholinesterase in the Brain. Neuron 33:275–285.

Pert CB, Kuhar MJ, Snyder SH (1976) Opiate receptor: autoradiographic localization in rat brain. Proc National Acad Sci 73:3729–3733.

Petryszyn S, Paolo TD, Parent A, Parent M (2016) The number of striatal cholinergic interneurons expressing calretinin is increased in parkinsonian monkeys. Neurobiol Dis 95:46–53.

Phelps PE, Houser CR, Vaughn JE (1985) Immunocytochemical localization of choline acetyltransferase within the rat neostriatum: A correlated light and electron microscopic study of cholinergic neurons and synapses. J Comp Neurol 238:286–307.

Phillips PEM, Hancock PJ, Stamford JA (2002) Time window of autoreceptor-mediated inhibition of limbic and striatal dopamine release. Synapse 44:15–22.

Phillips PEM, Stuber GD, Heien MLAV, Wightman RM, Carelli RM (2003) Subsecond dopamine release promotes cocaine seeking. Nature 422:614–618.

Pisani A, Bernardi G, Ding J, Surmeier DJ (2007) Re-emergence of striatal cholinergic interneurons in movement disorders. Trends Neurosci 30:545–553.

Pissadaki EK, Bolam JP (2013) The energy cost of action potential propagation in dopamine neurons: clues to susceptibility in Parkinson's disease. Front Comput Neurosc 7:13.

Planert H, Berger TK, Silberberg G (2013) Membrane Properties of Striatal Direct and Indirect Pathway Neurons in Mouse and Rat Slices and Their Modulation by Dopamine. Plos One 8:e57054.

Planert H, Szydlowski SN, Hjorth JJJ, Grillner S, Silberberg G (2010) Dynamics of Synaptic Transmission between Fast-Spiking Interneurons and Striatal Projection Neurons of the Direct and Indirect Pathways. J Neurosci 30:3499–3507.

Plasse G van der, Schrama R, Seters SP van, Vanderschuren LJMJ, Westenberg HGM (2012) Deep Brain Stimulation Reveals a Dissociation of Consummatory and Motivated Behaviour in the Medial and Lateral Nucleus Accumbens Shell of the Rat. Plos One 7:e33455.

Poewe W, Seppi K, Tanner CM, Halliday GM, Brundin P, Volkmann J, Schrag A-E, Lang AE (2017) Parkinson disease. Nat Rev Dis Primers 3:17013.

Poewe W, Wolters E, Emre M, Onofrj M, Hsu C, Tekin S, Lane R (2006) Long-term benefits of rivastigmine in dementia associated with Parkinson's disease: An active treatment extension study. Movement Disord 21:456–461.

Poppi LA, Ho-Nguyen KT, Shi A, Daut CT, Tischfield MA (2021) Recurrent Implication of Striatal Cholinergic Interneurons in a Range of Neurodevelopmental, Neurodegenerative, and Neuropsychiatric Disorders. Cells 10:907.

Povlock SL, Schenk JO (1997) A Multisubstrate Kinetic Mechanism of Dopamine Transport in the Nucleus Accumbens and Its Inhibition by Cocaine. J Neurochem 69:1093–1105.

Prakriya M, Mennerick S (2000) Selective Depression of Low–Release Probability Excitatory Synapses by Sodium Channel Blockers. Neuron 26:671–682.

Prendergast BJ, Onishi KG, Zucker I (2014) Female mice liberated for inclusion in neuroscience and biomedical research. Neurosci Biobehav Rev 40:1–5.

Puighermanal E, Castell L, Esteve-Codina A, Melser S, Kaganovsky K, Zussy C, Boubaker-Vitre J, Gut M, Rialle S, Kellendonk C, Sanz E, Quintana A, Marsicano G, Martin M, Rubinstein M, Girault J-A, Ding JB, Valjent E (2020) Functional and molecular heterogeneity of D2R neurons along dorsal ventral axis in the striatum. Nat Commun 11:1957.

Quick MW, Lester RAJ (2002) Desensitization of neuronal nicotinic receptors. J Neurobiol 53:457–478.

Quik M, Bordia T, O'Leary K (2007) Nicotinic receptors as CNS targets for Parkinson's disease. Biochem Pharmacol 74:1224–1234.

Quinn JJ, Pittenger C, Lee AS, Pierson JL, Taylor JR (2013) Striatum-dependent habits are insensitive to both increases and decreases in reinforcer value in mice. Eur J Neurosci 37:1012–1021.

Ragozzino ME (2003) Acetylcholine actions in the dorsomedial striatum support the flexible shifting of response patterns. Neurobiol Learn Mem 80:257–267.

Ragozzino ME, Mohler EG, Prior M, Palencia CA, Rozman S (2009) Acetylcholine activity in selective striatal regions supports behavioral flexibility. Neurobiol Learn Mem 91:13–22.

Ramanathan S, Hanley JJ, Deniau J-M, Bolam JP (2002) Synaptic Convergence of Motor and Somatosensory Cortical Afferents onto GABAergic Interneurons in the Rat Striatum. J Neurosci 22:8158–8169.

Ravotto L, Duffet L, Zhou X, Weber B, Patriarchi T (2020) A Bright and Colorful Future for G-Protein Coupled Receptor Sensors. Front Cell Neurosci 14:67.

Rice ME, Cragg SJ (2004) Nicotine amplifies reward-related dopamine signals in striatum. Nat Neurosci 7:583–584.

Rice ME, Cragg SJ (2008) Dopamine spillover after quantal release: Rethinking dopamine transmission in the nigrostriatal pathway. Brain Res Rev 58:303–313.

Rice ME, Patel JC, Cragg SJ (2011) Dopamine release in the basal ganglia. Neuroscience 198:112–137.

Rivera A, Alberti I, Martín AB, Narváez JA, Calle ADL, Moratalla R (2002) Molecular phenotype of rat striatal neurons expressing the dopamine D5 receptor subtype. Eur J Neurosci 16:2049–2058.

Roberts BM, Doig NM, Brimblecombe KR, Lopes EF, Siddorn RE, Threlfell S, Connor-Robson N, Bengoa-Vergniory N, Pasternack N, Wade-Martins R, Magill PJ, Cragg SJ (2020) GABA uptake transporters support dopamine release in dorsal striatum with maladaptive downregulation in a parkinsonism model. Nat Commun 11:4958.

Roberts BM, Lambert E, Livesey JA, Wu Z, Li Y, Cragg SJ (2022) Dopamine Release in Nucleus Accumbens Is under Tonic Inhibition by Adenosine A 1 Receptors Regulated by Astrocytic ENT1 and Dysregulated by Ethanol. J Neurosci 42:1738–1751.

Roberts BM, Lopes EF, Cragg SJ (2021) Axonal Modulation of Striatal Dopamine Release by Local γ-Aminobutyric Acid (GABA) Signalling. Cells 10:709.

Rocca WA (2018) The burden of Parkinson's disease: a worldwide perspective. Lancet Neurology 17:928–929.

Rodŕiguez-Pallares J, Labandeira-García JL, Muñoz A, Caruncho HJ (2000) Morphology and neurochemistry of two striatal neuronal subtypes expressing the GABAA receptor α3-subunit in the rat. Brain Res 876:124–130.

Roesch MR, Calu DJ, Schoenbaum G (2007) Dopamine neurons encode the better option in rats deciding between differently delayed or sized rewards. Nat Neurosci 10:1615–1624.

Roitman MF (2004) Dopamine Operates as a Subsecond Modulator of Food Seeking. J Neurosci 24:1265–1271.

Rolinski M, Fox C, Maidment I, McShane R (2012) Cholinesterase inhibitors for dementia with Lewy bodies, Parkinson's disease dementia and cognitive impairment in Parkinson's disease. Cochrane Db Syst Rev 3:CD006504.

Romo R, Schultz W (1990) Dopamine neurons of the monkey midbrain: contingencies of responses to active touch during self-initiated arm movements. J Neurophysiol 63:592–606.

Rozov A, Bolshakov AP, Valiullina-Rakhmatullina F (2019) The Ever-Growing Puzzle of Asynchronous Release. Front Cell Neurosci 13:28.

Rutledge RB, Dean M, Caplin A, Glimcher PW (2010) Testing the Reward Prediction Error Hypothesis with an Axiomatic Model. J Neurosci 30:13525–13536.

Sabatini BL (2019) The impact of reporter kinetics on the interpretation of data gathered with fluorescent reporters. Biorxiv:834895.

Sakamoto S, Goto S, Ito H, Hirano A (1992) Striosornal organization of substance P-like immunoreactivity in parkinsonian patients. Neurology 42:1071–1071.

Sanchez G, Rodriguez MJ, Pomata P, Rela L, Murer MG (2011) Reduction of an Afterhyperpolarization Current Increases Excitability in Striatal Cholinergic Interneurons in Rat Parkinsonism. J Neurosci 31:6553–6564.

Sandor NT, Zelles T, Kiss J, Sershen H, Torocsik A, Lajtha A, Vizi ES (1991) Effect of nicotine on dopaminergic-cholinergic interaction in the striatum. Brain Res 567:313–316.

Santiago JA, Potashkin JA (2013) Integrative Network Analysis Unveils Convergent Molecular Pathways in Parkinson's Disease and Diabetes. Plos One 8:e83940.

Santiago JA, Potashkin JA (2014) System-based approaches to decode the molecular links in Parkinson's disease and diabetes. Neurobiol Dis 72:84–91.

Santos RM, Sirota A (2021) Phasic oxygen dynamics confounds fast choline-sensitive biosensor signals in the brain of behaving rodents. Elife 10:e61940.

Sarno P de, Giacobini E, Downen M (1987) Release of acetylcholinesterase from the caudate nucleus of the rat. J Neurosci Res 18:578–590.

Sato A, Sasaoka T, Nishijo T, Momiyama T (2014) GABAergic synaptic transmission onto striatal cholinergic interneurons in dopamine D2 receptor knock-out mice. Neuroscience 263:138–147.

Sauer H, Oertel WH (1994) Progressive degeneration of nigrostriatal dopamine neurons following intrastriatal terminal lesions with 6-hydroxydopamine: A combined retrograde tracing and immunocytochemical study in the rat. Neuroscience 59:401–415.

Schaeffer E, Pilotto A, Berg D (2014) Pharmacological Strategies for the Management of Levodopa-Induced Dyskinesia in Patients with Parkinson's Disease. Cns Drugs 28:1155–1184.

Schmidt H (2012) Three functional facets of calbindin D-28k. Front Mol Neurosci 5:25.

Schmidt H, Schwaller B, Eilers J (2005) Calbindin D28k targets myo-inositol monophosphatase in spines and dendrites of cerebellar Purkinje neurons. Proc National Acad Sci 102:5850–5855.

Schultz W (1998) Predictive Reward Signal of Dopamine Neurons. J Neurophysiol 80:1–27.

Schultz W, Dayan P, Montague PR (1997) A Neural Substrate of Prediction and Reward. Science 275:1593–1599.

Schultz W, Ruffieux A, Aebischer P (1983) The activity of pars compacta neurons of the monkey substantia nigra in relation to motor activation. Exp Brain Res 51:377–387.

Schuvailo ON, Dzyadevych SV, El'skaya AV, Gautier-Sauvigné S, Csöregi E, Cespuglio R, Soldatkin AP (2005) Carbon fibre-based microbiosensors for in vivo measurements of acetylcholine and choline. Biosens Bioelectron 21:87–94.

Senior SL, Ninkina N, Deacon R, Bannerman D, Buchman VL, Cragg SJ, Wade-Martins R (2008) Increased striatal dopamine release and hyperdopaminergic-like behaviour in mice lacking both alpha-synuclein and gamma-synuclein. Eur J Neurosci 27:947–957.

Sharott A, Doig NM, Mallet N, Magill PJ (2012) Relationships between the Firing of Identified Striatal Interneurons and Spontaneous and Driven Cortical Activities In Vivo. J Neurosci 32:13221–13236.

Shim KH, Go HG, Bae H, Jeong D-E, Kim D, Youn YC, Kim S, An SSA, Kang MJ (2021) Decreased Exosomal Acetylcholinesterase Activity in the Plasma of Patients With Parkinson's Disease. Front Aging Neurosci 13:665400.

Shin JH, Adrover MF, Alvarez VA (2017) Distinctive Modulation of Dopamine Release in the Nucleus Accumbens Shell Mediated by Dopamine and Acetylcholine Receptors. J Neurosci 37:11166–11180.

Shin JH, Adrover MF, Wess J, Alvarez VA (2015) Muscarinic regulation of dopamine and glutamate transmission in the nucleus accumbens. Proc National Acad Sci 112:8124–8129.

Siffrin V, Radbruch H, Glumm R, Niesner R, Paterka M, Herz J, Leuenberger T, Lehmann SM, Luenstedt S, Rinnenthal JL, Laube G, Luche H, Lehnardt S, Fehling H-J, Griesbeck O, Zipp F (2010) In Vivo Imaging of Partially Reversible Th17 Cell-Induced Neuronal Dysfunction in the Course of Encephalomyelitis. Immunity 33:424–436.

Singleton AB et al. (2003) alpha-Synuclein locus triplication causes Parkinson's disease. Sci New York N Y 302:841.

Smedley EB, DiLeo A, Smith KS (2019) Circuit directionality for motivation: Lateral accumbens-pallidum, but not pallidum-accumbens, connections regulate motivational attraction to reward cues. Neurobiol Learn Mem 162:23–35.

Smith AD, Bolam JP (1990) The neural network of the basal ganglia as revealed by the study of synaptic connections of identified neurones. Trends Neurosci 13:259–265.

Soliakov L, Wonnacott S (1996) Voltage-sensitive Ca2+ channels involved in nicotinic receptor-mediated [H] dopamine release from rat stratal synaptosomes. J Neurochem.

Somogyi P, Bolam JP, Smith AD (1981) Monosynaptic cortical input and local axon collaterals of identified striatonigral neurons. A light and electron microscopic study using the golgi-peroxidase transport-degeneration procedure. J Comp Neurol 195:567–584.

Sossi V, Fuente-Fernández R de la, Holden JE, Schulzer M, Ruth TJ, Stoessl J (2004) Changes of Dopamine Turnover in the Progression of Parkinson's Disease as Measured by Positron Emission Tomography: Their Relation to Disease-Compensatory Mechanisms. J Cereb Blood Flow Metabolism 24:869–876.

Specht CG, Schoepfer R (2001) Deletion of the alpha-synuclein locus in a subpopulation of C57BL/6J inbred mice. BMC Neurosci:11.

Spillantini MG, Crowther RA, Jakes R, Hasegawa M, Goedert M (1998) α-Synuclein in filamentous inclusions of Lewy bodies from Parkinson's disease and dementia with Lewy bodies. Proc National Acad Sci 95:6469–6473.

Steiner H, Gerfen CR (1998) Role of dynorphin and enkephalin in the regulation of striatal output pathways and behavior. Exp Brain Res 123:60–76.

Stevens TR, Krueger SR, Fitzsimonds RM, Picciotto MR (2003) Neuroprotection by Nicotine in Mouse Primary Cortical Cultures Involves Activation of Calcineurin and L-Type Calcium Channel Inactivation. J Neurosci 23:10093–10099.

Stouffer MA, Woods CA, Patel JC, Lee CR, Witkovsky P, Bao L, Machold RP, Jones KT, Vaca SC de, Reith MEA, Carr KD, Rice ME (2015) Insulin enhances striatal dopamine release by activating cholinergic interneurons and thereby signals reward. Nat Commun 6:8543.

Straub C, Saulnier JL, Bègue A, Feng DD, Huang KW, Sabatini BL (2016) Principles of Synaptic Organization of GABAergic Interneurons in the Striatum. Neuron 92:84–92.

Straub C, Tritsch NX, Hagan NA, Gu C, Sabatini BL (2014) Multiphasic Modulation of Cholinergic Interneurons by Nigrostriatal Afferents. J Neurosci 34:8557–8569.

Sullivan MA, Chen H, Morikawa H (2008) Recurrent Inhibitory Network among Striatal Cholinergic Interneurons. J Neurosci 28:8682–8690.

Sulzer D, Cragg SJ, Rice ME (2016) Striatal dopamine neurotransmission: Regulation of release and uptake. Basal Ganglia 6:123–148.

Sun F et al. (2018) A Genetically Encoded Fluorescent Sensor Enables Rapid and Specific Detection of Dopamine in Flies, Fish, and Mice. Cell 174:481-496.e19.

Sun F, Zhou J, Dai B, Qian T, Zeng J, Li X, Zhuo Y, Zhang Y, Wang Y, Qian C, Tan K, Feng J, Dong H, Lin D, Cui G, Li Y (2020) Next-generation GRAB sensors for monitoring dopaminergic activity in vivo. Nat Methods 17:1156–1166.

Sun Y, Chang Y-H, Chen H-F, Su Y-H, Su H-F, Li C-Y (2012) Risk of Parkinson Disease Onset in Patients With Diabetes. Diabetes Care 35:1047–1049.

Surmeier DJ, Song W-J, Yan Z (1996) Coordinated Expression of Dopamine Receptors in Neostriatal Medium Spiny Neurons. J Neurosci 16:6579–6591.

Surmeier DJ, Sulzer D (2013) The pathology roadmap in Parkinson disease. Prion 7:85–91.

Syed ECJ, Grima LL, Magill PJ, Bogacz R, Brown P, Walton ME (2016) Action Initiation Shapes Mesolimbic Dopamine Encoding of Future Rewards. Nat Neurosci 19:34–36.

Szydlowski SN, Dorocic IP, Planert H, Carlén M, Meletis K, Silberberg G (2013) Target Selectivity of Feedforward Inhibition by Striatal Fast-Spiking Interneurons. J Neurosci 33:1678–1683.

Taschenberger G, Garrido M, Tereshchenko Y, Bähr M, Zweckstetter M, Kügler S (2012) Aggregation of αSynuclein promotes progressive in vivo neurotoxicity in adult rat dopaminergic neurons. Acta Neuropathol 123:671–683.

Taverna S, Ilijic E, Surmeier DJ (2008) Recurrent Collateral Connections of Striatal Medium Spiny Neurons Are Disrupted in Models of Parkinson's Disease. J Neurosci 28:5504–5512.

Tepper JM, Bolam JP (2004) Functional diversity and specificity of neostriatal interneurons. Curr Opin Neurobiol 14:685–692.

Tepper JM, Koós T, Ibanez-Sandoval O, Tecuapetla F, Faust TW, Assous M (2018) Heterogeneity and Diversity of Striatal GABAergic Interneurons: Update 2018. Front Neuroanat 12:91.

Tepper JM, Tecuapetla F, Koós T, Ibáñez-Sandoval O (2010) Heterogeneity and Diversity of Striatal GABAergic Interneurons. Front Neuroanat 4:150.

Thestrup T et al. (2014) Optimized ratiometric calcium sensors for functional in vivo imaging of neurons and T lymphocytes. Nat Methods 11:175–182.

Thorn CA, Graybiel AM (2014) Differential Entrainment and Learning-Related Dynamics of Spike and Local Field Potential Activity in the Sensorimotor and Associative Striatum. J Neurosci 34:2845–2859.

Threlfell S, Clements MA, Khodai T, Pienaar IS, Exley R, Wess J, Cragg SJ (2010) Striatal Muscarinic Receptors Promote Activity Dependence of Dopamine Transmission via Distinct Receptor Subtypes on Cholinergic Interneurons in Ventral versus Dorsal Striatum. J Neurosci 30:3398–3408.

Threlfell S, Cragg SJ (2011) Dopamine Signaling in Dorsal Versus Ventral Striatum: The Dynamic Role of Cholinergic Interneurons. Frontiers Syst Neurosci 5:11.

Threlfell S, Lalic T, Platt NJ, Jennings KA, Deisseroth K, Cragg SJ (2012) Striatal Dopamine Release Is Triggered by Synchronized Activity in Cholinergic Interneurons. Neuron 75:58–64.

Threlfell S, Mohammadi AS, Ryan BJ, Connor-Robson N, Platt NJ, Anand R, Serres F, Sharp T, Bengoa-Vergniory N, Wade-Martins R, Ewing A, Cragg SJ, Brimblecombe KR (2021) Striatal Dopamine Transporter Function Is Facilitated by Converging Biology of α-Synuclein and Cholesterol. Front Cell Neurosci 15:658244.

Tobler PN, Fiorillo CD, Schultz W (2005) Adaptive Coding of Reward Value by Dopamine Neurons. Science 307:1642–1645.

Tritsch NX, Ding JB, Sabatini BL (2012) Dopaminergic neurons inhibit striatal output via non-canonical release of GABA. Nature 490:262–266.

Tsuneki H, Klink R, Léna C, Korn H, Changeux J (2000) Calcium mobilisation elicited by two types of nicotinic acetylcholine receptors in mouse substantial migra pars compacta. European Journal of Neuroscience.

Tubert C, Murer MG (2021) What's wrong with the striatal cholinergic interneurons in Parkinson's disease? Focus on intrinsic excitability. Eur J Neurosci 53:2100–2116.

Tunstall MJ, Oorschot DE, Kean A, Wickens JR (2002) Inhibitory Interactions Between Spiny Projection Neurons in the Rat Striatum. J Neurophysiol 88:1263–1269.

Usiello A, Baik J-H, Rougé-Pont F, Picetti R, Dierich A, LeMeur M, Piazza PV, Borrelli E (2000) Distinct functions of the two isoforms of dopamine D2 receptors. Nature 408:199–203.

Venda LL, Cragg SJ, Buchman VL, Wade-Martins R (2010) α-Synuclein and dopamine at the crossroads of Parkinson's disease. Trends Neurosci 33:559–568.

Vilaró MT, Palacios JoséM, Mengod G (1990) Localization of m5 muscarinic receptor mRNA in rat brain examined by in situ hybridization histochemistry. Neurosci Lett 114:154–159.

Villalba RM, Pare J-F, Lee S, Lee S, Smith Y (2019) Thalamic degeneration in MPTP-treated Parkinsonian monkeys: impact upon glutamatergic innervation of striatal cholinergic interneurons. Brain Struct Funct 224:3321–3338.

Visanji NP, Brotchie JM, Kalia LV, Koprich JB, Tandon A, Watts JC, Lang AE (2016) α-Synuclein-Based Animal Models of Parkinson's Disease: Challenges and Opportunities in a New Era. Trends Neurosci 39:750–762.

Voorn P, Vanderschuren LJMJ, Groenewegen HJ, Robbins TW, Pennartz CMA (2004) Putting a spin on the dorsal–ventral divide of the striatum. Trends Neurosci 27:468–474.

Vuillet J, Dimova R-, Nieoullon A, Goff LK-L (1992) Ultrastructural relationships between choline acetyltransferase- and neuropeptide Y-containing neurons in the rat striatum. Neuroscience 46:351–360.

Vuillet J, Kerkerian L, Kachidian P, Bosler O, Nieoullon A (1989a) Ultrastructural correlates of functional relationships between nigral dopaminergic or cortical afferent fibers and neuropeptide Y-containing neurons in the rat striatum. Neurosci Lett 100:99–104.

Vuillet J, Kerkerian L, Salin P, Nieoullon A (1989b) Ultrastructural features of NPY-containing neurons in the rat striatum. Brain Res 477:241–251.

Waldvogel HJ, Fritschy J -M., Mohler H, Faull RLM (1998) GABAA receptors in the primate basal ganglia: An autoradiographic and a light and electron microscopic immunohistochemical study of the α1 and β2,3 subunits in the baboon brain. J Comp Neurol 397:297–325.

Wall NR, De La Parra M, Callaway EM, Kreitzer AC (2013) Differential Innervation of Direct- and Indirect-Pathway Striatal Projection Neurons. Neuron 79:347–360.

Wang H, Jing M, Li Y (2018) Lighting up the brain: genetically encoded fluorescent sensors for imaging neurotransmitters and neuromodulators. Curr Opin Neurobiol 50:171–178.

Wang H-F, Yu J-T, Tang S-W, Jiang T, Tan C-C, Meng X-F, Wang C, Tan M-S, Tan L (2015) Efficacy and safety of cholinesterase inhibitors and memantine in cognitive impairment in Parkinson's disease, Parkinson's disease dementia, and dementia with Lewy bodies: systematic review with meta-analysis and trial sequential analysis. J Neurology Neurosurg Psychiatry 86:135.

Wang L, Shang S, Kang X, Teng S, Zhu F, Liu B, Wu Q, Li M, Liu W, Xu H, Zhou L, Jiao R, Dou H, Zuo P, Zhang X, Zheng L, Wang S, Wang C, Zhou Z (2014a) Modulation of dopamine release in the striatum by physiologically relevant levels of nicotine. Nat Commun 5:3925.

Wang L, Zhang X, Xu H, Zhou L, Jiao R, Liu W, Zhu F, Kang X, Liu B, Teng S, Wu Q, Li M, Dou H, Zuo P, Wang C, Wang S, Zhou Z (2014b) Temporal components of cholinergic terminal to dopaminergic terminal transmission in dorsal striatum slices of mice. J Physiology 592:3559–3576.

Wang M, Roman GT, Schultz K, Jennings C, Kennedy RT (2008) Improved Temporal Resolution for in Vivo Microdialysis by Using Segmented Flow. Anal Chem 80:5607–5615.

Weiner DM, Levey AI, Brann MR (1990) Expression of muscarinic acetylcholine and dopamine receptor mRNAs in rat basal ganglia. Proc National Acad Sci 87:7050–7054.

Wess J (1996) Molecular Biology of Muscarinic Acetylcholine Receptors. Crit Rev Neurobiol 10:69–99.

Will TR, Proaño SB, Thomas AM, Kunz LM, Thompson KC, Ginnari LA, Jones CH, Lucas S-C, Reavis EM, Dorris DM, Meitzen J (2017) Problems and Progress regarding Sex Bias and Omission in Neuroscience Research. Eneuro 4:ENEURO.0278-17.2017.

Wilson C, Chang H, Kitai S (1990) Firing patterns and synaptic potentials of identified giant aspiny interneurons in the rat neostriatum. J Neurosci 10:508–519.

Witten IB, Lin S-C, Brodsky M, Prakash R, Diester I, Anikeeva P, Gradinaru V, Ramakrishnan C, Deisseroth K (2010) Cholinergic Interneurons Control Local Circuit Activity and Cocaine Conditioning. Science 330:1677–1681.

Woolf NJ, Butcher LL (1986) Cholinergic systems in the rat brain: III. Projections from the pontomesencephalic tegmentum to the thalamus, tectum, basal ganglia, and basal forebrain. Brain Res Bull 16:603–637.

Wooltorton JRA, Pidoplichko VI, Broide RS, Dani JA (2003) Differential Desensitization and Distribution of Nicotinic Acetylcholine Receptor Subtypes in Midbrain Dopamine Areas. J Neurosci 23:3176–3185.

Xenias HS, Ibáñez-Sandoval O, Koós T, Tepper JM (2015) Are Striatal Tyrosine Hydroxylase Interneurons Dopaminergic? J Neurosci 35:6584–6599.

Xu M, Nakamura Y, Yamamoto T, Natori K, Irie T, Utsumi H, Kato T (1991) Determination of basal acetylcholine release in vivo by rat brain dialysis with a U-shaped cannula: effect of SM-10888, a putative therapeutic drug for Alzheimer's disease. Neurosci Lett 123:179–182.

Xu Q, Park Y, Huang X, Hollenbeck A, Blair A, Schatzkin A, Chen H (2011) Diabetes and Risk of Parkinson's Disease. Diabetes Care 34:910–915.

Yamamoto K, Ebihara K, Koshikawa N, Kobayashi M (2013) Reciprocal regulation of inhibitory synaptic transmission by nicotinic and muscarinic receptors in rat nucleus accumbens shell. J Physiology 591:5745–5763.

Yan Z, Song W-J, Surmeier DJ (1997) D2 Dopamine Receptors Reduce N-Type Ca2+ Currents in Rat Neostriatal Cholinergic Interneurons Through a Membrane-Delimited, Protein-Kinase-C-Insensitive Pathway. J Neurophysiol 77:1003–1015.

Yan Z, Surmeier D (1996) Muscarinic (m2/m4) receptors reduce N- and P-type Ca2+ currents in rat neostriatal cholinergic interneurons through a fast, membrane-delimited, G-protein pathway. J Neurosci 16:2592–2604.

Yang H, Jong JW de, Tak Y, Peck J, Bateup HS, Lammel S (2018) Nucleus Accumbens Subnuclei Regulate Motivated Behavior via Direct Inhibition and Disinhibition of VTA Dopamine Subpopulations. Neuron 97:434-449.e4.

Yang Y-W, Hsieh T-F, Li C-I, Liu C-S, Lin W-Y, Chiang J-H, Li T-C, Lin C-C (2017) Increased risk of Parkinson disease with diabetes mellitus in a population-based study. Medicine 96:e5921.

Yetnikoff L, Lavezzi HN, Reichard RA, Zahm DS (2014) An update on the connections of the ventral mesencephalic dopaminergic complex. Neuroscience 282:23–48.

Yin HH, Knowlton BJ, Balleine BW (2004) Lesions of dorsolateral striatum preserve outcome expectancy but disrupt habit formation in instrumental learning. Eur J Neurosci 19:181–189.

Yung KKL, Bolam JP, Smith AD, Hersch SM, Ciliax BJ, Levey AI (1995) Immunocytochemical localization of D1 and D2 dopamine receptors in the basal ganglia of the rat: Light and electron microscopy. Neuroscience 65:709–730.

Yung KKL, Ng TKY, Wong CKC (1999) Subpopulations of neurons in the rat neostriatum display GABABR1 receptor immunoreactivity. Brain Res 830:345–352.

Zahm DS (1999) Functional-anatomical Implications of the Nucleus Accumbens Core and Shell Subterritories. Ann Ny Acad Sci 877:113–128.

Zeng J, Shu SY, Bao X, Zou F, Ji A, Ye J (1999) Properties of acetylcholine receptor channels in the acutely dissociated neurons of the marginal division in the rat striatum. Neurochemical research.

Zhang H, Sulzer D (2004) Frequency-dependent modulation of dopamine release by nicotine. Nat Neurosci 7:581–582.

Zhang W, Yamada M, Gomeza J, Basile AS, Wess J (2002) Multiple Muscarinic Acetylcholine Receptor Subtypes Modulate Striatal Dopamine Release, as Studied with M1–M5 Muscarinic Receptor Knock-Out Mice. J Neurosci 22:6347–6352.

Zhang Y-F, Reynolds JNJ, Cragg SJ (2018) Pauses in Cholinergic Interneuron Activity Are Driven by Excitatory Input and Delayed Rectification, with Dopamine Modulation. Neuron.

Zhou F, Wilson CJ, Dani JA (2002) Cholinergic interneuron characteristics and nicotinic properties in the striatum. J Neurobiol 53:590–605.

Zhou F-M, Liang Y, Dani JA (2001) Endogenous nicotinic cholinergic activity regulates dopamine release in the striatum. Nat Neurosci 4:nn769.

Zhu PK, Zheng WS, Zhang P, Jing M, Borden PM, Ali F, Guo K, Feng J, Marvin JS, Wang Y, Wan J, Gan L, Kwan AC, Lin L, Looger LL, Li Y, Zhang Y (2020) Nanoscopic Visualization of Restricted Nonvolume Cholinergic and Monoaminergic Transmission with Genetically Encoded Sensors. Nano Lett 20:4073–4083.

Ziegler N, Bätz J, Zabel U, Lohse MJ, Hoffmann C (2011) FRET-based sensors for the human M1-, M3-, and M5-acetylcholine receptors. Bioorgan Med Chem 19:1048–1054.

Ztaou S, Maurice N, Camon J, Guiraudie-Capraz G, Goff LK-L, Beurrier C, Liberge M, Amalric M (2016) Involvement of Striatal Cholinergic Interneurons and M1 and M4 Muscarinic Receptors in Motor Symptoms of Parkinson's Disease. J Neurosci 36:9161–9172.